UNIVERSITY OF CALIFORNIA SAN DIEGO

Use of Enzymes for Amplified Signal Generation

A dissertation submitted in partial satisfaction of the requirements for the degree
Doctor of Philosophy

in

Chemistry

by

Brandon T. Cisneros

Committee in charge:

Professor Neal K. Devaraj, Chair
Professor Ulrich F. Müller
Professor Maike Sander
Professor Jerry Yang
Professor Brian M. Zid

2020

The Dissertation of Brandon T. Cisneros is approved, and it is acceptable in quality and form for publication on microfilm and electronically:

Chair

University of California San Diego

2020

Epigraph

To experience science as nihilism is to experience the hopelessness that can result as you watch one cherished thought after another bite the dust, to be replaced by ideas that offer little or no comfort.

Venkatesh Rao

Table of Contents

List of Abbreviations

DMEM	Dulbecco's modified Eagle's medium
FBS	fetal bovine serum
DMF	dimethylformamide
DMSO	dimethylsulfoxide
TFA	trifluoroacetic acid
eq(s)	equivalent(s)
PBS	phosphate buffered saline
HBSS	Hank's balanced salt solution
EDTA	ethylenediamine tetraacetic acid
ORF	open reading frame
PCR	polymerase chain reaction
nt	nucleotide
bp	base pair
BSA	bovine serum albumin
K_m	Michaelis constant in Michaelis-Menten kinetics
DIEA	diisopropylethylamine
qPCR	quantitativePCR
Ct	cycle threshold number

List of Figures

List of Schemes

List of Tables

Acknowledgements

I would like to acknowledge the individuals who have played an instrumental role in my past and current success. I want to thank my family. Thank you to my parents, Jas and Ed, for a lifetime of supporting (or at least tolerating) the things my curiosity drove me to do. Really, thank you. It takes a lot of patience to put up with the assortment of things I did, from disassembling all the appliances to cleaning and rebuilding an opossum skeleton from roadkill. Thank you to my sister, Breanne, for commiserating with me about the difficulties of graduate school and helping keep me off my high horse. Thank you to my brother, Dean, who has been a role model for sincerity, kindness, and unrelenting work ethic to me for as long as I can remember. Thank you to my partner, Vy, who has been understanding and loving throughout this long journey through school. I could never have done this without you.

I would like to thank some of the influential teachers I had. Dr. Tilahaun Yimenu, your positive encouragement and passion helped me learn to enjoy the study of chemistry. Dr. Jake Sapiro, the rigor of your Anatomy and Physiology courses has built a foundation of knowledge that I still use on a near daily basis. Dr. Blythe Tellefsen, your classes and mentoring helped me be a bit less self-serious and showed me that it was possible for me to both enjoy and excel at non-science subjects. Thank you all.

I would like to thank my Pathfinder game night group, Alie, Micah, Steve, Cindy, Vlad and Vy, for their support throughout graduate school. Our weekly game nights were often the only social contact I would have during the week and were often one of the only breaks I had from work. Thank you to my lifelong friend, Jake Johnson. Our semi-weekly phone calls helped keep me grounded and were always a welcome relief to whatever I had going on.

I would like to thank my previous research advisors. Dr. Lon J. Wilson, you were an incredible mentor. The environment you cultivated in your lab allowed me to learn from many people. You helped ensure that I was engaged with work even though I was still a novice. Dr. Steven Curley, you provided me with many opportunities that were beyond the scope of my training and trusted that I could succeed in them. I am grateful for the confidence you had in me.

Thank you, Dr. Neal Devaraj, for letting me be part of your lab. Thanks to you, I have had many opportunities to learn new skills and explore different research directions that I would not have been able to do elsewhere. You have supported me in many ways over the years and I sincerely appreciate it.

Thank you to my fellow lab mates, current and former, who have been colleagues and mentors in their own way. From my previous labs, I would like to thank Dr. Jeyrama Ananta, Dr. Mike Matson, Dr. Lesa Tran, and Dr. Mustafa Raoof for their guidance and mentorship in Houston. From the Devaraj lab, I would like to thank Ahanjit for always being open to discussing interesting scientific literature, especially if it was not related to our own work. I would like to thank Kayla Busby and Dr. Andrew Rudd for all your help with experiments over the years.

Finally, I would owe a huge debt of gratitude to Dr. James P. Webb, former scientific director at Orange County Vector Control District. He was the first professional scientist I had any real contact with and showed me the value of having a wide breadth of academic interests. He would give me papers to read from physics, epigenetics, ecology, virology, biochemistry, etc. When I doubted the utility of such far flung reading, he responded quoting Robert Heinlein, “Specialization is for insects.” Thank you, Jim, giving me the opportunity to spend several years learning from and working with professional scientists when I was only a child of sixteen. I wish you could be here today to see what I have accomplished.

Chapter two, in full, is a reprint (with co-author permission) of the material as it appears in the publication: Cisneros, B. T., Devaraj, N. K., Laccase-mediated catalyzed fluorescent reporter deposition for live cell imaging. ChemBioChem 2019, 20. I would like to thank Neal Devaraj for his scientific oversight and assistance in preparing the manuscript. The author of the dissertation is the primary author of this manuscript.

Chapter three, in part, is being prepared for submission for publication of the material. Cisneros, B. T., Devaraj, N. K. The dissertation author is the primary investigator and author of this material.

Vita

Education

2011 Bachelor of Science, Chemistry, Rice University, Houston, TX

2015 Master of Science, Chemistry, University of California San Diego

2020 Doctor of Philosophy, Chemistry, University of California San Diego

Employment

2011 ACS Nuclear Chemistry Summer School, Teaching Assistant

2011-2013 MD Anderson Cancer Center, Research Assistant

Publications

Cisneros, B. T.; Devaraj, N. K. Laccase-mediated catalyzed fluorescent reporter deposition for live cell imaging. *ChemBioChem* 2019, 20.

Corr, S. J.; Shamsudeen, S.; Vergara, L. A.; Ho, J. C.; Ware, M. J.; Keshishian, V.; Yokoi, K.; Savage, D. J.; Meraz, I. M.; Kaluarachchi, W.; **Cisneros, B. T.;** Raoof, M.; Nguyen, D. T.; Zhang, Y.; Wilson, L. J.; Summers, H.; Rees, P.; Curley, S.A.; Serda, R.E. A New Imaging Platform for Visualizing Biological Effects of Non-Invasive Radiofrequency Electric-Field Cancer Hyperthermia. *PLoS One*. 2015, 10(8), e0136382.

Corr, S. J.; Raoof, M.; **Cisneros, B. T**.; Orbaek, A. W.; Cheney, M. A.; Law, J. J.; Lara, N.C.; Barron, A. R.; Wilson, L. J.; Curley, S. A. Radiofrequency electric-field heating behaviors of highly enriched semiconducting and metallic single-walled carbon nanotubes. *Nano Research* 2015, 8, 2859-2870.

Wu, H.; **Cisneros, B. T**.; Cole, C. M.; Devaraj, N. K. Bioorthogonal tetrazine-mediated transfer reactions facilitate reaction turnover in nucleic acid-templated detection of microRNA. *Journal of the American Chemical Society* 2014, 136, 17942-17945.

Raoof, M.; Zhu, C.; **Cisneros, B. T**., Liu, H., Corr, S. J.; Wilson, L. J.; Curley, S. A. Hyperthermia Inhibits Recombination Repair of Gemcitabine-Stalled Replication Forks. *Journal of the National Cancer Institute* 2014, 106, dju183.

Rosenberg, J. T.; **Cisneros, B. T**.; Matson, M.; Sokoll, M.; Sachi-Kocher, A.; Bejarano, F. C.; Wilson, L. J.; Grant, S. C. Encapsulated gadolinium and dysprosium ions within ultra-short carbon nanotubes for MR microscopy at 11.75 and 21.1 T. *Contrast Media & Molecular Imaging* 2014, 9, 92-99.

Cisneros, B. T.; Law, J. J.; Matson, M. L.; Azhdarinia, A.; Sevick-Muraca, E. M.; Wilson, L. J. Stable confinement of positron emission tomography and magnetic resonance agents within carbon nanotubes for bimodal imaging. *Nanomedicine* 2014, 9, 2499-2509.

Raoof, M.; Corr, S. J.; Zhu, C.; **Cisneros, B. T**.; Kaluarachchi, W. D.; Phounsavath, S.; Wilson, L. J.; Curley, S. A. Gold nanoparticles and radiofrequency in experimental models for hepatocellular carcinoma. *Nanomedicine: Nanotechnology, Biology and Medicine* 2014, 10, 1121-1130.

Corr, S. J.; **Cisneros, B. T.**; Green, L.; Raoof, M.; Curley, S. A. Protocols for Assessing Radiofrequency Interactions with Nanoparticles and Biological Systems for Non-Invasive Hyperthermia Cancer Therapy. *Journal of Visualized Experiments: JoVE* 2013, 78.

Kaluarachchi, W. D.; **Cisneros, B. T**.; Corr, S. J.; Albert, N. D.; Curley, S. A.; Kontoyiannis, D. P. Aspergillus fumigatus Hyphal Damage Caused by Noninvasive Radiofrequency Field-Induced Hyperthermia. *Antimicrobial Agents and Chemotherapy* 2013, 57, 4444-4448.

Mackeyev, Y.; Raoof, M.; **Cisneros, B**.; Koshkina, N.; Berger, C.; Wilson, L.; Curley, S. Toward Paclitaxel-[60] Fullerene Immunoconjugates as a Targeted Prodrug against Cancer. *Nanosystems*, 67.

Raoof, M.; **Cisneros, B. T**.; Corr, S. J.; Palalon, F.; Curley, S. A.; Koshkina, N. V. Tumor selective hyperthermia induced by short-wave capacitively-coupled RF electric-fields. *PloS ONE* 2013, 8, e68506.

Raoof, M.; **Cisneros, B. T**.; Guven, A.; Phounsavath, S.; Corr, S. J.; Wilson, L. J.; Curley, S. A. Remotely triggered cisplatin release from carbon nanocapsules by radiofrequency fields. *Biomaterials* 2013, 34, 1862-1869.

Corr, S. J.; Raoof, M.; **Cisneros, B. T**.; Kuznetsov, O.; Massey, K.; Kaluarachchi, W. D.; Cheney, M. A.; Billups, E. W.; Wilson, L. J.,;Curley, S. A. Cytotoxicity and variant cellular internalization behavior of water-soluble sulfonated nanographene sheets in liver cancer cells. *Nanoscale Research Letters* 2013, 8, 1-10

Corr, S. J.; Raoof, M.; Mackeyev, Y.; Phounsavath, S.; Cheney, M. A.; **Cisneros, B. T.;** Shur, M.; Gozin, M.; McNally, P. J.; Wilson, L. J. Citrate-capped gold nanoparticle electrophoretic heat production in response to a time-varying radio-frequency electric field. *The Journal of Physical Chemistry C* 2012, 116, 24380-24389.

Tang, A. M.; Ananta, J. S.; Zhao, H.; **Cisneros, B. T**.; Lam, E. Y.; Wong, S. T.; Wilson, L. J.; Wong, K. K. Cellular uptake and imaging studies of gadolinium-loaded single-walled carbon nanotubes as MRI contrast agents. *Contrast Media & Molecular Imaging* 2011, 6, 93-99.

Fellowships and Awards

2018 San Diego Fellowship

2013 National Science Foundation Graduate Research Fellowship

2013 Katzin Prize

2013 Cota Robles Fellowship

2013 Stanley Miller Award

2011 Richard B. Turner Memorial Award for Chemistry

2010 ACS Nuclear Chemistry Summer School Outstanding Student Award

2010 ACS Nuclear Chemistry Summer School Undergraduate Fellowship

2008 Joel D. Hail Memorial Scholarship for Chemistry

Abstract of the Dissertation

Use of Enzymes for Amplified Signal Generation

by

Brandon T. Cisneros

Doctor of Philosophy in Chemistry

University of California San Diego, 2020

Professor Neal K. Devaraj, Chair

This dissertation will explore two different methods of generating enzymatically-amplified signals in response to cell surface features. The first method uses a variation on traditional catalyzed reporter deposition employing the enzyme laccase to covalently deposit a fluorescent ferulic acid derivative. This enzyme has distinct properties that make it more suitable for use with catalyzed reporter deposition in living systems. The second portion of this thesis focuses on the development of xanthine methylating enzymes as a reporter protein. It demonstrates how synthetic juxtacrine signaling receptors can be used to induce expression of enzymes capable of methylating

a variety of xanthines to produce a detectable, biocompatible small molecule reporter. This approach required heterologous expression of many xanthine methyltransferase enzymes in human cells for the first time so that their properties could be evaluated. In addition to being potentially useful as a reporter protein, the use of xanthine methylating enzymes in mammalian cells has potential connections to synthetic biology and the development of synthetic paracrine signaling pathways using small molecules.

CHAPTER 1

1. Introduction

1.1 Early Use of Tinctorial Methods in Histology

Exogenous agents have been used since the dawn of microscopy to colorize samples to help visualize their features. The processes of using dyes to stain or selectively stain samples are referred to as tinctorial methods. Early microscopists Leeuwenhoek and Hooke both used cochineal, a dye extracted from cochineal beetles, to stain samples.[1] Iodine was used to colorize starches in plants. Haematoxylin extracted from tropical logwood tree was used as a crude nuclear stain.[1] The key feature of these dyes was that they differentially colored features within samples. By selectively staining some features and not others, these dyes allowed microscopists to distinguish cellular compartments and organelles and gain insight into their composition. Being able to distinguish a feature from its surroundings is essential to careful observation.

1.2 Development of Immunofluorescence Microscopy

The origin of fluorescence microscopy can be traced back to 1904, when August Köhler made an ultraviolet light microscope for the purpose of producing higher resolution images using the shorter wavelength light.[2] He noted the emission of light at a longer wavelength from the samples. This phenomenon was used to develop a microscope specifically to look at the light re-emitted from a sample in 1911 by Oskar Heimstädt,[3] but the technique did not become especially useful until exogenous fluorescent compounds began being added to samples.[2] A rudimentary epi-fluorescence microscope was developed in 1929 by Ellinger and Hirt which was used to image fluorescent fluorescein and trypaflavin in rodent tissue.

The specificity of fluorescent staining took a dramatic leap forward in 1941,[4] when Coons et al. reacted anthracene isothiocyanate with antipneumococcus I and II antibodies.[5] They noted that this would not be useful in mammalian tissues due to the blue autofluorescence that interfered with observations. The following year, Coons et al. produced antibodies fluorescently-labeled with fluorescein isocyanate which could be easily observed in tissues.[5] This method of making fluorescent antibodies is still in use, albeit with slight modifications (e.g. fluorescein isothiocyanate is used today).

In 1966, Graham and Karnovsky reported the first use of the antibodies labeled with the enzyme horseradish peroxidase for microscopy.[6] Parallel work by Nakane and Pierce demonstrated the same principle with acid phosphatase as well as horseradish peroxidase.[7] Rather than stoichiometrically labeling a target with a fluorophore, this technique uses the catalytic properties of the bound enzyme to oxidize a large amount of 3,3'-diaminobenzidine (DAB) which can be seen via light microscopy. The use of enzymes to enhance signal obtained from specimens was further developed by Bobrow, et al. in the technique of catalyzed reporter deposition (CARD).[8] In this elaboration on the use of horseradish peroxidase, a biotinylated tyramide probe is deposited instead of DAB, but the initial approach was not suitable for microscopy. Later improvements on this technique enabled indirect[9,10] and direct[11] fluorescent detection using microscopy. These advances led to an even better ability to resolve specific, minute features and gain an even better understanding of biological world.

1.3 Reporter Proteins

The microscopy techniques discussed above were powerful tools for studying fixed microscopy specimens, but were much less useful for studying dynamic, living samples. Proteins that have easily detected features or produce easily detected enzymatic products are known as

reporter proteins. Reporter proteins are immensely valuable in the study of living systems because they do not require an organism or tissue to be fixed and unchanging in order to detect their presence. In the 1980s, firefly luciferase,[12] bacterial luciferase,[13] and β-galactosidase[14] were all developed as reporter proteins for biological studies. By the end of the decade, transgenic mice expressing luciferase were available as a new research tool.[15] In 1994, green fluorescent protein (GFP) was first used as a reporter protein[16] and unlike other reporter proteins it did not require an exogenous substrate. Subsequent improvement of GFP led to its proliferation in research as a valuable tool. Development of different colored fluorescent proteins only further increased the value of this class of reporter proteins.[17,18] Reporter proteins have revolutionized the study of living organisms and will continue to be a valuable tool in the future.

This dissertation will explore the development of new tools for use in generating amplified signals from biological systems with enzymes. Recent work will be presented which demonstrates a derivative of CARD using laccase that has features more suitable for use in living systems. Additional work will be presented which documents the development of xanthine methylating enzymes as enzymatic reporters for mammalian cells. In conclusion, I can only adapt the closing sentiment[3] Oskar Heimstädt from his work developing the fluorescence microscopy: if and to what degree my research will be used by others only the future will show.

CHAPTER 2

2 Laccase-Mediated Catalyzed Fluorescent Reporter Deposition for Live Cell Imaging

2.1 Abstract

Catalyzed reporter deposition (CARD) is a widely established method for labeling biological samples analyzed using microscopy. Horseradish peroxidase, commonly used in CARD to amplify reporter signals, requires the addition of hydrogen peroxide which may perturb samples used in live-cell microscopy. Herein we describe an alternative method of performing CARD using a laccase enzyme, which does not require exogenous hydrogen peroxide. Laccase is an oxidative enzyme which can carry out single-electron oxidations of phenols and related compounds by reducing molecular oxygen. We demonstrate proof-of-concept for this technique through the non-targeted covalent labeling of bovine serum albumin using a fluorescently-labeled ferulic acid derivative as the laccase re-porter substrate. We further demonstrate the viability of this approach by performing live-cell CARD with an antibody-conjugated laccase against a surface bound target. CARD using laccase produces an amplified fluorescence signal by labeling cells without the need for exogenous hydrogen peroxide.

2.2 Introduction

Laccases (EC 1.10.3.2, benzenediol:oxygen oxidoreductase) are a family of enzymes which couple the reduction of molecular oxygen to the oxidation of a substrate, typically a phenol or aromatic amine. Laccases carry out four one-electron oxidations of its substrate and use these electrons to reduce oxygen to water. This process is mediated by a cluster of four copper atoms in its active site. Laccases are found in many organisms, notably fungi[19] and plants, but also in insects[20] and bacteria,[21] and they show variable substrate specificity across species.

Owing to the versatile nature of the chemical transformation they carry out, laccases have been adopted or proposed for use in many industrial processes.[22] Much of laccase's utility in industry has focused on decolorizing dye[23] or treating wood pulp used to produce paper.[24] Moreover, laccase has been suggested as a useful agent for treating contaminated water,[25] and removing phenol constituents in various food or beverages[26]. In academic research, laccase has been used for the chemical transformations of small molecules,[27] production of polymers,[28] as an enzyme in ELISA,[29–31] and in biosensing applications.[32] This research has led to the development of modified laccases with a variety of properties, including stability in organic solvents[33] and improved reactivity in biological media.[34]

Catalyzed reporter deposition (CARD) is a technique that is frequently used in the preparation of tissues or cells for microscopy.[8] In this technique, an analyte-dependent reporter enzyme is used to deposit an easily-detectable reporter molecule near the desired target. This is often achieved by modifying the enzyme with an affinity tag, typically by linking it to an antibody, and using it to chemically activate a biotin-labeled or fluorophore-labeled substrate.[35,36] The activated substrate can then covalently bind to the targeted cell (**Figure 2.1 A**).[8] Enzyme turnover allows for many more fluorescent labels to be deposited per antibody delivered compared to an antibody that has been directly labeled with a fluorescent tag. This approach has been widely used with horseradish peroxidase (HRP) but has also been used with other enzymes such as alkaline phosphatase.[36]

More recently, genetically encoded engineered ascorbate peroxidase (APEX) has been used for amplified imaging in cells for fluorescent microscopy,[37] electron microscopy,[38] and proteomic labeling.[39] Unlike typical CARD methodologies, APEX uses a genetically encoded reporter enzyme as a label. The addition of heme during cell culture allows for reconstitution of

enzyme activity that can subsequently be used to deposit a probe (e.g. biotin-phenol). Using reporter enzymes to provide an amplified signal for imaging and labeling has proven to be a useful tool in studying biological systems in many different contexts.[35,39–43]

One caveat of using a peroxidase such as HRP or APEX is that these techniques use exogenous hydrogen peroxide as the oxidizing agent. Hydrogen peroxide has been shown to have a number of effects on cells at various concentrations, including inducing differentiation, proliferation,[44] DNA lesions,[45] and apoptosis.[46] Even at lower concentrations, hydrogen peroxide is recognized to alter cell signaling,[47] particularly in sensitive cells like neurons.[48] These effects are highly dependent on the specific conditions and identity of the cells in question.[49] The diversity of effects over a range of concentrations makes it difficult to predict what might happen upon addition of hydrogen peroxide to any given cell line. As a result, CARD with peroxidases can have limitations when used for live cell imaging.

We hypothesized that laccase could be used to carry out CARD for live cell fluorescence microscopy imaging. This seemed plausible because laccase and HRP can both oxidize various phenolic substrates and carry out similar chemical transformations of their substrates albeit via distinct mechanisms.[50–52] Since laccase uses oxygen as the oxidizing agent and produces water, cells would not be exposed to unnecessarily levels of hydrogen peroxide required by HRP. Because laccases oxidize their substrates to products that are identical to those produced by peroxidases, these products are expected to react with tyrosine residues to form adducts (**Figure 2.1 B**).[53]

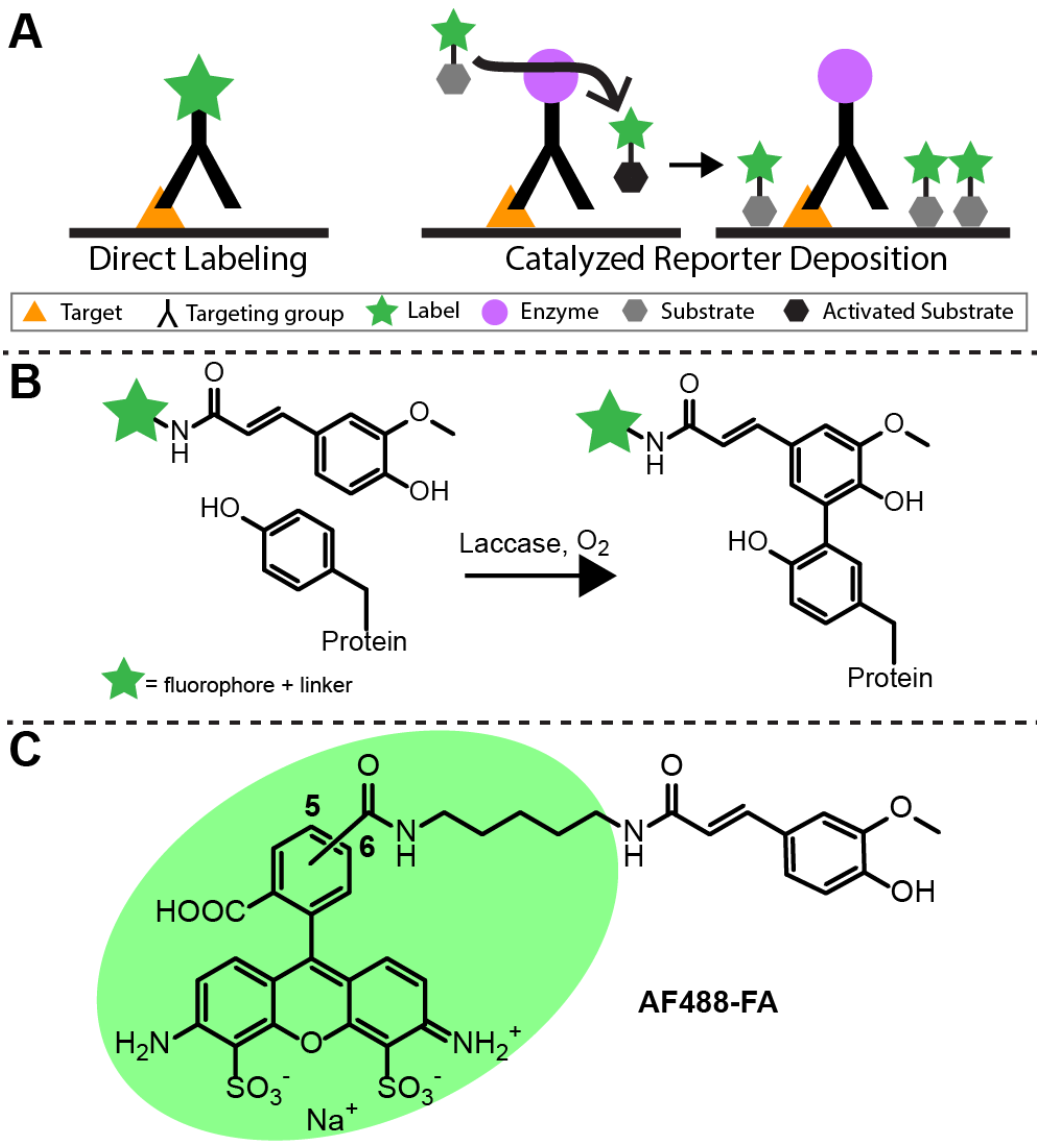

Figure 2.1: A) Graphical depiction comparing direct labeling to CARD. The fluorescent label is covalently attached to the targeting group in direct labeling, whereas the fluorescent label is covalently deposited in the area near the target in CARD. B) Schematic representation of the way by which AF488-FA could covalently bind to tyrosine residues in a protein. C) Structure of AF488-FA which consists of ferulic acid bound to Alexa Fluor 488 via a cadaverine linker.

2.3 Results

To test whether laccase could serve as a suitable enzyme for carrying out CARD, we used two commercially available laccases derived from different organisms: Chinese lacquer tree (*Toxicodendron vernicifluum*, formerly *Rhus vernicifera*) and turkey tail mushroom (*Trametes versicolor*). Initial attempts at verifying previously reported enzyme activities and pH optima using

syringaldazine[54–56] were difficult to reproduce, possibly due to the heterogenous quality of the enzyme preparations. Reproducibility was considerably improved by triturating the enzyme powder with a minimum quantity of buffer in a hand homogenizer before adding the remaining quantity of buffer. This suspension was then syringe filtered to remove large particles and concentrated via spin filtration to produce a transparent, stable solution of laccase.

To assess the viability of using laccase to perform CARD, we selected ferulic acid as a suitable substrate due to its high rate of reaction with our chosen laccases.[56] We designed a probe (**Figure 2.1 C**) consisting of Alexa Fluor 488 conjugated to ferulic acid via a cadaverine linker. The probe was synthesized by reaction of succinimidyl ferulate with Alexa Fluor 488 cadaverine and subsequently purified by semi-preparative HPLC. The resulting probe (AF488-FA) was dissolved in dimethyl sulfoxide and was used in all subsequent CARD tests.

We tested the ability for laccase to perform CARD first in an untargeted fashion (**Figure 2.2 A**). By co-incubating laccase with the probe and a soluble protein target, bovine serum albumin (BSA), we expected that some of the probe should be oxidized to the ferulic acid semiquinone. The oxidized probe could then react with tyrosine residues on the protein target, leading to conjugation. After performing such an incubation, the solutions were subjected to repeated washing and spin dialysis. Washes included both denaturing and ethanolic conditions to ensure that non-covalently bound AF488-FA was removed. Both laccases were found to be able to modify BSA in solution but *T. versicolor* laccase provided better conjugation yields at pH 7.0 150 mM phosphate buffer, 19.5 μM AF488-FA, and 0.5% (w/v) BSA (**Figure 2.2 B**). Variable concentrations of BSA showed that increasing concentrations of BSA do not noticeably increase non-specific binding (**Figure 2.2 C**).

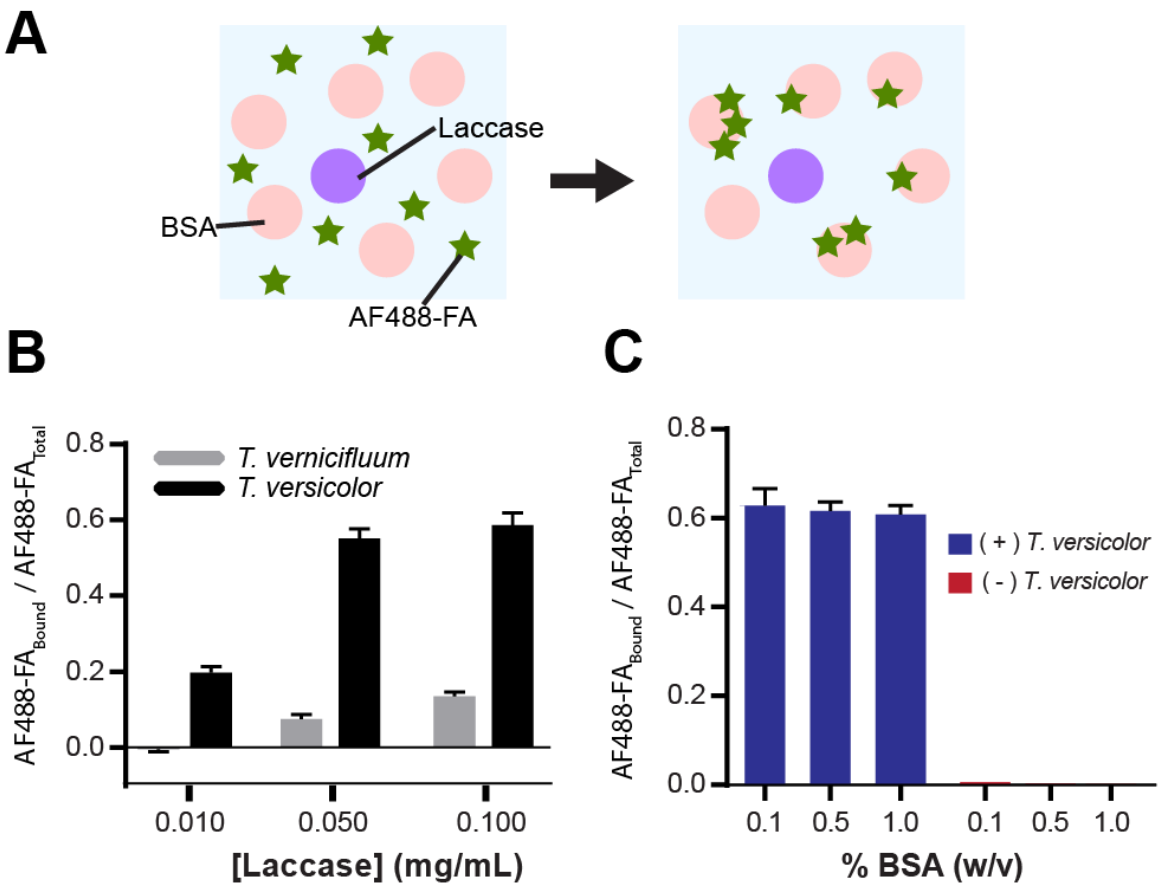

Figure 2.2: A) Representation of non-targeted labeling of BSA with AF488-FA using laccase. BSA in the general proximity of a laccase can be covalently labeled when activated AF488-FA diffuses close to it and reacts with amino acid residues (e.g. tyrosine) in its structure. B) Fraction of AF488-FA bound to BSA after washing with various concentrations of laccase showing superior performance of T. versicolor at all enzyme concentrations. Refer to Supplementary Information for detailed conditions. C) Dependence of BSA modification on BSA concentration

We set out to determine if laccase could be used to fluorescently label the surface of living cells with AF488-FA via CARD. We labeled cells with a biotinylated primary antibody followed by a laccase-streptavidin conjugate (laccase-SA) (**Scheme 2.1 A**). Our approach mimicked the use of a primary antibody followed by an enzyme-conjugated secondary antibody for fluorescent labeling of fixed cells as in CARD. The modular nature of this approach could allow the laccase-SA to be used for other biotinylated antibodies or targets. In addition, an antibody that has laccase attached to it could be easily prepared by pre-incubating the laccase-SA with a biotinylated antibody.

To create the laccase-SA, streptavidin and laccase were modified with amine-reactive succinimidyl 6-hydrazinonicotinate acetone hydrazone (HyNic-NHS) and succinimidyl 4-formylbenzoate (4-FB-NHS), respectively, using a Solulink protein-modification kit (**Scheme 2.1 B**). The derivatized proteins were subsequently reacted with one another to yield the streptavidin-laccase conjugate. The resulting product was found to have 1.1 laccases per streptavidin molecule based on the optical detection of the hydrazone formed between HyNic and 4-FB. Conjugation was further validated by measuring laccase enzymatic activity using syringaldazine[57] as a colorimetric substrate.

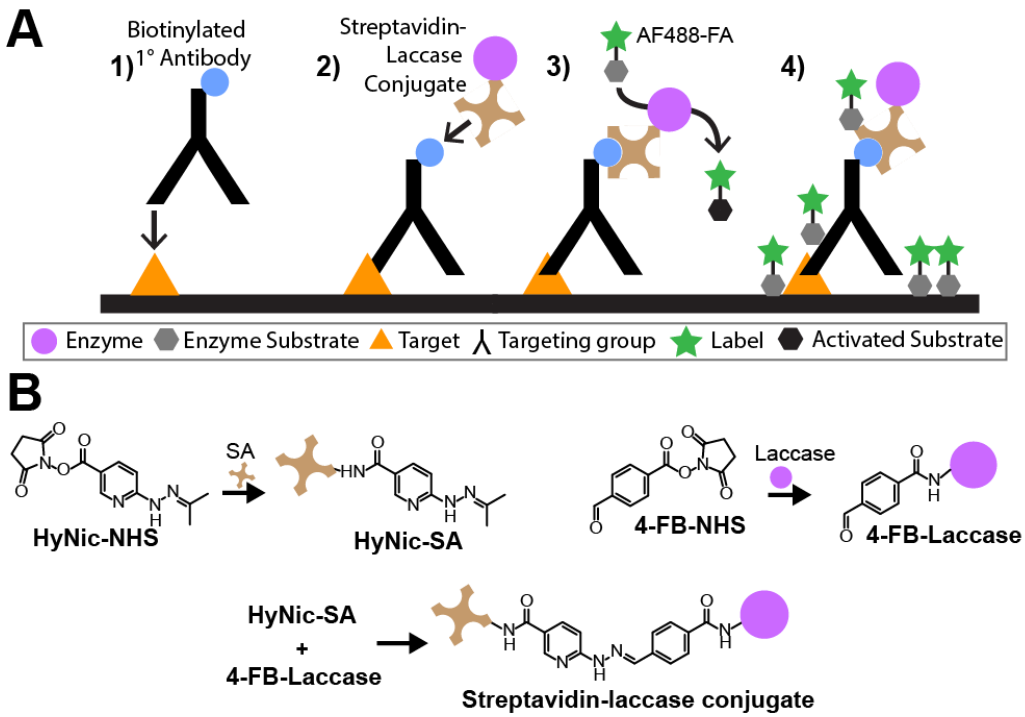

Scheme 2.1: A) A biotinylated primary antibody can interact with a target on the surface of a cell (1). The streptavidin moiety of a laccase-SA can bind to biotin on the primary antibody (2). Exposure to the AF488-FA probe will cause the probe to become activated by the laccase (3). The activated probe can react with amino acids on the cell surface proteins nearby (4). B) Synthesis of HyNic-modified streptavidin, 4-FB-modified laccase, and streptavidin-laccase conjugate.

To test laccase CARD on live cells, we chose to target epidermal growth factor receptor (EGFR) on the surface of A431 cells. A431 is a human squamous cell carcinoma cell line that has

high levels of surface-expressed EGFR.[58] EGFR has been intensively studied as a therapeutic and imaging target, and has been used as a model system for surface receptor internalization and recycling.[59]

For our imaging experiments, we grew A431 cells in 8-well chamber slides. Prior to imaging, the cells were sequentially incubated with the biotinylated anti-EGFR primary antibody at 4 °C for 30 min, laccase-SA for 15 min at room temperature, and the AF488-FA in phosphate buffer at 37 °C for 30 min. The low temperatures were used to minimize receptor internalization.[60] As a comparison, cells were also treated with commercial Alexa Fluor 488-labeled streptavidin (SA-488) (4 fluorophores/protein) using the same duration, temperature, and concentration of streptavidin as was used for the streptavidin-laccase conjugate. The confocal fluorescence microscopy images of these cells indicate substantial signal amplification of the laccase-SA and AF488-FA treated cells compared to the Alexa Fluor 488-streptavidin conjugate (**Figure 2.3 A** and **Figure 2.7)**.

We set out to quantify the amplified fluorescence signal produced by this method for a population of cells. Cells were grown in a black-bottomed 96-well culture plate and were fluorescently labeled with laccase/AF488-FA or SA-488. The cells were fluorescently labeled using the same methods as were used for microscopy. The total fluorescence for each well was measured on a plate reader (**Figure 2.8**). These data also indicate that the total fluorescence was greater for the laccase-SA treated cells than for the SA-488 treated cells. This indicates that the quantity of fluorophores deposited per cell and thus the total fluorescence was amplified relative to the stoichiometric labeling method. These results could be readily improved with further research and optimization of conditions such as concentration of AF488-FA, duration of incubation, or identity of the fluorescent substrate.

To qualitatively assess the specificity of this approach in a mixed cell population, we labeled and imaged co-cultured cells. A431 cells (+EGFR) and mCherry-expressing HEK293 cells (-EGFR) were grown together in chamber slides and were prepared in the same manner as other live-cell imaging experiments. The epifluorescence microscopy images obtained (**Figure 2.4 B** and **Figure 2.9**) show that the EGFR-expressing A431 cells (-mCherry) show high levels of probe deposition by AF488-FA whereas the EGFR-deficient HEK293 cells (+mCherry) do not. This demonstrates that CARD with laccase can selectively label live cells expressing a target of interest in mixed cell populations.

We then tested whether CARD with laccase changes the uptake of epidermal growth factor (**Figure 2.10**). A431 cells were labeled with laccase, as before, but were subsequently treated with 20 ng/μL Alexa Fluor 555 EGF Complex (EGF-AF555) for 1h at 4 °C to allow EGF-AF555 to bind. Cells were then incubated at 37 °C for 30 minutes to elicit endocytosis.[61] Confocal microscopy of these cells shows that the overall signal is diminished in cells treated with the anti-EGFR antibody compared to those without. Puncta are observed in both cases, but this suggests that the primary anti-EGFR antibody used for CARD with laccase reduces the overall intensity of EGF-AF555 signal observed. As a result, CARD with laccase could plausibly inhibit EGF signaling to some degree. This observation is likely caused by a combination of two factors: direct antibody interference with the EGF binding site on EGFR and receptor endocytosis during laccase labeling.[62] Optimization of the amount of primary antibody needed could potentially improve EGF receptor/ligand binding.

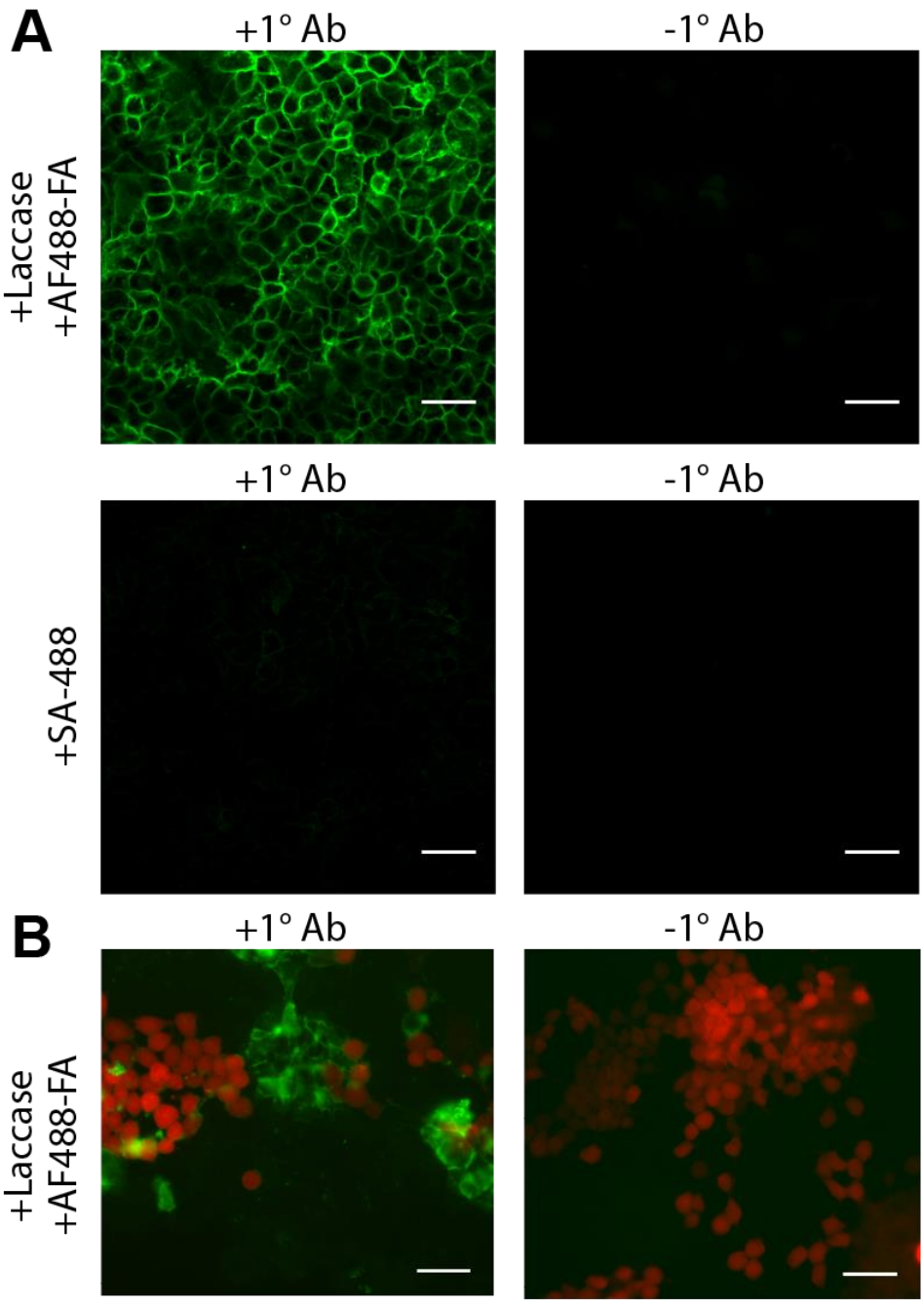

Figure 2.3: A) Confocal microscopy images of A431 cells treated with biotinylated anti-EGFR primary antibody followed by either laccase-SA/AF488-FA or SA-488. Control cells ("-1° Ab") were subjected to the same conditions but without the primary antibody. Scale bar = 50 µm. B) Epifluorescence microscopy images of merged AF488 and mCherry channels of co-culture of A431 cells and mCherry-expressing HEK293 cells. Scale bar = 50 µm All microscopy images here are window-leveled identically.

2.4 Conclusions

We have demonstrated that laccase can be used to fluorescently label proteins via CARD. Antibody-targeted laccases enable biomarker dependent amplification of imaging signals. We

selectively labeled live cells with AF488-FA and imaged them without fixation, even in the presence of other cell types. This technique allows for signal amplification in a manner akin to APEX or CARD with horseradish peroxidase, but it does not require exogenous hydrogen peroxide. While this improvement does not obviate potential issues with covalent modification proteins in situ, it removes a barrier to using CARD in live cells. With further evaluation of other laccases and laccase substrates, this technique could be modified to accept different reporter substrates and have improved reactivity, optimal pH, ion sensitivity, etc. We envision that laccase-based CARD techniques could be potentially useful for many labeling applications and could serve as a basis for an improved method of performing amplified reporter deposition of live cells in biomarker fluorescence imaging, electron microscopy, and proteomics.

2.5 Experimental Procedures

2.5.1 Materials and Instrument Details

Laccases (*Trametes versicolor* and *Toxicodendron vernicifluum*), syringaldazine, dicylcohexylcarbodiimide solution, and THF purchased from Sigma Aldrich (St. Louis, MO). trans-Ferulic acid was purchased from Tokyo Chemical Inc. (Tokyo, Japan). All other reagents and solvents were obtained from Fisher Scientific. Solulink Protein-Protein Conjugation kit (S-9010) was purchased from TriLink Biotechnologies (San Diego, CA). Biotinylated anti-EGFR antibody clone 528 (#MA5-12872), AlexaFluor 488-cadaverine, streptavidin-AlexaFluor 488, and AlexaFluor 555 EGF Complex (EGF-AF555) were purchased Thermo Fisher (Waltham, MA). Fetal bovine serum (FBS) was purchased from Corning (Corning, NY). All unspecified products (e.g. buffer components, etc.) were purchased from Fisher Scientific (Waltham, MA). pHR_Gal4UAS_tBFP_PGK_mCherry[63] was a gift from Wendell Lim (Addgene plasmid # 79130). pLP1 (gal-pol) and pLP2 (rev) were obtained from Invitrogen (Waltham, MA). pCMV-G

was obtained from the Friedmann lab.[64] No unexpected or unusually high safety hazards were encountered.

UV-Vis spectroscopy for BCA assay, fluorophore concentration determination, and kinetics assays were performed on a Nandrop 2000 (Thermo Fisher, Waltham, MA).

Reverse-phase HPLC purification was performed using an Agilent 1100 series Infinity HPLC (Santa Clara, CA). Agilent Zorbax SB-C18 semi-prep column (ID 9.4 x 250 mm, 5 µm, 80 Å) using a water/acetonitrile gradient containing 0.1% trifluoroacetic acid using a variable wavelength detector wavelength of 495 nm. High resolution mass spectroscopy was collected on an Agilent Infinity 1260 LC and tandem Agilent 6230 high resolution time of flight (TOF) mass spectrometer managed by the UCSD Department of Chemistry and Biochemistry Molecular Mass Spectroscopy Facility.

Confocal fluorescence microscopy imaging was performed on an Axio Observer Z1 motorized inverted microscope (Carl Zeiss Microscopy GmbH, Germany) with Yokogawa CSU-X1 spinning disk confocal unit to and an Evolve 512x512 EMCCD camera (Photometrics, Canada) using ZEN imaging software (Carl Zeiss Microscopy GmbH, Germany). Fluorophores were excited with laser diodes (488 nm; 30 mW). Epifluorescence microscopy imaging for coculture experiments was performed on an Axio Observer D1 inverted microscope (Carl Zeiss Microscopy, GmbH, Germany) with an Axiocam MRm camera (Carl Zeiss, Microscopy, GmbH, Germany) and an HBO-100 mercury arc lamp epifluorescence source (Carl Zeiss Microscopy, GmbH, Germany). A 49008 ET mCH/TR filter cube (Chroma Technology Group, Bellows Falls, VT) and 38 HE filter cube (Carl Zeiss Microscopy, GmbH, Germany) were used for imaging of fluorophores. Images were processed using Image J[65] with Fiji.[66] Microscopy images shown in a given figure are window-leveled in the same manner as one another.

2.5.2 Synthesis of N-succinimidyl ferulate (NHS-FA)

FA **NHS-FA**

Scheme 2.2: Synthesis of N-succinimidyl ferulate

250 mg of ferulic acid (1.27 mmol, 1 eq.) and 146 mg (1.26 mmol, 1 eq.) of NHS were dissolved in 5 mL tetrahydrofuran. This solution was chilled over ice and 1.91 mL (1.91 mmol, 1.5 eq.) of 1 M dicyclohexyl carbodiimide (DCC) was added to the reaction. The reaction was monitored with TLC (1:1 hexane:ethyl acetate). After 24 hours, the reaction filtered over a medium frit and rotary evaporated to dryness. The residue was suspended in methylene chloride causing formation of a white precipitate. The solution was filtered through a short plug of silica and purified by column chromatography (1:1 hexane:ethyl acetate).

2.5.3 Synthesis of AlexaFluor 488-cadaverine-ferulate (AF488-FA)

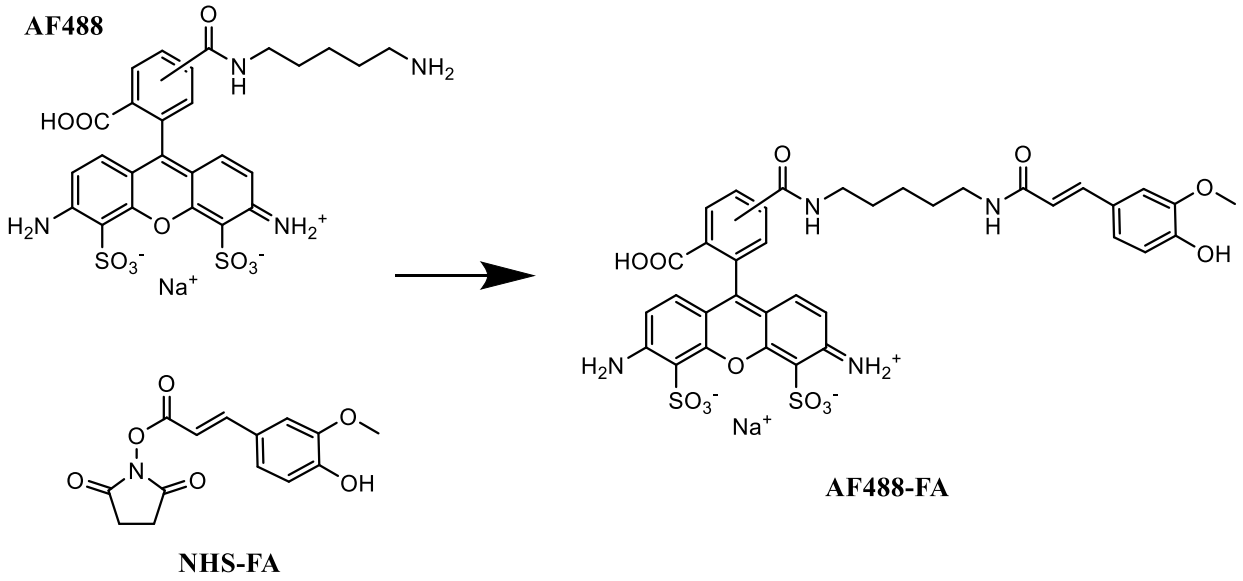

Scheme 2.3: Synthesis of AlexaFluor 488-cadaverine-ferulate (AF488-FA)

Solutions of AlexaFluor 488-cadaverine and NHS-FA in DMF were prepared at 2.0 mg/mL and 1.0 mg/mL, respectively. 100 µL (0.31 µmol) of the AlexaFluor 488 cadaverine solution, 180 µL (0.65 µmol, ~2 eq.) of the NHS-FA solution, and 8 µL (0.046 µmol, 0.15 eq.) of diisopropylethylamine were combined and incubated at 45 °C for 8 hours while shaking. The solution was concentrated in vacuo, dissolved in acetonitrile, and purified by HPLC. Recovered yield: 0.13 mg (53%) as determined by UV-Vis spectroscopy. HRMS (ESI-TOF) calculated for $[C_{36}H_{33}N_4O_{13}S_2]^-$ ($[M]^-$) 793.1491, found 793.1484 (Figure 2.4)

Table 2.1: HPLC gradient conditions for purification of A488-FA

Time[a]	Water + 0.1% TFA	Acetonitrile + 0.1% TFA
0 min	95%	5%
5 min	80%	20%
12 min	70%	30%
15 min	70%	30%

[a] The product eluted at approximately 12-12.4 min.

2.5.4 High-Resolution Time-of-Flight Mass Spectrometry of AF488-FA

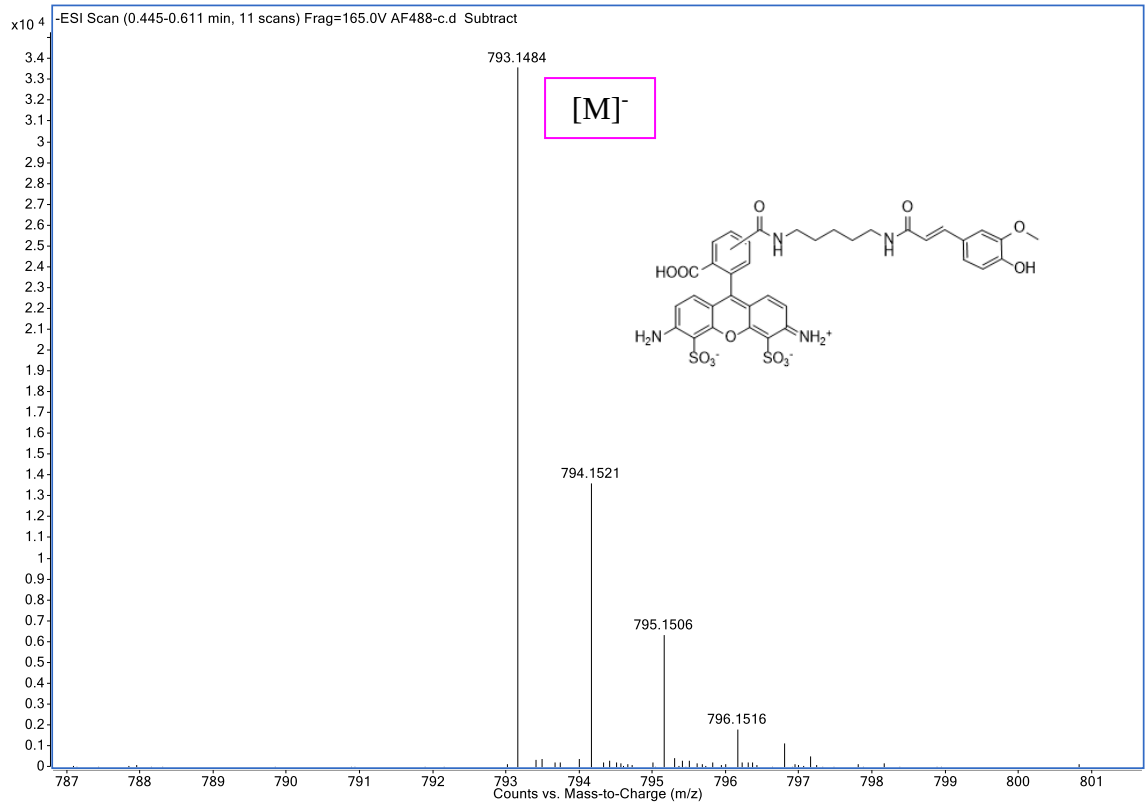

Figure 2.4: HRMS spectrum of AF488-FA

Table 2.2: HRMS results data for AF488-FA

Mass Measured	Theoretical Mass	Delta (ppm)	Composition
793.1484	793.1491	-0.9	$[C36H33N4O13S2]^-$

2.5.5 Laccase Resuspension

Laccase was brought into solution prior to modification and conjugation. To suspend, laccase was triturated with warm (~37 °C) buffer (typically pH 7.0 150 mM sodium phosphate buffer) in a Dounce homogenizer. Buffer was added in small portions and removed, being careful to not pipet any enzyme powder that remains undissolved. This was continued until all buffer had been thoroughly triturated with the enzyme. The resulting suspensions were dark and turbid with

some visible sediment. These were incubated at 37 °C for 1 hour with gentle shaking. After incubating, the samples were centrifuged at 5,000 rcf for 5 minutes. The supernatant was syringe filtered with a 0.22 micron filter to remove large particles. The resulting transparent, light brown/yellow solution was concentrated with a centrifuge filter (e.g. Amicon Ultra 10 kDa or similar) to produce a dark yellow-brown solution that lacked turbidity. This solution was stable for 1 month at 4 °C without significant loss of activity.

Protein concentration of these solutions were determined with BCA assay and enzymatic activity was determined with a syringaldazine assay.

2.5.6 Syringaldazine Laccase Activity Assay

A 0.216 mM solution of syringaldazine was prepared in methanol. Laccase was suspended in an appropriate buffer at the desired pH. 2.2 mL of buffer and 0.5 mL of laccase solution were added to a UV-Vis cuvette with a stir bar and the solution was allowed to reach 37 °C in a UV-Vis spectrometer. Upon equilibration, 0.3 mL of the 0.216 mM syringaldazine solution (pre-warmed to 37 °C) was added and A530 was measured every 5 seconds for 10 minutes. From the linear portion of the resulting graph, units of laccase activity was calculated as follows:

$$\frac{Units}{mL}\ enzyme = \frac{\Delta A_{530}}{0.001\ \times\ 0.5\ mL}$$

Figure 2.5: Equation for determining laccase activity

This same protocol can be adapted to a microscale format where measurements of 2 microliter samples are taken at longer time intervals on the pedestal of the Nandrop instead of in a cuvette. The above equation can be used slight alteration. Care should be taken to use 1 cm absorbance measurements instead of 1 mm absorbance measurements in this case.

2.5.7 Kinetic data of T. versicolor and T. vernicifluum

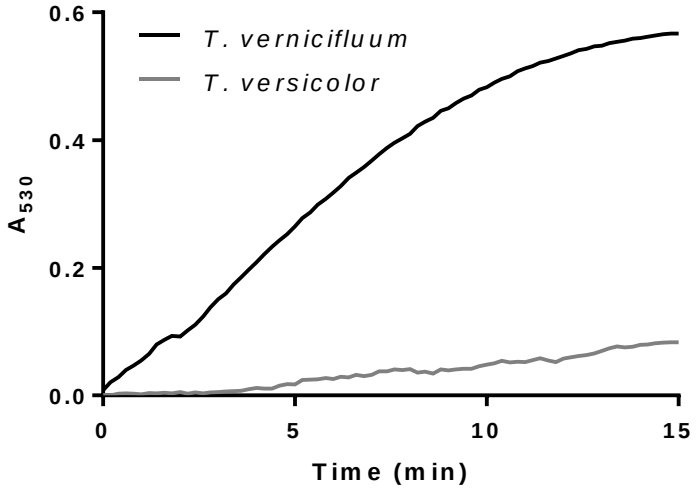

Figure 2.6: Representative kinetic curves of *T. vernicifluum* and *T. versicolor* at final concentration of 0.0167 mg/mL in 3 mL pH 7.0 150 mM sodium phosphate buffer with 10% MeOH, and 0.0216 mM syringaldazine at 37 °C.

If too many units of laccase are added to this assay, the absorbance from the colored product will begin to disappear over the observation scale of a kinetics experiment as the product is likely further oxidized. In this case, the amount of enzyme added to the assay and it should be decreased and the assay repeated.

2.5.8 Non-targeted BSA Labeling Assay

Variable enzyme concentration experimental conditions: Incubation conditions: pH 7.0 phosphate buffer, 37 °C, 90 min, 19.5 µM AF488-FA, 0.5% (w/v) BSA. The sample was then concentrated and subsequently washed in a 30k MWCO spin filter with: 1 × 8M urea, 1 × 50%(v/v) EtOH in pH 7.0 phosphate buffer, 5 × pH 7.0 phosphate buffer. Concentration of bound and unbound AF488-FA was determined spectrophotometrically using UV-Vis.

Variable BSA experimental conditions: Same as above but a fixed concentration of enzyme at 0.1 mg/mL final concentration.

2.5.9 Protein-Protein Conjugation

A slightly modified version of the SoluLink protein conjugation protocol was followed. In brief: The proteins to be modified were suspended/buffer exchanged into 250 mM sodium phosphate pH 8.0 and protein concentration was determined with BCA assay. The protein was concentrated to a >2 mg/mL for optimal reaction. The manufacturer-provided protein-conjugation excel spreadsheet was used to determine the amount of the S-4FB and S-HyNic reagents to add using a 10x excess of the succinimidyl ester. S-HyNic was reacted with laccase and S-4FB was reacted with streptavidin. They were incubated for 4 hours.

After reaction, the proteins were desalted using a buffer exchange column into pH 6 150 mM sodium phosphate. Protein concentration was determined using BCA assay and degree of modification was assessed by UV-Vis (as per manufacturer instructions). Modified laccase and streptavidin were combined at a 1:2 ratio and incubated at room temperature overnight. It is critical to not add the TurboLink catalyst. This catalyst is aniline based and will act as a substrate to laccase under the reaction conditions causing formation of a dark polymeric precipitate.

Resulting product was subjected to spin filtration with a 100kD MWCO to eliminate unconjugated laccase. UV-Vis was used to estimate degree of labeling of the proteins. Protein concentration was determined with BCA assay. Activity per mg of protein was determined with the syringaldazine laccase assay to further validate the degree of labeling determined by UV-Vis.

2.5.10 Cell Culture

A431, HEK293, and HEK293T cells (American Type Culture Collection), were cultured in DMEM with glutamine and pyruvate (GIBCO Thermo Fisher, Waltham, MA) 10% FBS (Corning, Corning, NY). Cells were detached for passaging using TrypLE Express (Thermo

Fisher, Waltham, MA). LabTekII 8-well chamber slides were purchased from Nunc (Thermo Fisher, Waltham, MA).

2.5.11 Lentiviral Production and Transduction

HIV1-based lentivirus vectors were produced by transient co-transfection of HEK293T cells. HEK293T cells in ten 150 mm dishes were co-transfected by polyethyleneimine (PEI) method with pHR_Gal4UAS_tBFP_PGK_mCherry, pLP1 (gal-pol), pLP2 (rev), and pCMV-G1. 12 μg of pHR_Gal4UAS-tBFP_PGK_mCherry, 12 μg pLP1, 10 μg pLP2, 6 μg pCMV-G, and 90 μg PEI were used per 150 mm plate. Conditioned media at day 1, 2, and 3 post-transfection were collected, filtered through a 0.45 micron filter, and concentrated by centrifugation at 7000 rpm for 16 hours at 4 °C with a Sorvall GS-3 rotor. The resulting pellets were resuspended with buffer containing 10 mM Tris HCl, pH 7.8, 1 mM MgCl2, and 3% (w/v) sucrose.

HEK293 cells were transduced with the resulting lentivirus by adding 30 microliters of concentrated virus to the HEK293 cells that were grown in a single well of a 24-well plate with 1 mL of DMEM with 10% FBS. The medium was changed after 2 days. Fluorescence revealed mCherry expression was sufficient for co-culture experiments.

2.5.12 Live-Cell Microscopy Protocol

Cells were grown in 8 well chamber slides (Nunc LabTek II) to a desired confluency (~70-90%). Culture medium was removed carefully by gently aspirating it from the corner of a slide with a pipette while tilting the slide. Being gentle is important as to not disrupt the monolayer of cells. Cells were incubated with biotinylated anti-EGFR antibody at a concentration of 0.002 mg/mL in whole media (including FBS) at 4 °C for 30 min. Longer incubation times can be used to improve labeling, but the kinetics of EGFR receptor internalization do not allow for particularly long labeling times (e.g. overnight at 37 °C). The cells are then washed three times by gentling

rocking them in room temperature Ca- and Mg-free Hank's Balanced Salt Solution. The supernatant is aspirated and replaced with either streptavidin-AlexaFluor 488 (SA-488) or the laccase-streptavidin conjugate.

The laccase-streptavidin conjugate was added to each well to a final concentration of 0.002 mg/mL. SA-488 was added to a final concentration of 0.00084 mg/mL. This concentration corresponds to an equivalent concentration of streptavidin as the laccase-streptavidin. These were incubated at room temperature for 15 min and then the cells were washed as before. For SA-488-treated cells, the media was replaced with pH 7 phosphate buffer. For laccase-streptavidin treated cells, the media was replaced with AF488-FA at 19.5 μM in pH 7 phosphate buffer. The samples were then incubated for 30 min at 37 °C. They were then washed as above and pH 7.4 phosphate buffered saline was added. The cells were then promptly imaged.

For fluorescent labeling experiments with EGF-AF555, after labeling cells with laccase, cells are washed with ice cold PBS and 20 ng/ μL EGF-AF555 in cold 0.3% (w/v) BSA in DMEM and cells were incubated for 1hr at 4 °C. Cells were then incubated at 37 °C for 30 minutes to promote receptor endocytosis.

2.5.13 Microscopy of Laccase-Streptavidin with AF488-FA and Streptavidin-Alexa Fluor 488

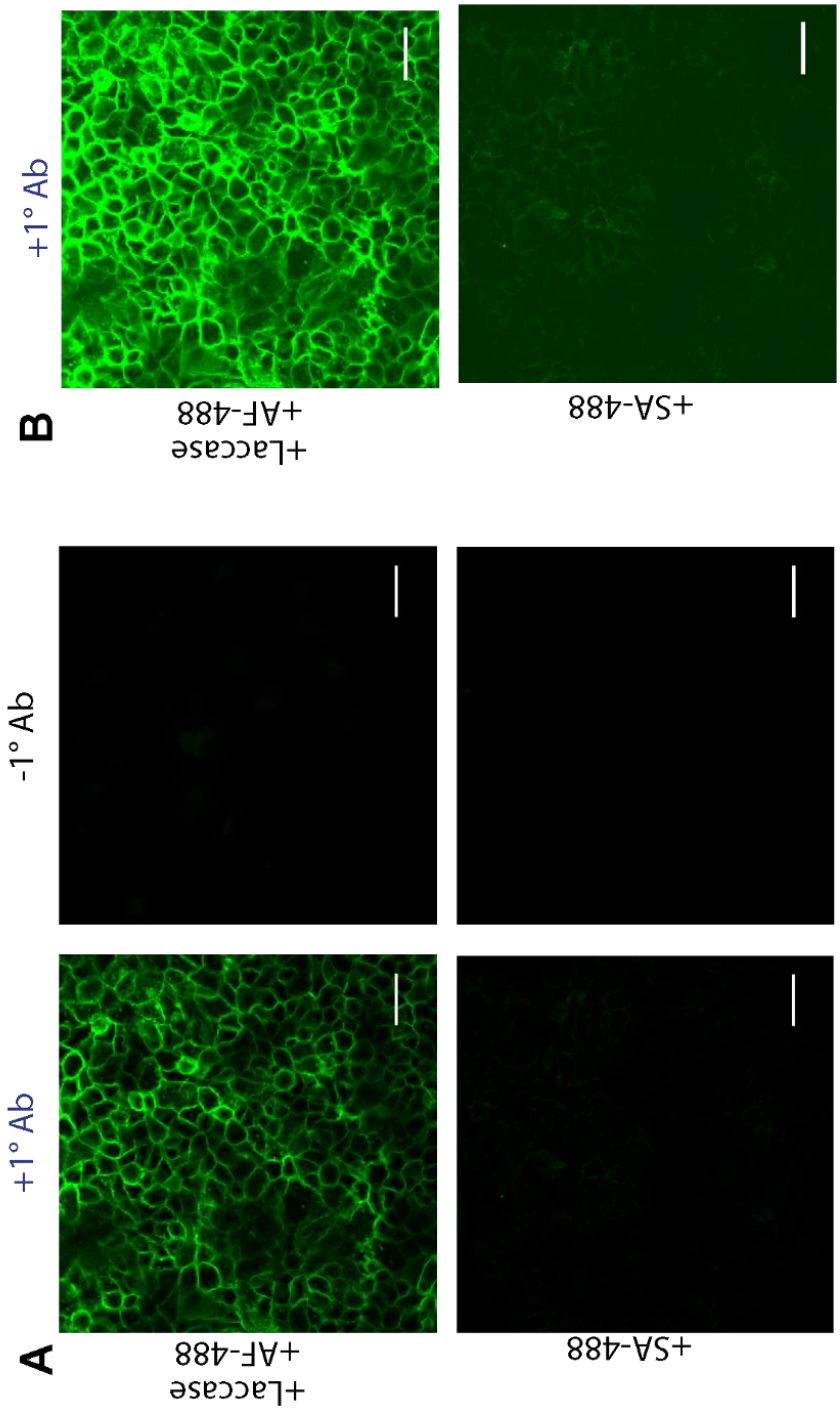

Figure 2.7: A) Fluorescence confocal microscopy images of signal amplification from probe deposition by laccase-streptavidin as compared to streptavidin-AlexaFluor 488. Images are taken under the same conditions and window-leveled identically. B) Images brightened to show similar pattern of fluorescence labeling for both SA-488-labeled and AF488-FA. Scale bar = 50 μm.

2.5.14 Plate reader assay of Laccase/AF-488 and SA-488 cells

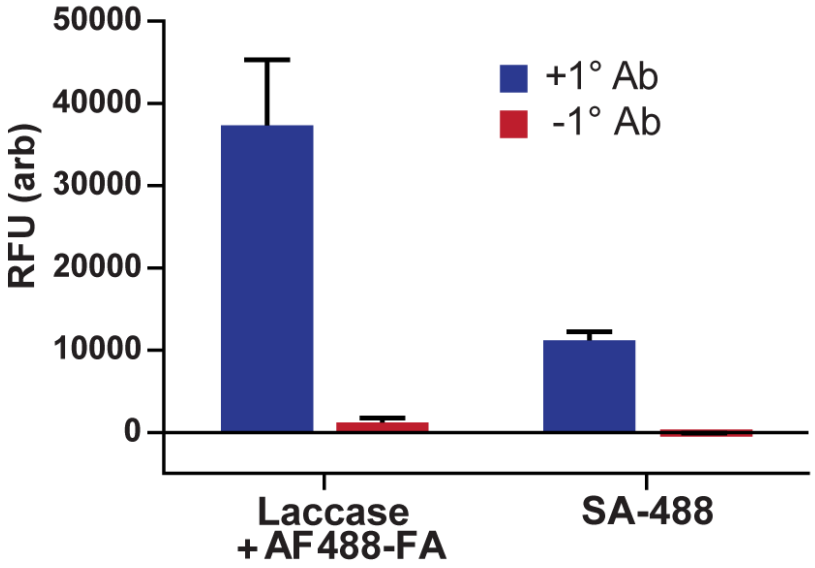

Figure 2.8: Bulk fluorescence measurements of cells obtained with a fluorescence plate reader, after being treated by the same method used for microscopy.

2.5.15 Representative Co-Culture Microscopy Images

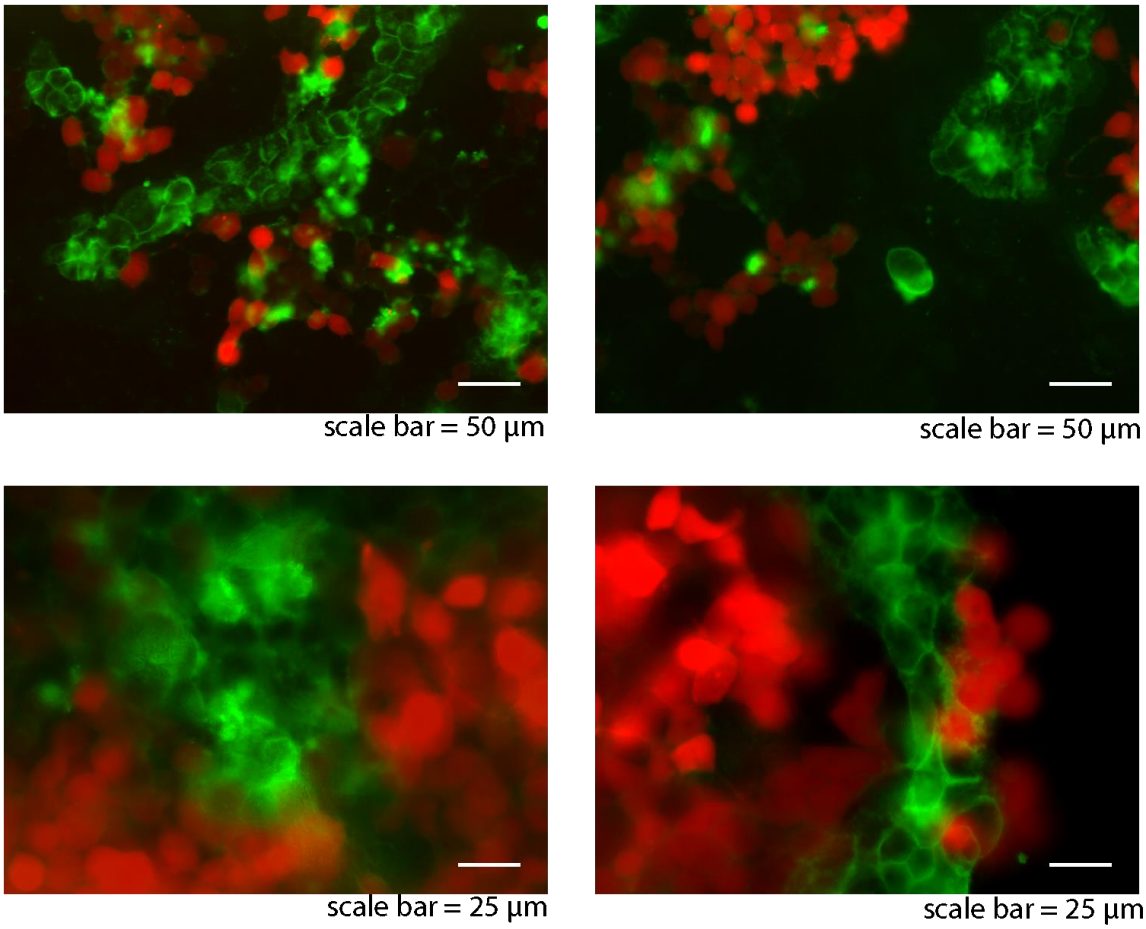

Figure 2.9: More example representative images of mCherry-expressing HEK293 (red) and AF488-FA labelled A431 cells (green). The top row of images are at 20x magnification and the lower row are at 40x magnification. All fluorescent images were acquired with epifluorescence microscopy.

2.5.16 Fluorescent Epidermal Growth Factor Internalization Microscopy Images

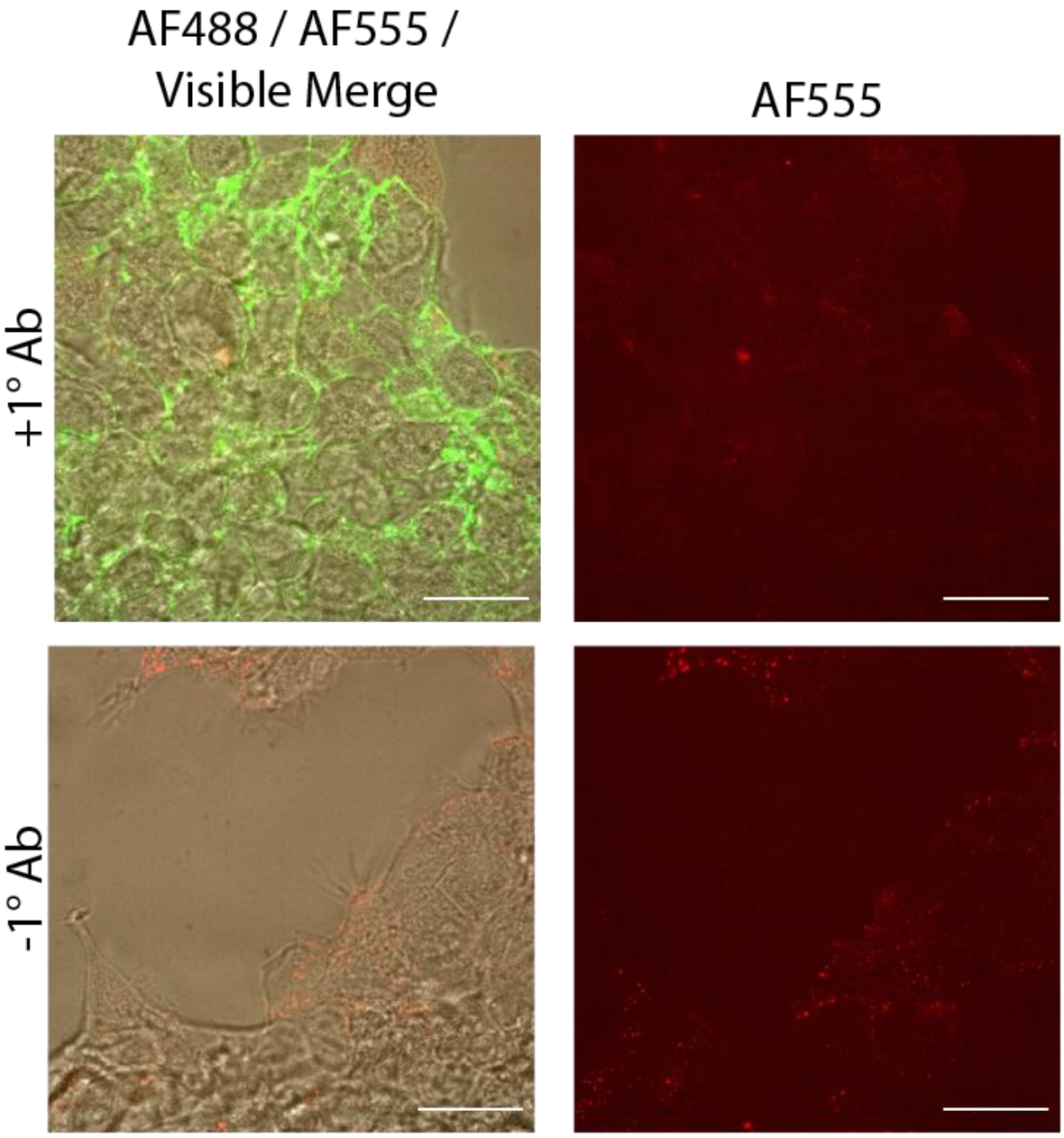

Figure 2.10: Confocal microscopy images of A431 cells treated with biotinylated anti-EGFR primary antibody followed sequentially by laccase-streptavidin, AF488-FA, and EGF-Alexa Fluor 555 conjugate. Cells were incubated for 30 minutes at 37 °C to elicit endocytosis. Control cells ("-1° Ab") were subjected to the same conditions but without the primary antibody. Scale bar = 25 μm. All microscopy images here are window-leveled identically.

Chapter two, in full, is a reprint (with co-author permission) of the material as it appears in the publication: Cisneros, B. T., Devaraj, N. K., Laccase-mediated catalyzed fluorescent reporter deposition for live cell imaging. ChemBioChem 2019, 20. I would like to thank Neal Devaraj for his scientific oversight and assistance in preparing the manuscript. The author of the dissertation is the primary author of this manuscript.

CHAPTER 3

3 Heterologous Expression of Methylxanthine Synthesis Enzymes in Mammalian Cells and Use as a Reporter Protein

3.1 Abstract

This work makes progress toward the development of methylxanthine synthesis enzymes as reporter enzymes that can produce a detectable small molecule output for use in mammalian cells. Previously, a variety of enzymes involved in caffeine synthesis (methylxanthine synthesis enzymes) from plants have been characterized *in vitro* and have been heterologously-expressed in yeast or bacteria. In this work, I heterologously express caffeine synthesis enzymes from tea, coffee, and guarana in human cells. I show that they have similar patterns of activity with a set of xanthine substrates in human cells as they do *in vitro*. I show the effect that several structural modifications have on the function of some of these enzymes. I demonstrate that the activity of these enzymes can be used as a reporter for juxtacrine cell-cell signaling by coupling the expression of methylxanthine synthesis enzymes to synNotch activation by surface-expressed GFP on adjacent cells.

3.2 Introduction

This project attempted to solve some of the problems faced when using laccase for amplified imaging. Although catalyzed reporter deposition using laccase can generate an amplified, detectable signal in response to a cell surface marker,[67] its ability to selectively deposit a probe is limited by the properties of the antibody used for targeting. For the *in vitro* and *in vivo* labeling of rare targets, background will contribute a disproportionate amount to the signal

observed.[68] Given that human immune cells can respond with sensitivity and specificity to their specific targets, I had the larger overall vision of using engineered cells, akin to those used in CAR-T immunotherapy for cancer, as a vector for a receptor-reporter system that could be used to detecting cell surface targets in a large animal target. Unfortunately, the most obvious reporter choices—luciferase and fluorescent proteins—are unsuitable for use in large animal models.[69,70] As such, I sought an enzymatic reporter capable of producing a small molecule that could be detectable in the blood or urine instead of a reporter that would generate light. This led me to the study of caffeine synthesis, as these small molecules were known to be non-toxic enough for humans to consume willingly.

3.3 Background

Xanthine is ubiquitous in life as a degradation product of the purine bases found in DNA. Xanthine has three nitrogen atoms that can be methylated (at positions 1, 3, and 7, respectively). As such, methylxanthines as a group (**Figure 3.1**) includes monomethylxanthines (1-methylxanthine, 3-methylxanthine, 7-methylxanthine), dimethylxanthines (1,3-dimethylxanthine, 1,7-dimethylxanthine, and 3,7-dimethylxanthine), and 1,3,7-trimethylxanthine. The methylated derivatives of xanthine are of significant human interest.

Several methylxanthines have notable pharmacologic properties that are of relevance to humans: theophylline, theobromine, and caffeine particularly. Theophylline and its derivatives are used in medicine often for their effects on the respiratory system or as stimulants.[71] Theobromine is a mild stimulant found in chocolate.[72] Caffeine is a stimulant drug and is by far the xanthine derivative of most interest to people. It is consumed by roughly 85% of Americans on a daily basis[73] and the cultivation of caffeine-containing plants is of immense economic value in the

present day and historically.[74] As summarized[75] by poet Dale Pendell: “Every office, large or small, has its shrine, however modest, to the coffee plant.”

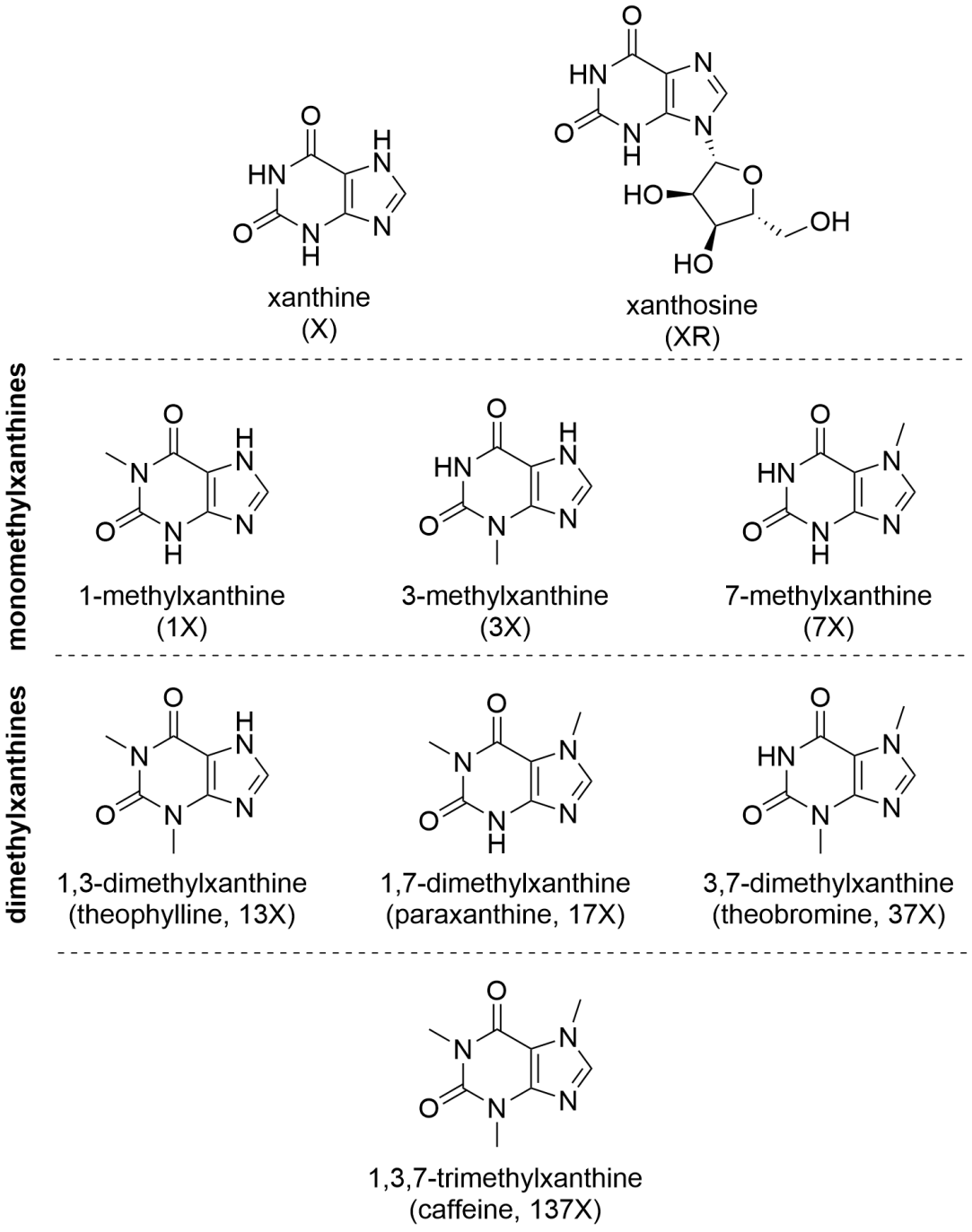

Figure 3.1: Structures of the xanthine derivatives pertinent to this research

A majority of caffeine consumed by people is derived from coffee (*Coffea spp.*, namely *Coffea arabica*) with most of the remainder coming from tea (*Camellia sinensis*), and a smaller contribution yet from other plants like guarana (*Paullinia cupana*) and yerba mate (*Ilex paraguariensis)*.[76] While humans have developed ethnobotanical relationships with these plants in the distant past, there are many other species that are not consumed for their pharmacological properties that produce caffeine and a menagerie of methylxanthines metabolites.

Despite being found in many plants, the species that produce caffeine prodigiously are not close relatives of one another.[77] Within those plants, enzymes performing different steps of the caffeine biosynthesis are more closely related than enzymes which perform the same step in different organisms.[78] This suggests that caffeine synthesis has arisen multiple times by way of convergent evolution by co-opting enzymes that carry out other functions in plants (e.g. production of odorants or hormones). Work in comparative genomics and evolutionary reconstruction of ancestral enzymes has produced strong evidence in support of this view.[78–81]

The study of enzymatic production of caffeine began with examinations of plant extracts to identify the location of purine alkaloids[82] followed by studies examining the various enzymatic transformations that plant extracts could perform.[83] Careful study of individual transformations led to the identification of the major enzymes and their genes in coffee, tea, and guarana.[84–90] More recently, genome sequencing data has become available and is being used to build a more thorough understanding of the enzymes involved in caffeine synthesis.[79–81,91–93] Because this work will not be focused on the nuances of caffeine production and regulation in plants, I will limit the discussion to the dominant enzymes in coffee, tea, and guarana (**Scheme 3.1** and **Scheme 3.2**).

In coffee, the dominant pathway involves conversion of xanthosine to 7X (I), 7X to 37X (II), and 37X to 137X (III). This is carried out by CaXMT1 (*Coffea arabica* xanthosine

methyltransferase 1, also known as CaXRS1), CaMXMT (*Coffea arabica* methylxanthine methyltransferase), and CaDXMT (*Coffea arabica* dimethylxanthine methyltransferase). Coffee additionally contains the multi-functional enzyme CCS1 (coffee caffeine synthase 1) which can perform carry out steps II and III, but this enzyme does not appear to be primarily responsible for caffeine production in coffee.[89] In tea, TCS2 (tea caffeine synthase 2) carries out step I and TCS1 (tea caffeine synthase 1) carries out steps II and III. In guarana, steps I-III are carried out by PcCS1 (*Paullinia cupana* caffeine synthase 1), PcCS2 (*Paullinia cupana* caffeine synthase 2), and PcCS (*Paullinia cupana* caffeine synthase), respectively.[78] All these methylating enzymes use S-adenosylmethionine (SAM) as a methyl donor.

	I	II	III
Camellia sinensis	TCS2	TCS1	TCS1
Coffea arabica	CaXMT1	CaMXMT	CaDXMT

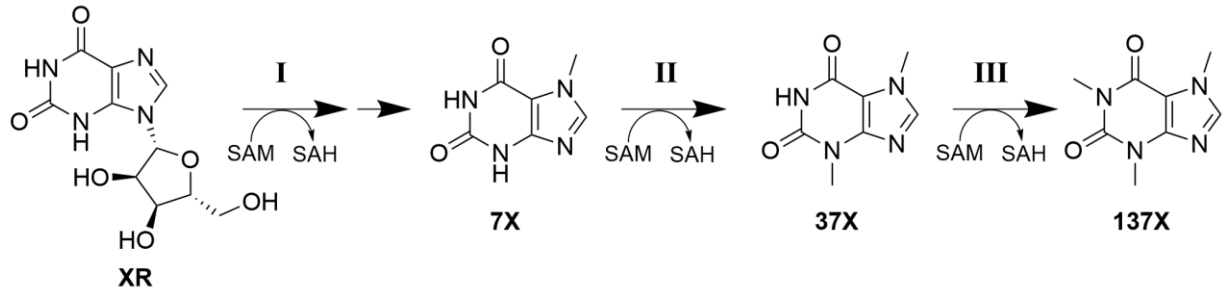

Scheme 3.1: Pathway for biosynthesis of caffeine in tea and coffee. The cleavage of ribose from 7-methylxanthosine after step I is not shown, as the mechanistic details are yet unknown.

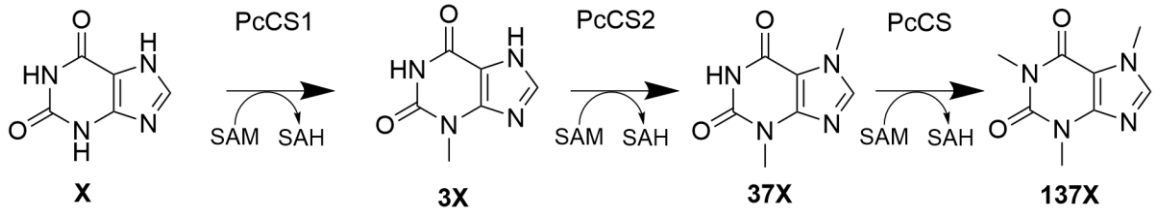

Scheme 3.2: Pathway for the biosynthesis of caffeine in guarana

After key enzymes and pathways were identified, researchers attempted to reconstitute caffeine synthesis pathways in *E. coli*[94,95] and *S. cerevisiae*.[95,96] Several of these attempts were successful at generating large quantities of caffeine from liquid cultures of bacteria or yeast using glucose as a starting material. The overall simplicity of the caffeine synthesis pathway and the successful reconstitution of it in other organisms suggested to me that it may be feasible to introduce this pathway to mammalian cells.

3.4 Heterologous Expression of Methylxanthine Synthesis Enzymes

I set out to determine if caffeine synthesis enzymes could be heterologously expressed in mammalian cells. Several methylxanthine synthesis enzymes from three plants were chosen to potentially express in mammalian cells: CaXMT1, CaMXMT, CaDXMT, CCS1 from *Coffea arabica;* TCS1 and TCS2 from *Camellia sinensis*; and PcCS from *Paullinia cupana.* In addition, I chose to express two putative ancestral enzymes CamelliaAncCS and PaulliniaAncCS2, hereafter referred to as CsAncCS and PcAncCS2, respectively. Previous work suggested that these two enzymes may possess the ability to produce some quantity of paraxanthine.[97] This activity has not been previously observed in any known xanthine methylating enzymes. The whole set enzymes chosen ought to cover a wide range of transformations in the pathways for methylating xanthines.

Table 3.1: Dominant methylation activity of natural xanthine methylating enzymes

Source	Enzyme	Dominant Reaction(s)			
		N-7 methylation	N-3 methylation		N-1 methylation
Coffea arabica	CaXMT1	XR → 7X	-	-	-
	CaMXMT	-	-	-	7X → 37X
	CaDXMT	-	-	37X → 137X	-
	CCS1	-	17X → 137X	37X → 137X	7X → 37X
Camellia sinensis	TCS2	XR → 7X	-	-	-
	TCS1	-	17X → 137X	37X → 137X	7X → 37X
Paullinia cupana	PcCS	-	-	37X → 137X	-

I then constructed expression vectors for each of the chosen enzymes. I chose to use pSBBi-RP and pSBBi-GB[98] as a basis for my vectors due to several advantages for future studies. The expression cassette within pSBBi vectors is part of a Sleeping Beauty transposon, allowing it to be stably integrated into the host cell's genome in the presence of Sleeping Beauty transposase.[99,100] The cassette encodes constitutive expression of a selectable antibiotic resistance gene and a fluorescent protein as well as a constitutive expression of a gene-of-interest. This allows for rapid generation of stable cell lines as well as the ability to include multiple, independent antibiotic selectable markers or fluorescent reporters in a single cell, if so desired.

I then produced stable cell lines expressing each of the xanthine methylating enzyme genes I had chosen to study. I transiently transfected human embryonic kidney cells, HEK-293T, with each plasmid and pSB100X[101] to stably integrate the specific methyltransferase gene into the cells' genomes. I then performed an antibiotic selection using puromycin or blasticidin (for pSBBi-RP and pSBBi-GB plasmid variants, respectively). All enzymes were inserted into the pSBBi-RP backbone except for CaXMT1 and TCS2 which were inserted into pSBBi-GB. This was done to enable more facile co-expression and orthogonal selection for future researchers. All cells produced showed strong and stable integration of the transposon as observed by fluorescence microscopy. Pellets of the transduced cells were visibly tinted from the fluorescent reporter protein as well. Doubling time slightly slowed across all transduced lines, but cell morphology remained unchanged. Because all of these enzymes were expressed in HEK-293T cells, cells will be referred to simply by the enzyme name, e.g. CCS1 cells.

3.5 Xanthine Methyltransferases Are Functional in Mammalian Cells

With cell lines successfully expressing my chosen xanthine methylating enzymes, I then set out to determine if these enzymes were active in human cells and if their observed

methyltransferase activities were consistent with those observed *in vitro* for these enzymes. To do this, I grew cells in 12-well plates and exposed them to a fixed concentration (200 µM) of each of the following substrates: xanthine (X), 1-methylxanthine (1X), 3-methylxanthine (3X), 7-methylxanthine (7X), 1,3-dimethylxanthine (13X, theophylline, or TPH), 1,7-dimethylxanthine (17X, paraxanthine, or PX), 3,7-dimethylxanthine (37X, theobromine, or TBR), and xanthosine (XR) (for enzymes with expected activity against this substrate). After 72 h of growth, the supernatant was harvested and analyzed by high performance liquid chromatography.

Table 3.2: Expected Methylation of Xanthine Substrates by Methyltransferase Enzymes

	1-N Methylation				**3-N Methylation**				**7-N Methylation**			
Substrate	X	3X	7X	37X (TB)	X	1X	7X	17X (PX)	XR	1X	3X	13X (TP)
CaXMT1[86]									+			
CaMXMT[86,102]							+	+				
CaDXMT[86]				+			+	+				
CCS1[89]		+		+		+	+	+				
TCS2[78]	+	+	+					+	+	+	+	+
TCS1[84]		+		+	+	+	+	+				+
PcCS[85]				+			+					
CsAncCS[97]	+		+		+		+					
PcAncCS2[97]			+		+		+				+	
Product	1X	13X (TP)	17X (PX)	137X (CAF)	3X	13X (TP)	37X (TB)	137X (CAF)	7X	17X (PX)	37X (TB)	137X (CAF)

Table 3.3: Observed Methylation of Xanthine Substrates by Methyltransferase Enzymes. "+" indicates observed activity, "-" indicates unobserved activity, "tr." indicates trace activity, filled dark grey squares indicate tests were not performed, and boxed squares indicate a discrepancy with previous reports.

	1-N Methylation				**3-N Methylation**				**7-N Methylation**			
Substrate	X	3X	7X	37X (TB)	X	1X	7X	17X (PX)	XR	1X	3X	13X (TP)
CaXMT1	-	-	-	-	-	-	-	-	+	-	-	-
CaMXMT							+					
CaDXMT	-	-	-	+	-	-	+	+	-	-	-	-
CCS1	-	+	-	+	-	+	+	+	-	-	-	-
TCS2	-	-	-	-	-	-	-	tr.	+	-	tr.	-
TCS1	-	+	-	+	+	+	+	+	-	-	tr.	+
PcCS	-	-	-	-	-	-	-	-	-	-	-	-
CsAncCS	+	tr.	tr.	-	+	-	+	-	-	-	-	-
PcAncCS2	tr.	-	tr.	-	+	-	+	-	-	-	+	-
Product	1X	13X (TP)	17X (PX)	137X (CAF)	3X	13X (TP)	37X (TB)	137X (CAF)	7X	17X (PX)	37X (TB)	137X CAF

The activity for each enzyme to the given substrates consistent with previous reports in the literature. Several reported activities for various substrates were not observed likely due to the low reported activity with the enzyme for those substrates (e.g. TCS2 with many substrates). However, several activities were observed which had not previously been reported. Trace formation of 37X from 3X was observed with TCS1, trace formation of 1X from X was observed with PcAncCS2, and trace formation of 13X was observed from 3X with CsAncCS. Extracted ion intensity from mass spectrometry was too low to definitively verify the formation of these products, but the reliable appearance of these peaks with retention times that match other known methylxanthines is certainly suggestive. Representative chromatograms showing separation of the various xanthine derivative peaks are shown in **Figure 3.2**.

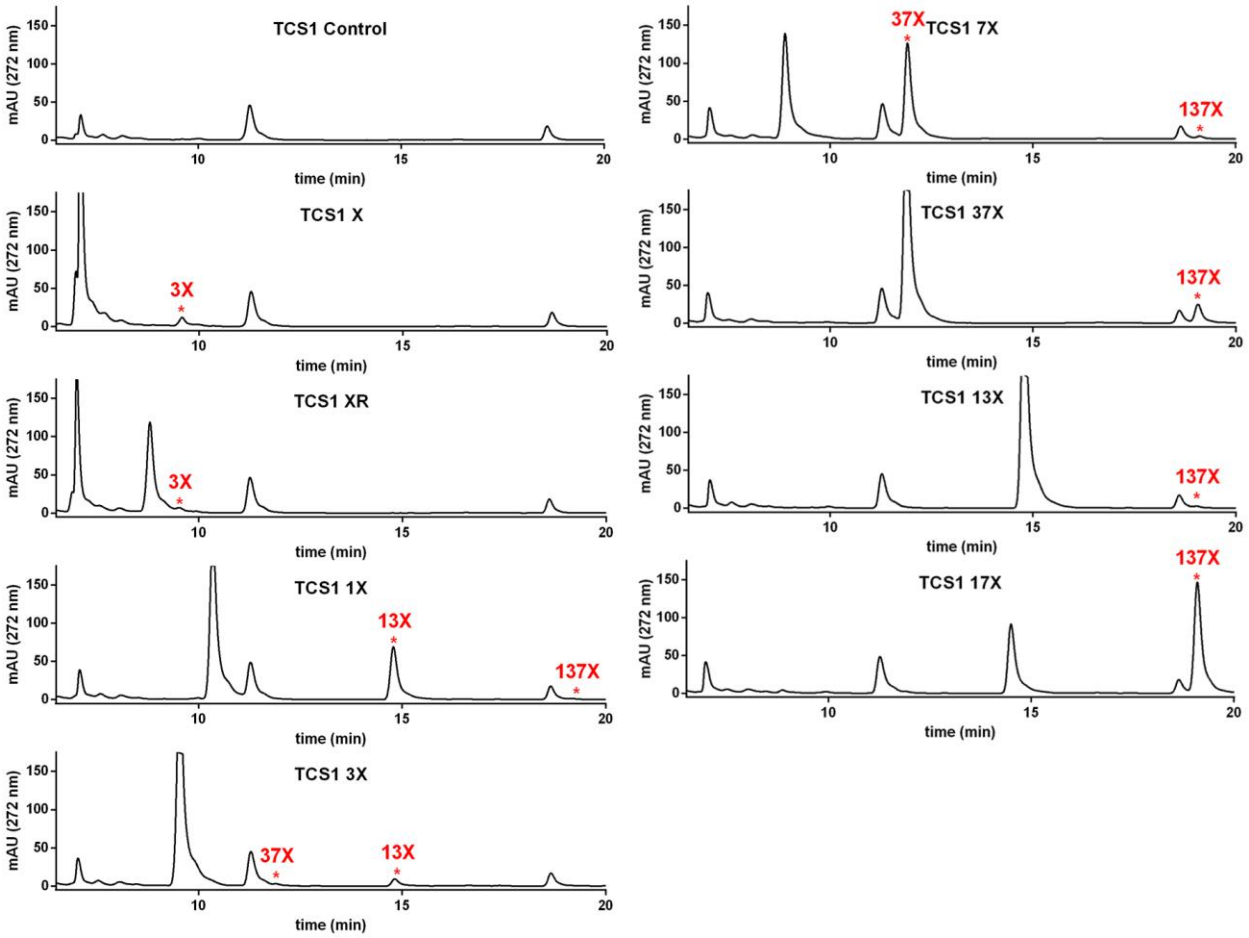

Figure 3.2: Representative chromatograms of TCS1 cells with various xanthine derivatives. Product peaks are shown in red with an asterisk.

3.5.1 Production of 7-Methylxanthine From Xanthosine by TCS2 and CaXMT1 Can Be Verified by Reconstituting Caffeine Synthesis Pathways

As shown above (**Figure 3.2**), when XR was supplied as a substrate multiple peaks are produced even though TCS1 is not known to cannot act on xanthosine. The low retention time peak in the XR chromatogram appears to consist, at least in part, of xanthine. This is evidenced by the presence of a small amount of the same product being formed from xanthosine as is formed from xanthine, i.e. 3X is found as a product in X and XR chromatograms for TCS1. This is

consistent with xanthosine being degraded to xanthine as part of normal purine degradation pathways.[103]

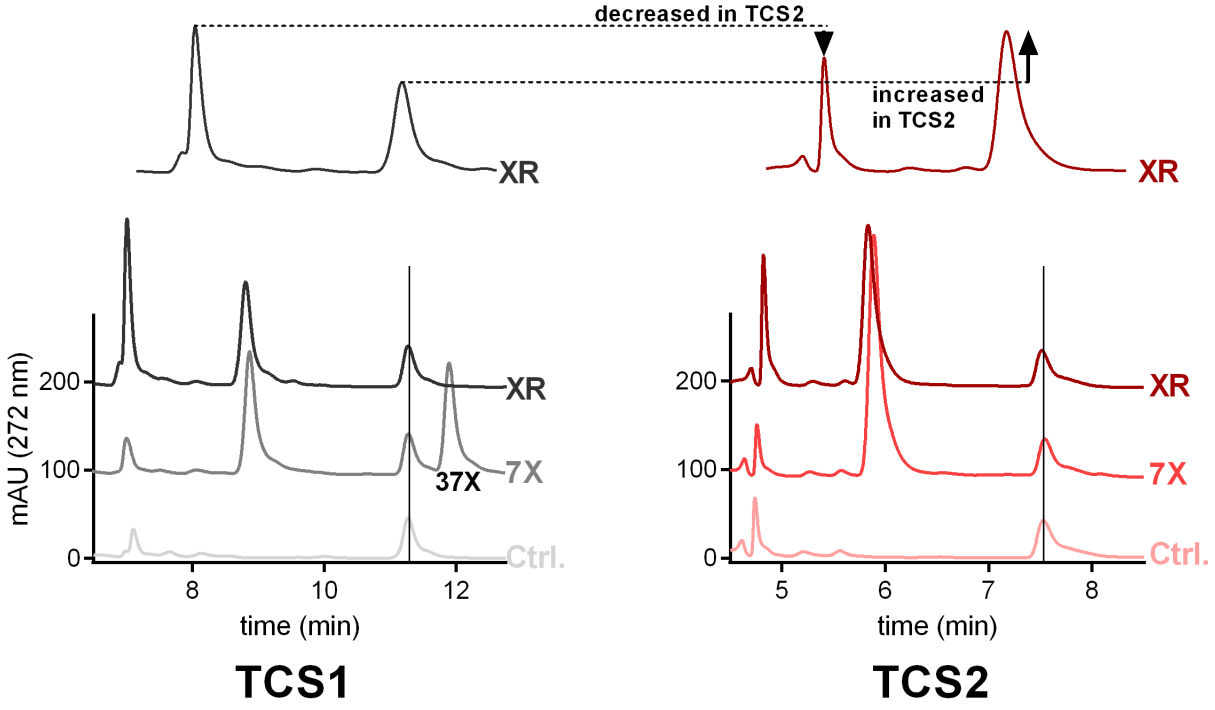

Figure 3.3: Comparison of product peaks for TCS1 and TCS2 cells for control, 7X, and XR substrates demonstrating difficulty of demonstrating 7X production of TCS2 with XR. Chromatograms were aligned to a background peak found in all conditions. Differences in elution time result from differences in column condition when samples were analyzed. 37X is not produced in TCS1 despite presence of peak with nearly identical retention time as 7X. Relative peak abundances for the two peaks differs between TCS1 and TCS2.

Unfortunately, the other peak present when XR is used as a substrate has a nearly identical retention time to the 7X. As such, the presence (and integrated intensity) of the 7X product peak could not be used to definitively show that TCS2 and CaXMT1 definitively synthesize 7X from XR in mammalian cells. It was evident that this peak did not contain 7X in enzymes which did not methylate XR, such as TCS1. TCS1 is highly active toward 7-methylxanthine and yet no theobromine was produced from XR whereas a similarly sized peak of 7X causes formation of large quantities of theobromine.

To verify that this peak contained 7X for CaXMT1 and TCS2, I decided to use other caffeine synthesis enzymes to convert any 7X present into products that could be clearly identified.

I conducted experiments with three conditions: CCS1 cells alone, CaXMT1/TCS2 cells alone, and co-cultured CCS1 cells with CaXMT1/TCS2 cells. All three conditions were cultured in 400 µM XR and harvested after 72 h. As shown in **Figure 3.4** and **Figure 3.5**, CCS1 cells alone with XR produced a single peak in the chromatogram. TCS2 cells produce the same peak which overlaps with a 7X peak. When TCS2 and CCS1 were co-cultured, however, the intensity of the 7X peak decreased and the presence of a 37X peak appeared. This was confirmed by comparison to authentic theobromine. The same scenario was true for CaXMT1. As such, this demonstrated that CaXMT1 and TCS2 definitively produced 7-methylxanthine from xanthosine in mammalian cells.

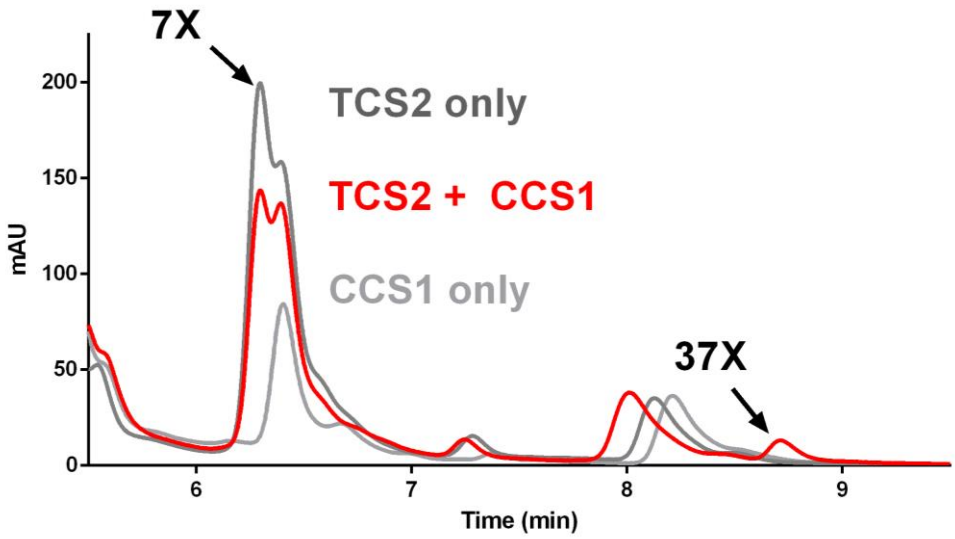

Figure 3.4: Overlaid chromatograms for HPLC of TCS2 cells, CCS1 cells, and TCS2 cells + CCS1 cells grown in 400 µM XR for 72 h.

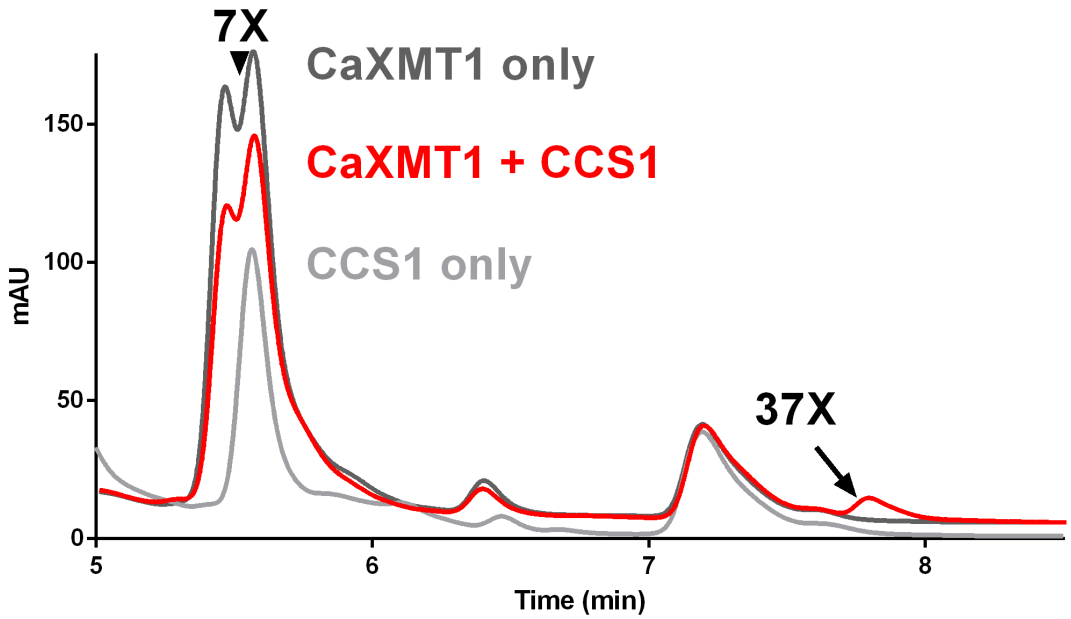

Figure 3.5: Overlaid chromatograms for HPLC of CaXMT1 cells, CCS1 cells, and TCS2 cells + CCS1 cells grown in 400 µM XR for 72 h.

3.5.2 Endogenous Xanthine Can Be Used for Production of Methylxanthines

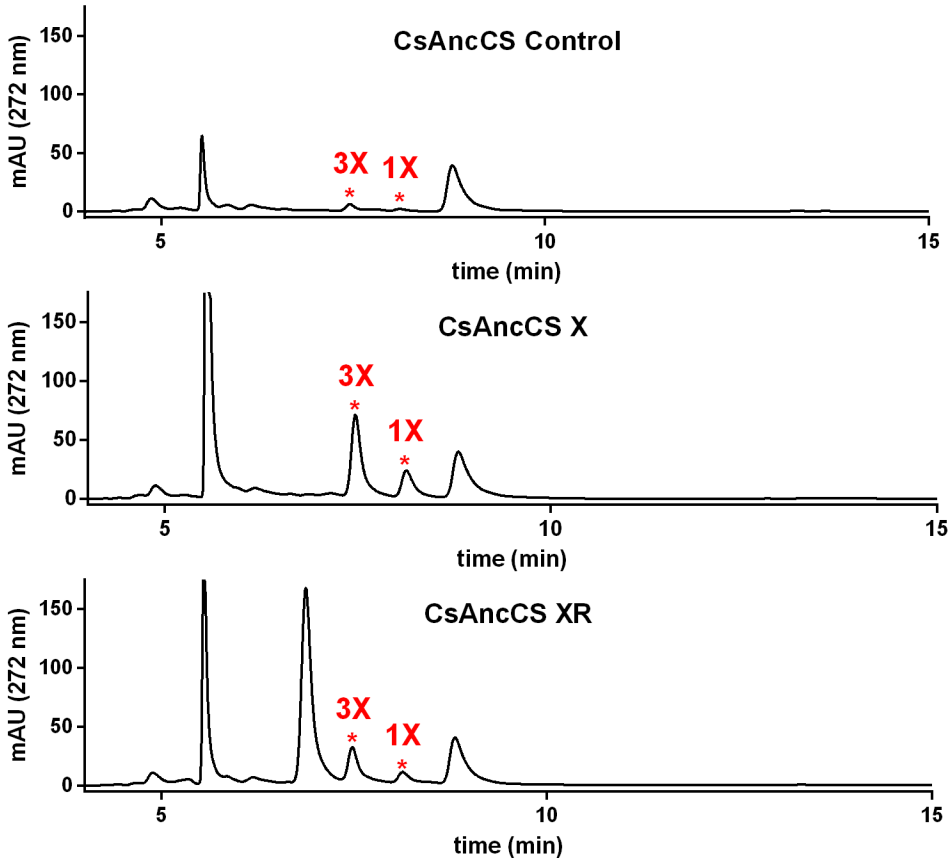

Figure 3.6: Control, X, and XR chromatograms for CsAncCS. Product peaks are colored red and marked with an asterisk.

CsAncCS cells were particularly active against the substrate xanthine and produced 1X and 3X in large quantity (Figure 3.6). As with other xanthine-modifying enzymes, use of XR as a substrate provides the same products as X but with lower yields. Of particular interest in this example is the presence of 3X and 1X in the control sample in small but detectable quantities. Indeed, 1X and 3X can be found in the other chromatograms for CsAncCS with different substrates (refer to **Supplemental Data**) This suggests that CsAncCS has a low enough K_m for xanthine that it can produce methylated products it in a detectable yield with only intracellular xanthine pools as a substrate. It also demonstrates the plausibility of completely *de novo* caffeine synthesis in

mammalian cells, as conceivably these products could be successively methylated to become caffeine.

3.5.3 Highly Active Enzymes Slow Cell Growth in the Presence of Preferred Substrates

Upon harvesting the cell media, I had observed that the phenol red indicator in the medium was noticeably pinker (thus more basic) in some of the wells in some plates. Microscopy showed that there were fewer cells in these wells indicating that cell growth was slower, but cell growth was not similarly diminished for cells grown in 200 μM caffeine. This effect was therefore not caused by some toxic effect of the caffeine being produced. The substrates that slowed cell growth varied from cell line to cell line, and the degree to which it inhibited cell growth varied too. Comparing the HPLC results with these patterns revealed that cell growth was slowed when the enzyme expressed was highly active with a substrate, e.g. CCS1 cells showed slowed growth when exposed to paraxanthine, with which it is highly active.

The methylation of xanthine substrates by the methylxanthine synthesis enzymes requires S-adenosylmethionine (SAM). SAM is the primary methyl donor in cells and is essential for the synthesis of polyamines, glutathione,[104] and phosphatidylethanolamines.[105] Through many direct and indirect mechanisms, SAM can regulate cell proliferation in a cell-type specific manner.[104,106,107] CCS1 cells in 300 μM paraxanthine were cultured with and without supplemental 300 μM SAM. At 72 hours, I qualitatively evaluated the cells via light microscopy and did not observe any difference in how much either group had proliferated. Samples of the cell medium were analyzed by HPLC and the concentration of caffeine produced in each was determined. The medium was found to contain 104.0 μM caffeine for CCS1 cells without supplemental SAM and only 46.8 μM caffeine for CCS1 cells with supplemental SAM. This showed that even if SAM

depletion caused hindered proliferation, this concentration of supplemental SAM is not effective in increasing proliferation and in fact causes decreased production of caffeine.

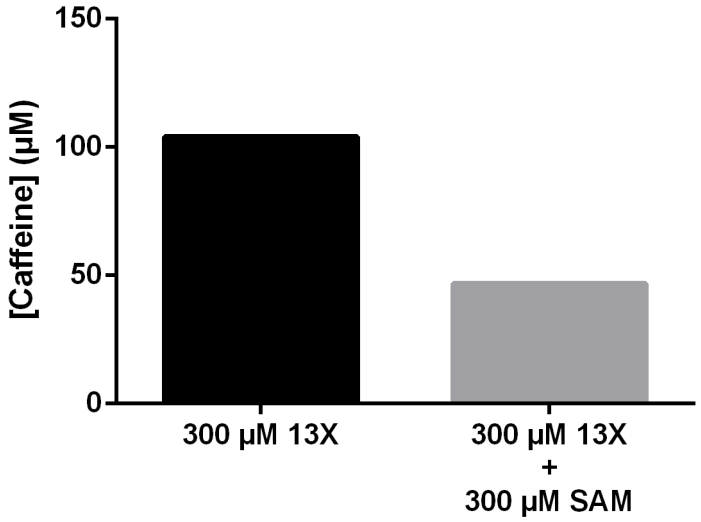

Figure 3.7: Effect of supplemental SAM on caffeine synthesis in CCS1 cells. Decreased caffeine concentration is observed after 72h of incubation when cells are grown with 300 µM SAM compared to cells grown without it.

One plausible explanation for this observed effect is a combination of inhibition by S-adenosylhomocysteine (SAH) and the insufficiency of SAM regeneration pathways. SAH binds to most methyltransferases with higher affinity than SAM,[77,108] a fact noted as a possible explanation for discrepancies in reported *in vitro* K_m values for enzymes.[109] If SAM is being depleted within a cell (i.e. the balance between SAM and SAH is not correct) this indicates that the throughput for the SAH recycling pathway is not sufficient to replenish the SAM that is being consumed. Supplying excess SAM would not increase methyltransferase activity, as SAH would continue to build up and further competitively inhibit the SAM binding sites in methyltransferase enzymes. Future attempts at maximizing methylxanthine synthesis in mammalian cells should consider modifications to the pathways for recycling SAH or supplementation with other small molecules that would increase efficiency of SAH recycling.

3.6 Effect of N-terminal Glutathione Transferase Fusion on CCS1 and TCS1 Activity

In previous work, fusion proteins of caffeine synthesis pathway enzymes and glutathione transferase (GST) or thioredoxin (Trx) have been made and studied.[89] These types of protein fusions are often made to improve the stability of the expressed protein, increase protein yield/solubility, or be used as an affinity tag for purification (for GST).[110] It is notable that the isolated protein from these experiments had improved K_m compared to the native protein. Native CCS1 had a K_m value of 125.6 μM whereas the Trx-fusion had a K_m value of 75.1 μM.[89] Native CaMXMT had a K_m value of 873 μM whereas the GST-fusion had a K_m value of 50 μM.[89,102] One possible explanation is that the improved activity of the fusion protein relative to the native protein was due to improved stability of the fusion protein during the purification process.[87] However, the redox activity of Trx or dimerization of GST could conceivably contribute to altered enzymatic activity.

The strong dimerization of GST was of interest as previous studies of CaXMT, CaMXMT, and CaDXMT have demonstrated that these enzymes all form homodimers and heterodimers readily.[111] Many enzymes[112] are known to have enhanced activity or show activity only when dimerized such as caspase-9[113] and guanylate cyclase.[114] No studies have been done which examine the effects of enhancing or inhibiting the ability for caffeine synthases to dimerize. As such, I decided to make plasmids encoding GST fusions of CCS1 and TCS1 and transformed cells with these to determine if this modification has any effect in mammalian cells.

I prepared the N-terminal GST fusion plasmids, transduced HEK-293T cell lines, and selected them as before. The N-GST fusions and wild type enzymes cell lines were plated, grown in and media was harvested at 72h. Even though selection conditions are identical, the non-deterministic nature of the transduction and selection process can generate cell populations that do

not necessarily express equivalent amounts of protein. Direct comparisons of product yields cannot necessarily inform you about overall changes in enzyme activity. Both CCS1 and TCS1 have highest reaction velocity and lowest K_m with paraxanthine as a substrate. Since this will best approximate the maximal performance of the enzyme and this reaction velocity should be least affected by the concentration of substrate, the yield of caffeine or theobromine in the other compared reactions will be normalized to the yield of paraxanthine for the same enzyme.

Table 3.4: Effect of N-terminal GST fusion on Relative Product Yields for CCS1 and TCS1 in mammalian cells

Reaction	Product	Relative Yield†			
		CCS1	CCS-G	TCS1	TCS1-G
17X → 137X	137X	1.0	1.0	1.0	1.0
7X → 37X → 137X	37X	0.45	0.60	0.76	0.35
	137X	0.10	0.072	0.025	--
37X → 137X	137X	0.57	0.56	0.15	0.029

†Relative Yield = $Yield^{Product}/Yield^{17X \rightarrow 137X}$ for a given enzyme at [17X] = 200 µM

Table 3.5: Effect of N-terminal GST fusion on Methylation Equivalents Consumed for CCS1 and TCS1 in mammalian cells

Reaction	Relative Methylation Equivalents Consumed†			
	CCS1	CCS-G	TCS1	TCS1-G
17X → 137X	1.0	1.0	1.0	1.0
7X → 37X → 137X	0.55	0.67	0.79	0.35
37X → 137X	0.57	0.56	0.15	0.029

†Relative Methylation Equivalents Consumed = ($2xRel.\ Yield^{137X}$ + $Rel.\ Yield^{37X}$) for reaction with 7X. Otherwise, RMEC = Relative Yield

From these data, it is apparent that the N-terminal GST fusions of CCS1 had relatively little effect on its activity compared to CCS1. The improved relative yield with 7X is consistent of an improved K_m for 7X. However, the N-terminal GST fusion of TCS1 had notably worse relative activity with 7X and 37X as substrates. The substantially decreased relative yield of with 7X and 37X as substrates for TCS1-G suggests an increase of the K_m or a decrease in the maximum

reaction velocity. Without an absolute quantification of enzyme present and data about the growth rate of the cells in question, the specific changes to enzyme kinetics cannot be determined. Regardless, N-terminal GST fusions of TCS1 do not appear to have any advantages over their wild-type counterparts in mammalian cells. Any future studies on protein dimerization would need to consider the deleterious effects of protein fusion on the activity of the xanthine methylating enzymes.

3.7 Effect of CCS-CTS Deletion on CCS1 Activity

CaXMT1 and CCS1 share a high degree of sequence similarity (**Figure 3.7**), yet they have quite distinct methylation specificity. These enzymes show a high sequence similarity, yet CaXMT1 is capable of 7-N methylation whereas CCS1 is capable of 3-N and 1-N methylation. In their studies as to which residues contribute to 3-N methylation activity, Mizuno, et al. found that the deletion of a 13-amino acid motif from CCS1 had a pronounced change on its activity.[115] When compared to wild-type CCS1, the relative methylation activities (normalized to 7-methylxanthine) of CCS1-delC13 increased 3.5-fold for paraxanthine and 2.6-fold for theobromine. It is not clear whether this is caused by an increase in overall enzyme activity with paraxanthine and theobromine or simply a decrease in activity with 7-methylxanthine. Regardless, this work suggests seems as though the CCS-CTS extended region plays a role in making CCS1 more selective for methylxanthines over dimethylxanthines.

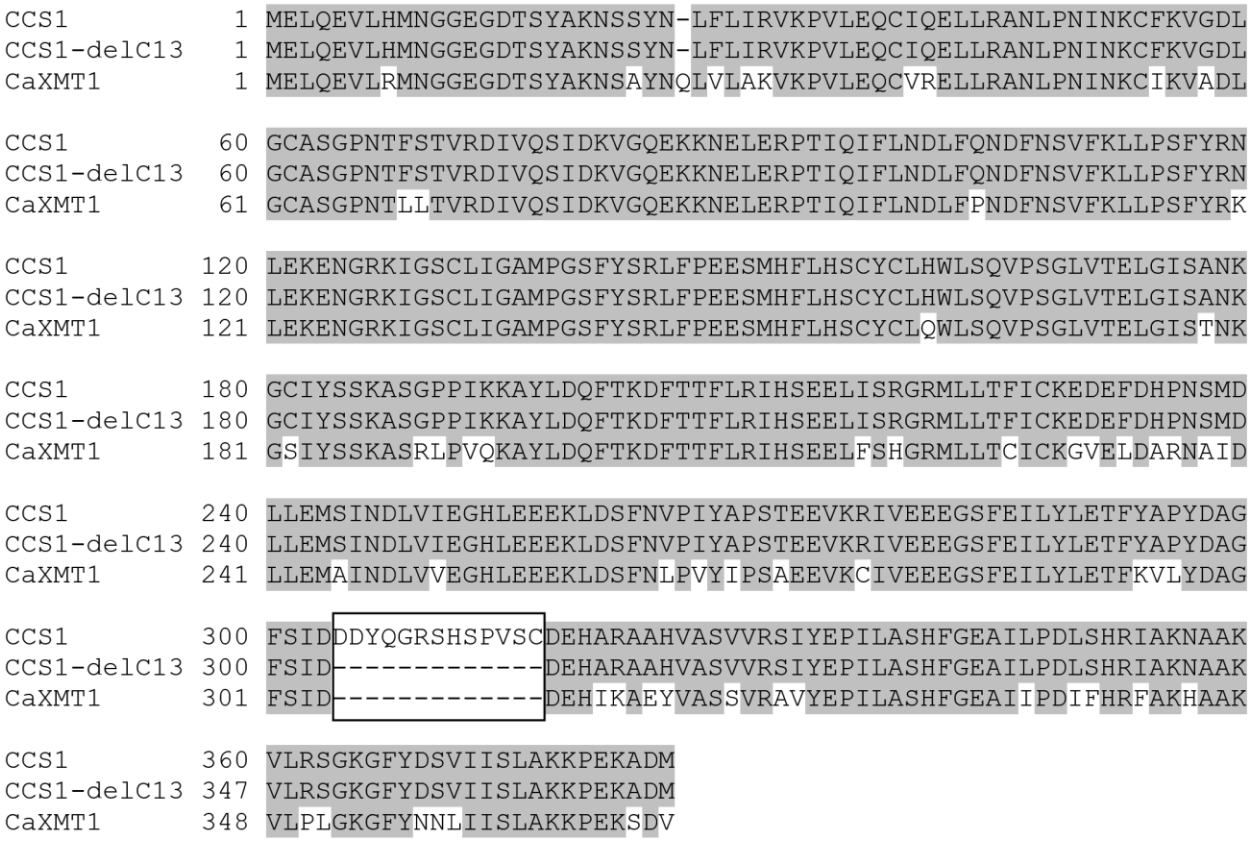

Figure 3.7: Sequence alignment of CCS1, CCS1-delC13, and CaXMT1. The boxed region is the CCS-CTS extended region.

I decided to make a CCS-CTS extended region deletion mutant and see if this effect would be borne out in mammalian cells as well. Cells were transformed with a plasmid containing the CCS-CTS extended region deletion mutant, CCS1(delC13). CCS1 and CCS1(delC13) cells were plated and allowed to incubate with the typical panel of substrates and harvested after 72h. In addition, three more conditions were assessed at 72h which matched the substrate concentrations used by Mizuno, et al.: 1000 µM 7X, 17X, and 37X.[115]

Table 3.6: Effect of CCS-CTS extended region deletion on Relative Yield for CCS1 in mammalian cells

Reaction	Product	Relative Yield†			
		CCS1		CCS1(delC13)	
		200 µM	1000 µM	200 µM	1000 µM
17X → 137X	137X	1.0	0.77	1.0	0.86
7X → 37X → 137X	37X	0.45	0.69	0.44	0.73
	137X	0.10	0.051	0.084	0.050
37X → 137X	137X	0.57	0.79	0.60	0.80

†Relative Yield = $Yield^{Product}/Yield^{17X \rightarrow 137X}$ for a given enzyme at [17X] =200 µM

Table 3.7: Effect of CCS-CTS extended region deletion on Relative Methylation Equivalents Consumed for CCS1 in mammalian cells

Reaction	Relative Methylation Equivalents Consumed†			
	CCS1		CCS1(delC13)	
	200 µM	1000 µM	200 µM	1000 µM
17X → 137X	1.0	0.77	1.0	0.86
7X → 37X → 137X	0.55	0.74	0.52	0.78
37X → 137X	0.57	0.79	0.60	0.80

†Relative Methylation Equivalents Consumed = (2 x Rel. $Yield^{137X}$ + Rel. $Yield^{37X}$) for reaction with 7X. Otherwise, RMEC = Relative Yield

In contrast to the results[90] observed by Mizuno, et al., I observed little meaningful difference between CCS1(delC13) and CCS1 at either 1000 µM or 200 µM substrate concentration. In both cases, increasing the concentration of paraxanthine from 200 to 1000 µM decreased the total relative yield of caffeine produced. Increasing theobromine concentrations modestly increased the relative yields of caffeine (by 39% and 33% for CCS1 and CCS1(delC13), respectively). Increasing 7-methylxanthine concentration increased the relative methylation equivalents consumed but decreased the yield of caffeine itself. This is likely due to the enzyme having a higher affinity 7-methylxanthine compared to theobromine. The total yield of products was slightly higher for CCS1(delC13) (refer to **Supplemental Data**), but this does not control for protein concentration per cell and so I cannot make a firm statement about changes in absolute enzyme activity. In addition, these experiments take place at 37 °C and at a different pH than the

in vitro experiments that were used to study the mechanisms of N-3 methylation by CCS1. It is possible that such changes could alter protein structure in such a way that affects the selectivity compared to the conditions used by Mizuno, et al.

If one conceives of cells simply as containers for enzymes, one would assume that increasing the substrate concentration ought to increase the reaction rate and thus increase total yield after a given period of time. In my experiments, the total relative methylation equivalents consumed slightly decreased at 1000 μM paraxanthine for both enzymes and slightly increased for 7-methylxanthine and theobromine at 1000 μM. This suggests that whatever increases in reaction velocity that might be seen due to the higher substrate concentration can be counteracted by increased cell toxicity, depletion of SAM, or some other mechanism. This suggests that choice of what substrate concentration to use to maximize total product yield might be informed as much by optimizing culture growth as it does by optimizing enzyme kinetics.

3.8 Synthesis of Methylxanthines as a Juxtacrine Signaling Reporter

To connect the synthesis of methylxanthines with other synthetic biological signaling pathways, I decided to test if methylxanthine synthesis enzymes could be made as a product of juxtacrine cell signaling. and if small molecule production could be used as a proxy measure for cell-cell contact. I chose to use synthetic Notch receptors[116–120] (synNotch) as a way of transducing extracellular binding events to produce a reporter enzyme.

Notch is an important developmental receptor that is ubiquitous in multicellular life.[121,122] Unlike many receptors, it has a comparatively simple mode of signal transduction wherein tension produced by binding to its target reveals protease cleavage sites.[121] After cleavage, the intracellular domain can directly act as a transcription factor.[123] Research has demonstrated that the extracellular domain can be replaced[124] and that the intracellular transcription factor domain can

be replaced with unnatural transcription factors.[125] This has led to the development of synNotch receptors that can be designed to respond to any number of targets and induce any number of intracellular events with synthetic transcription factors.[63,116] These have the feature of generating a stoichiometric response (one signaling event to one transcription factor) which ought to provide a more linear signal response curve to a given stimulus which is well suited for an output that is intrinsically amplified (i.e. enzymatic output).[63]

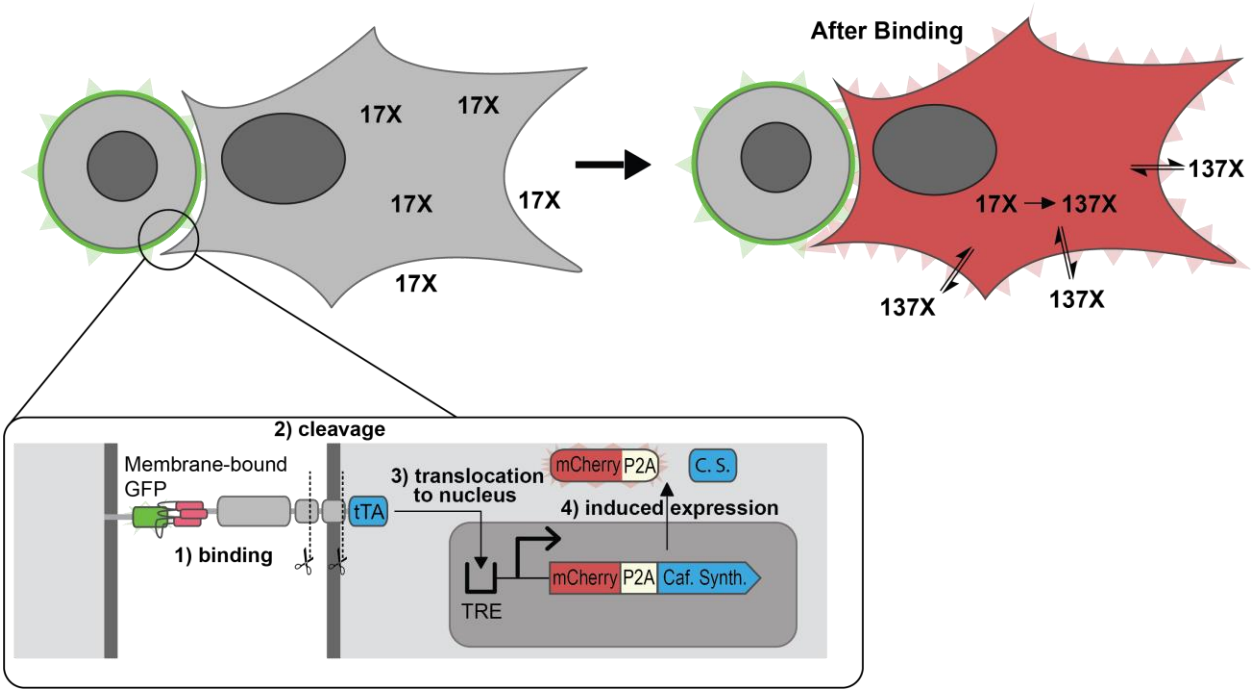

Figure 3.8: Depiction of how cell-cell contact between target cells and reporter cells can induce caffeine synthase enzyme expression upon juxtacrine signaling via synNotch. Expressed caffeine synthase can transform an existing substrate to the desired product. *Inset*: LaG17 binds surface-expressed GFP in K562 cells and subsequent cleavage events liberate TetRVP64 which translocates to the nucleus and interacts with the tetracycline response element (TRE) to induce gene expression. The expressed enzyme is capable of converting the surrounding paraxanthine (17X) to caffeine (137X).

I chose to use a LaG17-synNotch-TetRVP64 receptor for my experiments. This receptor is targeted against surface-expressed GFP using the anti-GFP nanobody LaG17[126] fused to the Notch core domain. The intracellular transcription factor is TetRVP64, an extended variant of the typical tetracycline trans-activator (tTA) with four repeats of VP16 instead of one. This trans-activator

can interact with a tetracycline response element (TRE) before an ORF and it can induce gene expression in the typical Tet-Off fashion.[127] I designed a reporter construct with a tight tetracycline regulatory element[128] ($TetO_7$ and minimal CMV promoter) followed by a fusion of mCherry and a caffeine synthase (CCS1, TCS1, or MXMT) separated by a self-cleaving P2A sequence. This P2A sequence allows for two proteins to be generated from a single transcript.[129] The caffeine synthase was placed downstream of the P2A element so that the only change to its sequence would be the addition of single amino acid residue after the P2A cleavage site. The synNotch and reporter constructs were inserted into orthogonally-selectable Sleeping Beauty plasmids (pSBBi-BH and pSBBi-GB backbones, respectively). HEK-293T cells were transduced with each pair of the plasmids and selected with the appropriate antibiotics. Cells with synNotch and a TRE reporter are called reporter cells, for short.

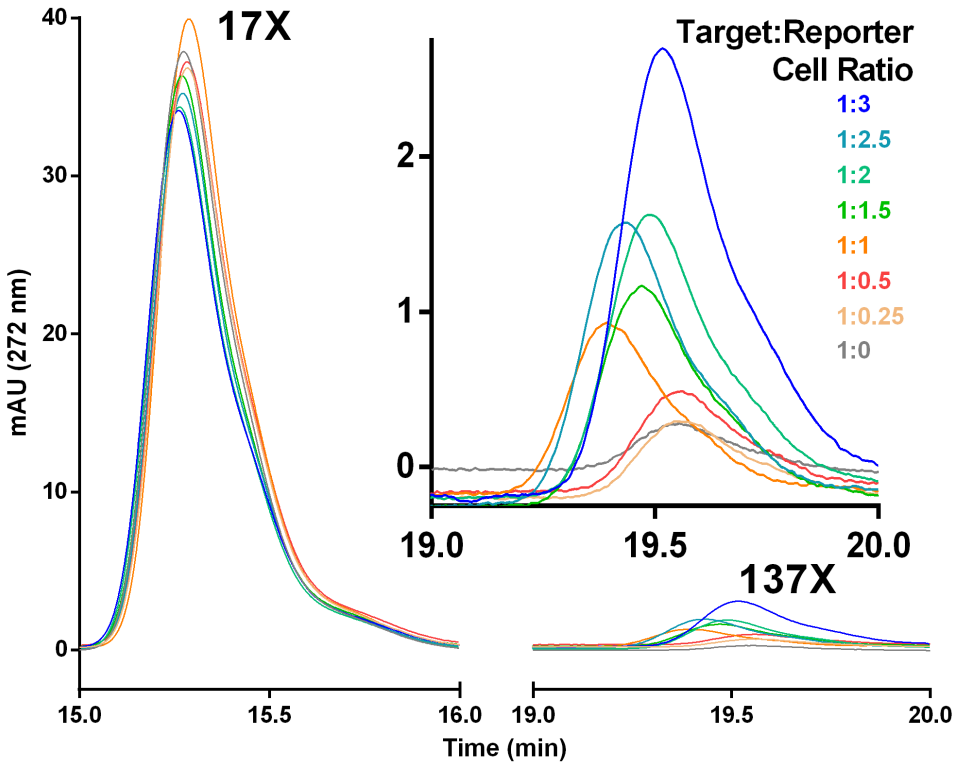

Figure 3.9: Portions of the chromatograms from coculture of target cells with LaG17-synNotch-TetRVP64 + TRE mCherry-P2A-CCS1 reporter cells. Inset shows more detail of the caffeine peak highlighting the relationship between target:reporter ratio and quantity of caffeine produced.

I then co-cultured the reporter cells with varying ratios of K562 cells expressing surface GFP (target cells) and 200 µM paraxanthine (**Figure 3.7** and **Figure 3.8**) When no target cells were present, only trace amounts (~1.0 µM) of caffeine was detected. This is likely due to baseline activation of the synNotch receptors. At a 3:1 ratio of target:reporter cells, 14.5 µM of caffeine was detected. A linear relationship was observed for these target:reporter cell ratios. The total amount of caffeine produced was notably lower than the amount produced by cells which constitutively produce CCS1. This suggests that improvements could yet be made in maximizing the yield obtained from reporter cells. Induction of reporter enzyme was also verified by qPCR using synNotch as a reference gene (see **Supplemental Data**). Reporter production was also demonstrated in cell lines with CaMXMT and TCS1 enzymes as well (see **Supplemental Data**). These experiments establish the viability of using induced methylxanthine production as a proxy for cell-cell contact in contexts where the feedstock is not limiting.

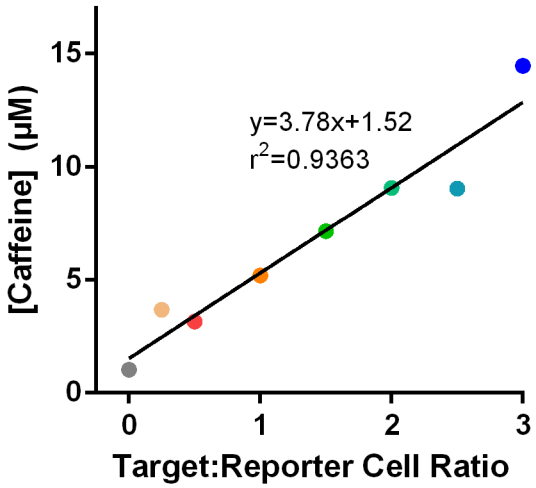

Figure 3.10: Final caffeine concentration for various target:reporter ratios. The linear regression demonstrates dose-response relationship for inducible enzyme expression and product production.

3.9 Attempts at Expanding the Functionality of SynNotch Receptors

In the process of using the synNotch receptor to induce expression of methylxanthine synthesis enzymes, I considered possible modifications to the synNotch platform that would add more functionality. I tested three variations of synNotch: 1) using a peptide for targeting, 2) *in situ* assembly of synNotch using a benzylguanylated targeting group and a SNAPtag-synNotch fusion, and 3) use of an amplifiable intracellular domain producing the intracellular response upon stimulation.

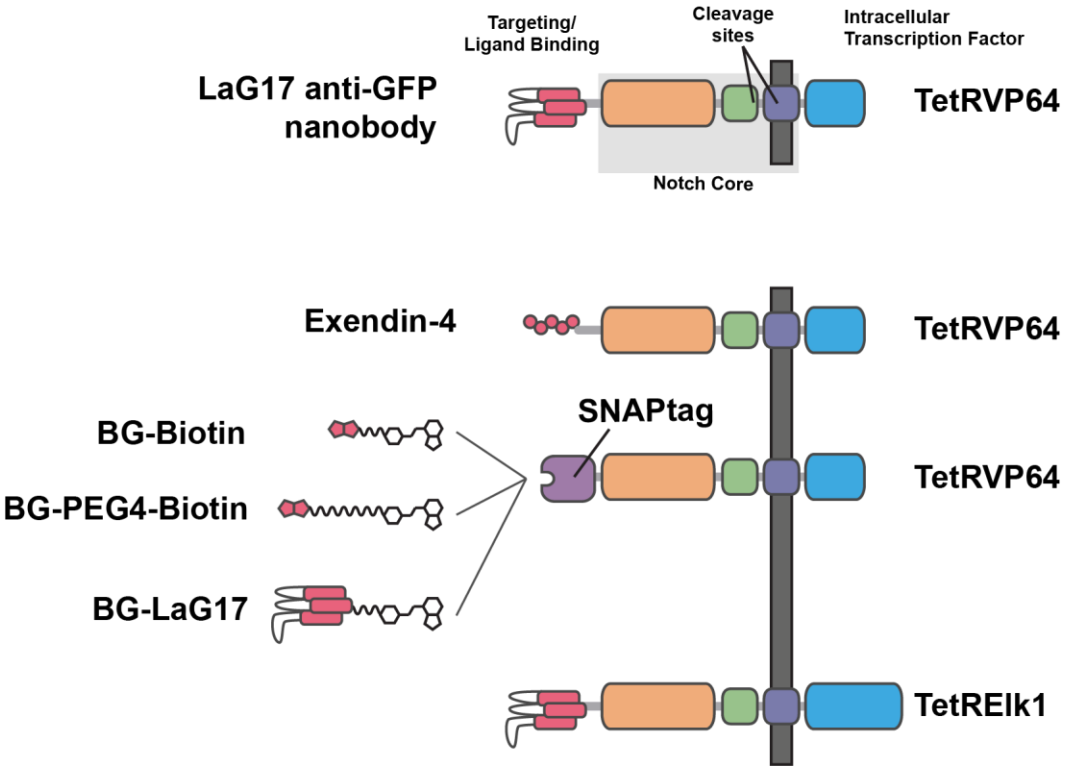

Figure 3.11: Depiction of LaG17 synNotch and synNotch variations tested. *Top*: Typical synNotch contains a targeting domain (red), Notch core, and an intracellular transcription factor (blue). Notch core comprises Lin-12 Notch repeats (orange), heterodimerization domains (green), and transmembrane domain (dark blue). *Middle*: synNotch targeting variants include peptide-targeted Exendin-4 (Ex4) synNotch and modular SNAPtag synNotch. SNAPtag synNotch can react with the pictured benzylguanylated targeting groups. *Bottom*: synNotch variant using amplifiable hybrid transcription factor TetRElk1.

One variation of synNotch employed use of a peptide as a targeting group instead of using an antibody. Exendin-4 (Ex4) is a high affinity peptide hormone found in the saliva of *H.*

horridium, the gila monster.[130] It interacts with the glucagon-like peptide 1 receptor (GLP-1R) and stimulates glucose-responsive insulin secretion in beta cells of the pancreas. A synthetic derivative of exendin-4 where the terminal carboxylic acid is simply amidated is used as a therapy for type 2 diabetes under the name exendatide.[131] The relative beta-specificity of Ex4 has also been used by researchers to target beta cells for MRI, PET imaging, and fluorescent imaging.[132–135] As such, I thought that this might be a potentially interesting affinity group to use to target GLP-1R.

To make the Ex4-synNotch fusion I inserted Ex4 and a small flexible linker[136] into LaG17-synNotch-TetRVP64, replacing the LaG17 nanobody, and inserted ORF into a selectable Sleeping Beauty transposon plasmid pSBBi-BH. I transduced HEK-293T cells with pSBBi-BH Ex4-synNotch-TetRVP64 along with the reporter plasmid pSBTRE-GB mCherrry-P2A-CCS1.
I then made the lentiviral transfer vector pHR SFFV GLP1R(S301A)-GFP plasmid which contains a GLP-1R-GFP fusion with a S301A mutation[137] to help maintain high membrane localization of the protein. I lentivirally transduced K562 cells with the GLP1R(S301A)-GFP plasmid and co-cultured these cells with the Ex4-synNotch cells as before. Unfortunately, no fluorescence was observed via microscopy after co-incubation for 72h, regardless of the number of target cells included. When 200 μM 17X was included in the culture medium, no formation of caffeine was observed. The native Notch protein sometimes includes variable repeats of the EGF repeat unit and previous work has shown that this can sometimes rescue activity of a receptor.[63] The same experiments were performed with Ex4-EGF-synNotch-TetRVP64 instead, but no activity was observed in these experiments either.

I then went on to test whether a SNAPtag-based synNotch receptor would be viable. SNAPtag is an engineered version of the O-6-methylguanine DNA methyltranferase enzyme which forms a covalent adduct upon reaction with a modified O-6-benzylguanine derivative.[138,139]

This allows for the facile formation of a covalent bond between an arbitrary molecule tagged with a benzylguanine and a SNAPtag-protein fusion. In this concept, a receptor would be a modular base unit that could be programmed to respond to a target by incubation with a benzylguanylated targeting group. I decided to test this with two targeting groups: biotin and the LaG17 nanobody.

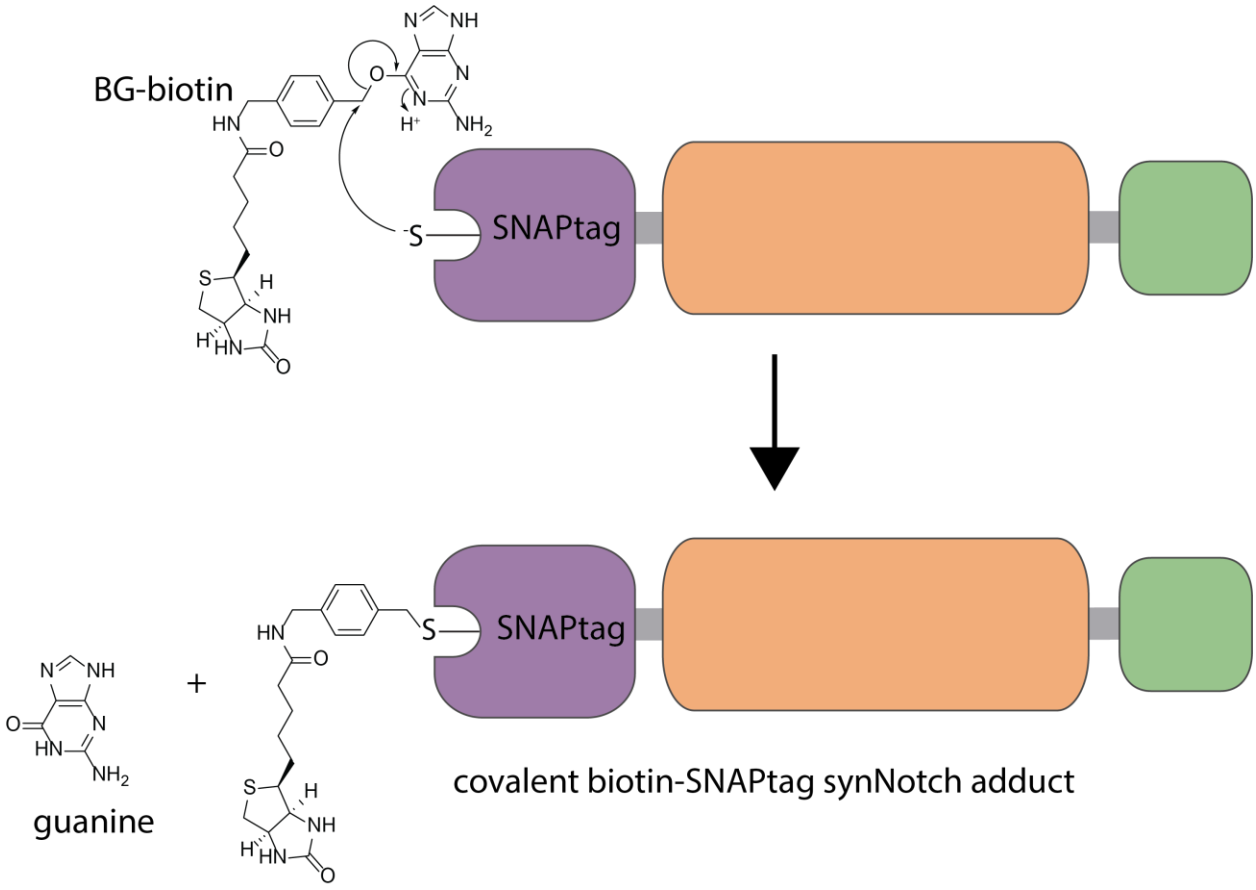

Scheme 3.3: Mechanism of how SNAPtag synNotch is covalently modified with a targeting group, demonstrated with BG-biotin.

The avidin-biotin interaction is well-known and used in many different biochemistry techniques to rapidly form strong interactions between elements.[140,141] This property has been widely used in techniques such as bioID,[142] affinity pulldowns,[143] and enzymatic amplifications.[144] Because of its strength and specificity, I thought that it could serve as a potentially viable targeting

group. Avidin and streptavidin, the most common of the proteins used to bind biotin, are both tetrameric.[141] I was concerned that surface expression of the avidin or streptavidin monomers might not allow the appropriate tetramers to form that are required for high affinity interaction with biotin. While tetrameric streptavidin has a K_d of ~10 fM for biotin,[140] a single monomer of streptavidin has a K_d of only 1.7 μM for biotin.[145] An engineered streptavidin monomer with modifications inspired by the dimeric biotin-binding protein rhizavidin from *Rhizobium etli*, however, has a K_d of 2.8 nM for biotin.[146] It has previously been used as a surface target in yeast.[146] As such, I made the appropriate plasmids and lentivirally transduced K562 cells with surface-expressed monomeric streptavidin (K562-mSA-EGFP-TM) and synthesized two biotin-benzylguanine compounds, BG-Biotin and BG-PEG4-Biotin. I chose to synthesize the PEG4 linker version with the idea that there could be too much steric hindrance from the SNAPtag biding binding pocket for benzylguanine to allow the biotin moiety to interact with monomeric streptavidin.

As with the other fusions, I prepared plasmids coding for a SNAPtag-synNotch-TetRVP64 fusion and transduced them in HEK-293T cells along with the Tet-inducible TRE mCherry-P2A-TCS1 reporter to make the reporter cells. I co-cultured cells, as before, but used three different methods of exposing the BG-Biotin or BG-PEG4-biotin to cells: pre-incubation with reporter cells, pre-incubation with target cells (K562-mSA-EGFP-TM), or addition during co-culture. After 72h cells were assessed via fluorescence microscopy, but no production of fluorescent reporter was observed in any of the conditions tested. When incubations were performed in the presence of 100 μM 17X, no formation of caffeine was observed for any conditions tested.

Current synNotch receptors use single chain antibodies (scFVs) or camelid VH antibodies (nanobodies) fused to the Notch core domain as a means to recognize the intended target.[63,147]

While this approach is effective, synNotch receptors can only be developed against targets for which a high quality scFv or nanobody exists. However, the process of producing a fusion protein, transfecting cells, and testing each cell line is time consuming. I considered that one possible solution would be to make a modular synNotch receptor with an extracellular SNAPtag domain instead of an affinity domain. If a suitable commercially-available antibody were modified with a benzylguanine group (e.g. via reaction with an NHS-ester of benzylguanine) then perhaps a functional synNotch receptor could be assembled *in situ*. This would forego the need to construct a new genetic construct for every potential target and allow for more rapid screening of viable antibody-synNotch pairings.

I then decided to test if it was possible to reconstitute a receptor similar to LaG17-synNotch-TetRVP64 *in situ* by using a benzylguanylated LaG17 nanobody with cells expressing SNAPtag-synNotch-TetRVP64 and a TRE mCherry-P2A-CCS1 reporter. I expressed and purified LaG17 which contained a had SGKGSKGSKSK added to the C-terminal portion of the protein from *E. coli*. I reasoned that the additional lysine residues would increase the probability of having a C-terminal benzylguanylation that seemed most likely to form a receptor with a similar structure to the reference LaG17-synNotch after reaction with SNAPtag-synNotch. I reacted the purified protein with BG-GLA-NHS (the N-hydroxsuccinimide activated ester of 4-aminomethylbenzylguanine with a glutaric acid linker) and used the benzylguanylated LaG17 for cell culture experiments. As before I tested pre-incubation with the target cells, pre-incubation with the reporter cells, and addition during cell culture. In all experiments antibody was added to 0.1 μM. Fluorescence microscopy of the cells revealed no production of fluorescent reporter for any condition tested. When incubated with 17X, no production of caffeine was detected either.

There are two plausible reasons for the failure of the SNAPtag-synNotch receptor in these experiments. One possibility is the that the receptor binding group reacts with the SNAPtag domain and forms the desired product but that interaction of this simply does not result in the appropriate structural change in Notch to transduce a binding event. The second possibility is that the strength of the interaction with the target is too weak to survive the force needed to cause the structural change that is key in transducing biding events in Notch signaling. This latter explanation could be the case for the avidin- and GLP-1R-targeted synNotch receptors. This cannot be the case with the membrane-bound GFP-targeted synNotch receptor, however, as LaG17-synNotch is capable of transducing a binding event when the whole receptor is produced as a single protein. In this case, a possible explanation is that the additional length of the SNAPtag and short linker are acting similar to an extra EGF-repeat. Extra EGF-repeats have been shown to diminish the ability of synNotch receptors to transduce signals when the receptor functions normally without it.[63]

3.10 Attempts at Making an Amplifiable SynNotch Receptor

One key distinction between synNotch and many other receptors is that it generates a stoichiometric response instead of an amplified response because the cleaved intracellular portion of Notch acts directly as a transcription factor. However, by not having steps of amplification it means that there are fewer ways that synNotch can be made to interact with other natural and synthetic gene circuits other than through its ability to control gene expression. I wanted to make a synNotch receptor whose product was a hybrid transcription factor that was regulated by another cellular process.

TetRElk1 is a hybrid regulated transcription factor[148] that is combination of the DNA-binding, regulatory, and dimerization domains from tTA2s with the regulatory and transcriptional activation domains of Elk-1. Activation of MAPK ERK Kinase 1 (MEK-1) results in activation of

extracellular signal-related kinase (ERK) which then phosphorylates TetRElk1to produce phospho-TetR-Elk1.[148] Phospho-TetRElk1 is a transcriptional activator, whereas TetRElk1 is not. I hypothesized that this should make a "gated" synNotch which could transduce a juxtacrine signaling event, but the cleaved portion of it would not serve as a promoter unless another process caused activation of ERK. Anti-caffeine synthetic receptor pDB395[149] is built upon a mouse fibroblast growth factor receptor fragment1 ($mFGFR1_{405\text{-}822}$) fused to an anti-caffeine nanobody (aCaffVHH). Homodimerization of this protein causes activation of MAPK (downstream of MEK 1/2) which is suitable for being rerouted through TetRElk1. pDB395 has been demonstrated to provide substantial activation of a reporter with as little as 0.1 µM caffeine.[149]

To test this, I made pSBBi-BH LaG17-synNotch-TetRElk1 and transduced cells with it and pSBTRE-GB mCherry-P2A-CCS1. I then transiently transfected these cells with synthetic caffeine receptor pDB395. I observed that with 0.1 µM caffeine there was substantial activation of reporter circuits as observed by fluorescence microscopy even in the absence of GFP-expressing target cells. It is not clear why this had such high baseline activation, but no further attempts were made to develop this system. This conceptual approach may have merit, but it may require use of a transcription factor that is not subject to so much amplification. The low level "leaky" activation of synNotch[122] may be enough to enable downstream signaling that, when amplified, becomes substantial.

3.11 Plausibility of Cell-Cell Signaling Using Methylxanthine Synthesis and Synthetic Caffeine Receptors

Recent work by Bojar, et al.[149] has generated several different caffeine receptors that can be used for synthetic biology applications which have sensitivities to caffeine ranging from 0.01 uM to 100 uM.[149] These receptors are all built around the dimerization of an anti-caffeine camelid

heavy-chain-only antibody fragment called aCaffVHH.[150–152] When aCaffVHH is fused to proteins that transduce a signal upon dimerization, the net result is that the presence of caffeine can induce the downstream signaling event. Although these are described as caffeine receptors, they are not exclusively responsive to caffeine[149] and do display some sensitivity to dimethylxanthines; theophylline, paraxanthine, and theobromine all show some activation of the STAT3-based caffeine receptor at 1 µM according to work in Bojar, et al., with these dimethylxanthines being listed in order of decreasing receptor activation.

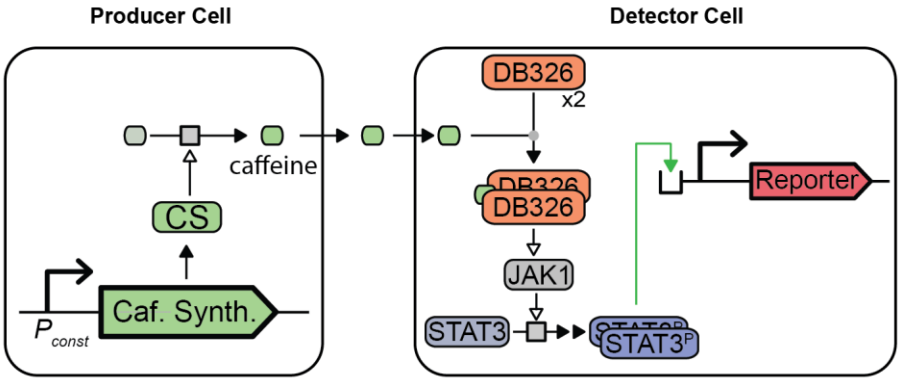

Figure 3.12: Simple circuit for cell-cell signaling from a caffeine (or other methylxanthine) producing cell to a detector cell containing DB326. DB326 homodimerizes in the presence of caffeine and activates JAK1 which activates the phosphorylation and dimerization of STAT3. The $STAT3^{P}$ dimer can then enable the expression of a STAT3-inducible reporter gene

The differential activation of the receptors for the dimethylxanthines is a result of how this antibody was developed. Caffeine was not used as a target and instead a 1,3-dimethylxanthine derivative with an extended alkyl carboxylate in the 7-position was used.[152] This allowed conjugation of the target molecule to proteins and peptides used for the selection process. As such, the regions of caffeine which interact with aCaffVHH dimers are more likely to be the N-1 and N-3 methyl groups. Indeed, this pattern of reactivity is observed in binding thermodynamics[151] and in cross reactivity with dimethylxanthines during immunoaffinity chromatography.[150] Recent

crystallography of the caffeine-aCaffVHH dimer further demonstrates that the N-1 and N-3 methyl groups are oriented toward the antibody when bound.

I had initially been interested in exploring the possibility of detecting caffeine production by cells using a paraxanthine feedstock due to the high activity of enzymes toward it and comparatively low K_m. Unfortunately, signal produced by DB326 starts to notably increase for theophylline at only 1 µM,[149] far below the K_m of any enzymes tested for any substrate. If dimethylxanthines achieve lower activation of this receptor than caffeine, then it was plausible that monomethylxanthines ought to achieve even less activation of this receptor than dimethylxanthines. This could allow for concentrations of a feedstock at levels closer to ideal for the enzymes without eliciting too much spurious activation of the receptor. Previous work developing a water quality immunoassay for caffeine using different monoclonal and polyclonal anti-caffeine antibodies indicated that xanthine produced negligible signal (<0.002% and <0.008% for mAb and pAb immunoassays, respectively).[153] I wanted to test the feasibility of using xanthine or monomethylxanthine as a feedstock to generate products detectable by pDB326 receptors.

I transduced HEK-293T cells with pDB326 with the typical Sleeping Beauty method to produce DB326 cells. These were selected with antibiotics, but unlike Bojar, et al., I did not perform a clonal selection and expansion. I plated and transfected DB326 cells with a plasmid containing a STAT3-inducible secreted embryonic alkaline phosphatase (SEAP) reporter gene[154] (P_{STAT3}-SEAP-pA_{SV40}, pLS13). Initial experiments showed only modest SEAP activity as determined by assay with 4-nitrophenylphosphate (pNPP). However, repeat of this transfection with pLS13[155] and constitutive STAT3 (P_{hCMV}-hSTAT3-pA, pLS15) notably increased the signal.

Based on these data, X, XR, and any of the monomethylxanthines are suitable to use with DB326 up to at least 50 µM without eliciting substantial receptor activation above background. It

is also apparent that optimization of the genetic circuit—namely clonal expansion of pDB326 cells and optimization of how much pLS13 and pLS15 are used—will be necessary to maximize signal while minimizing baseline (unstimulated) receptor activation.

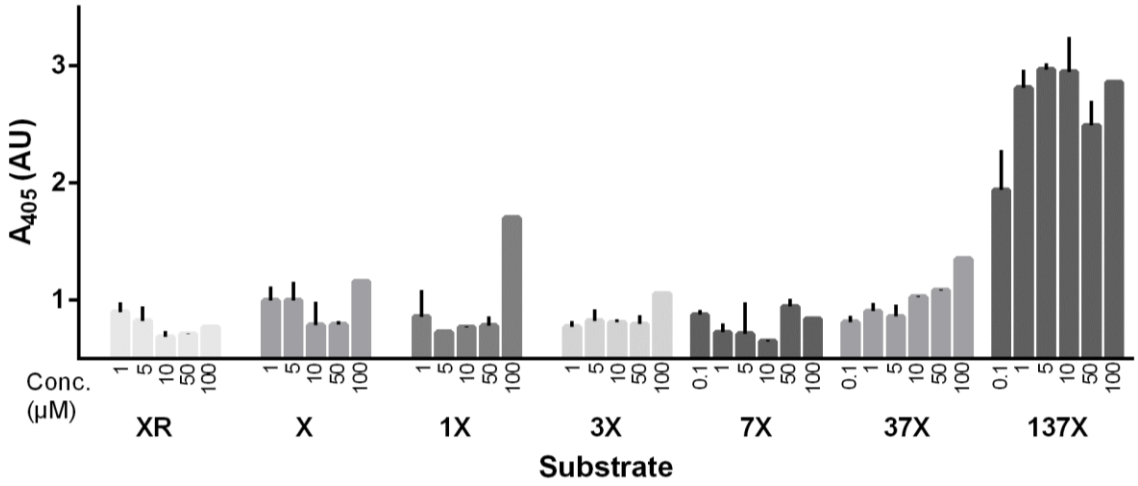

Figure 3.13: Cross Reactivity of Non-Preferred Xanthine Substrates with the STAT3-based caffeine receptor pDB326 assessed by SEAP assay. Error bars show standard deviation of duplicate experiments. 100 μM concentrations were not performed in duplicate.

3.12 Discussion and Future Work

This work has set the stage for small subset of future possible studies. There are two broad areas that deserve future investigation: fundamental studies of the properties of the caffeine synthesis pathways and enzymes, and further elaboration on mammalian synthesis of caffeine/methylxanthines. The findings from the former would go a long way to improving the viability of the latter research direction.

As more recent work has begun to reveal, the canonical pathway from xanthosine to 7-methylxanthine to theobromine to caffeine is not the only way to make caffeine.[78,156,157] Given that the roles that convergent evolution and enzyme exaption[78,97] have played in the development of the known caffeine biosynthesis pathways, it is not unreasonable to assume that may be diversity among the pathways in less-studied organisms. The potential role of theophylline in caffeine

biosynthesis in *Ilex paraguariensis*[156] is certainly suggestive of what surprises may lie in parts of the natural world that remain unstudied.

What is the role of hetero/homo-dimerization in coffee caffeine synthases? There is experimental[111] and structural[158] evidence for dimer formation yet its functional importance has not been determined. It is tempting to speculate on the potential for metabolon formation,[159] particularly since the dimerization interface is conserved within the coffee enzymes and is also found in the structurally-related salicylic acid methyltransferase class of enzymes.[160] While the interface is on the small side of protein dimerization surfaces,[158,161] that does not necessarily preclude it from conferring beneficial properties of dimerization[162] on caffeine synthesis enzymes. One possible next step in this direction is to design enzyme dimer fusions which would effectively force enzymes to adopt a dimer-like structure and see if this alters the enzymatic activity.

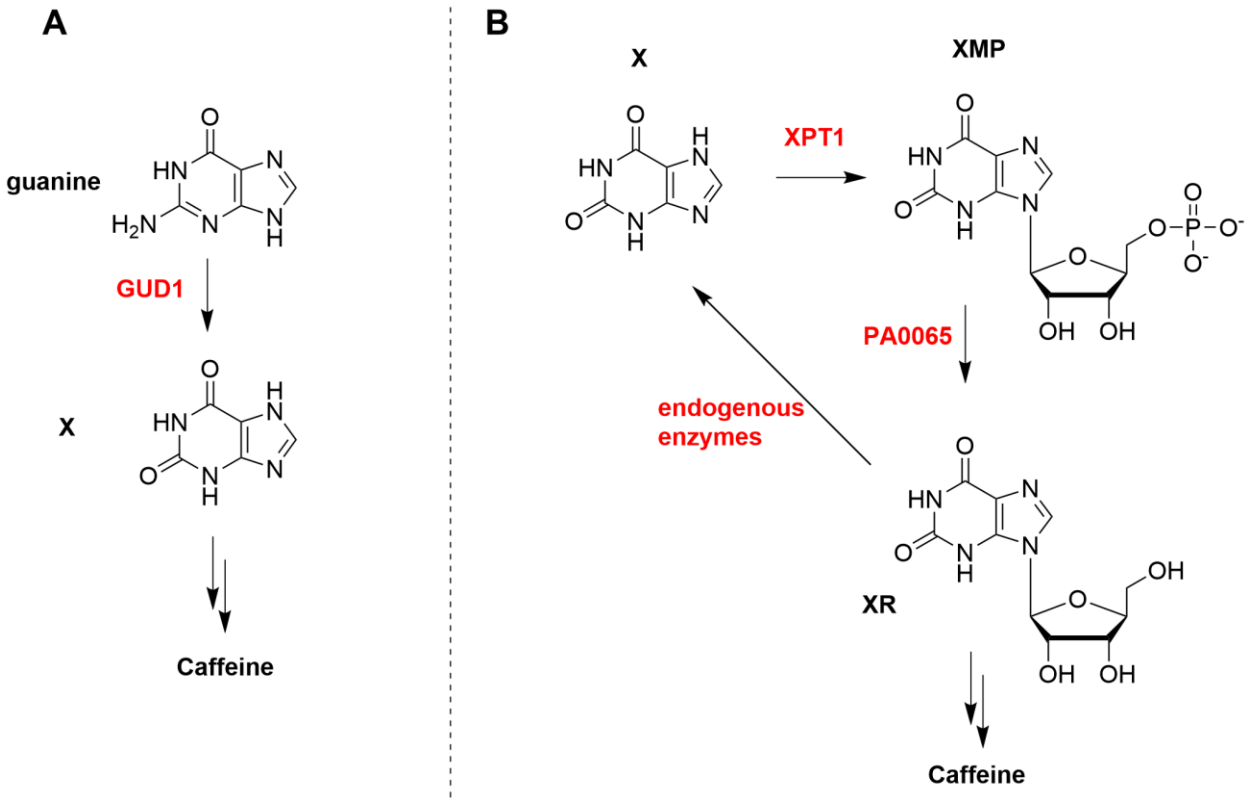

Scheme 3.4: Pathways for improved xanthine and xanthosine synthesis used previously. A) Shows the degradation of guanine used to increase xanthine concentrations in *E. coli*;[163] B) Shows cyclical interconversion of xanthine, xanthosine monophosphate (XMP), and xanthosine used in *S. cerevisiae*.[96]

While I have reconstituted and evaluated many methylxanthine synthesis enzymes, none of my work tackled the generation of the small molecule feedstock required for methylxanthine-generating cells. It is not unreasonable to achieve *de novo* formation of caffeine (or other methylxanthines) which originates from the pools of nucleotides that are already present in cells. Prior research demonstrated that caffeine can be made *de novo* in *E. coli*[163] and *S. cerevisiae.*[96] Successful production of large quantities of methylxanthines *de novo* in mammalian cells would likely require the same type of modifications that were needed in these other hosts (**Scheme 3.4**). In *S. cerevisiae*,[96] intracellular pools of xanthine were converted to xanthine monophosphate (XMP) by xanthine phosphoribosyltransferase 1 (XPT1) followed by hydrolysis with PA0065 (a

5′-nucleotidase from *Pseudomonas aeruginosa*) to form xanthosine. A different approach was taken in *E. coli,* where guanine deaminase 1 (GUD1) from yeast was used to enhance conversion of endogenous guanine into xanthine and TCS1 alone was used to triply methylate xanthine into caffeine. While I have shown that endogenous xanthine is sufficient to produce limited quantities of 1X and 3X using CsAncCS, much optimization could be done to maximize the yield. Either of these approaches would be worth trying in human cells, depending on the subsequent enzymatic transformations. Intracellular concentration of xanthine has been reported to be 20 μM in human cells.[164] Even if xanthosine was the desired end product there would likely be benefit of combining these approaches to use GUD1 to effectively enhance the concentration of products in the xanthine/XMP/xanothosine pool.

As mentioned previously, recent work has generated several viable synthetic caffeine receptors. Although I have laid some of the groundwork for using caffeine or other methylxanthines for cell-cell communication, there is much room for exploration of this concept. As I mentioned before, a simple example one could implement would enable detection of caffeine (or another methylxanthine) by reporter cells with DB326 (or another synthetic receptor) akin to the process shown in **Figure 3.12**. In this scheme, some feedstock present in solution like a monomethylxanthine could be methylated to become a dimethylxanthine or caffeine within producer cells. Because the monomethylxanthine does not strongly stimulate the receptor at the provided concentration, only upon buildup and diffusion of the methylated products (perhaps even caffeine) would DB326 be stimulated beyond background activation. This method of cell-cell communication could be construed as a form synthetic paracrine signaling and could be used as part of a self-organizing synthetic tissue.

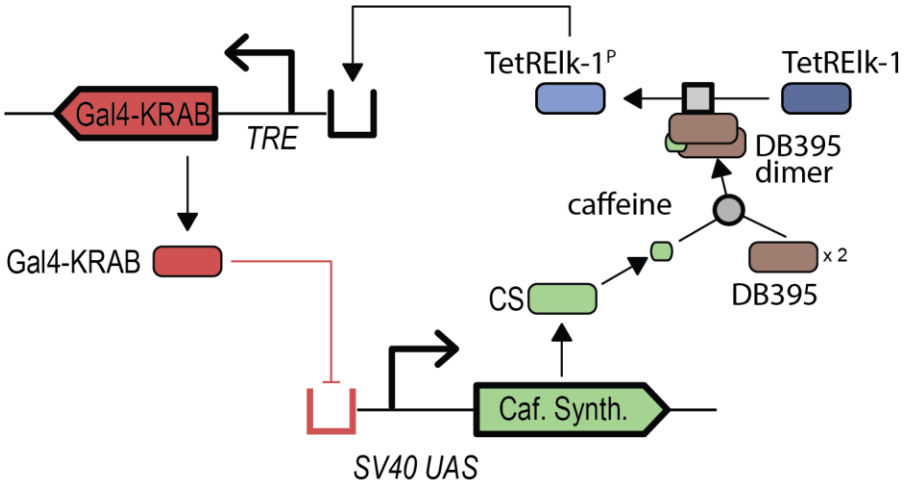

Figure 3.14: Schematic diagram of a hypothetical self-limiting caffeine production circuit. In this circuit, a caffeine synthase is ordinarily constitutive promoter SV40 UAS. The resulting caffeine synthase can go on to produce caffeine which can bind to DB395 (mFGFR1$_{405\text{-}822}$-aCaffVHH) and cause it to homodimerize. This can activate MEK 1/2 and lead to downstream phosphorylation of TetREIk-1. Phospho-TetREIk-1 will bind to the TRE promoter to induce Gal4-KRAB. Gal4-KRAB represses the SV40 UAS promoter, halting expression of the caffeine synthase.

Alternatively, one could easily imagine using a caffeine receptor co-expressed in a cell which produces methylxanthines to set a limit on how much caffeine is made (**Figure 3.14**). For example, a caffeine receptor could be used to induce production of Gal4-KRAB in a cell with constitutive caffeine synthase production controlled by a SV40/UAS promoter. In this situation the caffeine synthase enzyme would be unregulated until the caffeine concentration reached a high enough level to trigger the receptor. That would then result in repression of the enzyme responsible for caffeine production. Alternatively, one can imagine using one of the selective methylxanthine degrading enzymes from *Pseudomonas putida* CBB5[165] within a population of cells producing methylxanthines to limit production to a single product, e.g. theobromine, by selectively degrading others. The existence of so many functional proteins that can act upon caffeine and its metabolites could allow for a huge variety of experimentation in making gene circuits and synthetic cell-cell communication.

Finally, one could envision using production of methylxanthines as a reporter for otherwise invisible cellular states in a human recipient of a cell transplant. There are increasing numbers of cellular transplant therapies in clinical use or trials including transgenic immune cell transplants and islet cell transplants.[69,166–169] Unlike in animal studies, where it is common to include a non-invasive reporter for a functional endpoint, e.g. luciferase expression coupled to T-cell receptor activation in CAR-T, there is not an easy way to probe within the human body to look at cellular states. The poor penetrance[69] of luminescence in larger animals is enough of a problem to limit its use without even considering issues with systemic luciferin administration in humans.[70] Methylxanthines are well tolerated by humans and are not produced in endogenously. In a patient abstaining from caffeinated products, if methylxanthine synthesis were used as a reporter for some cellular state, it could serve as a unique, readily detectable biomarker for the correct functioning of the cellular therapy. Quantifying methylxanthines is not as convenient as quantifying luminescence, but it is feasible and compatible with human bodies.

3.13 Conclusion

I have demonstrated that enzymes involved in the biosynthesis of methylxanthines can be heterologously expressed in human cells and that many of these enzymes retain useful activity. I have shown that the endogenous levels of xanthine are sufficient to produce detectable monomethylxanthines in CsAncCS-expressing cells. I have assessed the effect of GST-fusion on CCS1 and TCS1 activity in human cells. I have shown that CCS-CTS deletion has relatively little effect on CCS1 activity in human cells compared to its effect *in vitro*. I have shown that enzyme activity can be induced using a synNotch receptor upon stimulation with correct target cells. I have also attempted to make several modifications to the synNotch receptor to increase the number of ways it could interact with its target without success. I have shown that quantity of target cells

used to stimulate a population of receptor/reporter cells correlates well with the quantity of methylxanthine product produced in response, suggesting that this technique could be used as a method of quantifying cell-cell interactions. Finally, I have demonstrated the potential viability of using a monomethylxanthine as a feedstock to produce dimethylxanthines or caffeine *in situ* for cell-cell signaling purposes.

3.14 Experimental Methods

3.14.1 Materials

All chemicals and reagents were of reagent grade or better. Unless otherwise stated, all reagents were purchased from Fisher Scientific (Waltham, MA) or Sigma Aldrich (St. Louis, MO). All solvents for reactions were anhydrous and purchased from Sigma Aldrich (St. Louis, MO). All solvents for liquid chromatography were HPLC grade or higher and were purchased from Sigma Aldrich or Fisher Scientific. Theobromine, theophylline, and 1-methylxanthine were purchased from Tokyo Chemical Industrial Co., Ltd. (Tokyo, Japan). 3-Methylxanthine was purchased from AK Scientific (Union City, CA). Xanthine was purchased from Chem Impex International (Wood Dale, IL). 7-Methylxanthine was purchased from Carbosynth (San Diego, CA). Caffeine was purchased from Alfa Aesar (Tewksbury, MA). Biotin-PEG4-N-hydroxysuccinimide ester was purchased from Click Chemistry Tools (Scottsdale, AZ).

Mammalian Cell Culture Supplies: Dulbecco's Modified Eagle's Medium (DMEM), HBSS, PBS, TrypLE, TRIzol Reagent, blasticidin S hydrochloride, and puromycin dihydrochloride were purchased from Thermo Fisher Scientific (Waltham, MA). Heat-inactivated fetal bovine serum was purchased from Omega Scientific (Tarzana, CA). Primocin was purchased from Invivogen (San Diego, CA). Cell culture dishes and flasks were purchased from VWR (Radnor, PA). Poly-L-lysine was purchased from Sigma Aldrich (St. Louis, MO). Accutase was

purchased from Innovative Cell Technologies (San Diego, CA). HEK-293T and K-562 cells were purchased from American Type Culture Collection (Manassas, VA).

Bacterial Cell Culture Supplies: Carbenicillin-containing (100 µg/mL) and kanamycin-containing (50 µg/mL) LB agar plates were purchased from Biopioneer (San Diego, CA). UltraPure Agarose, His-Pur Ni-NTA resin, and LB broth powder were purchased from Thermo Fisher Scientific (Waltham, MA). DH5a competent *E. coli* cells were obtained from Zymo Research (Irvine, CA). NEB Stable and BL21(DE3) competent *E. coli* cells were obtained from New England Biolabs (Ipswich, MA). Frozen aliquots of these cells were prepared with the "Mix & Go!" Transformation Kit (Zymo Research, Irvine, CA).

Biochemistry Supplies: All restriction enzymes, Q5 polymerase, HiFi Assembly 2X master mix, T4 DNA ligase, KLD enzyme mix, and murine RNAse inhibitor were purchased from New England Biosciences (Ipswich, MA). Maxima H-minus RT was purchased from Thermo Fisher Scientific (Waltham, MA). Pre-cast SDS-PAGE gels were purchased from Bio-Rad (Hercules, CA).

3.14.2 Plasmid Construction

3.14.2.1 General Information

SynNotch plasmids pHR_SFFV_LaG17_synNotch_TetRVP64, pHR_Gal4UAS_tBFP_ PGK_mCherry, pHR_EGFPligand, pHR_pGK_LaG17_synNotch _Gal4VP64, and pHR_SFFV were a gift from Wendell Lim (Addgene plasmid # 79128, 79130, 79129, 79127, and 79121, respectively). The Sleeping Beauty transposase plasmid pCMV(CAT) T7-SB100 was a gift from Zsuzsanna Izsvak (Addgene plasmid # 34879). The plasmid GLP1R-Tango[170] was a gift from Bryan Roth (Addgene plasmid # 66295). The Sleeping Beauty plasmids pSBBi-RP, pSBBi-GB, pSBBi-BH, and pSBTet-GB were a gift from Eric Kowarz (Addgene plasmid # 60513, 60520,

60515, and 60504, respectively). Plasmids pMD2.G and pCMV-dR8.2 dvpr were a gift from Didier Trono (Addgene plasmid # 12259 and 8455). Plasmid pACYC-GST was a gift from Cheryl Arrowsmith (Addgene plasmid # 62329) Plasmid pSNAPf was purchased from New England Biolabs (Ipswich, MA). Plasmid pET-11A(+)-PP, a modified version of pET-11A(+) containing a Precission protease cut site, was a gift from the Partho Ghosh (University of California, San Diego) lab.

All commercial or gifted plasmids were transformed into NEB Stable (for lentiviral plasmids) or DH5α (for all other plasmids) chemically competent cells according to the provided manufacturers' protocols. Minipreps and maxipreps were performed according to manufacturer's instructions using the Plasmid Miniprep Kit II and the Plasmid Maxi Kit, respectively, from Biomiga (San Diego, CA). Resultant plasmids were saved in water at -20 °C. Design and planning for plasmids was performed using SnapGene software (GSL Biotech; available at snapgene.com). All primers were synthesized by Eton Biosciences (San Diego, CA). All cloning operations were verified by sequencing performed by Eton Biosciences.

3.14.2.2 Preserving *E. coli* Cell Stocks

For frozen stocks of cultures, 0.5 mL of cultured LB was mixed with 0.5 mL of 50% (v/v) glycerol in water (autoclave sterilized) and immediately frozen at -80 °C. When many samples were saved for a short duration, a small portion (<5 µL) of cultured LB was pipetted) onto an agar plate, left at room temperature for several hours, and then stored at 4 °C for up to 2 weeks.

3.14.2.1 Agarose Gel Electrophoresis

Typically, a 0.8-1.0% (w/v) agarose gel was prepared by adding an appropriate amount of low melting agarose to 50 mL 1X TAE buffer (40 mM Tris, 20 mM acetic acid, 1 mM EDTA). This is heated in an 800W microwave in 30s increments until the gel is fully dissolved, swirling

the flask after each microwave treatment. After cooling slightly, 10,000X Gel Red or Gel Green (Biotium, Hayward, CA) is added to a final concentration of 1X (5 µL / 50 mL gel). After this the gel is pour into the mold and allowed to solidify at room temperature or 4 °C. 10X Loading buffer is added to the sample to a final concentration of 10-15% (v/v). The sample is mixed thoroughly, loaded into the gel alongside an appropriate ladder, and run at 120-140V until the bands had traveled sufficiently through the gel (>40 min). The completed gel is visualized using a [Gel Imager] or a Blue Light Gel Imager.

For visualizing small nucleic acid segments (<1000 bp), a 2% (w/v) agarose gel is prepared instead.

3.14.2.2 Gel Extraction

Gels intended to be subjected to gel extraction are prepared with Gel Green instead of Gel Red. After electrophoresis finishes, the desired bands are excised as neatly as possible using a new and clean razor blade on a blue light transilluminator. The bands are transferred into pre-weighed 1.7 mL centrifuge tubes. The DNA in the excised bands is extracted using a Qiaquick Gel Extraction Kit (Qiagen, Hilden, Germany) or a Monarch Gel Extraction kit (New England Biolabs, Waltham, MA) by following the manufacturer's instructions. Large plasmids (>10kb) were preferentially extracted using the NEB kit with a slight modification of the manufacturer's protocol: after the gel is dissolved using the appropriate buffer, a volume of water equal to the mass of the excised band is added to the dissolved gel prior to loading on a spin column. Otherwise, the manufacturers' protocols were followed as written.

3.14.2.3 Restriction Digest

For a typical single or double digestion, at least 500 µg of DNA template was diluted with 3 µL of 10X CutSmart buffer and enough water such that the final volume will be 30 µL after the

addition of the desired restriction enzyme(s). The restriction enzymes were always the final component added, typically using 0.25 µL of each enzyme. The samples were briefly vortexed to mix and then were digested for a minimum of 30 min at 37 °C on a thermal cycler. Depending on the nature of the sample and the downstream application, digested samples were: heat inactivated by incubating at 65 °C for 10 min and used directly, purified using a spin column, or run on an agarose gel and gel extracted.

Samples using restriction enzyme SfiI were digested at 50 °C for 45-60 min. Because the enzyme cannot be heat-inactivated, the digested fragment was always gel extracted or spin purified.

3.14.2.5 HiFi Assembly

Primers for HiFi assembly were typically created using the online NEBuilder Assembly Tool v2.2.6 from New England Biolabs (Ipswich, MA; available at nebuilder.neb.com). Primers were checked for off-target binding using SnapGene and for primer-dimer formation using the OligoAnalyzer Tool from Integrated DNA Technologies (Coralville, IA; available at www.idtdna.com/pages/tools/oligoanalyzer). The HiFi assembly was performed according to the manufacturer's instructions with the following modifications. The PCR products being assembled were treated with DpnI (0.25 µL DpnI directly to finished PCR reaction, incubated 15 min at 37 °C, then purified as usual) to ensure no PCR template carryover. The quantity of components for each reaction was determined by Table X.X. The HiFi assembly reaction was assembled at half scale (5 µL total) and incubated for 45 minutes at 50 °C and *E. coli* cells were transformed by the typical method.

Table 3.8: Reference for quantity of insert (ng) needed for a HiFi Assembly using 50 ng of vector

		Size of Insert (kb)							
		3.0	2.5	2.0	1.5	1.0	0.75	0.5	0.25
Size of Vector (kb)	14	21.4	17.9	14.3	10.7	7.1	5.4	3.6	1.8
	13	23.1	19.2	15.4	11.5	7.7	5.8	3.8	1.9
	12	25.0	20.8	16.7	12.5	8.3	6.3	4.2	2.1
	11	27.3	22.7	18.2	13.6	9.1	6.8	4.5	2.3
	10	30.0	25.0	20.0	15.0	10.0	7.5	5.0	2.5
	9	33.3	27.8	22.2	16.7	11.1	8.3	5.6	2.8
	8	37.5	31.3	25.0	18.8	12.5	9.4	6.3	3.1
	7	42.9	35.7	28.6	21.4	14.3	10.7	7.1	3.6
	6	50.0	41.7	33.3	25.0	16.7	12.5	8.3	4.2
	5	60.0	50.0	40.0	30.0	20.0	15.0	10.0	5.0

3.14.2.6 T4 Ligation

T4 ligations were performed according to manufacturer's instructions with minor changes to their protocol. All reactions were performed at half scale—10 µL instead of 20 µL —using fragments derived from restriction enzymes that generate sticky ends. The reactions were incubated at 25 °C for 30 minutes, 65 °C for 10 minutes, and 0 °C for 5 minutes. Then 2 µL of the reaction was promptly used to transform *E. coli* cells by the typical method.

3.14.2.7 Site-Directed Mutagenesis

Primers were designed using the NEBaseChanger v1.2.9, (available at nebasechanger.neb.com). Samples were amplified using Q5 polymerase as per the manufacturer's provided method, but with 30 amplification cycles instead of 25 amplification cycles. The kinase, ligase, and DpnI (KLD) treatment step was performed with a final volume of 5 µL instead of 10 µL. The entire KLD-treated sample was used to transform *E coli* cells by the typical method.

3.14.3 Mammalian Cell Culture

3.14.3.1 General Information

All mammalian cell culture was carried out in a biosafety cabinet using appropriate sterile technique. Cells were counted using a Bio-Rad TC20 cell counter. Adherent cells were detached with TrypLE. Cells were split when cultures reached >90% confluence for adherent cells or when the concentration exceeded 1.5 x 10^6 cells/mL for suspension cells. Antibiotics were not used routinely. All cell culture media consisted of 10% FBS in DMEM. Cells were tested for mycoplasma every 6 months.

3.14.3.2 Lentivirus Production

HEK-293T cells were grown to approximately 90% confluence in a 10-cm dish coated with poly-L-lysine to prevent detachment of cells. Plasmids were diluted to 250 µL in OptiMEM so that the final solution contained 8 µg pMD2.G, 18 µg pCMV-d8.2 dvpr, and 12 µg of the GOI-containing vector plasmid. A polyethyleneimine solution (114 µL of 1 µg/µL) is diluted to 250 µL using OptiMEM. The plasmid and PEI solutions are then combined and gently mixed and left to incubate at room temperature for 30 minutes. The solution is gently pipetted carefully across the whole surface of the plate and the plate was gently rocked side-to-side to mix. Conditioned media was collected at 24-hour intervals for 3 days, concentrated using a 100 kMW Amicon spin filter and frozen at -80 °C if not used immediately.

3.14.3.3 Lentiviral Transduction

A desired quantity of lentivirus concentrate was diluted in DMEM +10% FBS containing 8 µg/mL polybrene. K562 cells were centrifuged, washed once with HBSS, and resuspended with the cell culture medium containing lentivirus and polybrene to a final concentration of 2x10^5

cells/mL. 2 mL of this cell suspension was added to a well in a 6-well plate. The plate was sealed in two zipper-top bags and centrifuged in a pre-warmed swinging bucket centrifuge for 90 min at 33 °C at 1000 RCF. After incubating the plate for 24 hours at standard cell culture conditions, the medium was replaced with fresh cell culture medium and the cells were cultured as usual, splitting when the concentration exceeded $1x10^6$ cells/mL. After approximately 1 week, the cells were sorted to retain GFP-positive cells by flow-assisted cell sorting.

3.14.3.4 Cell Sorting

Cells to be sorted were detached using Accutase instead of TrypLE. The detachment was halted by addition of an excess of HBSS or PBS. The cells were pelleted by centrifugation. The supernatant was removed and the cells were washed 3 times with sort buffer (0.5% (w/v) BSA, and 25 mM HEPES in pH 7 PBS). The cell suspension was passed through a 40 µm cell strainer to produce a single-cell suspension. The cells were counted and then diluted to a final concentration of 3 to 7 million cells/mL.

Cells were sorted as the experiment needed using a BD Influx cell sorter (BD Biosciences, San Jose, CA) by staff at the UCSD Human Embryonic Stem Cell Core Facility at Sanford Consortium for Regenerative Medicine (La Jolla, CA). After sorting, they were re-plated at the desired concentration in 50% conditioned medium / 50% fresh medium with Primocin at a final concentration of 100 µg/mL. The Primocin is maintained in culture medium of sorted cells for at least 1 week after sorting to ensure the cells do not become contaminated.

3.14.3.5 Sleeping Beauty Transduction and Selection

HEK-293T cells were plated in poly-L-lysine-coated 24-well plates and grown until ~90% confluent in 500 µL of medium. Typically, 475 ng of transposon plasmid and 25 ng of pSB100X were diluted to 50 µL with Opti-MEM medium. 1.5 µL of Lipofectamine 2000 was added to 50

µL of Opti-MEM. The Lipofectamine 2000 and DNA solutions were mixed gently with a pipette tip and incubated at room temperature for 30 minutes. The prepared DNA lipoplexes were carefully pipetted over the surface of each well and the plate was gently rocked side to side to mix. The cells were left to grow for 24 hours in the incubator.

The next day, cells were inspected on the microscope to check for presence of the fluorescent reporter from the Sleeping Beauty transposon plasmid. If strong fluorescence was not observed, the cells are incubated for an additional 24 hours before re-inspecting. If strong fluorescence was not observed after 48 hours, the cells were discarded, and the transduction was repeated. Once strong fluorescence was observed, the culture was split to a 12-well plate well in 1 mL of medium containing puromycin, blasticidin, or hygromycin at the concentrations shown in **Table 3.11**. Approximately every 3 days, the selection antibiotic concentrations were increased to concentrations shown in the same table. Once the final concentration was reached, the selection antibiotics were maintained for a further 14 days. During this time, the cells populations were expanded and aliquots were frozen on day 14 upon cessation of antibiotic use.

Table 3.9: Antibiotic Selection Concentrations

Approximate Day	[Puromycin] (µg/mL)	[Blasticidin S] (µg/mL)	[Hygromycin] (µg/mL)
1	0.5	7.5	62.5
4	1.0	15.0	125.0
7	1.5	22.5	187.5
10	2.0	30.0	250.0

To transduce cells with two plasmids, the same process is carried out except the initial transduction includes two plasmids instead of one. In this case, the total quantity of DNA and lipofectamine were increased to 750 ng and 2.25 µL, respectively. The initial selection was started at the lowest listed concentration of each antibiotic, but the concentration was only increased when

it was visually evident that there were enough cells to continue the selection. The single-selection antibiotic schedule is too aggressive for a double selection.

3.14.3.5 RNA Extraction and Isolation

Cells were grown on a poly-L-lysine-coated 24-well plate for 72 hours at varying ratios of target (K562-GFP) and reporter cells (LaG17-synNotch-TetRVP64 / TRE mCherry-P2A-CCS1). At the end of the experiment the culture medium was removed and the cells were washed 3 times with HBSS. 300 µL of TRIzol was added to each well, gently pipetting the viscous solution to help distribute the TRIzol across the cells. It was left to sit for 5 minutes and then recovered from the wells. The TRIzol extract was centrifuged for 2 minutes at 10,000 RCF to pellet any cell debris and 250 µL of it was transferred to a new tube with an equal volume of ethanol.

The Direct-zol RNA Mini Prep kit (Zymo Research, Irvine, CA) was used to purify the RNA according to manufacturer's instructions. The optional DNAse I digestion step was performed. The purified RNA was eluted in 25 µL of water.

3.14.3.6 Enzyme Substrate Activity Assay

Cells that constitutively expressed the various xanthine methylating enzymes were all screened in the same fashion. Cells (0.5 mL of $2x10^5$ cells/mL) in standard medium were added to each well of a poly-l-lysine-coated 12-well plate. After 24 hours, 1 mL of 300 µM of one of the enzyme substrates was added to each well (final volume = 1.5 mL). These were incubated for 72 hours under standard conditions in a cell culture incubator. At 72h, the cell medium supernatant was removed in its entirety from each well and transferred to a pre-weighed sample tube. The tube was weighed, and its weight was recorded. The tubes are centrifuged for 2 minutes at 16,000 x RCF and 30 µL used for HPLC analysis. Metabolite peaks on the chromatogram from the diode array detector at 272 nm are positively identified by comparison with known standards. The peaks

are integrated and the concentration is determined using a calibration curve of known concentrations for each substance. The concentration is then scaled to what the concentration would have been without evaporation (i.e. it is multiplied by ratio of the masses of unevaporated medium to recovered medium). This is necessary because evaporation across the wells of a 12-well plate is much greater at wells that are closer to the outer edge of the plate and can distort results otherwise.

Table 3.10: Plating Diagram for Enzyme Substrate Activity Assay in a 12-Well Plate

200 µM X	200 µM XR	200 µM 1X	Variable
200 µM 3X	200 µM 7X	200 µM 37X	Variable
200 µM 13X	200 µM 17X	200 µM CTRL	Variable

3.14.3.7 Juxtacrine Signalling-Induced Expression of Caffeine Synthesis Enzymes

For all experiments, HEK-293T cells were doubly transduced (via Sleeping Beauty, as per usual) with pSBBi-P LaG17-synNotch-TetRVP64 and pSBTRE-GB mCherry-P2A-CCS1 (or the equivalent MXMT/TCS1 plasmid) and selected with blasticidin and puromycin, as described previously. These cells are referred to hereafter as reporter cells. The reporter cells were plated at an areal density of 40,000 cells/cm^2 with a culture medium volume to surface area ratio of 1 mL/5 cm^2, e.g. a T-25 flask would have 1 million reporter cells seeded and 5 mL of culture medium added. A relevant methylxanthine (1,7-dimethylxanthine for TCS1 and CCS1 and 7-methylxanthine for MXMT) was included at 200 µM. Target cells, K562 expressing surface GFP, were seeded simultaneously at any desired ratios. This plating scheme can be scaled for 24-well plates, 12-well plates, and T-25 flasks easily. The cell culture medium is harvested at 72 hours and

is analyzed by the typical method with HPLC. For qPCR experiments, RNA is extracted by the method in **Section 3.14.3.7**.

3.14.3.8 Verification of 7X Production by TCS2/CaXMT1 by Co-Culture

3.14.4 LaG17 Protein Production and Purification

BL21(DE3) competent *E. coli* cells (New England Biolabs, Ipswich, MA) were transformed with pET11-A+ eLaG17_(GSK)3_PP_Hisx6 by the standard heat shock method and grown on kanamycin-containing agar plates. A single colony was picked and grown overnight in a 10 mL starter culture while shaking at 37 °C. The next day, this was used to inoculate 1 L of LB which was grown at 37 °C with shaking. When this culture reached 0.6 OD_{600}, it was cooled in an ice water bath and IPTG was added to a final concentration of 1 mM to induce protein expression. It was then shaken for a further 20 h at 18 °C.

After 20 h, the culture was centrifuged at 5000 x RCF in a Beckman Coulter Avanti JXN-26 with a JLA-8.10000 rotor for 30 minutes at 4 °C to pellet the *E. coli* cells. The supernatant was decanted and the pellet was transferred to a 50 mL tube and frozen at -80 °C overnight. The next day, the pellet was resuspended in ice cold 10 mL of wash buffer (pH 8, 25 mM imidazole, 100 mM NaCl, 50 mM Tris-HCl, 5% (v/v) glycerol) containing 1 mM PMSF. While on ice, the suspension was sonicated for four times using a Branson Sonifier probe sonicator. Each cycle consisted of 30s sonication followed by a 90s delay. The duty cycle was set at 40% and the output control was set to 4. The bacterial lysate was centrifuged for 30 min at 10,000 x RCF and 4 °C to pellet cell debris. The supernatant was carefully removed and added to a tube containing 0.5 mL HisPur NiNTA Resin (Thermo Fisher Scientific, Waltham, MA) that had been washed and equilibrated with wash buffer, as per manufacturer instructions. The lysate supernatant was gently

inverted with the resin in a tube overnight at 4 °C to allow the His-tagged protein to bind to the resin.

After incubation, the resin and lysate supernatant solution was transferred to a spin column and centrifuged at 700 x RCF. The sample was washed 3 times with 1 mL of wash buffer, and then eluted successively with three 0.5 mL portions of wash buffer with 250 mM imidazole and one 0.5 mL portion of wash buffer with 500 mM imidazole. Samples of the washes and elutions were checked via SDS-PAGE to determine if they contained the desired protein.

The elution fractions were combined and concentrated using a 3 kDa molecular weight cutoff microcentrifuge filter. The buffer was exchanged to 1X PBS with 1 mM DTT using the same filter. 0.1 mg of His-tagged Precission Protease (a gift from the Partho Ghosh Lab) was added and the volume was brought up to 1 mL. The sample was gently tumbled overnight at 4 °C. The next morning, the buffer was exchanged to 1X PBS using a 3 kDa molecular weight cutoff microcentrifuge filter. The sample was tumbled with 0.2 mL of His resin (washed and equilibrated with 1X PBS) for two hours at 4 °C. It was then washed 3 times with PBS (0.4 mL each). This column was not eluted with a high concentration of imidazole so that the His-tagged Precission protease and any uncleaved LaG17 would remain bound. The elution fractions were combined, and protein concentration was determined by UV-Vis using a calculated extinction coefficient determined by the ExPASy ProtParam tool.[171]

3.14.5 LaG17 Labeling with BG-GLA-NHS

To 250 µL of a 1.56 mg/mL (102 µM) LaG17 solution, 2.3 µL of an 85% pure 10 mg/mL BG-GLA-NHS in DMSO was added. This corresponds to 1.5 eq. BG-GLA-NHS per LaG17. The reaction was tumbled overnight at 4 °C, concentrated via spin dialysis with a 3K MWCO filter, and resuspended in sterile PBS.

3.14.6 Microscopy

Epifluorescence microscopy imaging for coculture experiments was performed on an Axio Observer D1 inverted microscope (Carl Zeiss Microscopy, GmbH, Germany) with an Axiocam MRm camera (Carl Zeiss, Microscopy, GmbH, Germany) and an HBO-100 mercury arc lamp epifluorescence source (Carl Zeiss Microscopy, GmbH, Germany). Images were processed using Image J[65] with Fiji.[66] Microscopy images shown in a given figure are window-leveled in the same manner as one another.

3.14.7 Liquid Chromatography

Reverse phase high performance liquid chromatography (HPLC) and liquid chromatography with mass spectrometry (LCMS) were performed on an Agilent Infinity 1260 series (Santa Clara, CA) with diode-array detector (DAD) and a single quad mass spectrometer. An Agilent Polaris 5 C18-A column (180Å, 4.6 x 250 mm, 5 µm) or Polaris 5 C18-A (180Å, 10.0 x 250 mm, 5 µm) were used for all separations involving xanthine derivatives. The standard gradient conditions used can be found in the **Table 3.13**, but this method was modified as needed to account for degrading column conditions when necessary. For example, the solvent composition may be held at 83% water for an extended duration to allow for all peaks to fully elute before the acetonitrile concentration is increased. All quantifications were performed by integrating chromatogram peaks from absorbance at 272 nm and calculating the concentration of the substance using a linear regression obtained from a standard curve of known concentrations.

Reverse-phase HPLC purification was performed using an Agilent 1100 series Infinity HPLC and an Agilent Zorbax SB-C18 semi-prep column (ID 9.4 x 250 mm, 5 µm, 80 Å) using a water/acetonitrile gradient containing 0.1% trifluoroacetic acid using a variable wavelength detector wavelength of 280 nm.

Given the sample composition has a high ionic content, future revisions of the above method would likely use buffer solvents A and B instead of pure solvents.

Table 3.11: Generic HPLC method for separation of xanthines

Time (min)	% Solvent A (H_2O + 0.1% TFA)	% Solvent B (ACN + 0.1% TFA)
0	92	8
14	83	17
16	5	95
20	5	95
27.5	92	8
36	92	8

3.14.8 Synthesis of BG-GLA

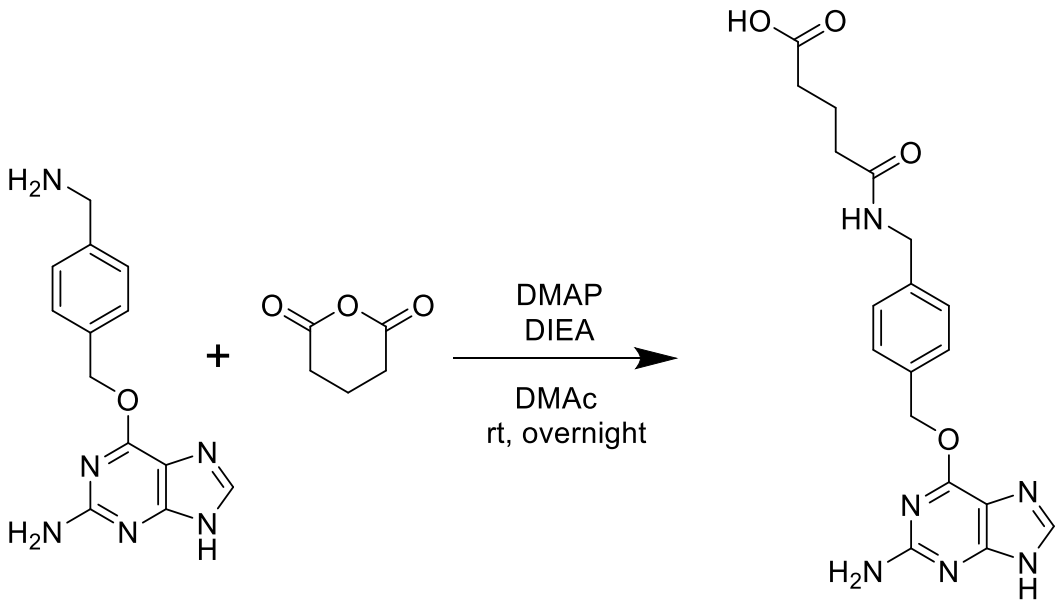

Scheme 3.5 Synthesis of BG-GLA

Adapting a previously published protocol,[172] 6-((4-(aminomethyl)benzyl)oxy)-7*H*-purin-2-amine (BG) (50.0 mg, 185 µmol, 1 eq.) and 1.2 mL of dimethylacetamide were added to a nitrogen-flushed 1-dram vial equipped with a stir bar. The sample was heated to 80 °C for 5

minutes with stirring to fully dissolve the BG. The sample was allowed to cool to room temperature. DMAP (10.0 mg, 81.9 µmol, 0.44 eq.) and DIEA (32.0 µL, 184 µmol, 1 eq.) were added to the reaction and it was left to stir overnight at room temperature. The reaction was added to a 15 mL of DI water using a Pasteur pipette and the pH was brought to ~4-5 using 1 M HCl. This caused a white precipitate to form. The precipitate was collected by gravity filtration through a filter paper and was dried under a high vacuum. It was used without any further purification. Yield: 52% (37.0 mg, 96.3 µmol). MS (ESI) m/2z $[M-2H]^-$ calc 1597.06; found 1597.65. HPLC (ELSD) Eclipse Plus C8 4.6 x 50mm 3.5 µm / H_2O:MeOH / 0-15min 5%-95% MeOH, 15-22min 95% MeOH.

3.14.9 Synthesis of BG-GLA-NHS

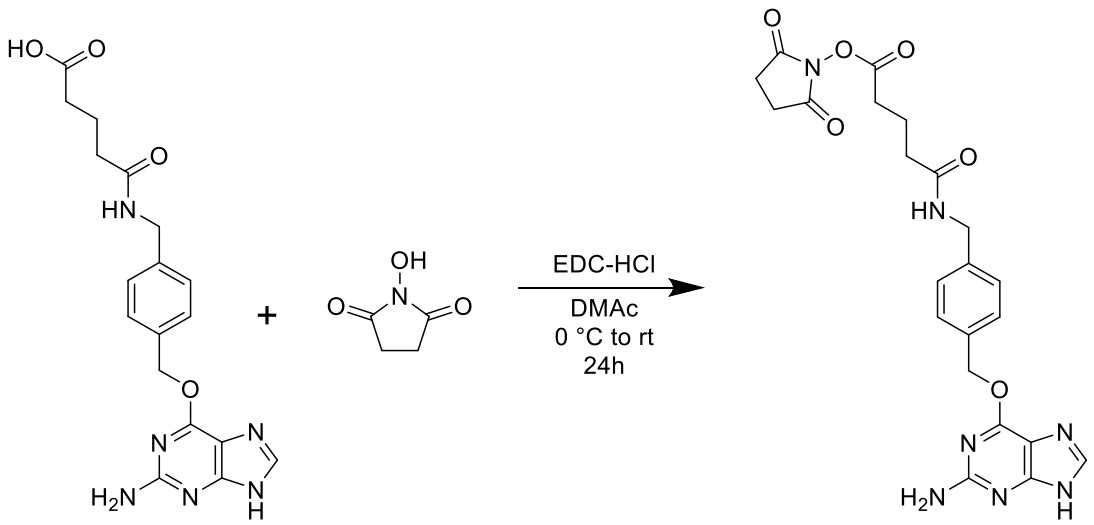

Scheme 3.6 Synthesis of BG-GLA-NHS

Adapting a previously published method,[172] BG-GLA (37.0 mg, 96.3 µmol, 1 eq.) was dissolved in 3.2 mL DMAc in a 2-dram vial equipped with a stir bar and cooled to 0 °C in an ice bath. N-hydroxysuccinimide (13.4 mg, 116 µmol 1.2 eq.) and N-ethyl-N′-(3-

dimethylaminopropyl)carbodiimide hydrochloride (EDC-HCl) (33.0 mg, 172 µmol, 1.8 eq.) were added, with the excess of EDC-HCl being added to compensate for the slightly degraded quality of the reagent. The reaction was allowed to warm to room temperature and was stirred for 24 hours. The reaction was poured into 180 mL of diethyl ether which caused formation of a precipitate. The ether was transferred to six 50-mL centrifuge tubes which were centrifuged at 5000 rcf for 15 min at 4 °C to pellet all of the precipitate residue that coated the sides of the tube. The diethyl ether was decanted off and the pellets from each were removed with a spatula and transferred to a single tube. The tube was centrifuged as before and the pellet was removed with a spatula and transferred to a new tube. HPLC analysis showed sufficiently high purity (~85%), as estimated via integration of the A^{280} absorbance peaks, for its intended use. As such, the product was used without further purification. It was dissolved in DMF and aliquots were stored at -80 °C. Recovered Yield: 86% (40.0 mg, 86.3 µmol), Estimated Product Yield: 71% (34 mg, 71 µmol) Eclipse Plus C8 4.6 x 50 mm 3.5 µm / H_2O:MeOH / 0 min 50% MeOH, 15-22 min MeOH.

3.14.10 Synthesis of BG-Biotin

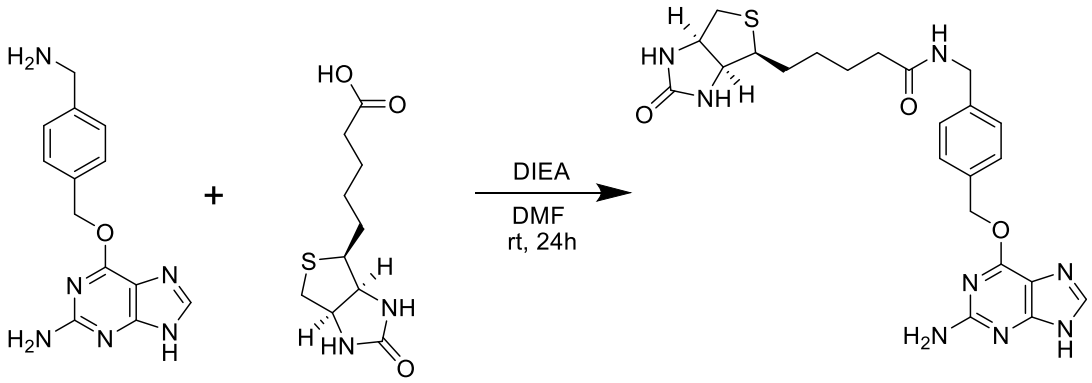

Scheme 3.7 Synthesis of BG-Biotin

6-((4-(aminomethyl)benzyl)oxy)-7*H*-purin-2-amine (11.5 mg, 42.5 µmol, 2.9 eq.), biotinyl N-hydroxysuccinimide ester (5.00 mg, 14.6 µmol, 1 eq.), and DIEA (12.75 µL, 73.2 µmol, 5.0 eq.) were added to 1 mL of anhydrous DMF in a 1-dram vial equipped with a stir bar. The reaction was stirred for 24 hours at room temperature. The solvent was removed under reduced pressure, taken up in methanol and purified by semi-preparative HPLC (DAD at 280 nm) Eclipse Plus C8 4.6 x 50 mm 3.5 µm / H_2O:MeOH / 0 min 50% MeOH, 15-22 min MeOH. Recovered Yield: 81% (5.87 mg, 11.8 µmol) solid. MS (ESI) 2m/z: $[M+H]^{2+}$ calc 249.11; found 294.2.

3.14.19 Synthesis of BG-PEG4-Biotin

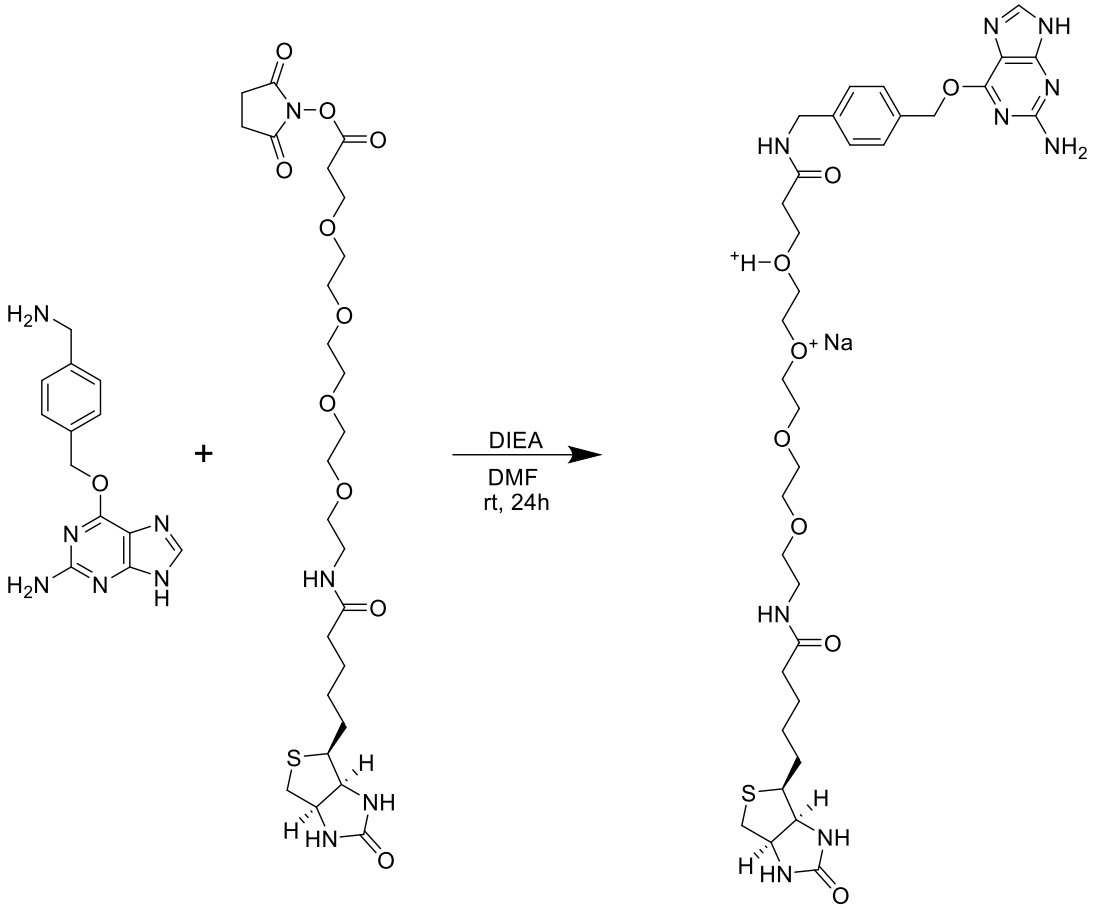

Scheme 3.8 Synthesis of BG-PEG4-Biotin

6-((4-(aminomethyl)benzyl)oxy)-7*H*-purin-2-amine (16.6 mg, 61.4 µmol, 2.4 eq.), biotin-PEG4-N-hydroxysuccinimide ester (15.0 mg, 25.5 µmol, 1 eq.), and DIEA (18.75 µL, 107.6 µmol, 4.2 eq.) were added to 1 mL of anhydrous DMSO in a scintillation vial equipped with a stir bar. The reaction was stirred for 24 hours at room temperature. The solvent was removed by heating under a high vacuum until dry. The residue was taken up in methanol and purified by semi-preparative HPLC (DAD at 280 nm) Eclipse Plus C8 4.6 x 50 mm 3.5 µm / H_2O:MeOH / 0 min 50% MeOH, 15-22 min MeOH. Recovered Yield: 64% (12.23 mg, 16.4 µmol). solid. MS (ESI) m/2z $[M+2H]^{2+}$ calc 372.68; found 372.8.

3.14.20 Reverse Transcriptase-qPCR Analysis of Induced CCS1 Expression

3.14.20.1 Induced CCS1 Expression

By the method in **3.14.3.7**, CCS1 reporter cells were grown with a target cell:receptor cell ratios of 0:1, 0.25:1, 0.5:1, 1:1, and 1.5:1 in a 24-well plate. RNA was harvested at 72 h.

3.14.20.2 qPCR Protocol

Primers for qPCR were chosen by entering the whole gene of interest into PRIMER-BLAST[173] and using a maximum primer length of 150 bp. The reverse transcriptase primer was chosen by selecting a primer which overlapped with the last 2-5 bp of the GOI and ended in a G or a C which had a melting temperature of approximately 55 °C.

Samples were prepared according to **Table 3.9** and **Table 3.10**. Reverse transcription was carried out at 50 °C for 45 minutes, followed by inactivation at 85 °C for 5 min.

Table 3.12: Reverse Transcription Primer Premix Recipe

Component	Volume
Water	85.0 µL
GOI Primer Stock (100 uM)	7.5 µL
Housekeeping Gene Primer Stock (100 uM)	7.5 µL

Table 3.13: Reverse Transcription Reaction Component Recipe

Component	Volume
RT Primer Premix	1.0 µL
10 mM dNTPs	1.0 µL
RT Buffer	4.0 µL
Maxima H-minus RT	1.0 µL
Murine RNAse Inhibitor	0.5 µL
Purified RNA	1.0 µL
Water	1.5 µL

Table 3.14: qPCR and Reverse Transcriptase Primers Used

Name	Sequence (5′ to 3′)
Notch-Forward	ATCAAGCGCTCTACAGTGGG
Notch-Reverse	ACATTGCCGGTTGTCGATCT
Notch-RT	GAGGATGACTGCACACATTG
CCS1-Forward	ACGACCTGTTCCAGAACGAC
CCS1-Reverse	CGGGGAACAGTCTGCTGTAG
CCS1-RT	GTGCATGGATTCCTCGG

The qPCR plate was prepared such that each well contained 25 µL: 12.5 µL of SYBR Green qPCR Master Mix, 6.25 µL of reverse transcriptase product dilution (10 µL reverse transcriptase product and 52.5 µL water), and 6.25 µL of qPCR primer dilution (7.5 µL of 100 µM forward primer, 7.5 µL of 100 µM reverse primer, and 610 µL water). Three replicates of each condition for each primer set were plated, i.e. 3 replicate samples of of 5 target:receptor cell ratios for two different genes. This was analyzed by qPCR on a Biorad CFX-96 real time PCR thermal cycler to obtain C_T values. C_T values were analyzed by the $2^{-\Delta\Delta CT}$ method[174] using CCS1 as a gene-of-interest and synNotch as a reference gene. Data were plotted as fold-change with error bars as standard deviation of three replicates.

3.15 Supplemental Data

3.15.1 Constitutive Xanthine Methylating Enzyme Expression Plasmid Maps and Notes

Nomenclature: The plasmid backbone is named first followed by the identity of the gene-of-interest inserted into the backbone. Fusions between components are indicated with dashes. Minor insertions, deletions, or mutations are not noted unless they were performed intentionally for specific effect.

Restriction Cloning with SfiI: Directional insertion of DNA into plasmids using SfiI can be easily performed using when distinct 5′ and 3′ SfiI recognition sequences. For simplicity's sake, flanking primers were designed such that they would result in a sequence like that found in **Figure 3.15.**

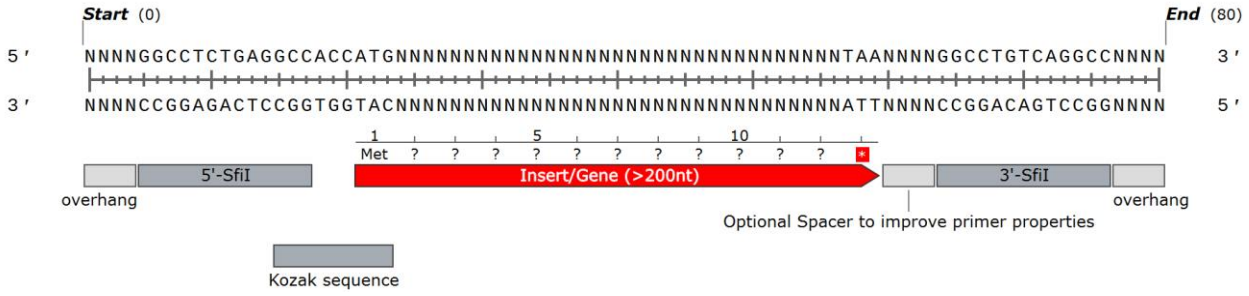

Figure 3.15: Example of 5′ and 3′ SfiI sites and design considerations for restriction cloning primer design

3.15.1.1 pSBBi-GB CaXMT1

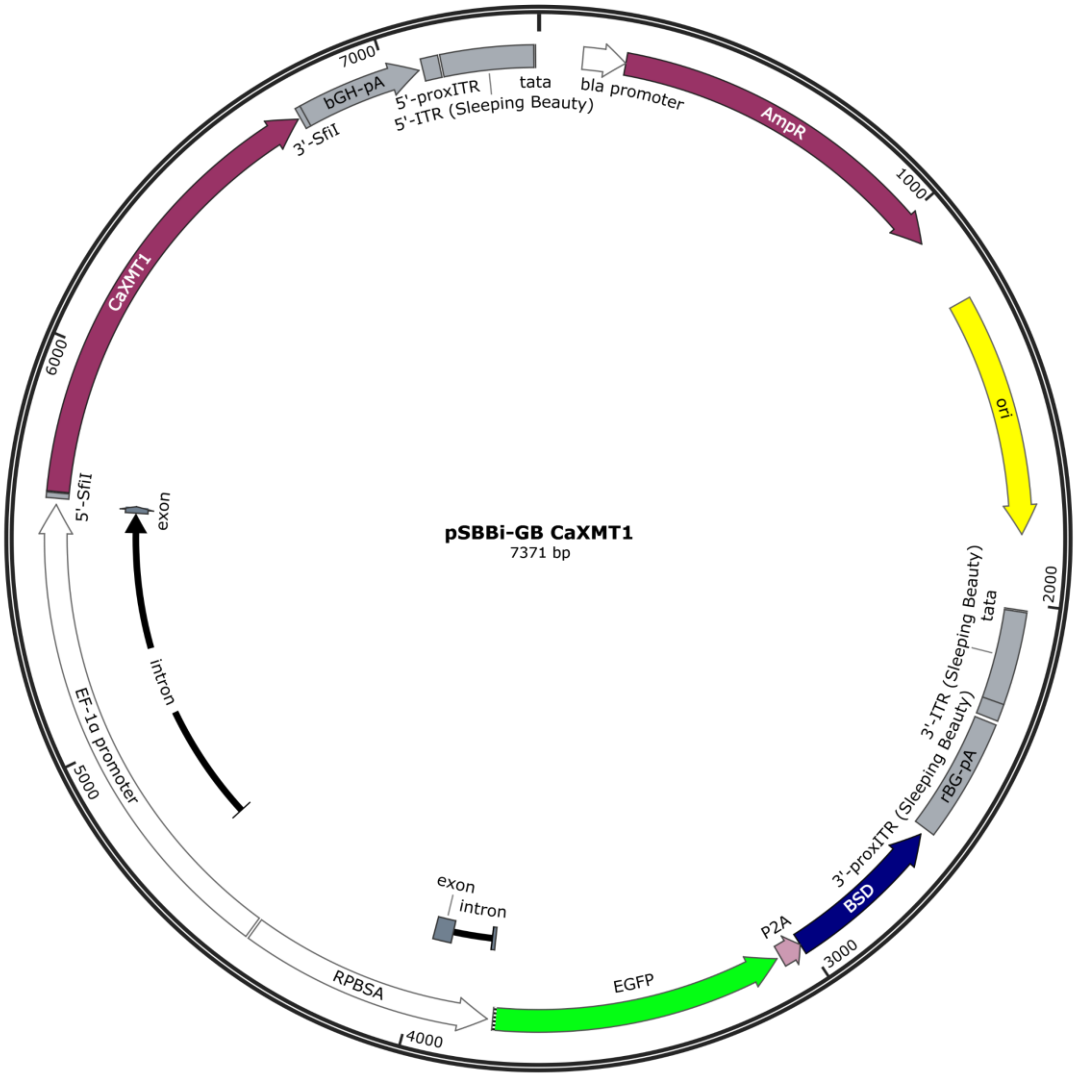

Figure 3.16: Plasmid map for pSBBi-GB CaXMT1 plasmid.

Construction Notes:

CaXMT1 was PCR amplified with flanking primers containing 5′ and 3′ SfiI cut sites. pSBBi-GB and this were each digested with SfiI and ligated with T4 ligase.

3.15.1.2 pSBBi-GB GST-CaXMT1

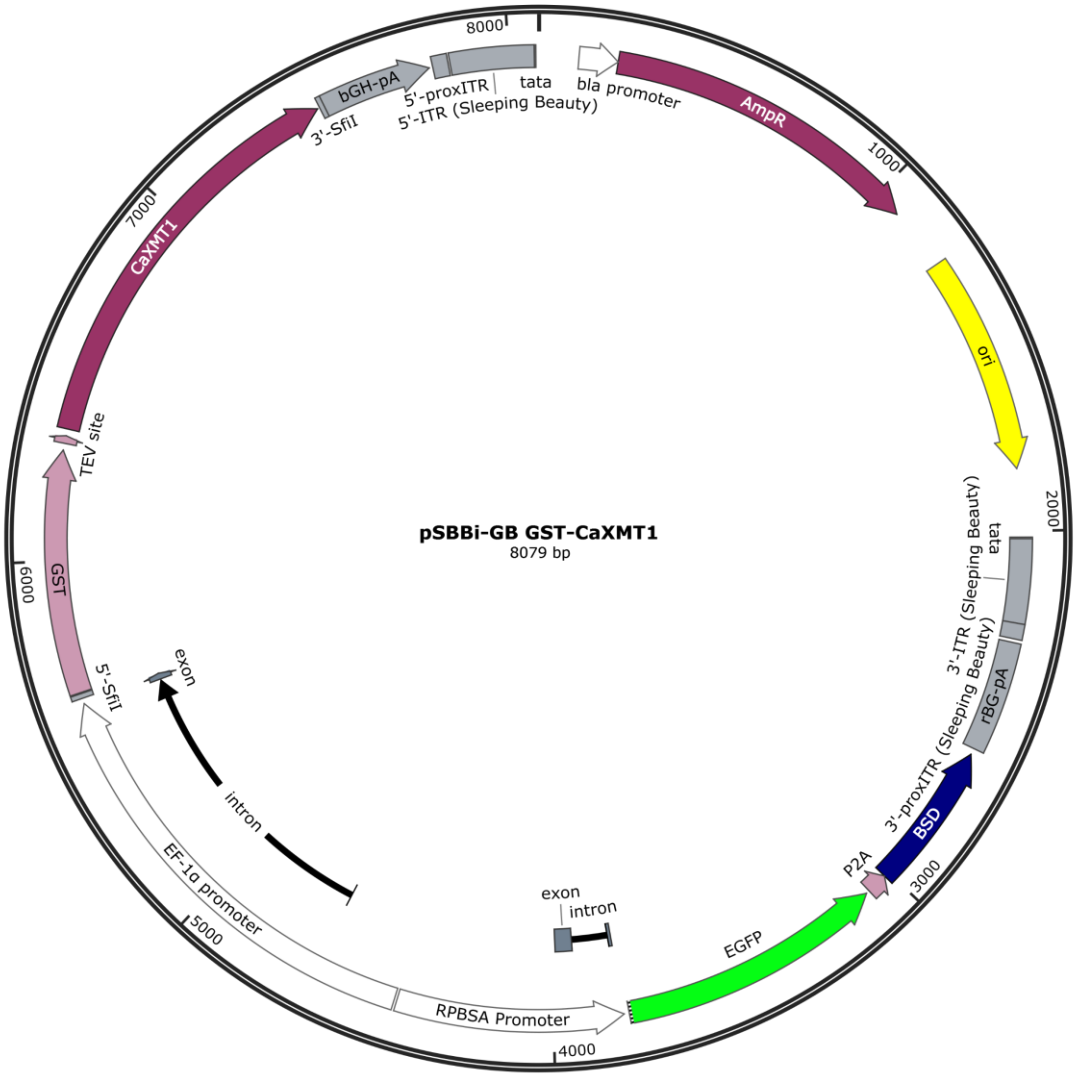

Figure 3.17: Plasmid map for pSBBi-GB GST-CaXMT1

Construction Notes:

This plasmid was constructed by HiFi assembly of N-terminal GST from pACYC-GST with pSBBi-GB CaXMT1

3.15.1.3 pSBBi-GB TCS2

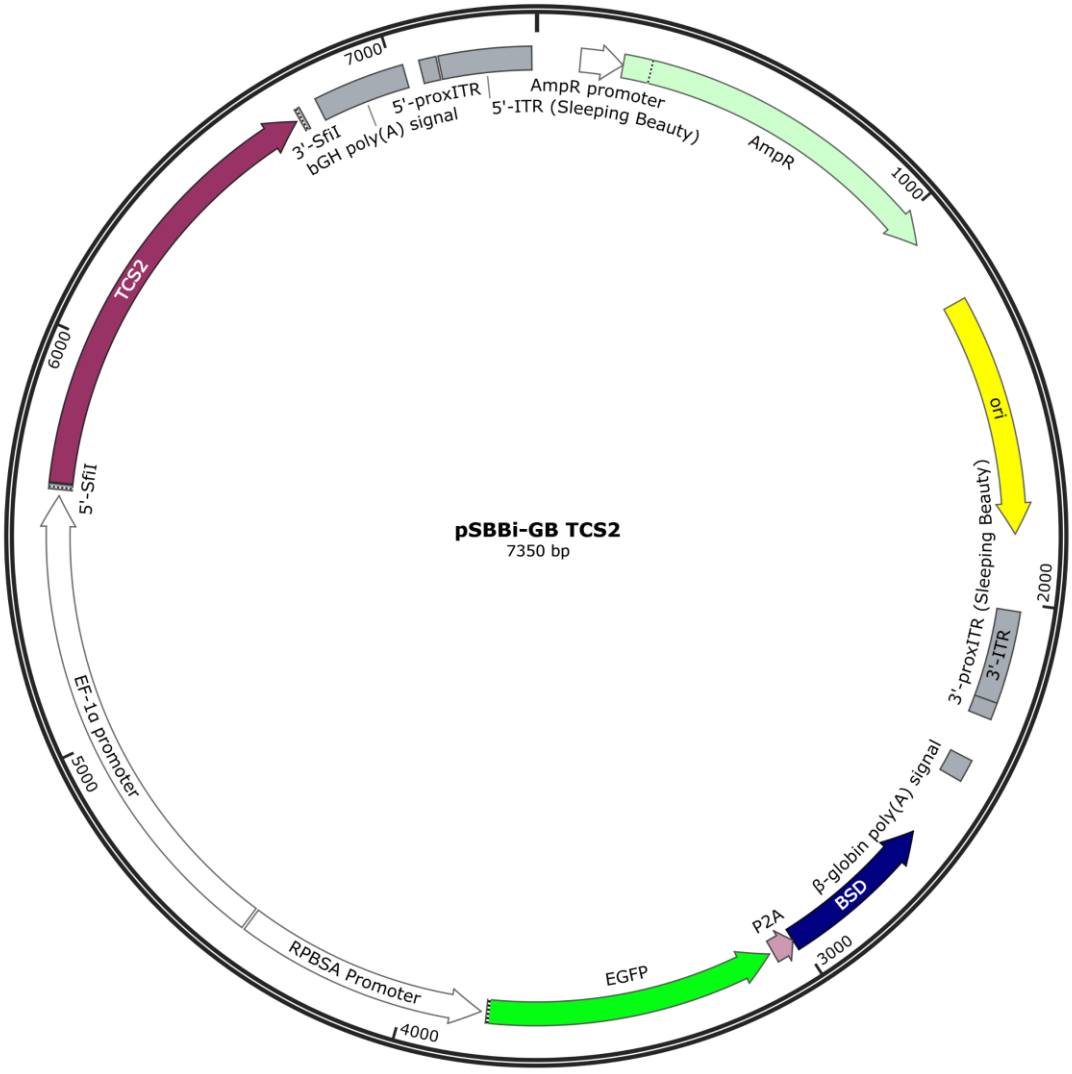

Figure 3.18: Plasmid map for pSBBi-GB TCS2

Construction Notes:

TCS2 was PCR amplified with flanking primers containing 5′ and 3′ SfiI cut sites. pSBBi-GB and this were each digested with SfiI and ligated with T4 ligase.

3.15.1.4 pSBBi-RP CaDXMT

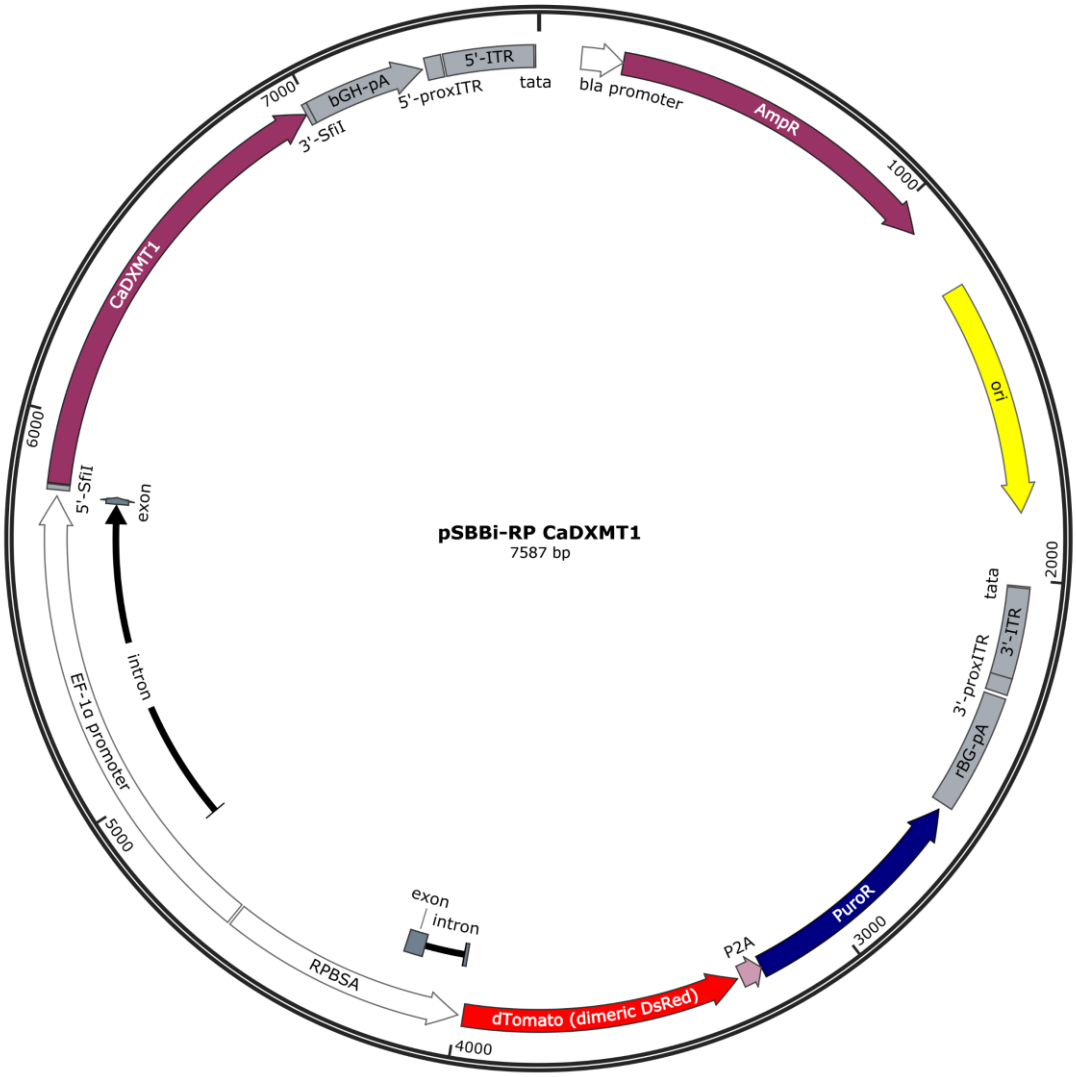

Figure 3.19: Plasmid map for pSBBi-RP CaDXMT

Construction Notes:

CaDXMT was PCR amplified with flanking primers containing 5′ and 3′ SfiI cut sites. pSBBi-RP and this were each digested with SfiI and ligated with T4 ligase.

3.15.1.5 pSBBi-RP CaMXMT

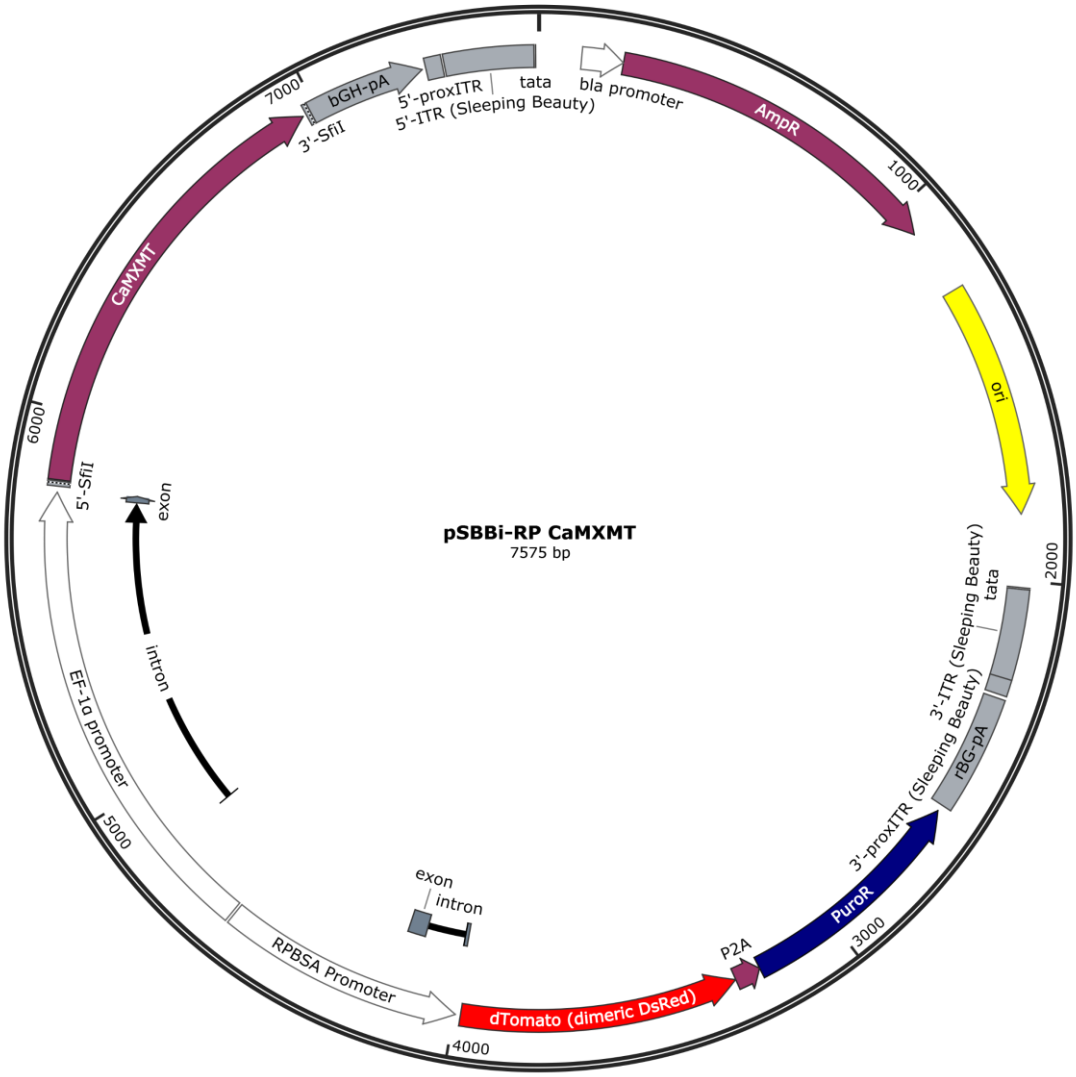

Figure 3.20: Plasmid map for pSBBi-RP CaMXMT

Construction Notes:

CaMXMT was PCR amplified with flanking primers containing 5′ and 3′ SfiI cut sites. pSBBi-RP and this were each digested with SfiI and ligated with T4 ligase.

3.15.1.6 pSBBi-RP CCS1

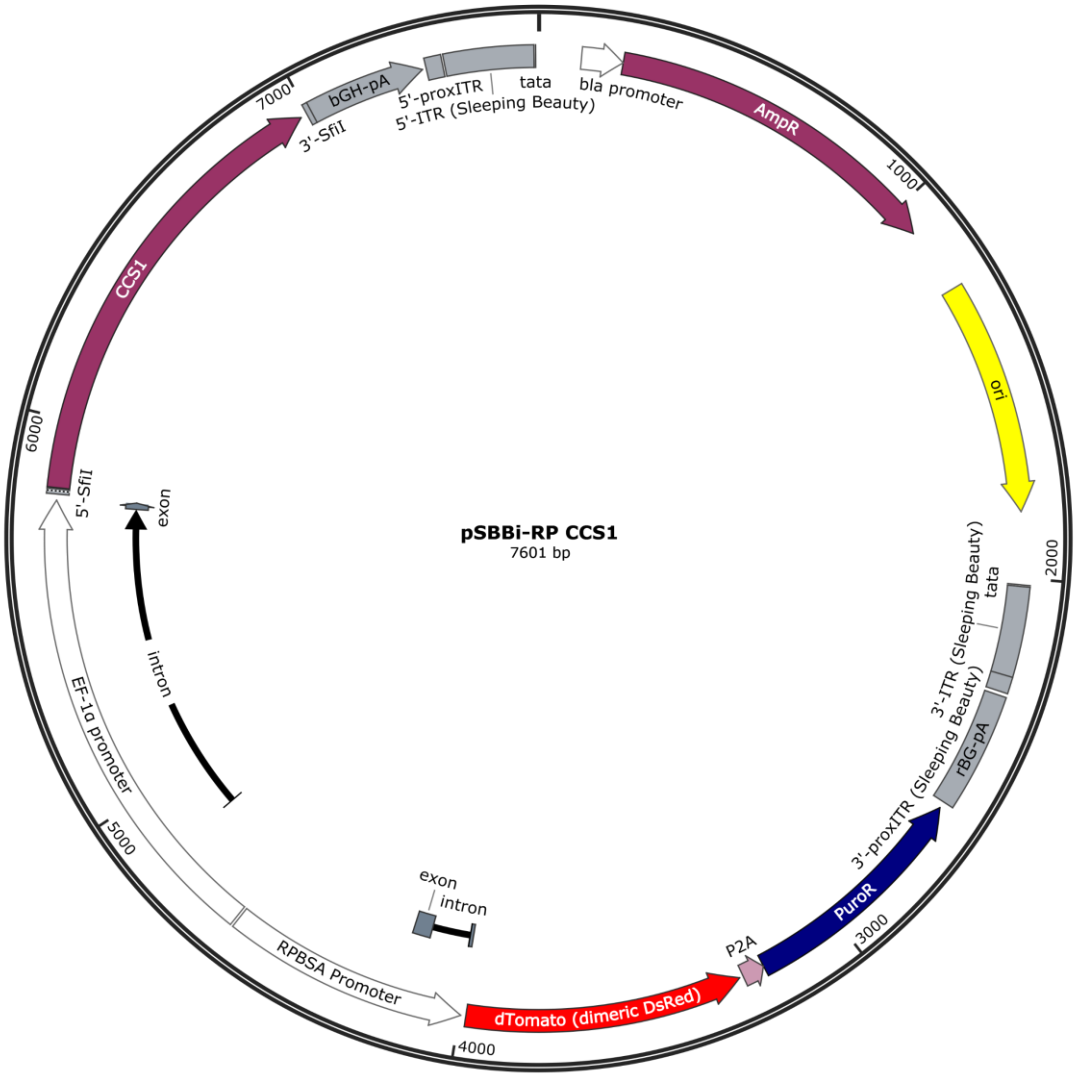

Figure 3.21: Plasmid map for pSBBI-RP CCS1

Construction Notes:

CCS1 was PCR amplified with flanking primers containing 5′ and 3′ SfiI cut sites. pSBBi-RP and this were each digested with SfiI and ligated with T4 ligase.

3.15.1.7 pSBBi-RP CCS1(delC13)

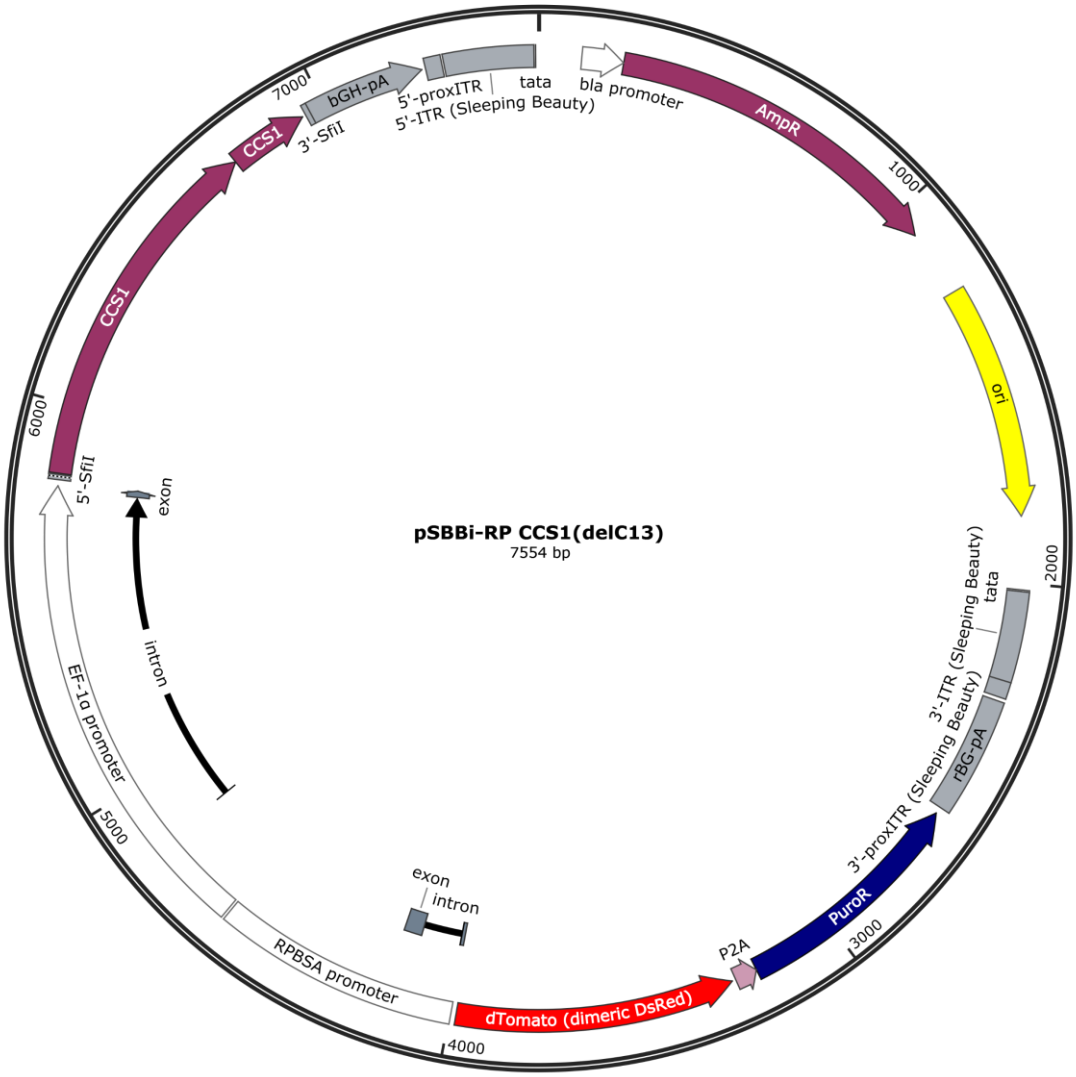

Figure 3.22: Plasmid map for pSBBi-RP CCS1(delC13)

Construction Notes:

CaDXMT1 was PCR amplified with flanking primers containing 5′ and 3′ SfiI cut sites. pSBBi-RP and this were each digested with SfiI and ligated with T4 ligase.

3.15.1.8 pSBBi-RP CsAncCS

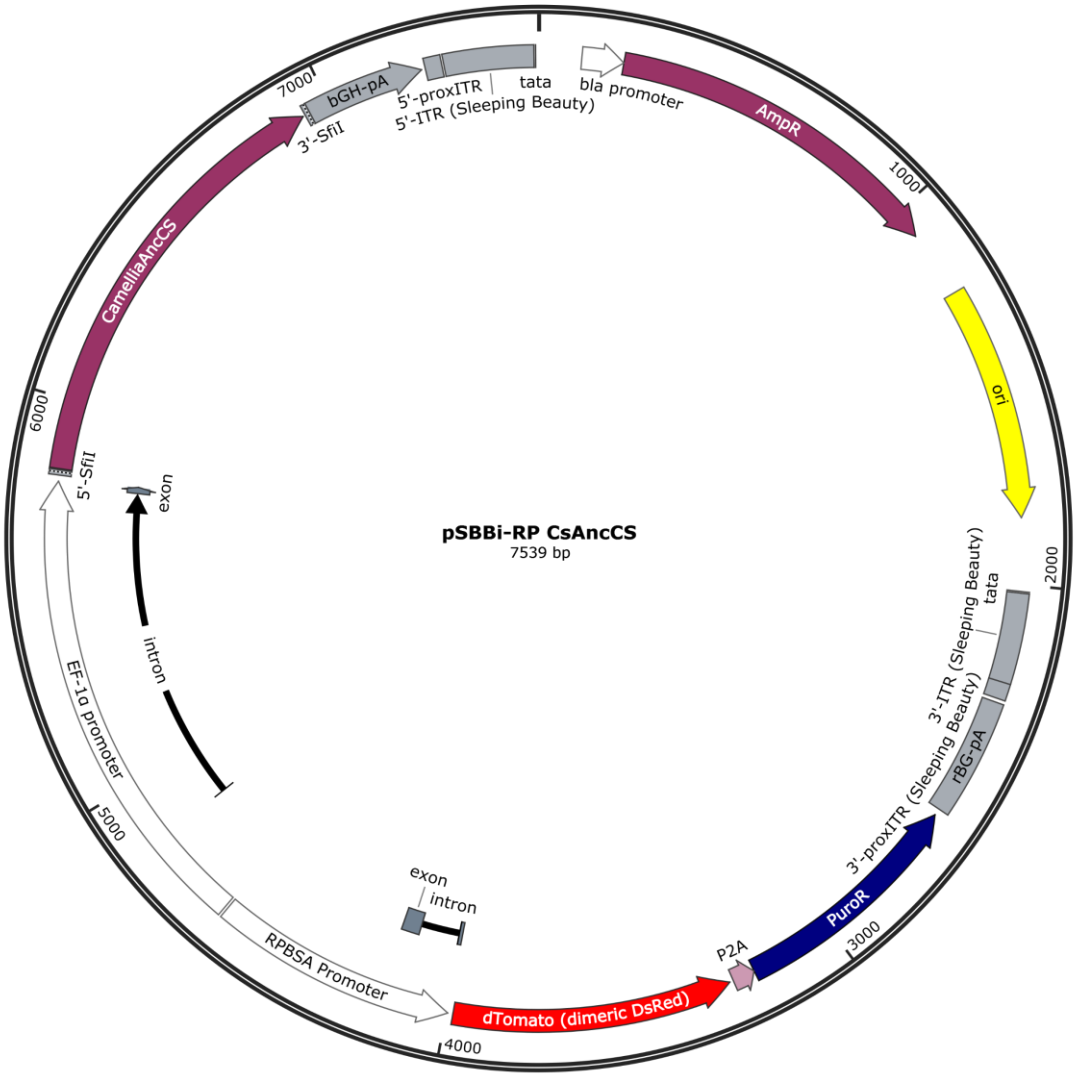

Figure 3.23: Plasmid map for pSBBi-RP CsAncCS

3.15.1.9 pSBBi-RP GST-CCS1

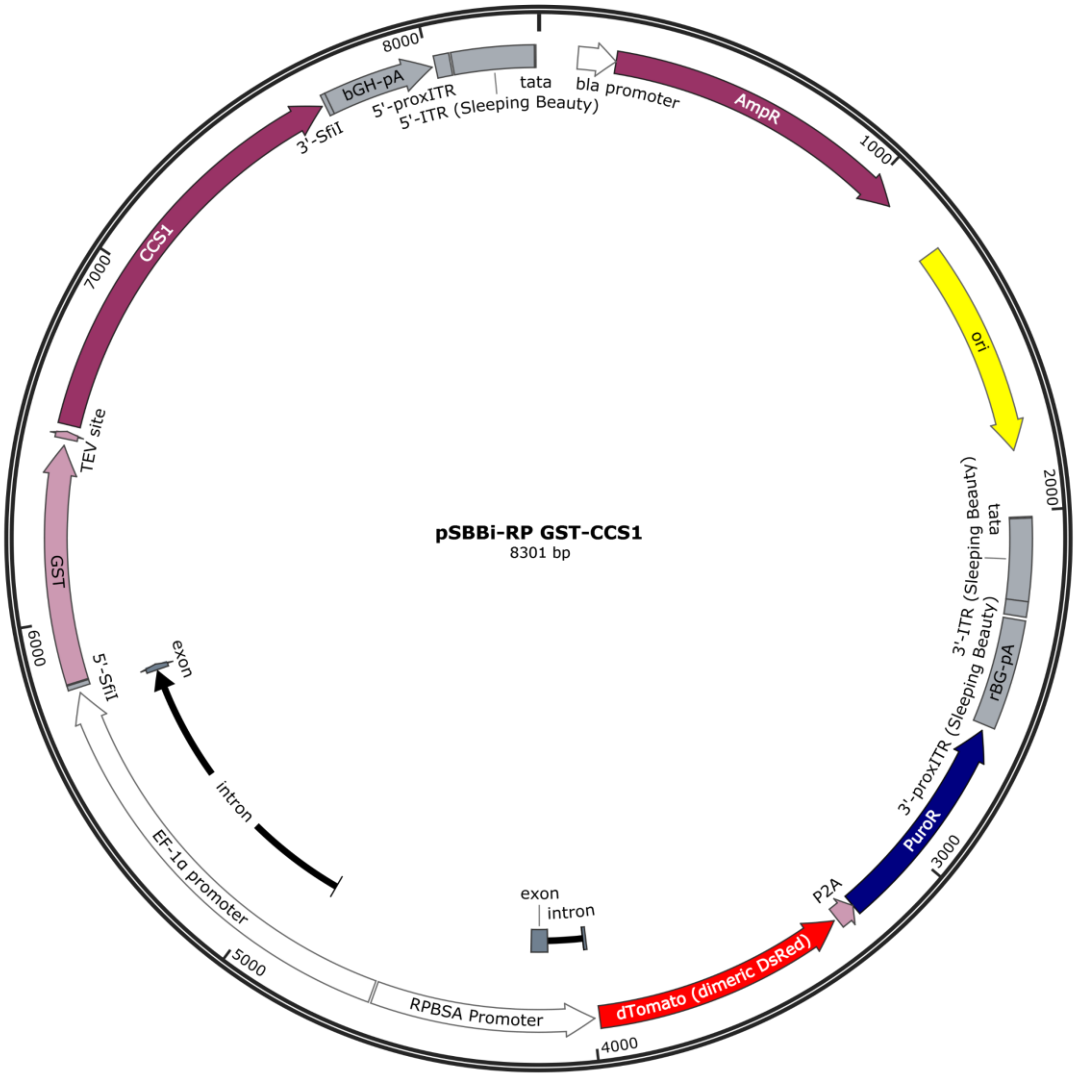

Figure 3.24: Plasmid map for pSBBi-RP GST-CCS1

3.15.1.10 pSBBi-RP GST-CCS1(delC13)

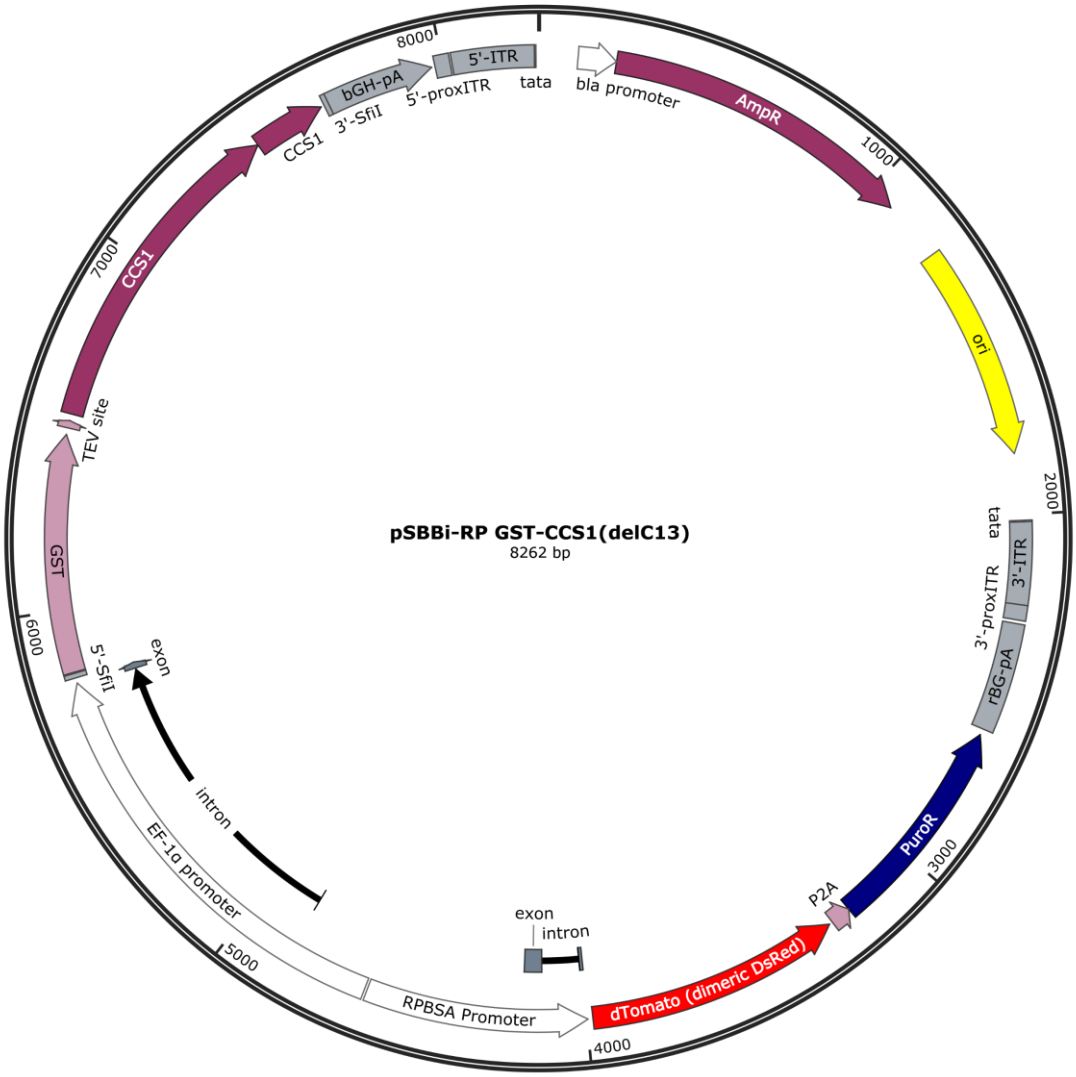

Figure 3.25: Plasmid map for pSBBi-RP GST-CCS1(delC13)

3.15.1.11 pSBBi-RP GST-PcCS

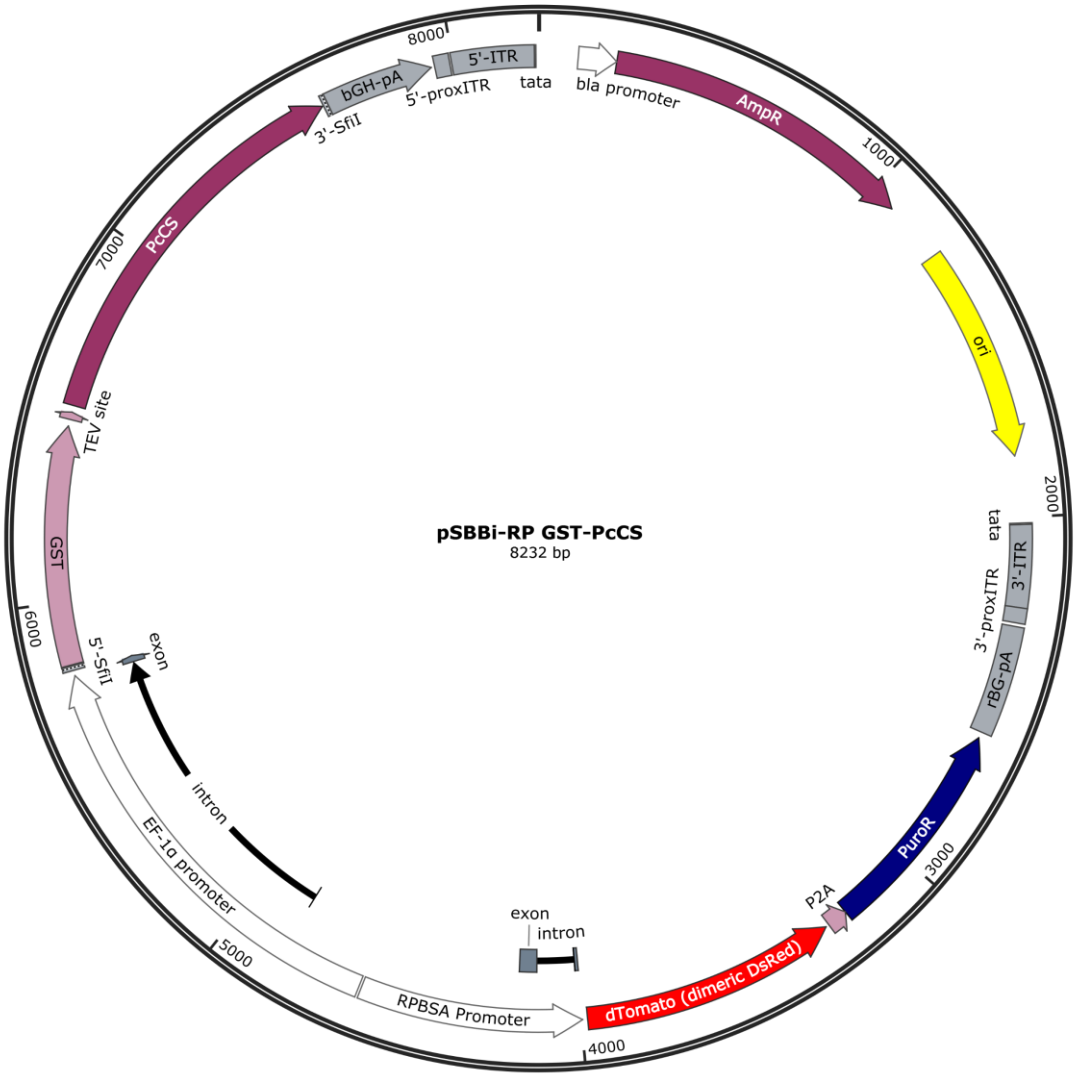

Figure 3.26: Plasmid map for pSBBi-RP GST-PcCS

3.15.1.12 pSBBi-RP GST-TCS1

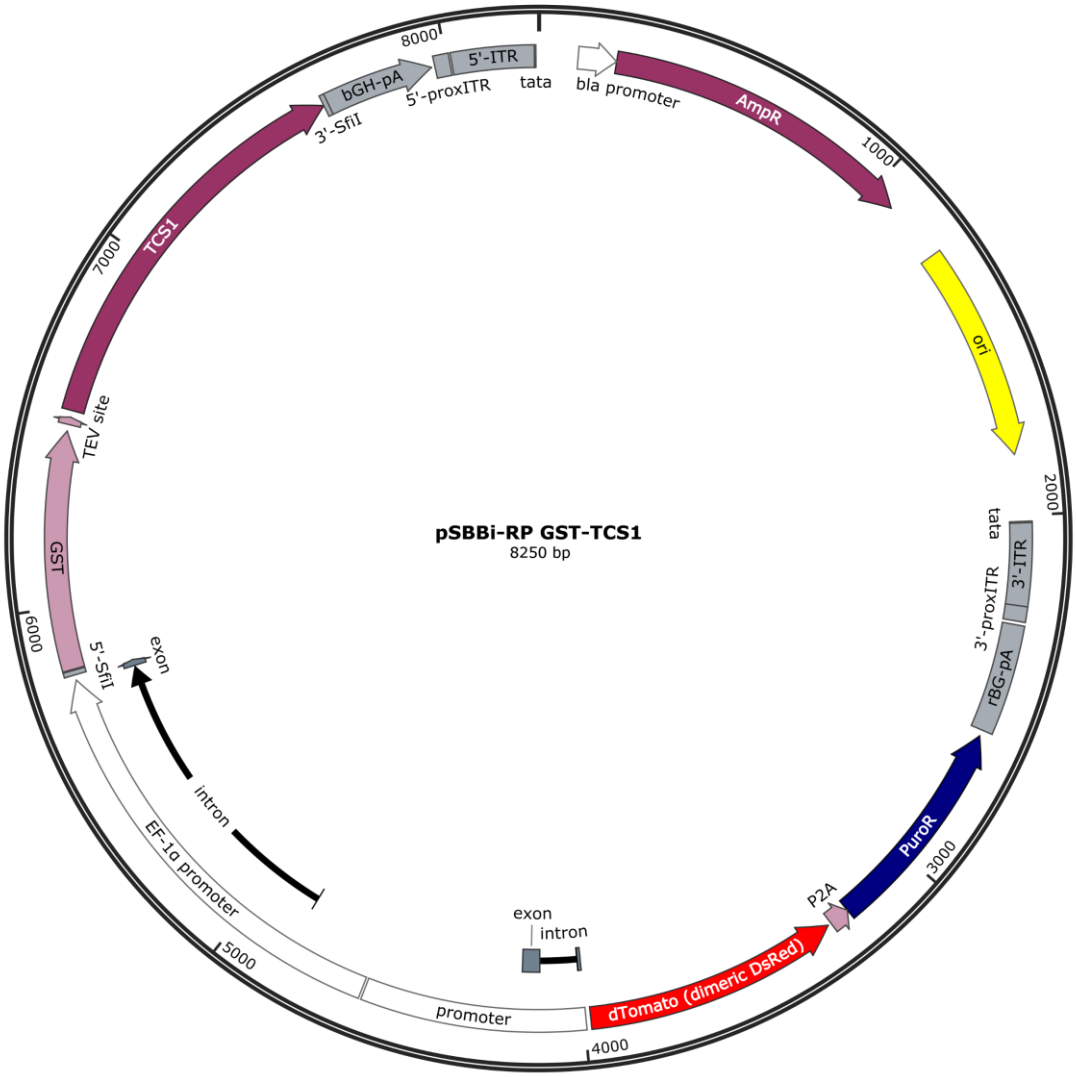

Figure 3.27: Plasmid map for pSBBi-RP GST-TCS1

3.15.1.13 pSBBi-RP TCS1

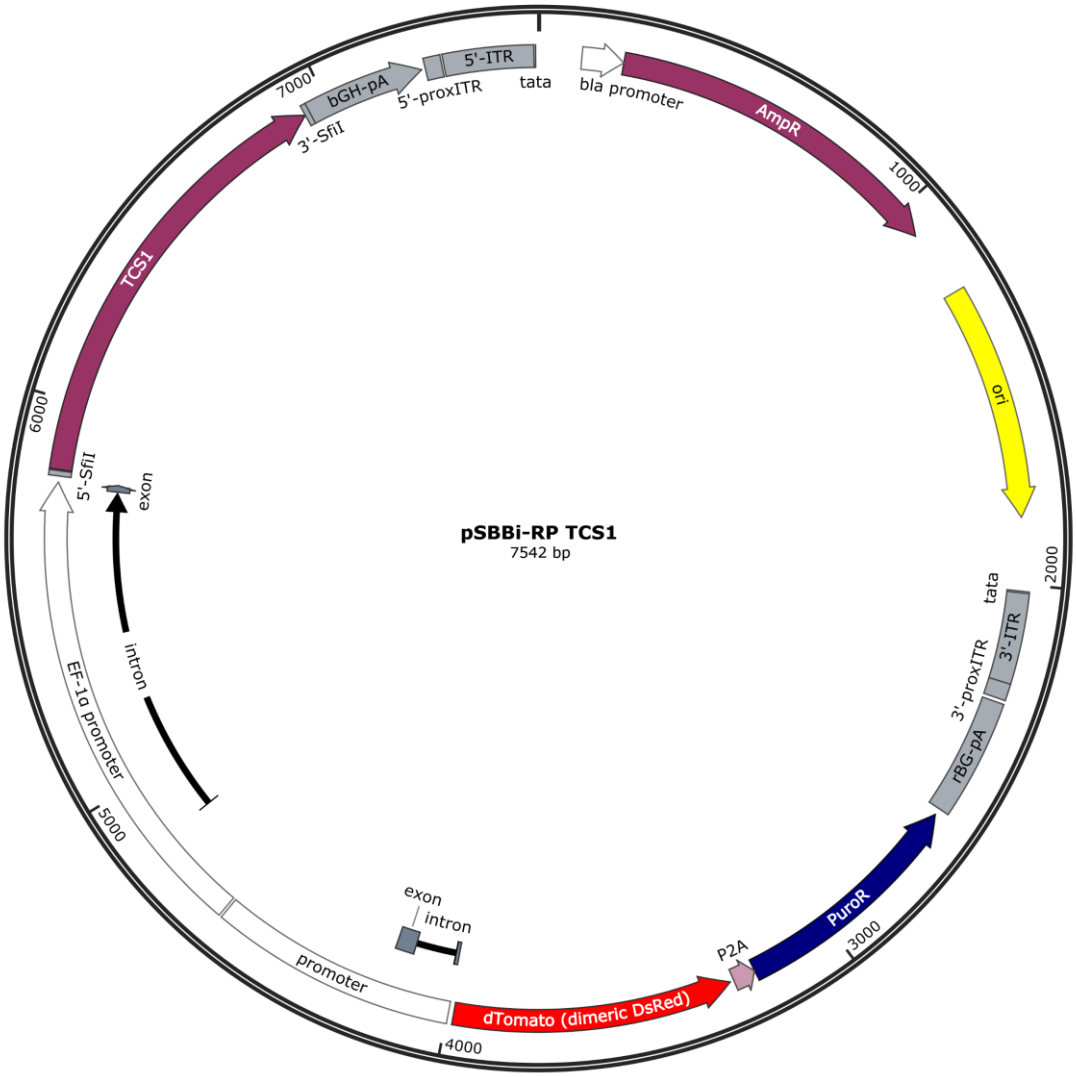

Figure 3.28: Plasmid map for pSBBi-RP TCS1

3.15.1.14 pSBBi-RP PcAncCS2

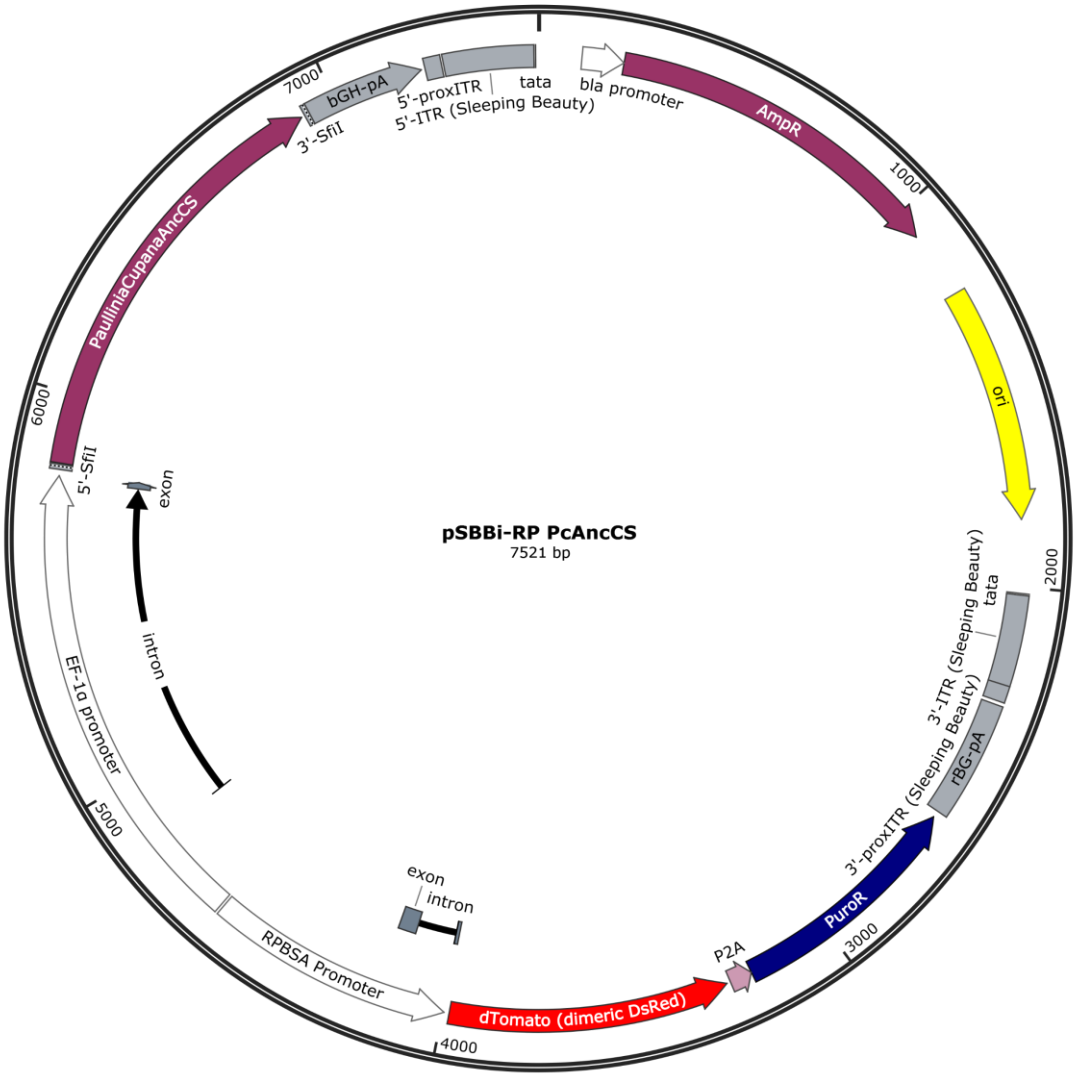

Figure 3.29: Plasmid map for pSBBi-RP PcAncCS2

3.15.1.15 pSBBi-RP PcCS

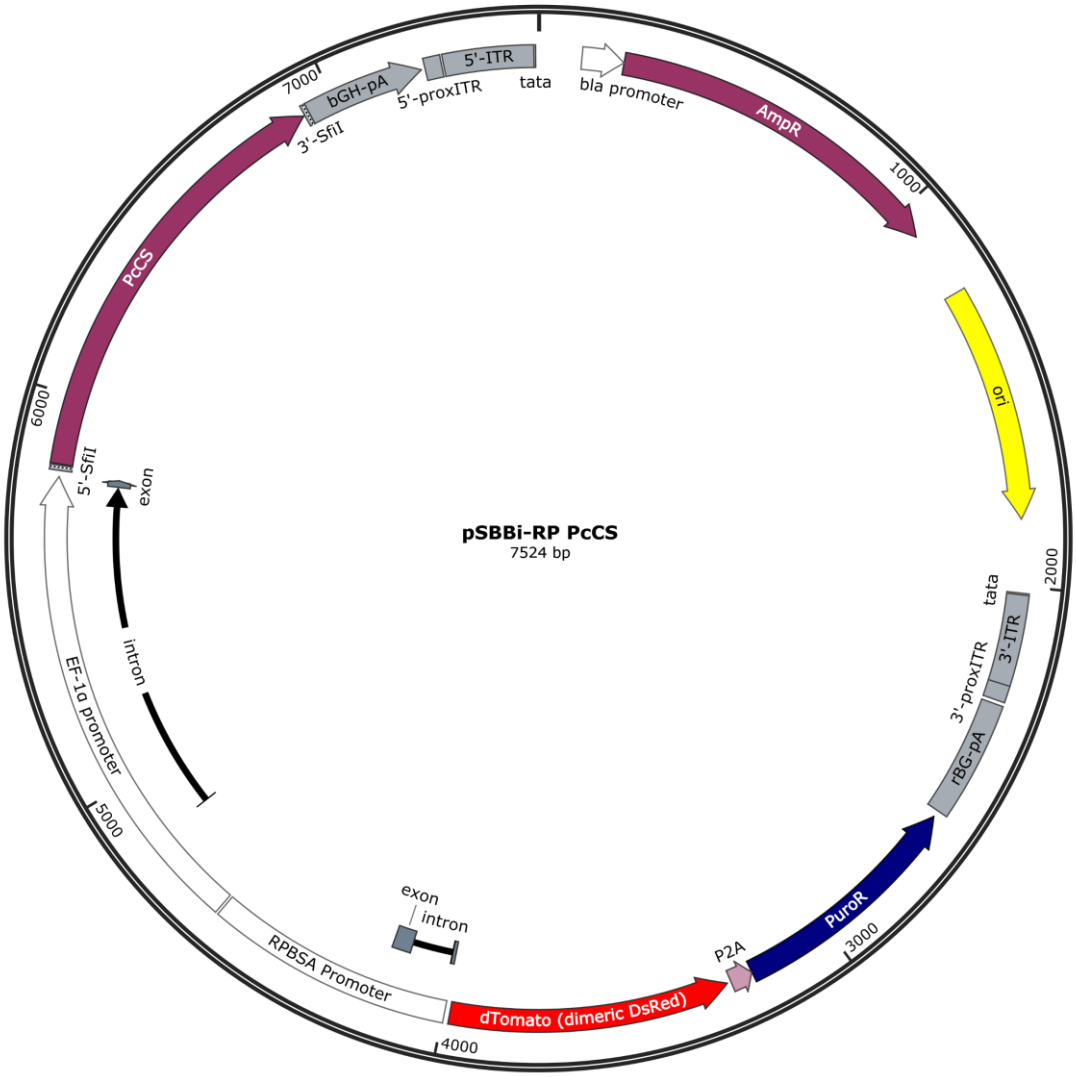

Figure 3.30: Plasmid map for pSBBi-RP PcCS

3.15.2 SynNotch Receptor Plasmid Maps and Notes

3.15.2.1 pSBBi-BH Exendin4-EGF-SynNotch-TetRVP64

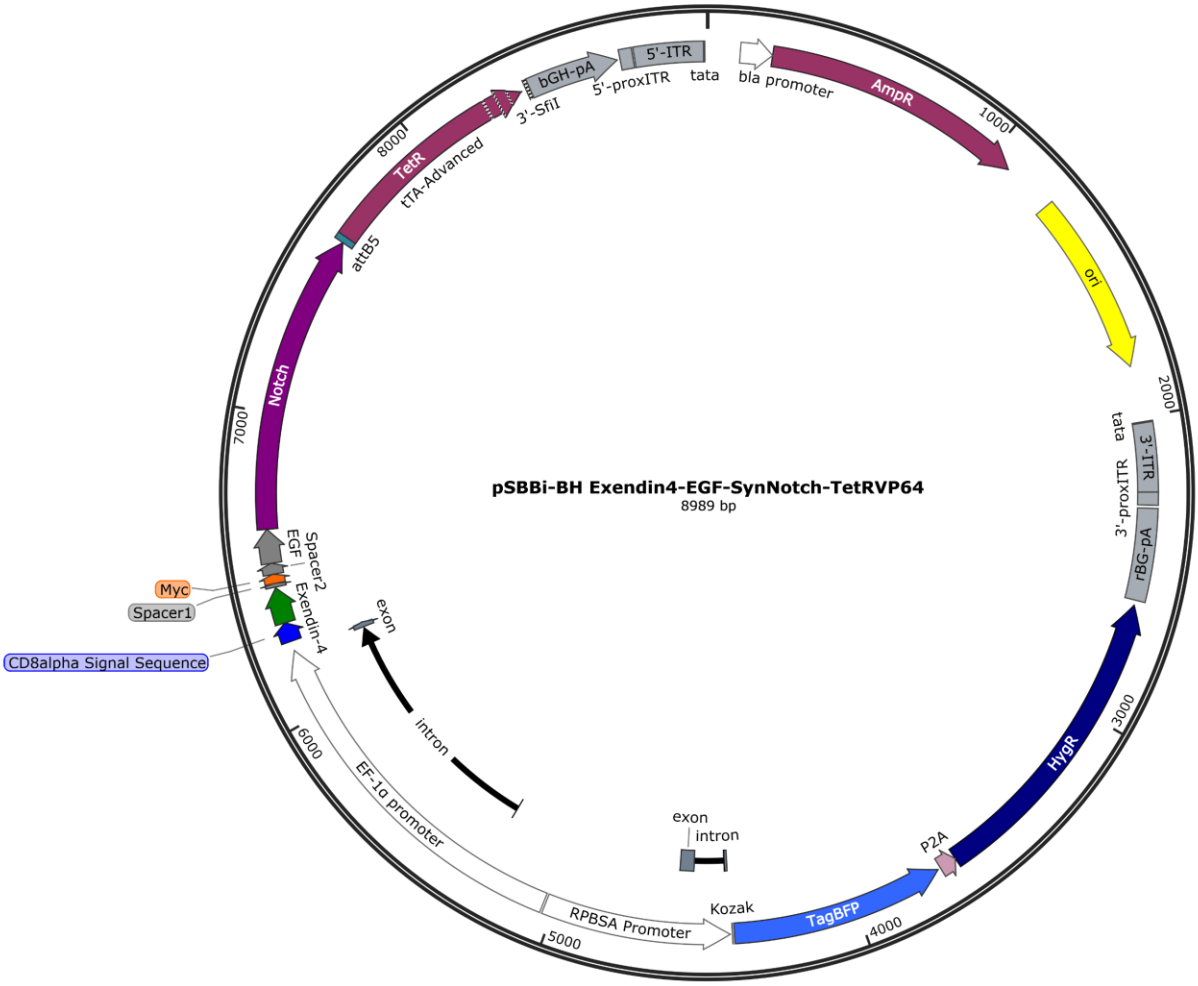

Figure 3.31: Plasmid map for pSBBi-BH Exendin4-EGF-SynNotch-TetRVP64

3.15.2.2 pSBBi-BH Exendin4-SynNotch-TetRVP64

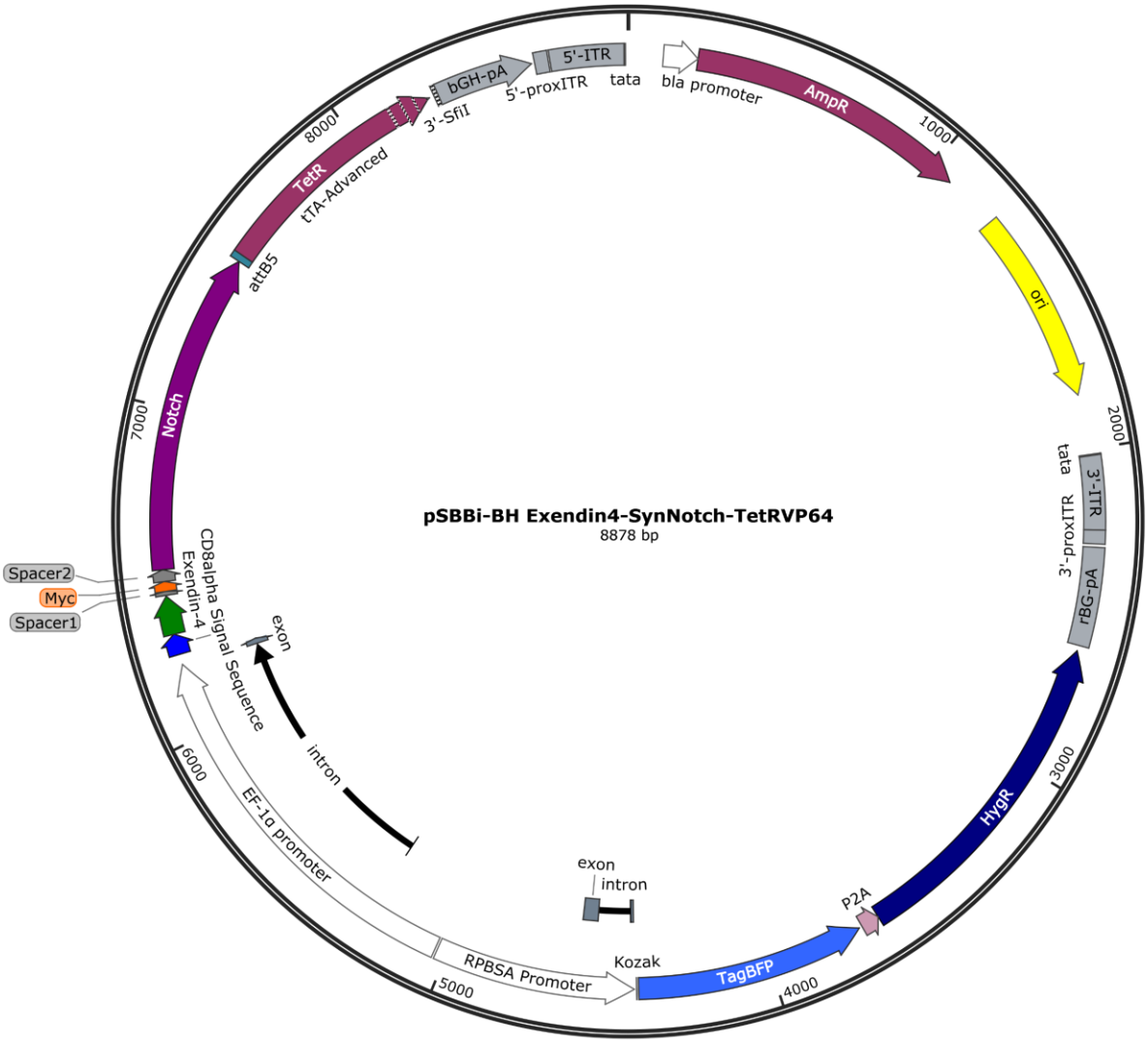

Figure 3.32: Plasmid map for pSBBi-BH Exendin4-SynNotch-TetRVP64

3.15.2.3 pSBBi-P Exendin4-EGF-SynNotch-Gal4VP64

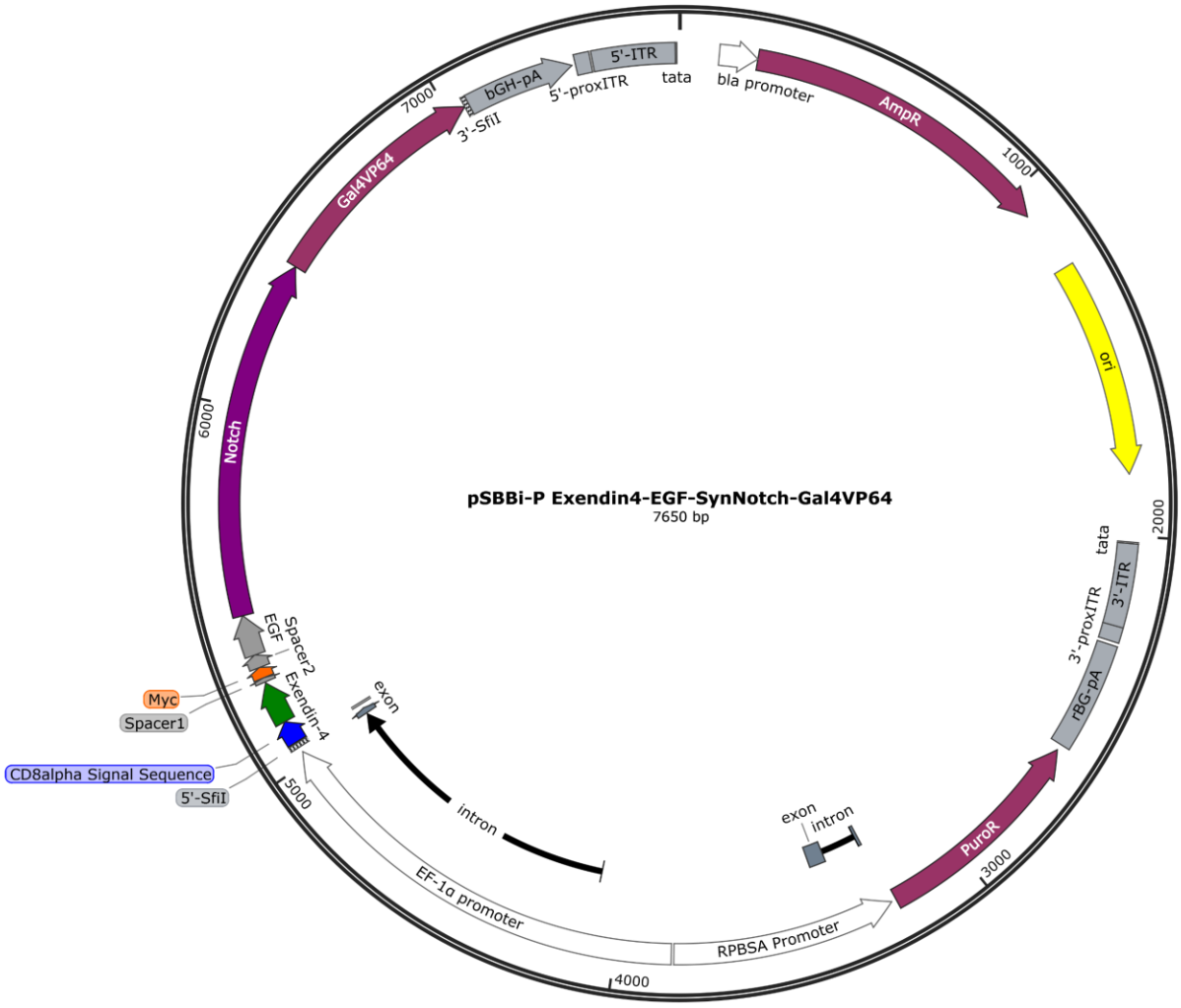

Figure 3.33: Plasmid map for pSBBi-P Exendin4-EGF-SynNotch-Gal4VP64

3.15.2.4 pSBBi-P Exendin4-EGF-SynNotch-TetRVP64

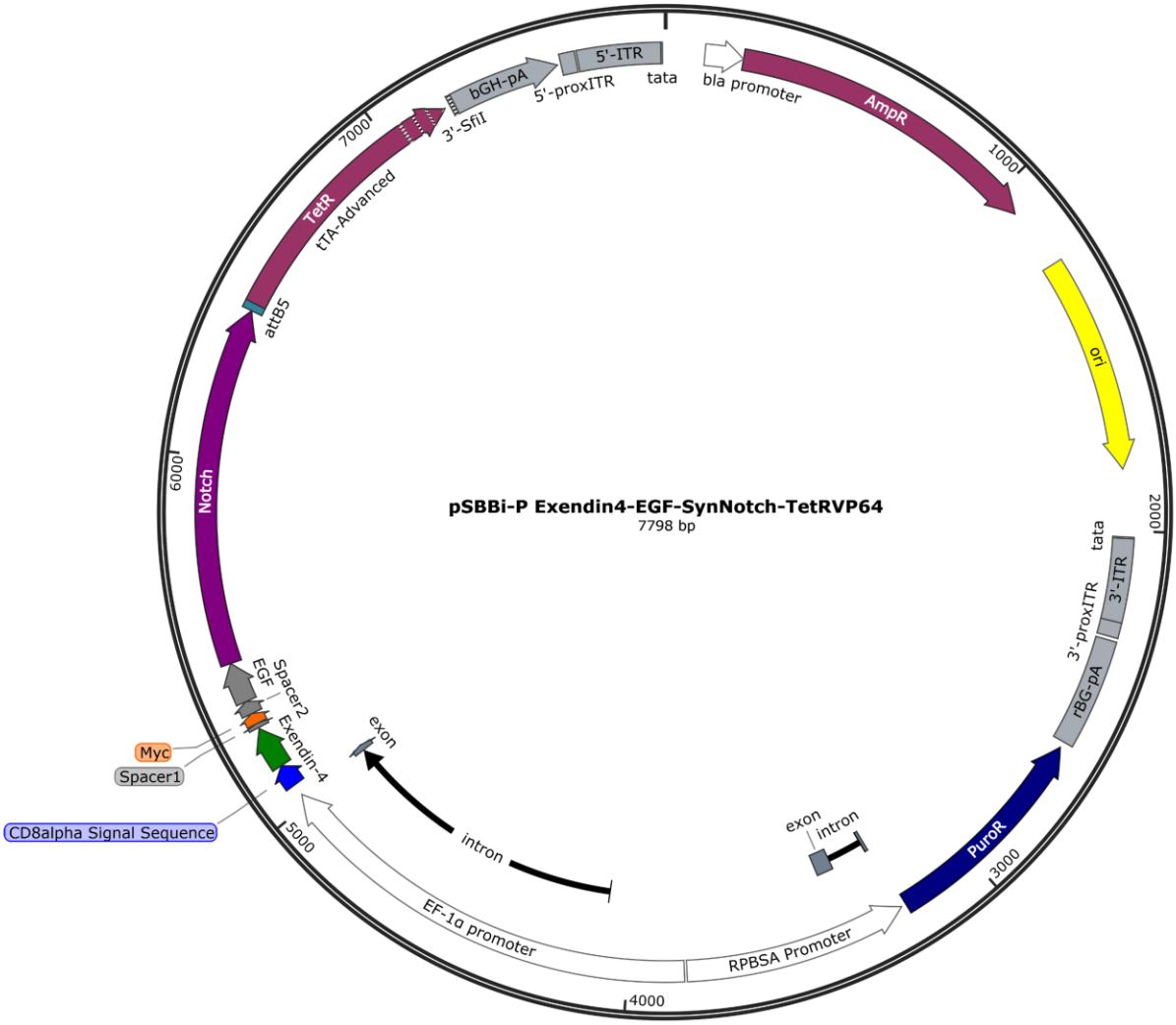

Figure 3.34: Plasmid map for pSBBi-P Exendin4-EGF-SynNotch-TetRVP64

3.15.2.5 pSBBi-P Exendin4-SynNotch-Gal4VP64

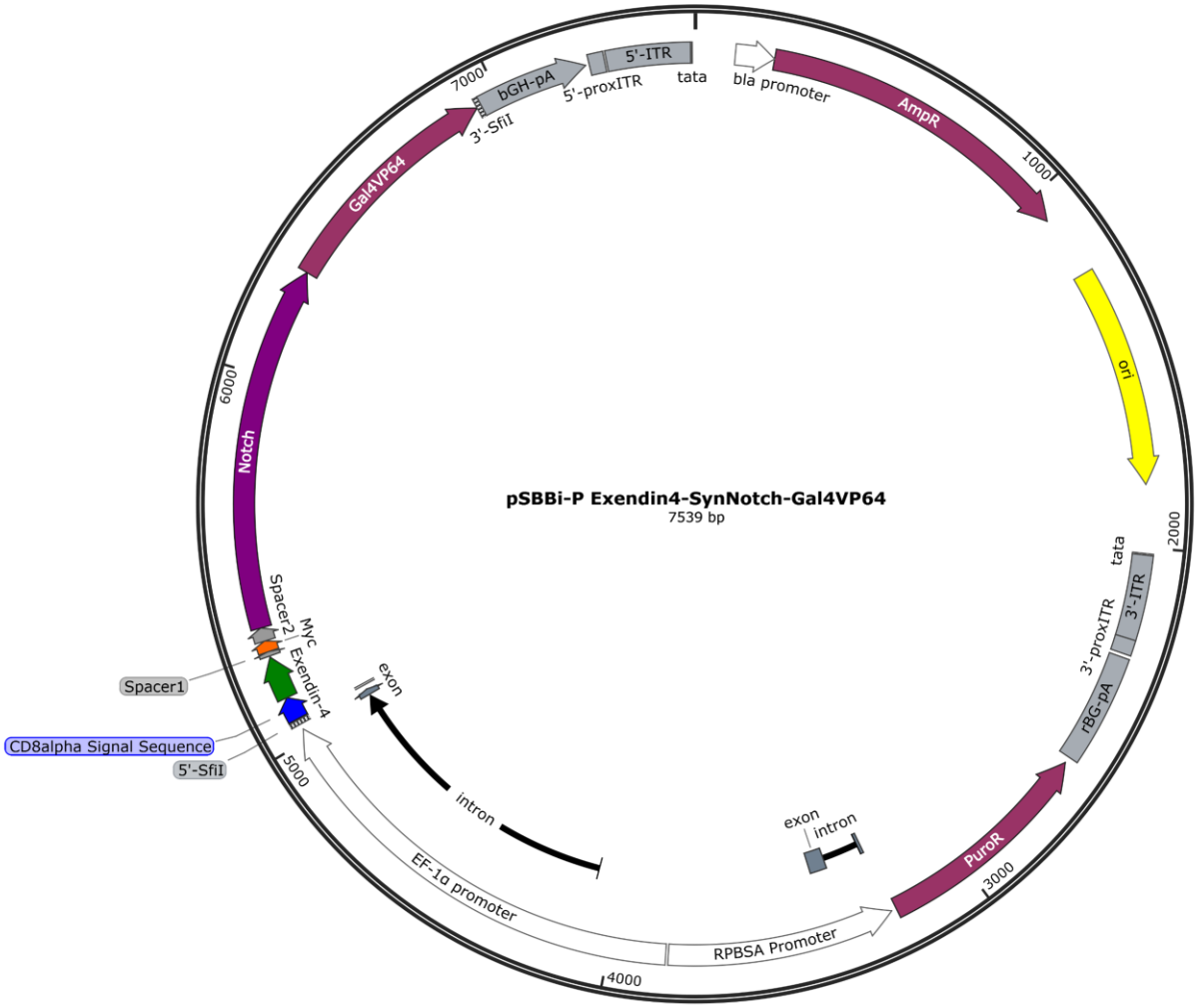

Figure 3.35: Plasmid map for pSBBi-P Exendin4-SynNotch-Gal4VP64

3.15.2.6 pSBBi-P Exendin4-SynNotch-TetRVP64

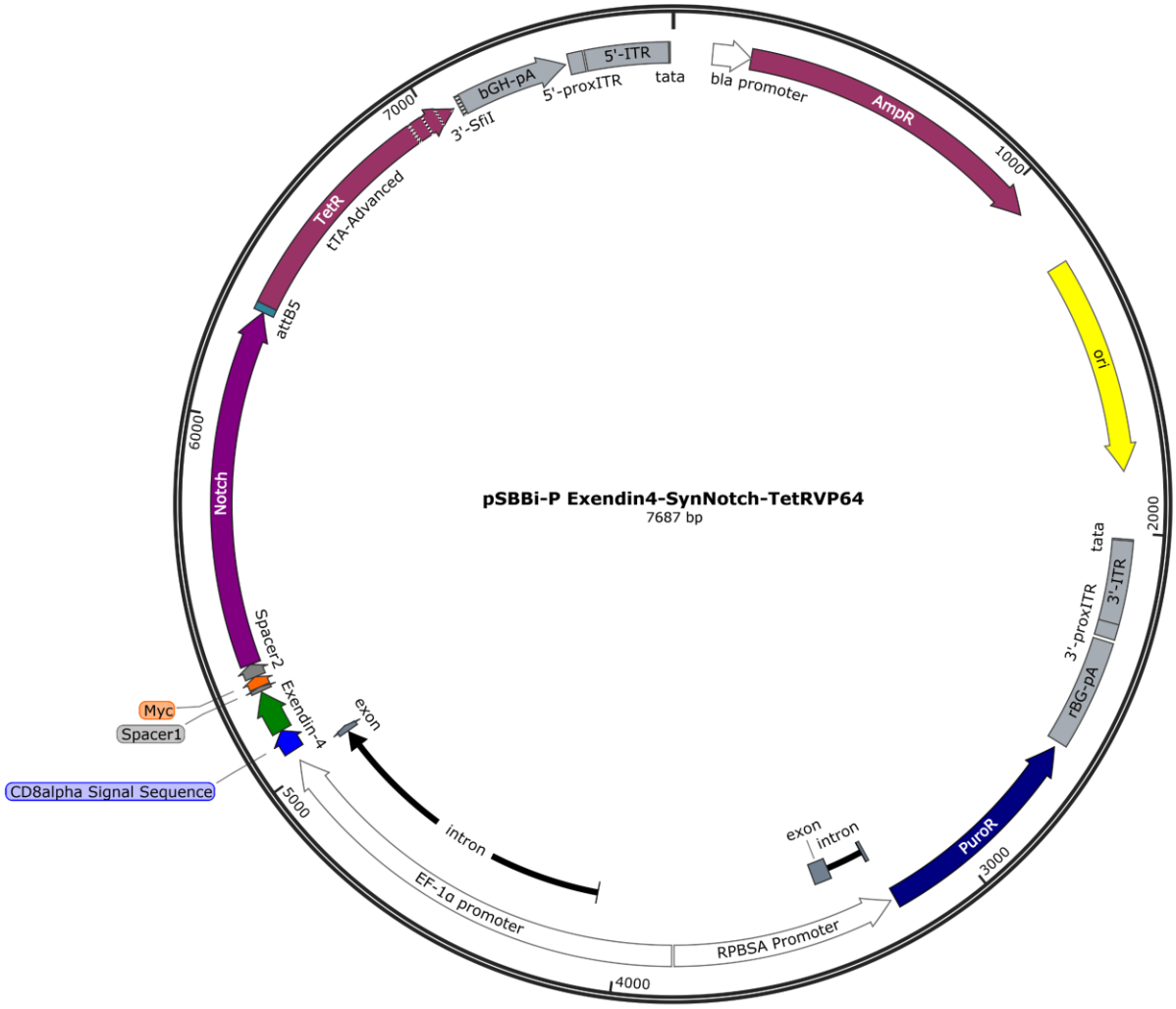

Figure 3.36: Plasmid map for pSBBi-P Exendin4-SynNotch-TetRVP64

3.15.2.7 pSBBi-P LaG17-SynNotch-Gal4VP64

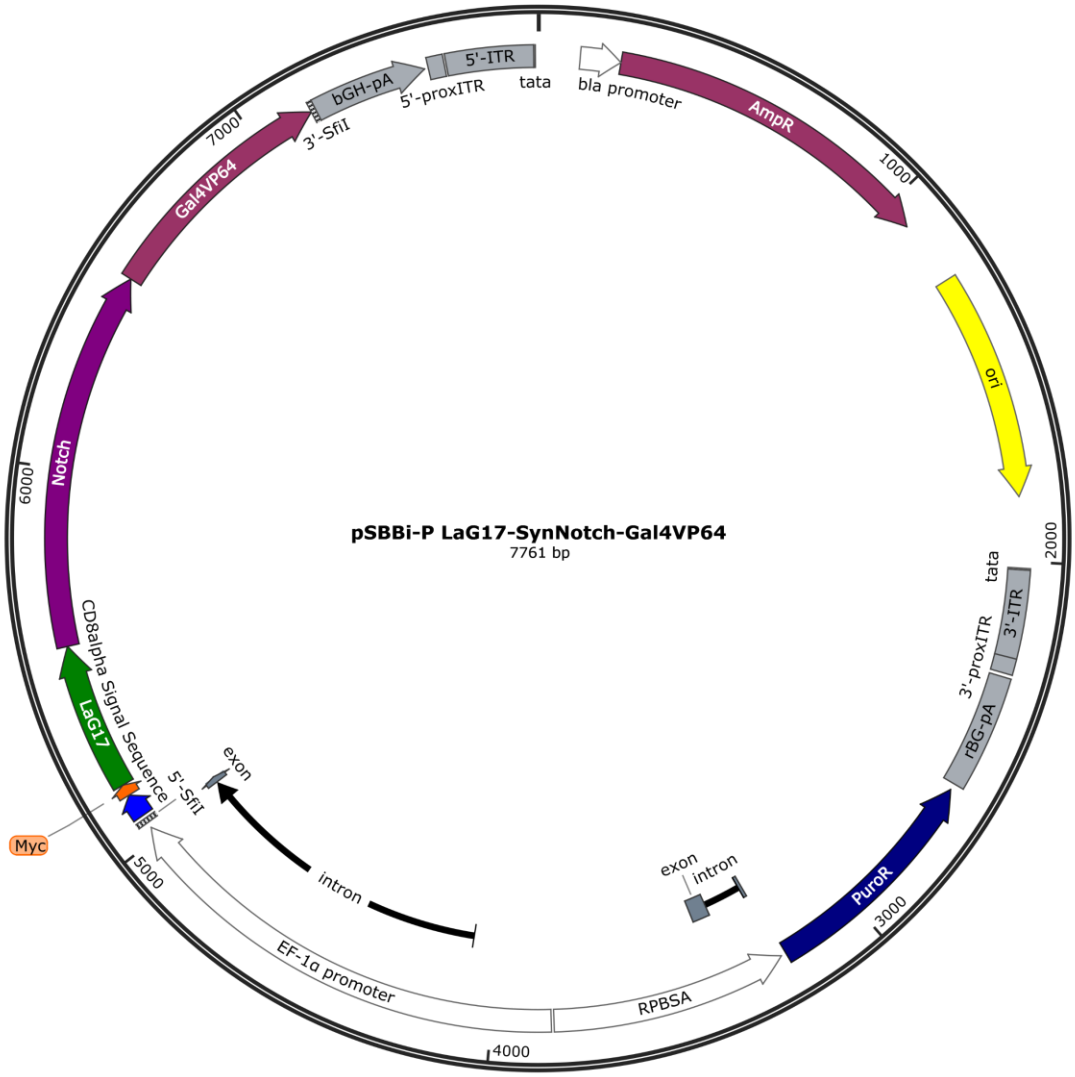

Figure 3.37: Plasmid map for pSBBi-P LaG17-SynNotch-Gal4VP64

3.15.2.8 pSBBi-P Lag17-SynNotch-TetRELK1

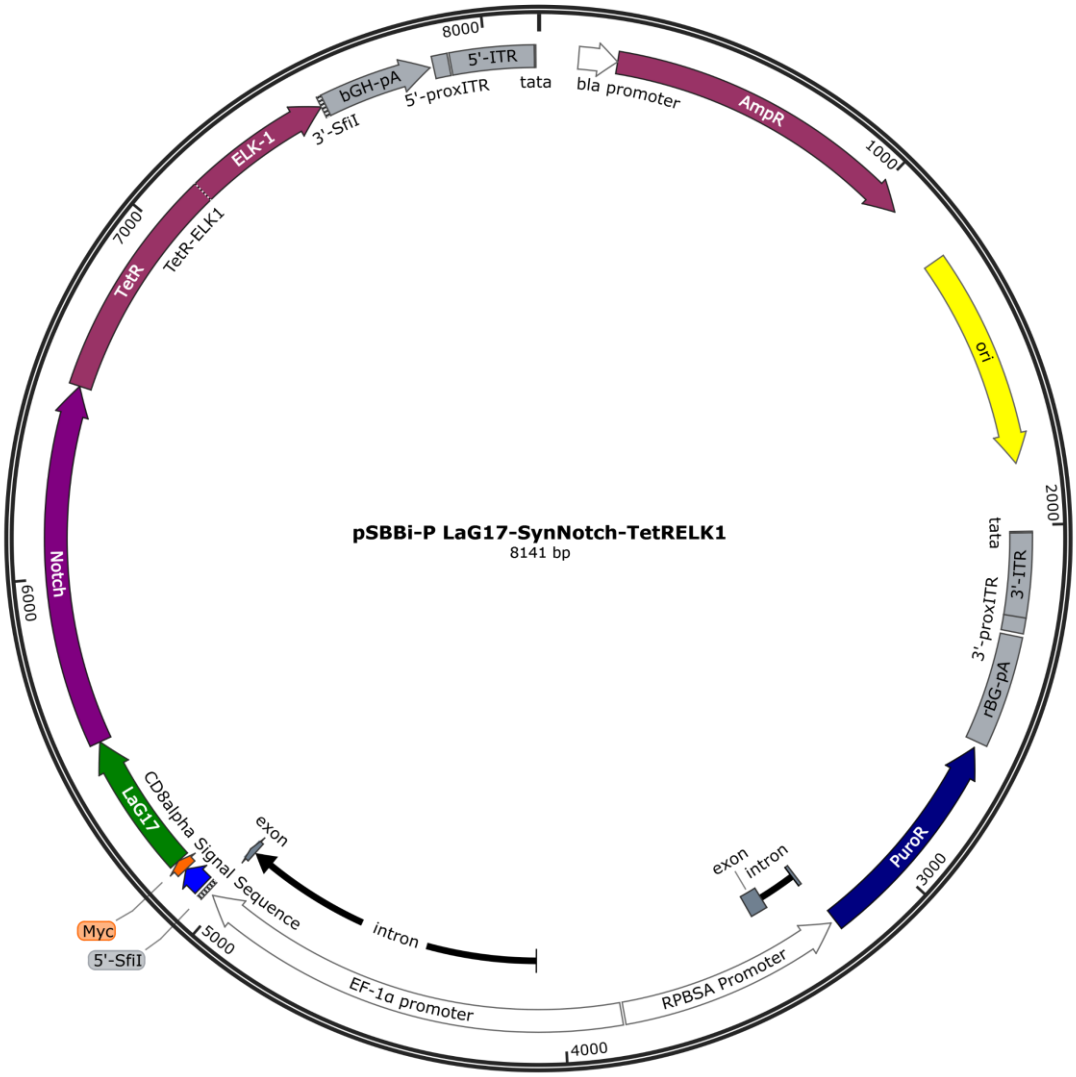

Figure 3.38: Plasmid map for pSBBi-P Lag17-SynNotch-TetRELK1

3.15.2.9 pSBBi-P LaG17-SynNotch-TetRVP64

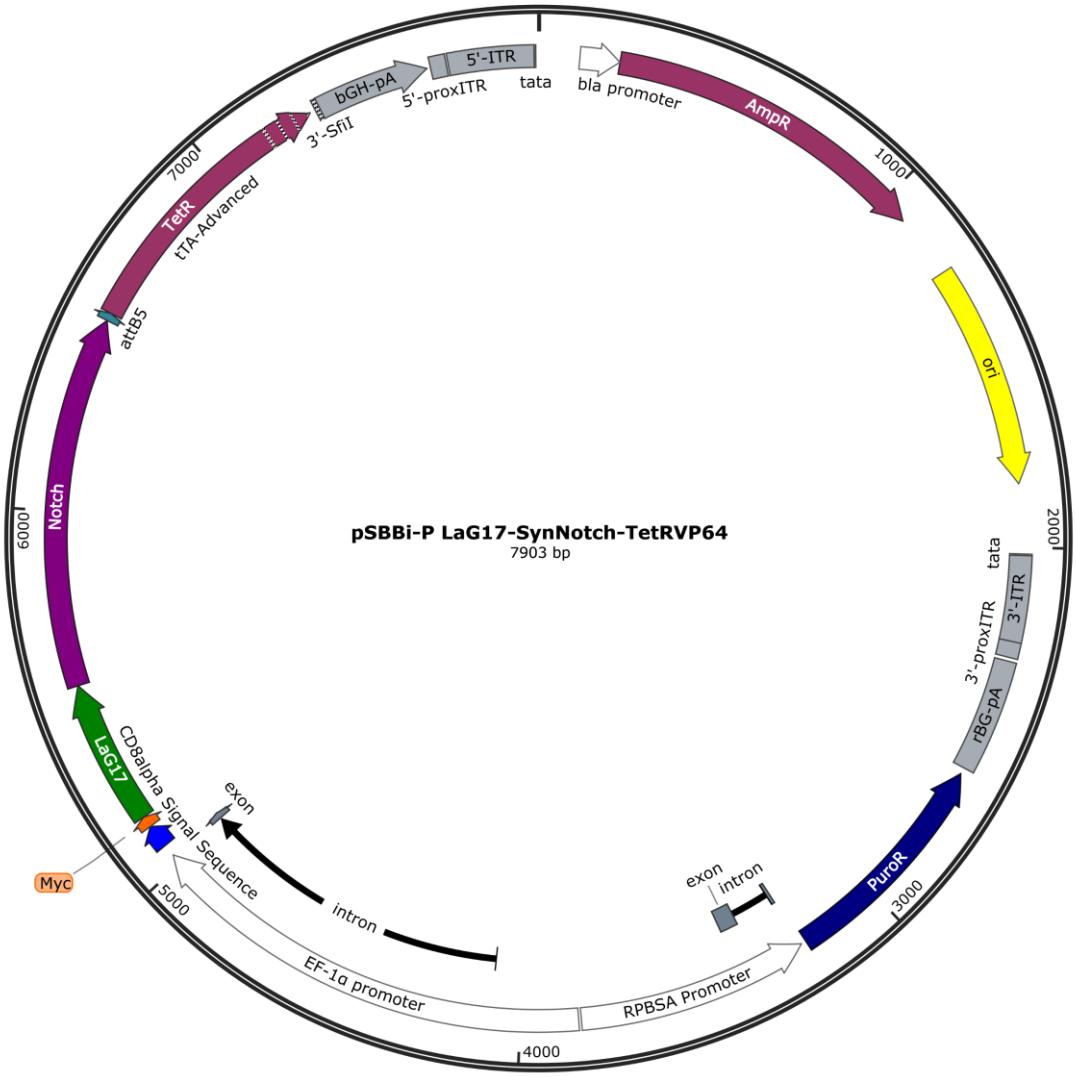

Figure 3.39: Plasmid map for pSBBi-P LaG17-SynNotch-TetRVP64

3.15.2.10 pSBBi-P SNAPtag-EGF-SynNotch-Gal4VP64

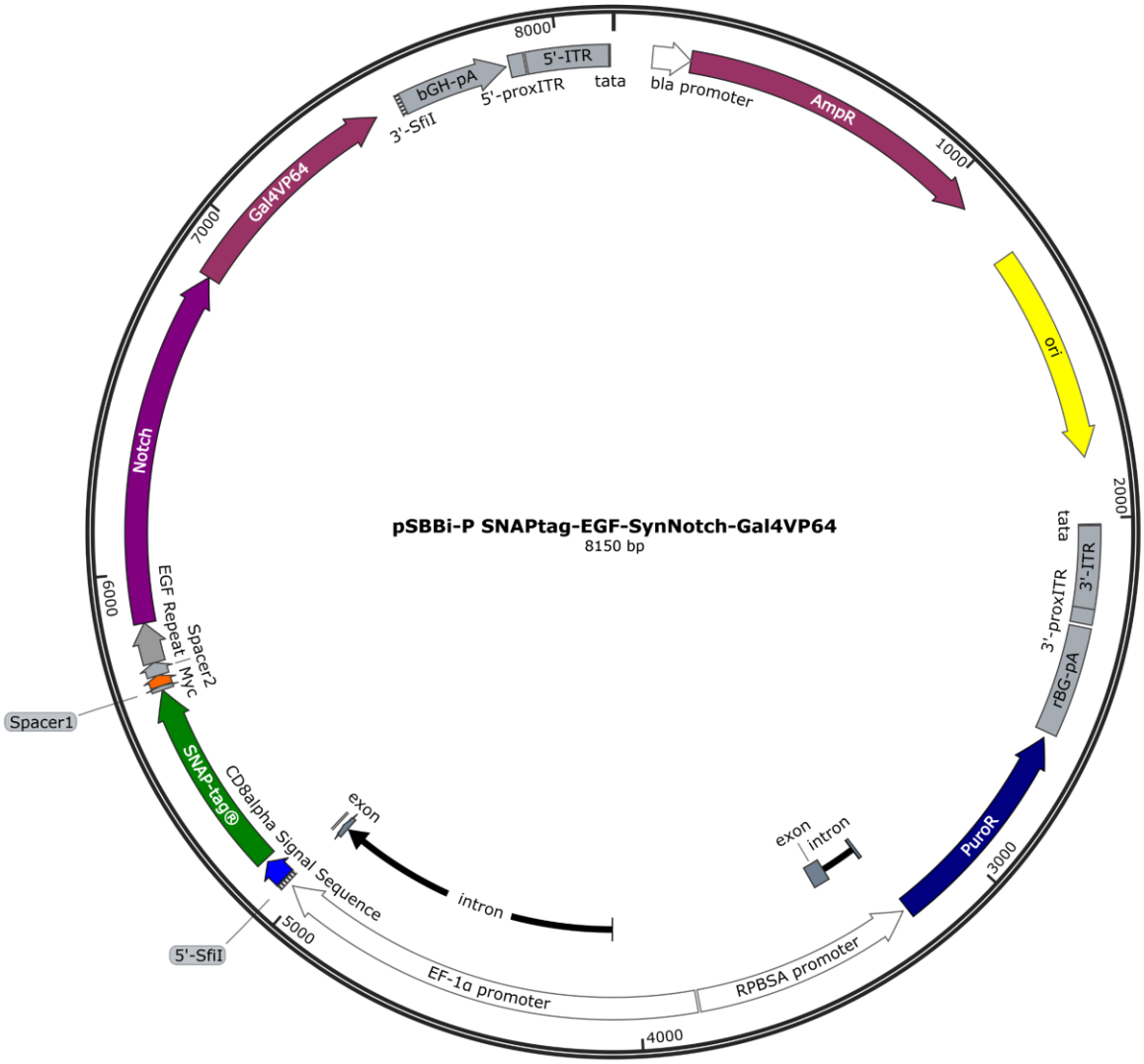

Figure 3.40: Plasmid map for pSBBi-P SNAPtag-EGF-SynNotch-Gal4VP64

3.15.2.11 pSBBi-P SNAPtag-EGF-SynNotch-TetRVP64

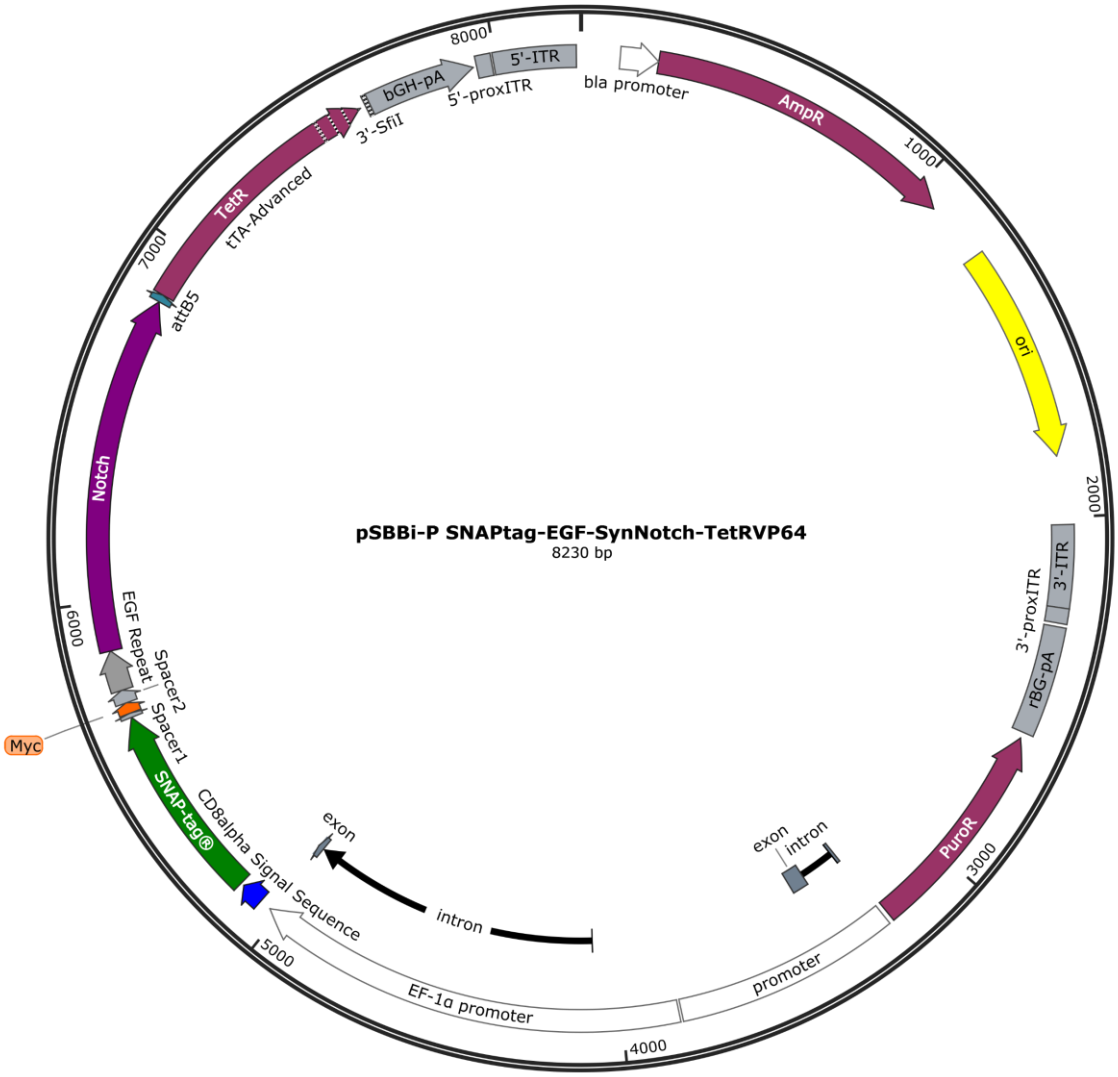

Figure 3.41: Plasmid map for pSBBi-P SNAPtag-EGF-SynNotch-TetRVP64

3.15.2.12 pSBBi-P SNAPtag-SynNotch-Gal4VP64

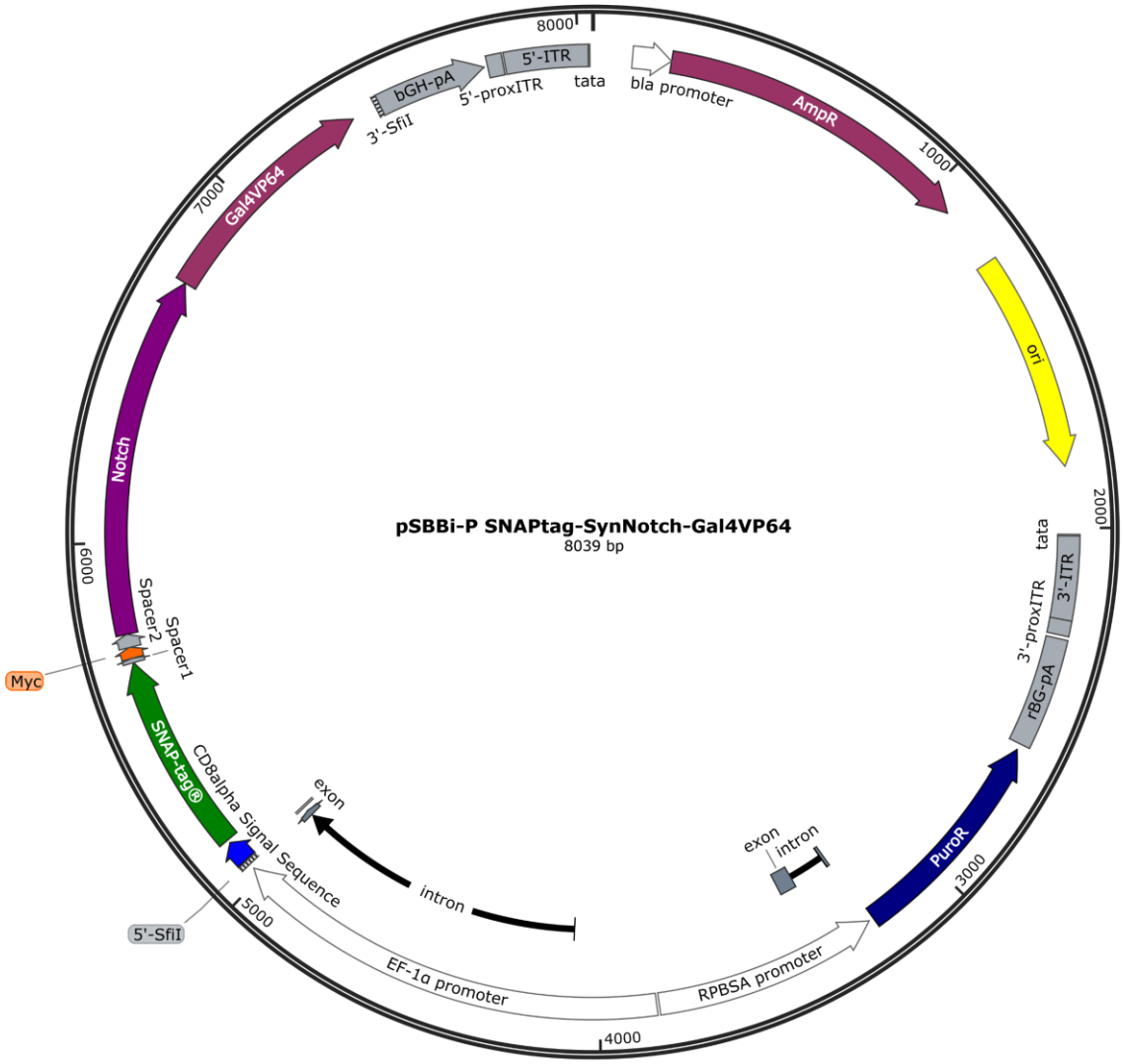

Figure 3.42: Plasmid map for pSBBi-P SNAPtag-SynNotch-Gal4VP64

3.15.2.13 pSBBi-P SNAPtag-SynNotch-TetRVP64

Figure 3.43: Plasmid map for pSBBi-P SNAPtag-SynNotch-TetRVP64

3.15.3 Targets for SynNotch Receptor Plasmid Maps and Notes

3.15.3.1 pSFFV mSA-EGFP-TM

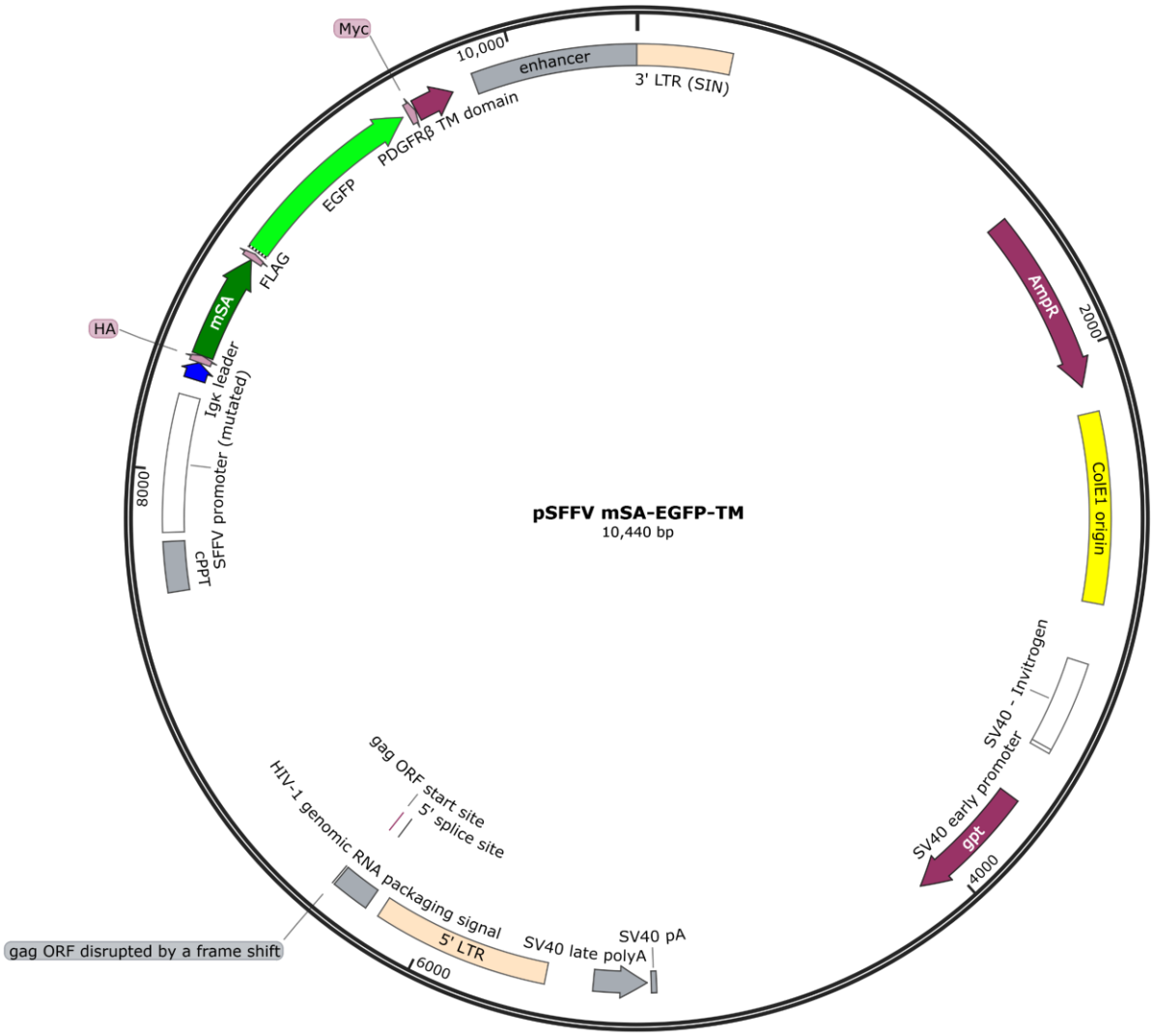

Figure 3.44: Plasmid map for pSFFV mSA-EGFP-TM

3.15.3.2 pSFFV GLP1R(S301A)EGFP

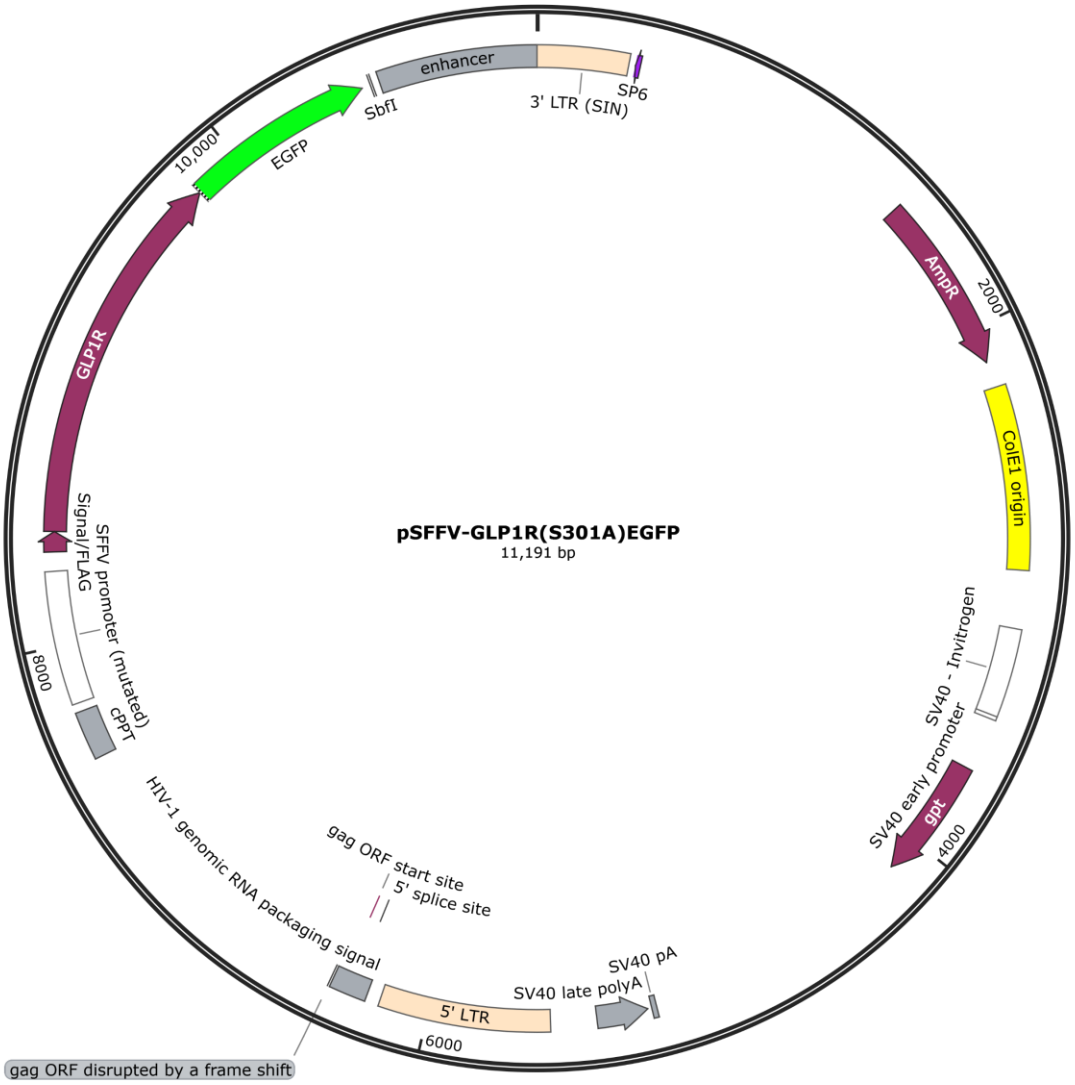

Figure 3.45: Plasmid map for pSFFV GLP1R(S301A)EGFP

3.15.3.3 pHR_EGFPligand

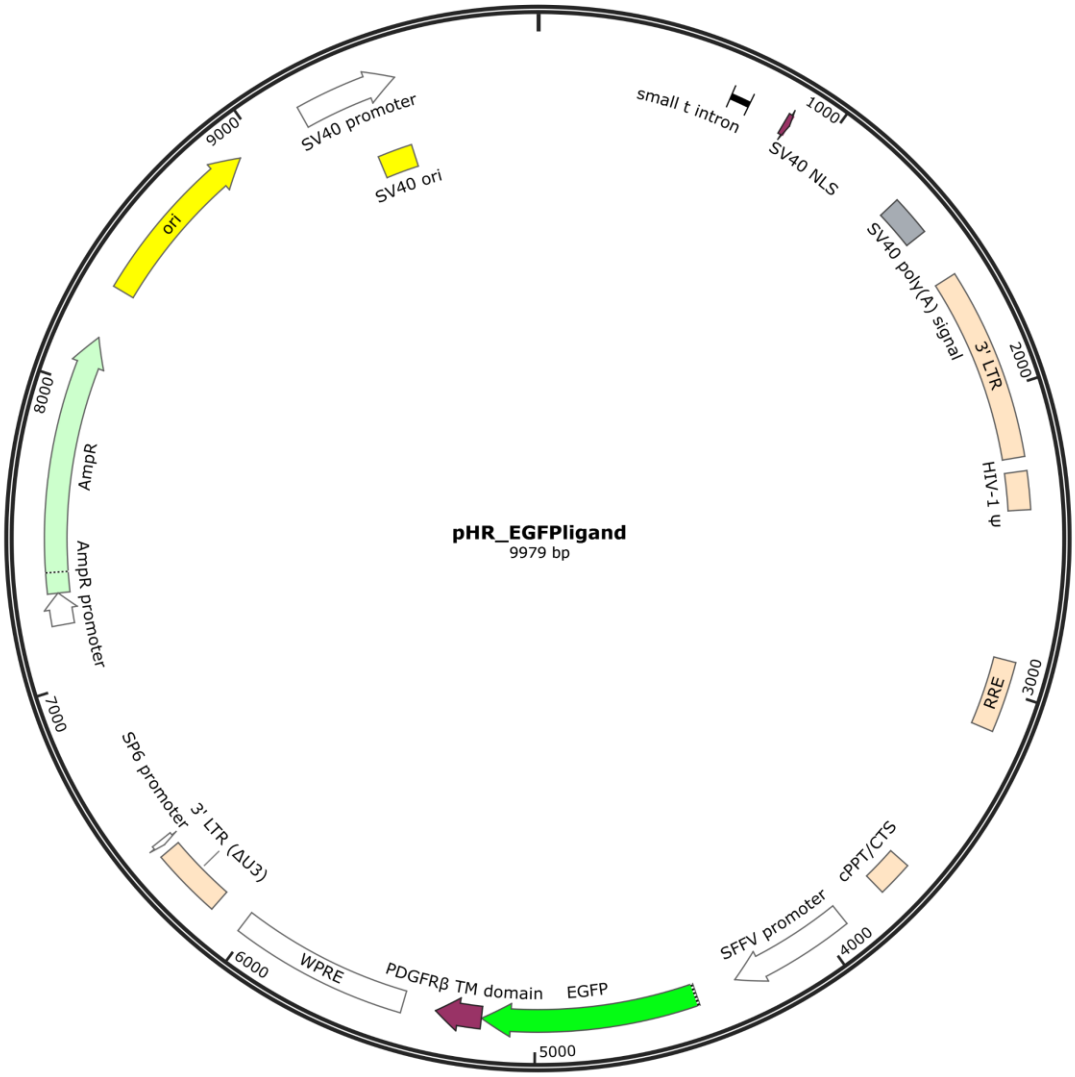

Figure 3.46: Plasmid map for pHR_EGFPligand

3.15.4 Tet-Inducible Plasmids

All Tet-inducible plasmids were made from a deletion mutant of pSBTet-GB wherein the rtTA-P2A was deleted. This backbone was named “pSBTRE-GB” to distinguish it from the parent plasmid. The reporter constructs (mCherry-P2A-GOI) were inserted downstream of the tight TRE promoter via HiFi assembly.

3.15.4.1 pSBTRE-GB mCherry-CCS1

Figure 3.47: Plasmid: Plasmid map for pSBTRE-GB mCherry-CCS1

3.15.4.2 pSBTRE-GB mCherry-P2A-CCS1

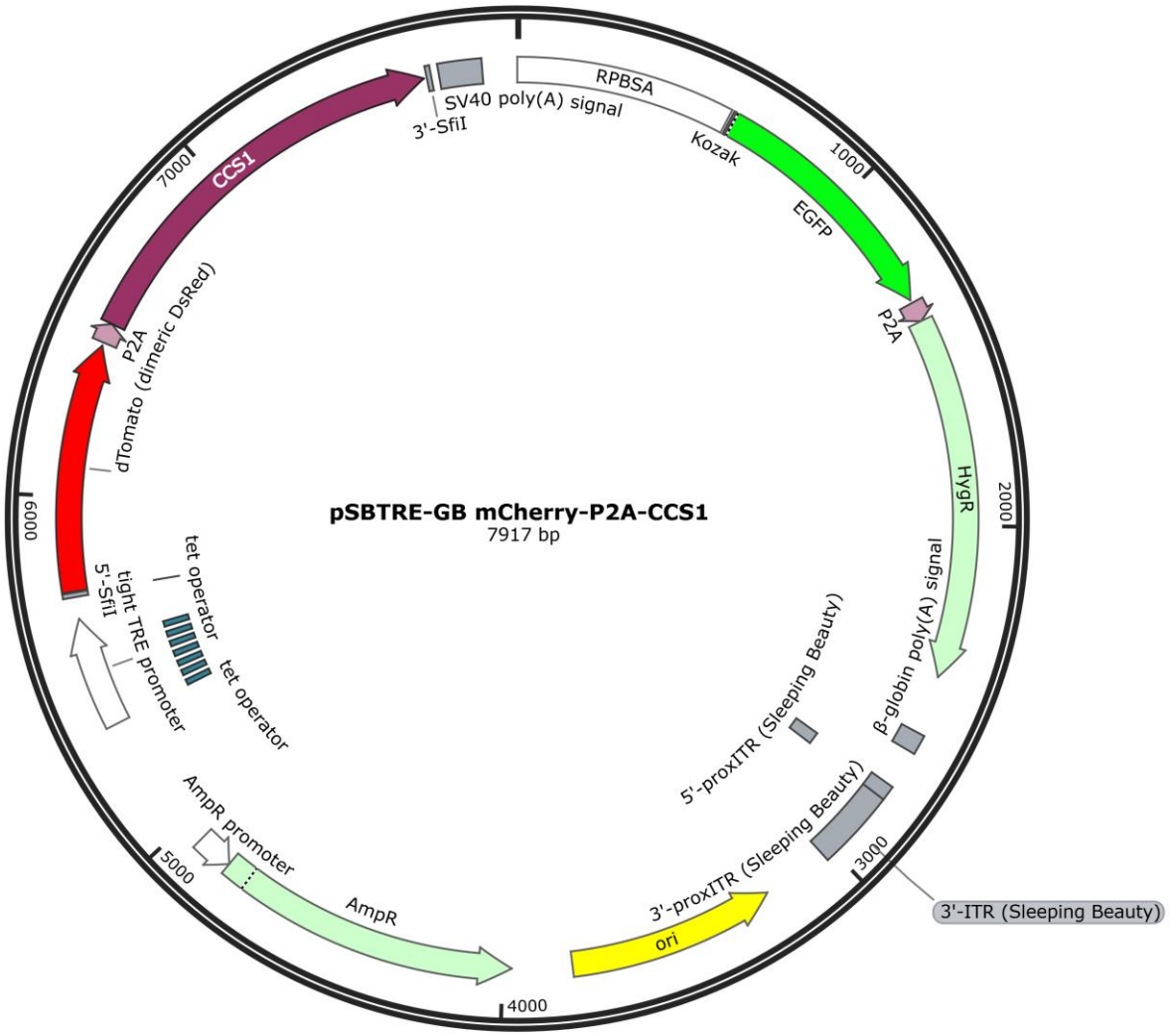

Figure 3.48: Plasmid: Plasmid map for pSBTRE-GB mCherry-P2A-CCS1

3.15.4.3 pSBTRE-GB mCherry-P2A-TCS1

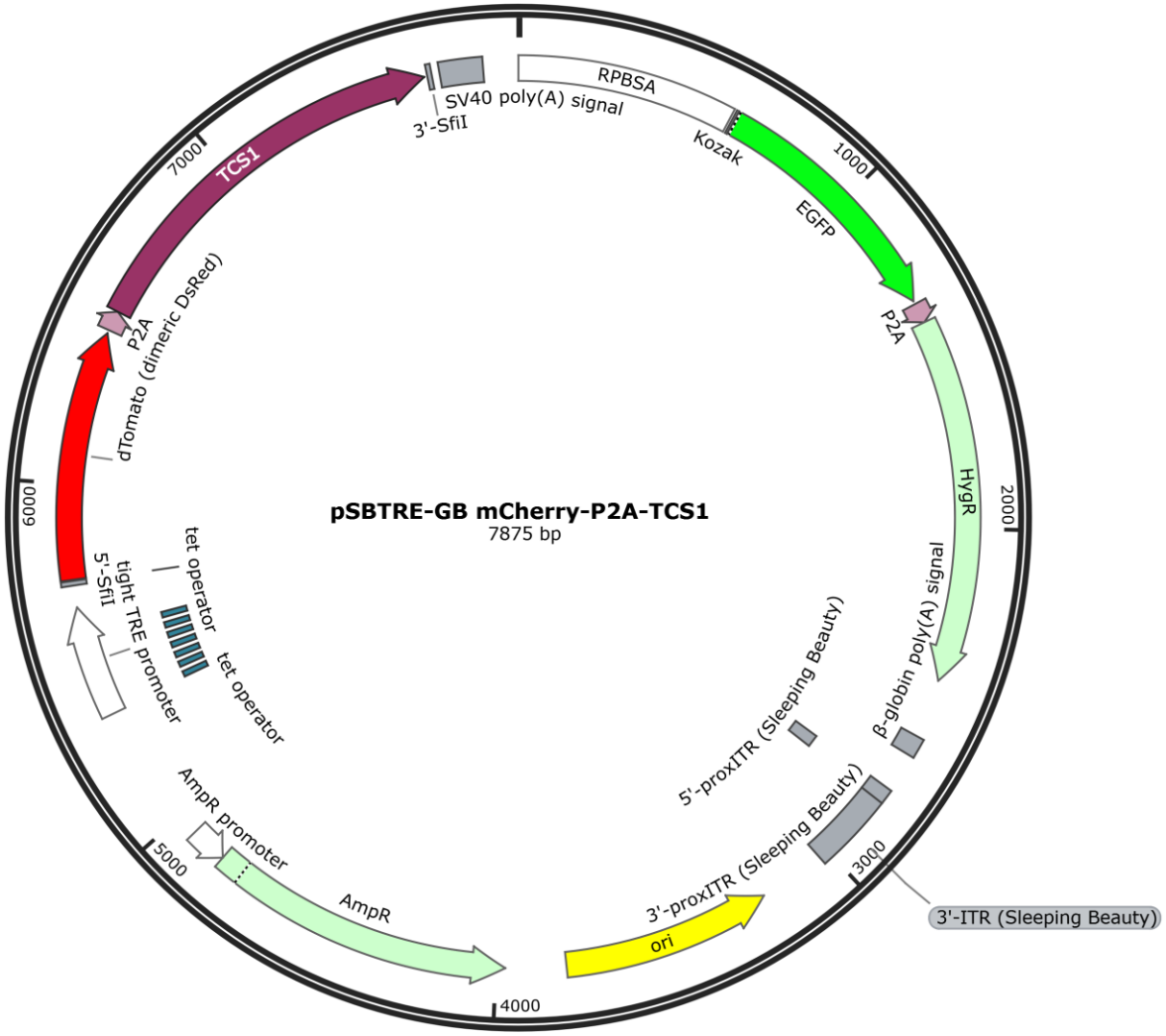

Figure 3.49: Plasmid map for pSBTRE-GB mCherry-P2A-TCS1

3.15.4.4 pSBTRE-GB mCherry-P2A-MXMT

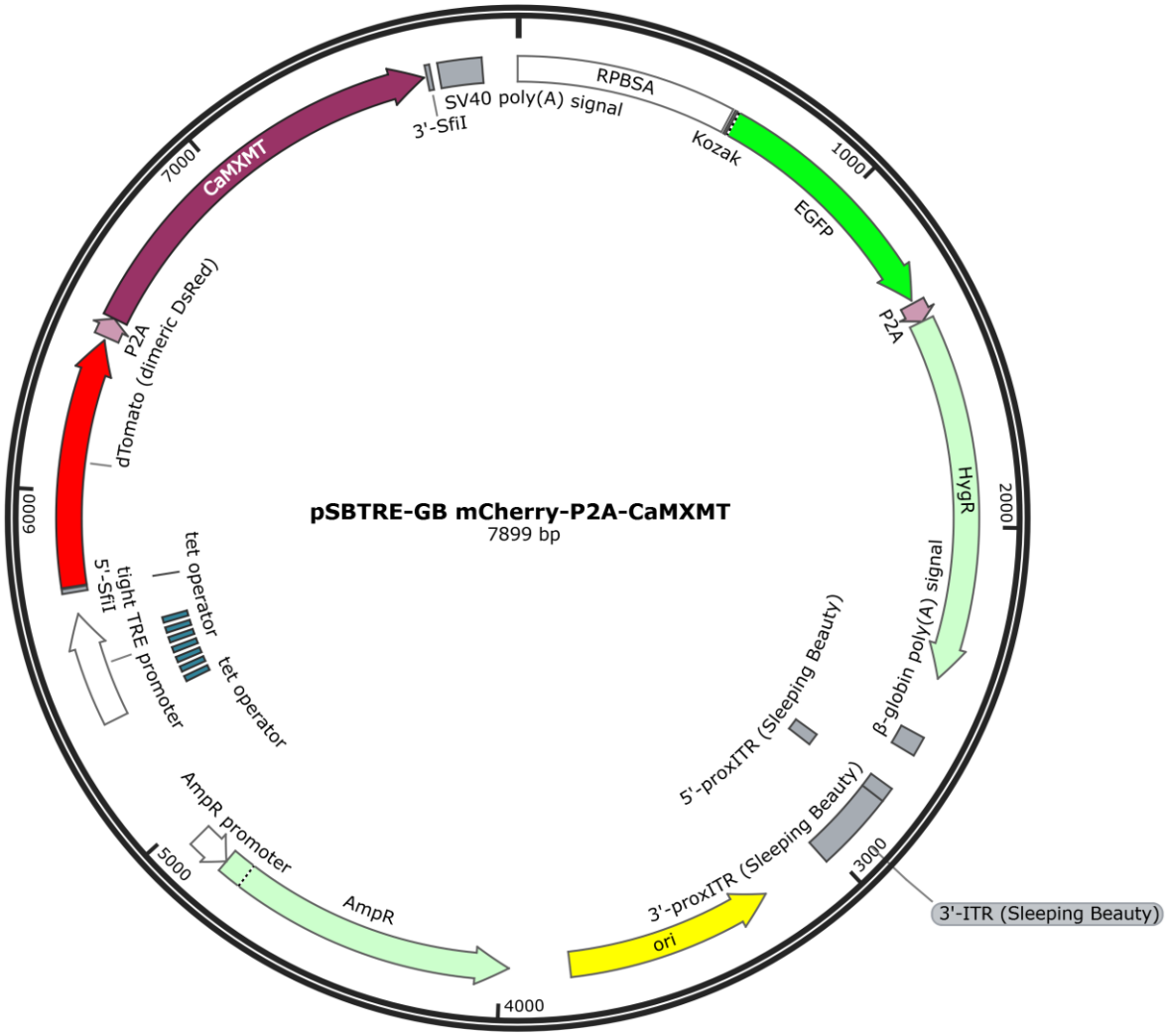

Figure 3.50: Plasmid map for pSBTRE-GB mCherry-P2A-CaMXMT

3.15.5 Other Plasmids

3.15.4.1 pET11-A+ eLaG17-SGKGSKGSKSK-Hisx6

Figure 3.51: Plasmid map for pET11A+ eLag17-SGKGSKGSKSK-Hisx6

3.15.6 HPLC Chromatograms

Retention times can be somewhat variable between samples. This is due to slowly degrading column condition as well as position in sequence. Samples earlier in the sequence elute differently than those later in a sequence due to column equilibration with the buffer constituents present in cell culture media. In the future, HPLC solvents probably should be buffer instead of just solvent + 0.1% TFA. Chromatographs were integrated in ChemStation and the peak area was used to calculate yield of products based on standard curves. When a product peak overlapped with a peak present in the control sample, the appropriate cell line's spectrum was integrated over the same time span as the peak and the result was subtracted from the integrated value for the sample in question.

3.15.6.1 HEK-293T LaG17-synNotch-TetRVP64 + TRE mCherry-P2A-CCS1 / K562-GFP Co-Culture

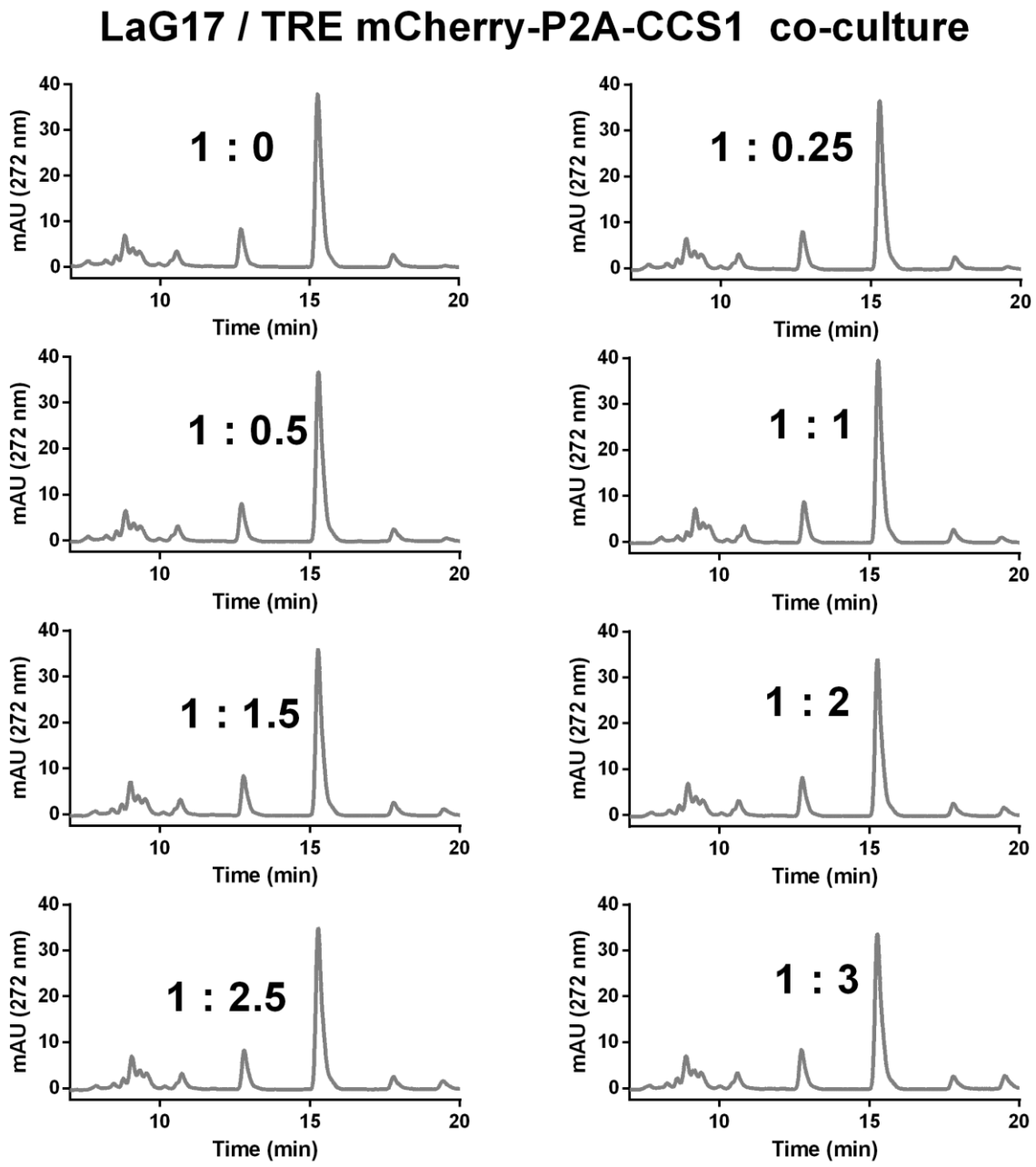

Figure 3.52: Chromatograms showing the formation of caffeine resulting from the coculture of receptor/reporter cells HEK-293T LaG17-synNotch-TetRVP64 + TRE mCherry-P2A-CCS1 with K562-GFP target cells in the presence of paraxanthine

3.15.6.2 CaDXMT1

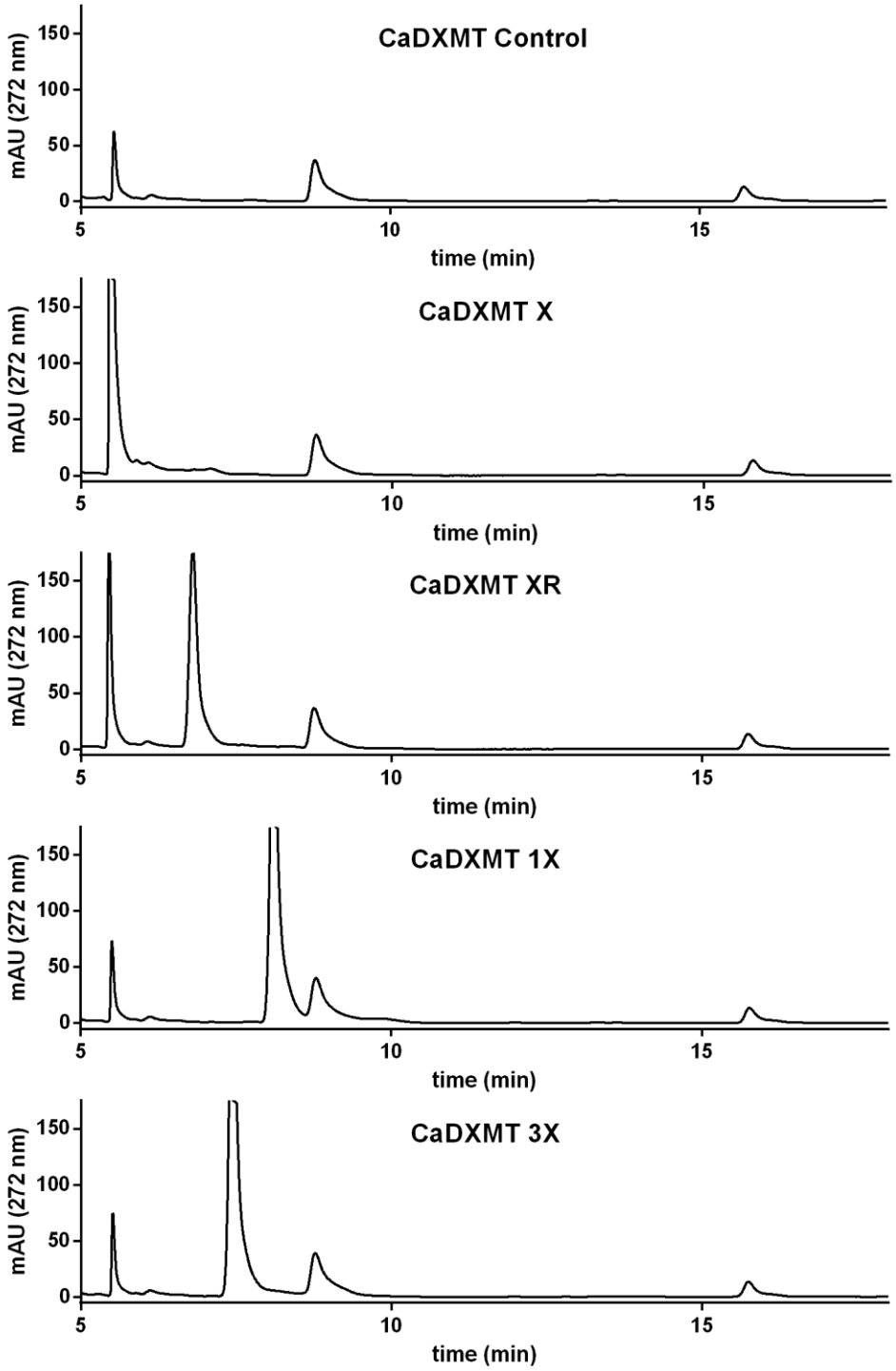

Figure 3.53: Control, X, XR, 1X, and 3X chromatograms from DAD (272 nm) for CsAncCS. Products are marked with an asterisk and are labeled in red.

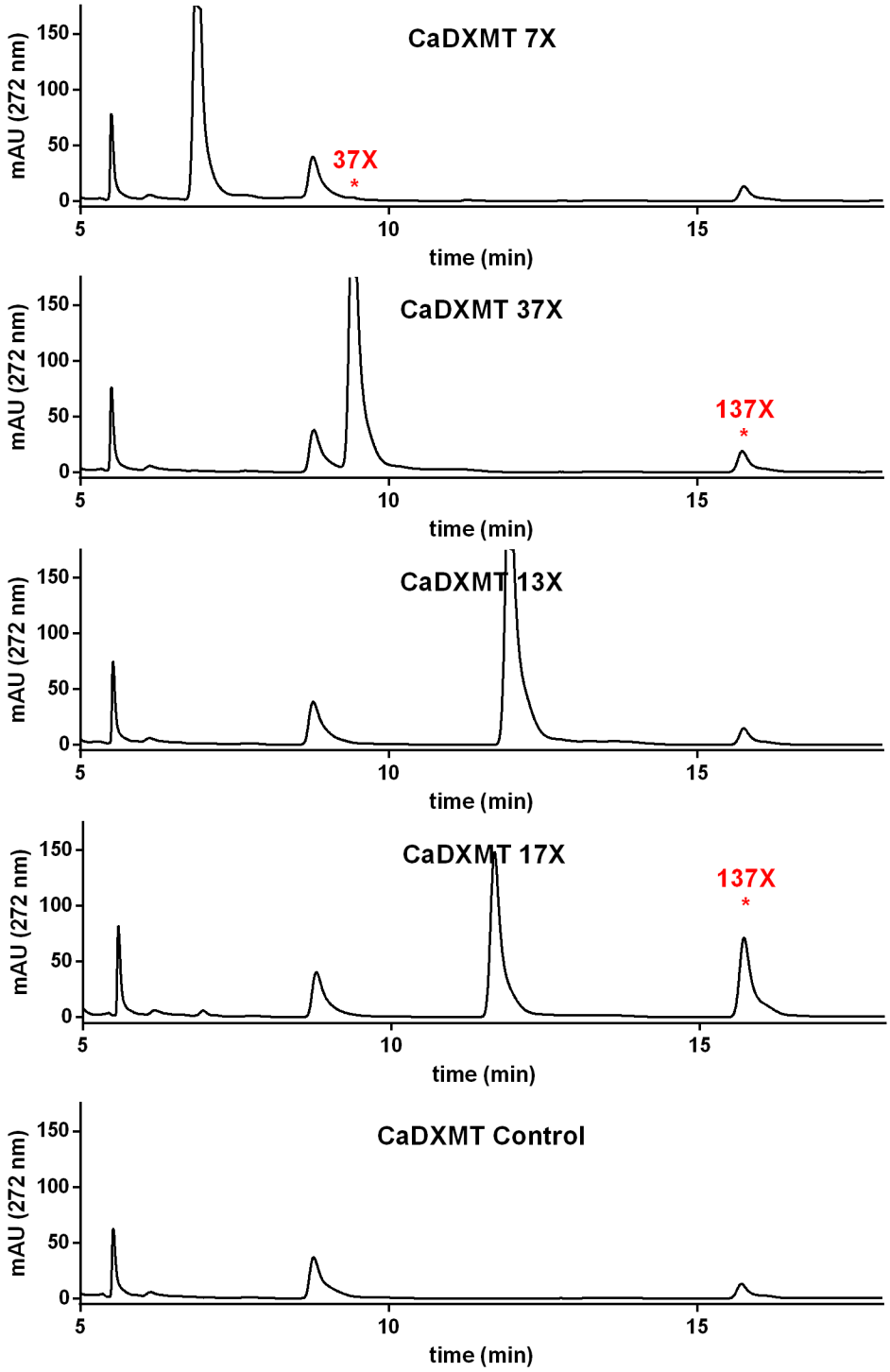

Figure 3.54: 7X, 37X, 13X, 17X, and control chromatograms from DAD (272 nm) for CsAncCS. Products are marked with an asterisk and are labeled in red.

3.15.6.3 CaMXMT

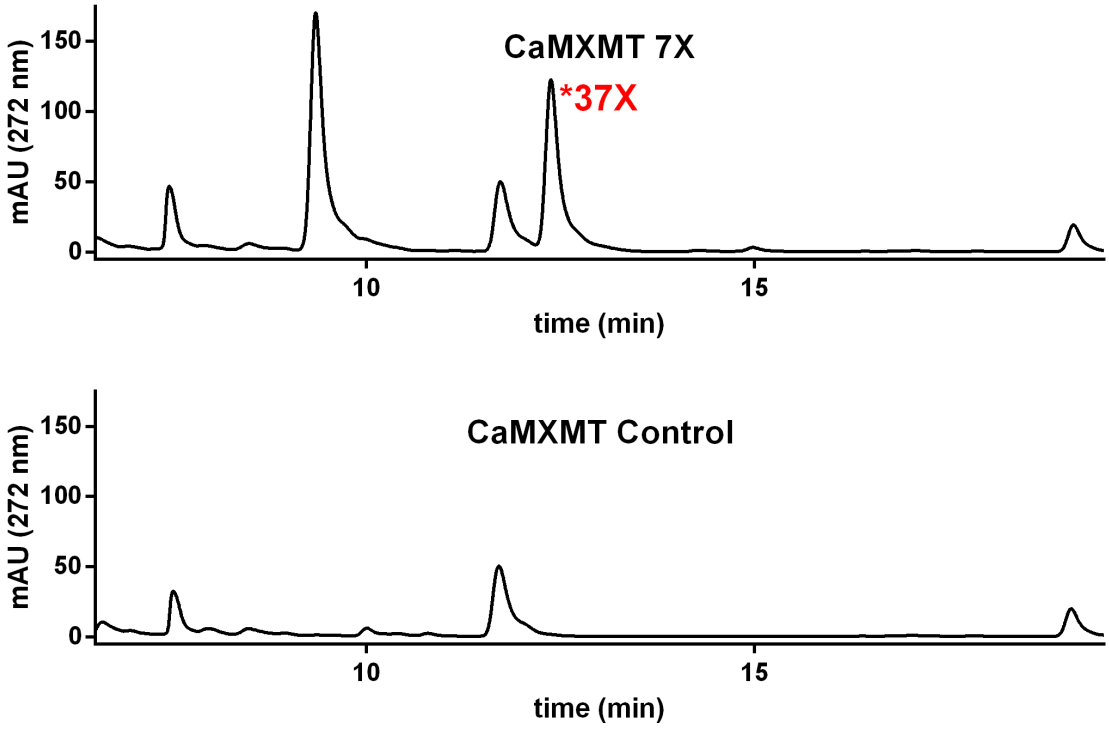

Figure 3.55: 7X and control chromatograms from DAD (272 nm) for CaMXMT. Products are marked with an asterisk and are labeled in red.

3.15.6.4 CaXMT1

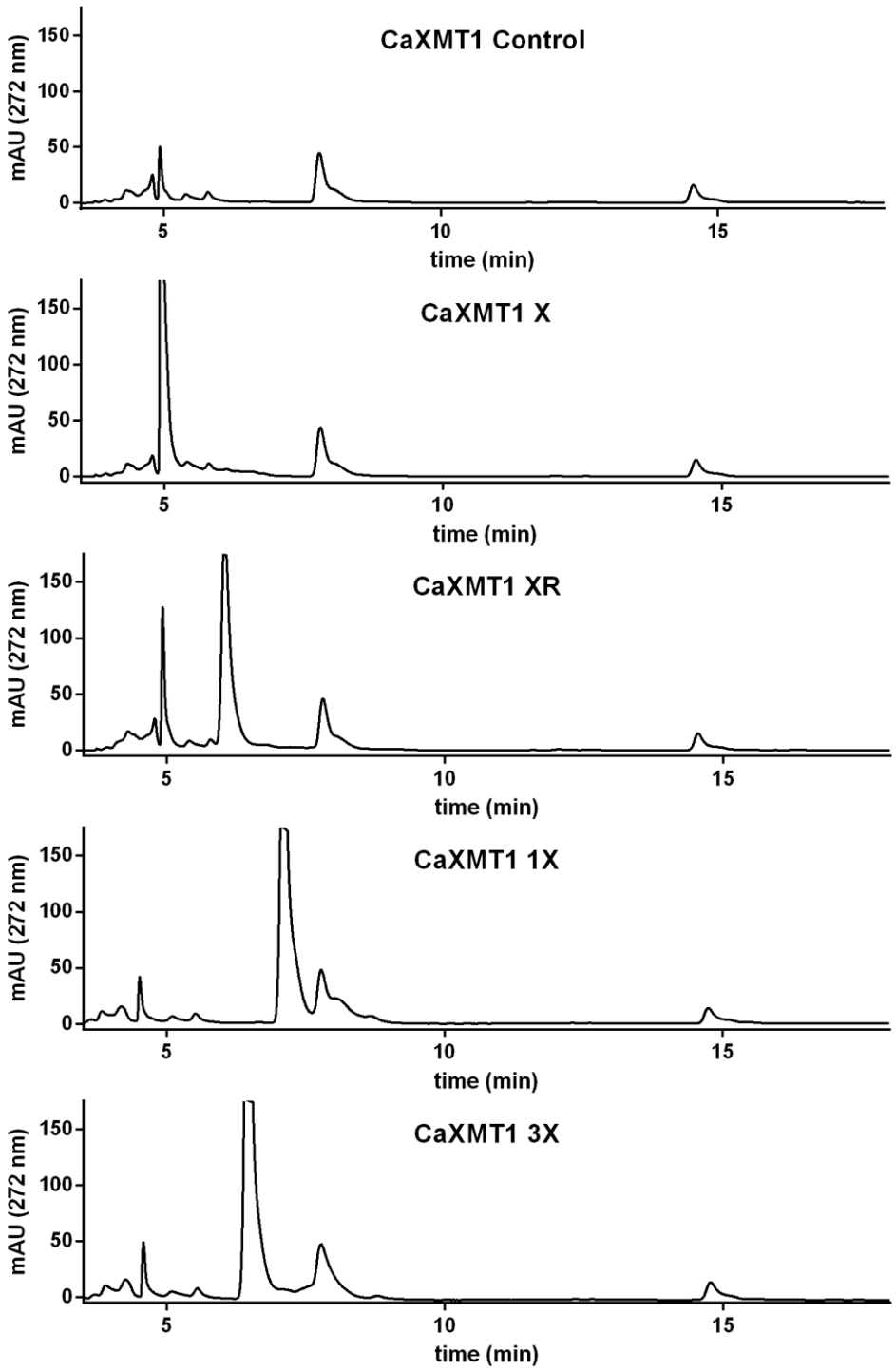

Figure 3.56: Control, X, XR, 1X, and 3X chromatograms from DAD (272 nm) for CsAncCS. Products are marked with an asterisk and are labeled in red.

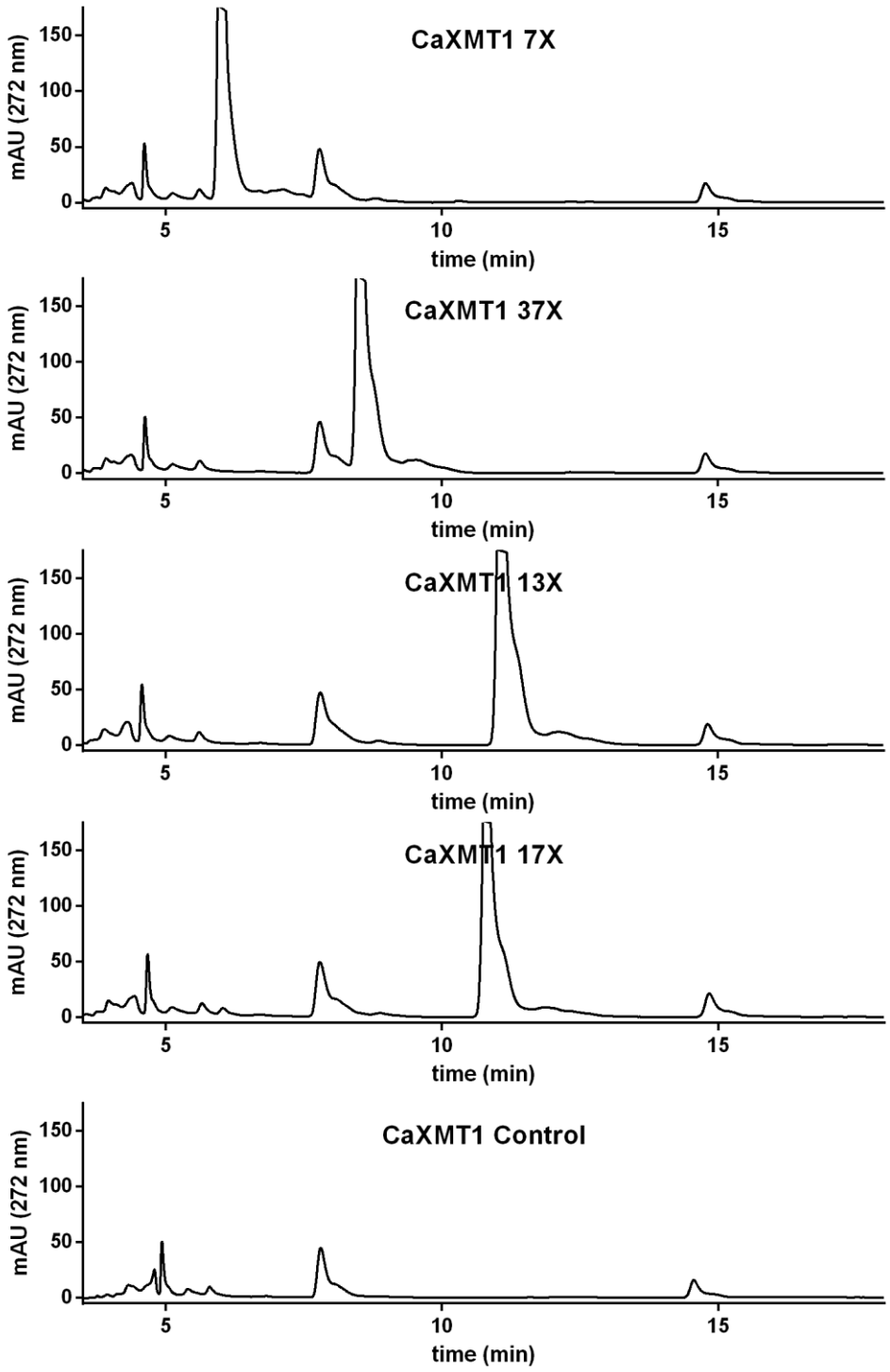

Figure 3.57: 7X, 37X, 13X, 17X, and control chromatograms from DAD (272 nm) for CsAncCS. Products are marked with an asterisk and are labeled in red.

3.15.6.4 CaXMT1-G

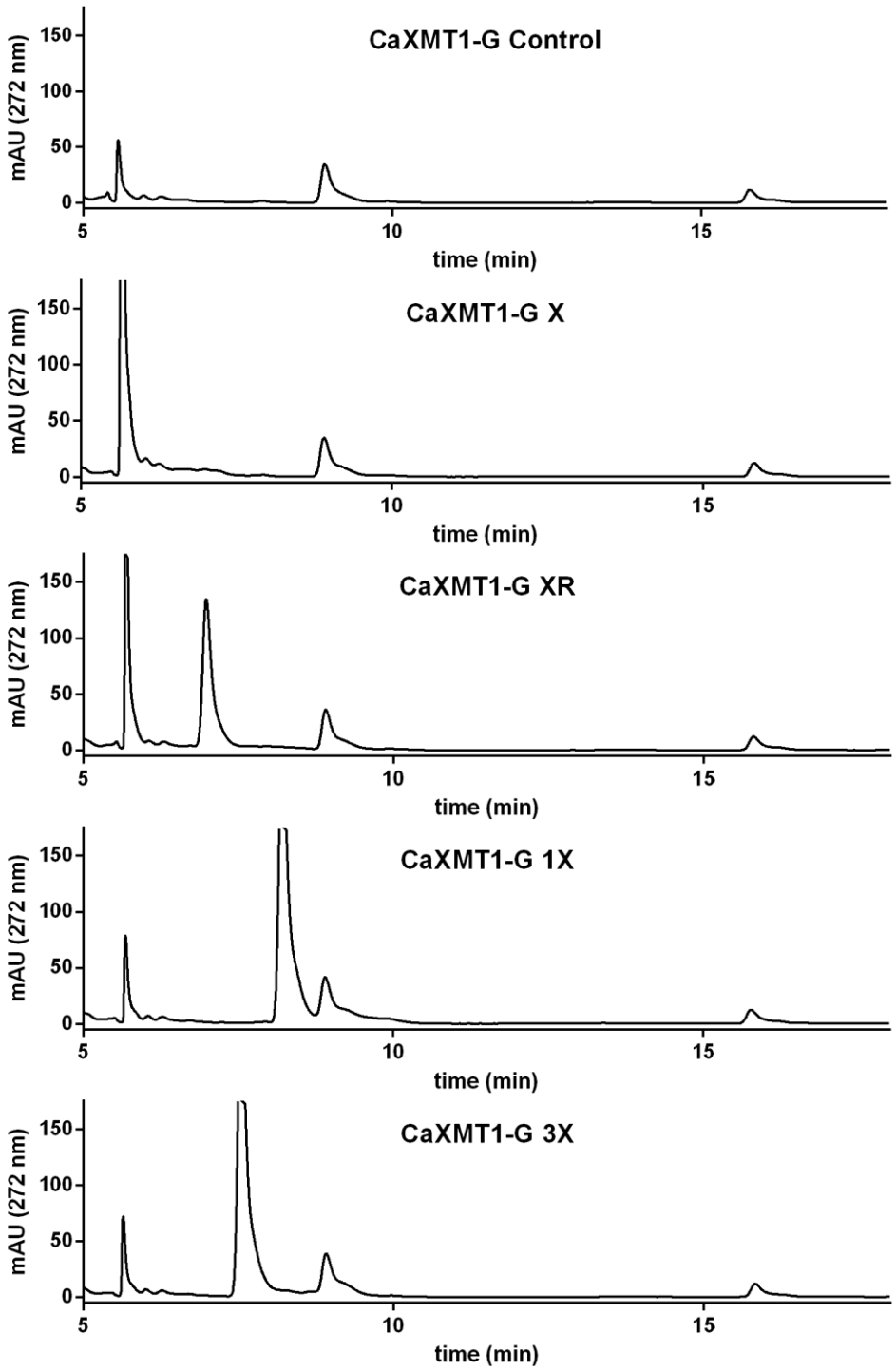

Figure 3.58: Control, X, XR, 1X, and 3X chromatograms from DAD (272 nm) for CsAncCS. Products are marked with an asterisk and are labeled in red.

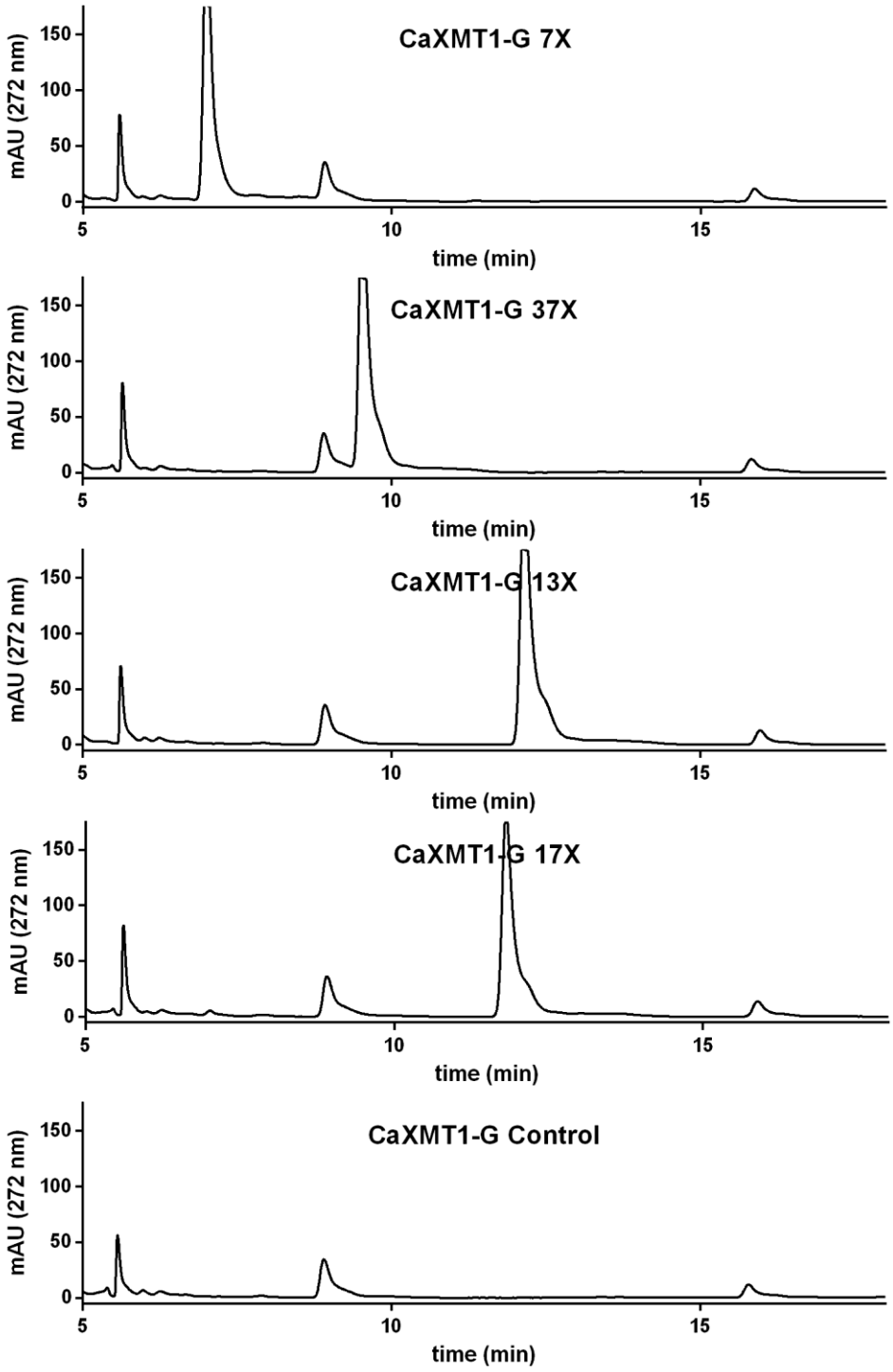

Figure 3.59: 7X, 37X, 13X, 17X, and control chromatograms from DAD (272 nm) for CsAncCS. Products are marked with an asterisk and are labeled in red.

3.15.6.5 CCS1

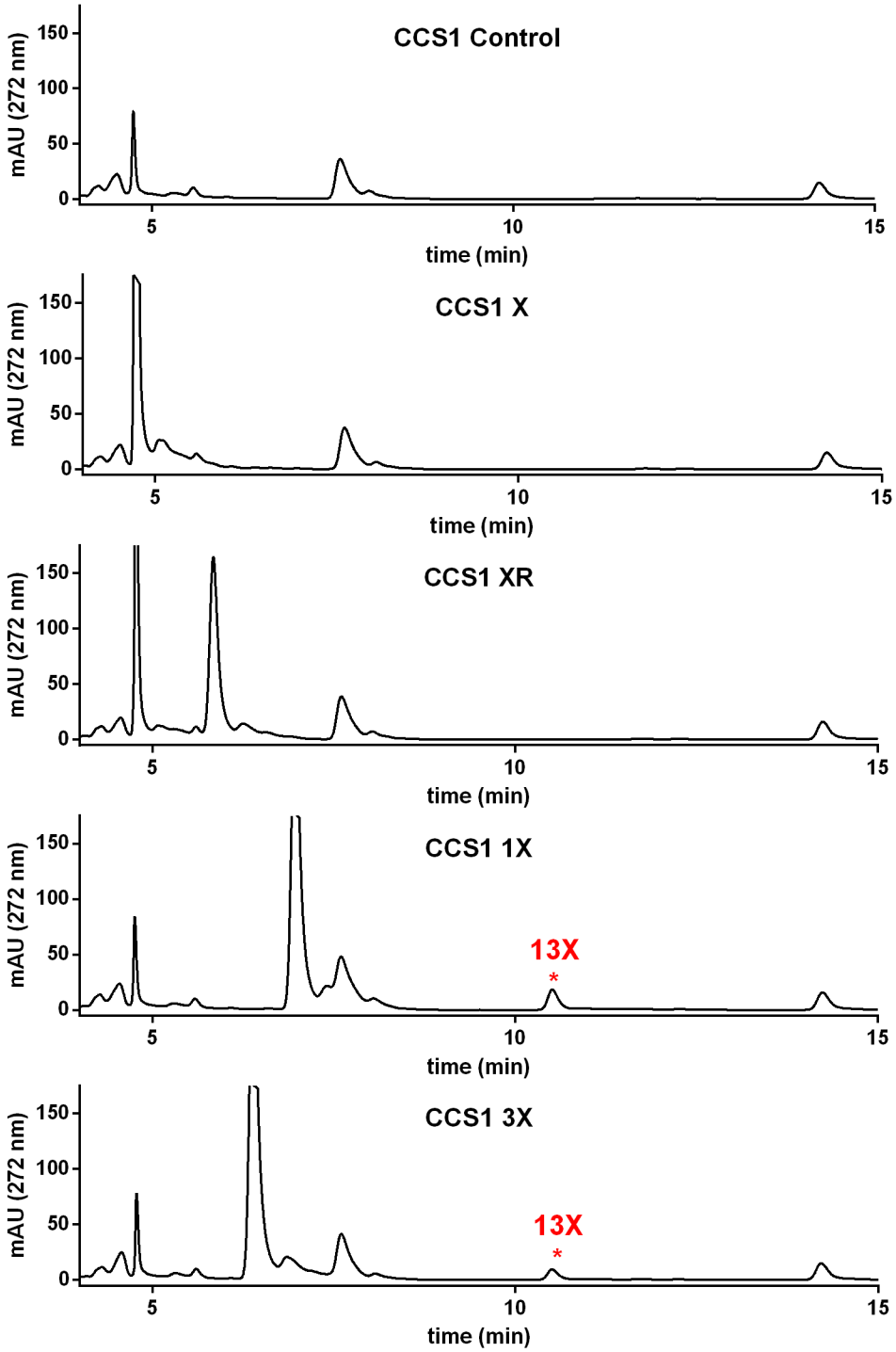

Figure 3.60: Control, X, XR, 1X, and 3X chromatograms from DAD (272 nm) for CsAncCS. Products are marked with an asterisk and are labeled in red.

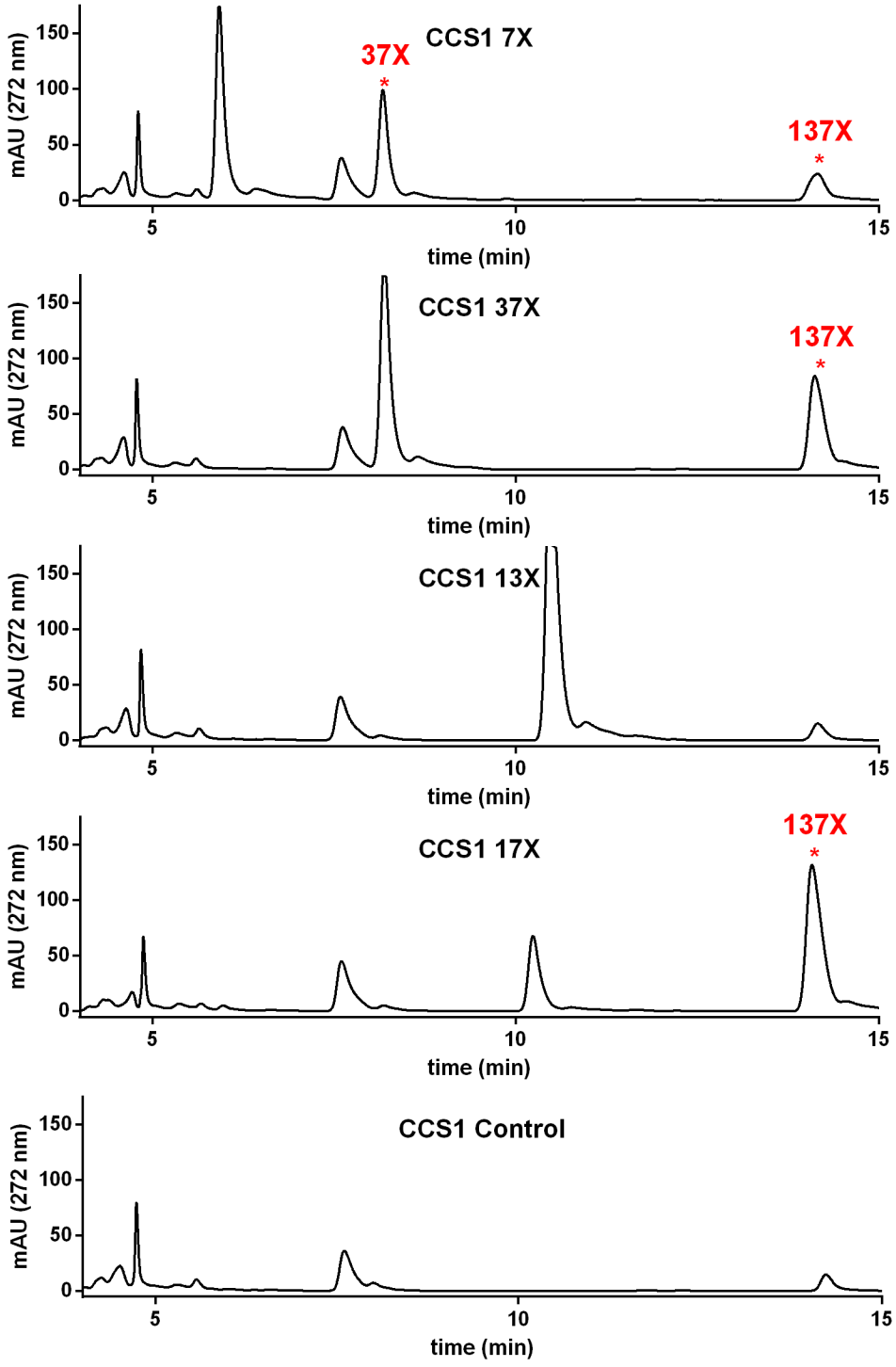

Figure 3.61: 7X, 37X, 13X, 17X, and control chromatograms from DAD (272 nm) for CsAncCS. Products are marked with an asterisk and are labeled in red.

3.15.6.6 CCS1-G

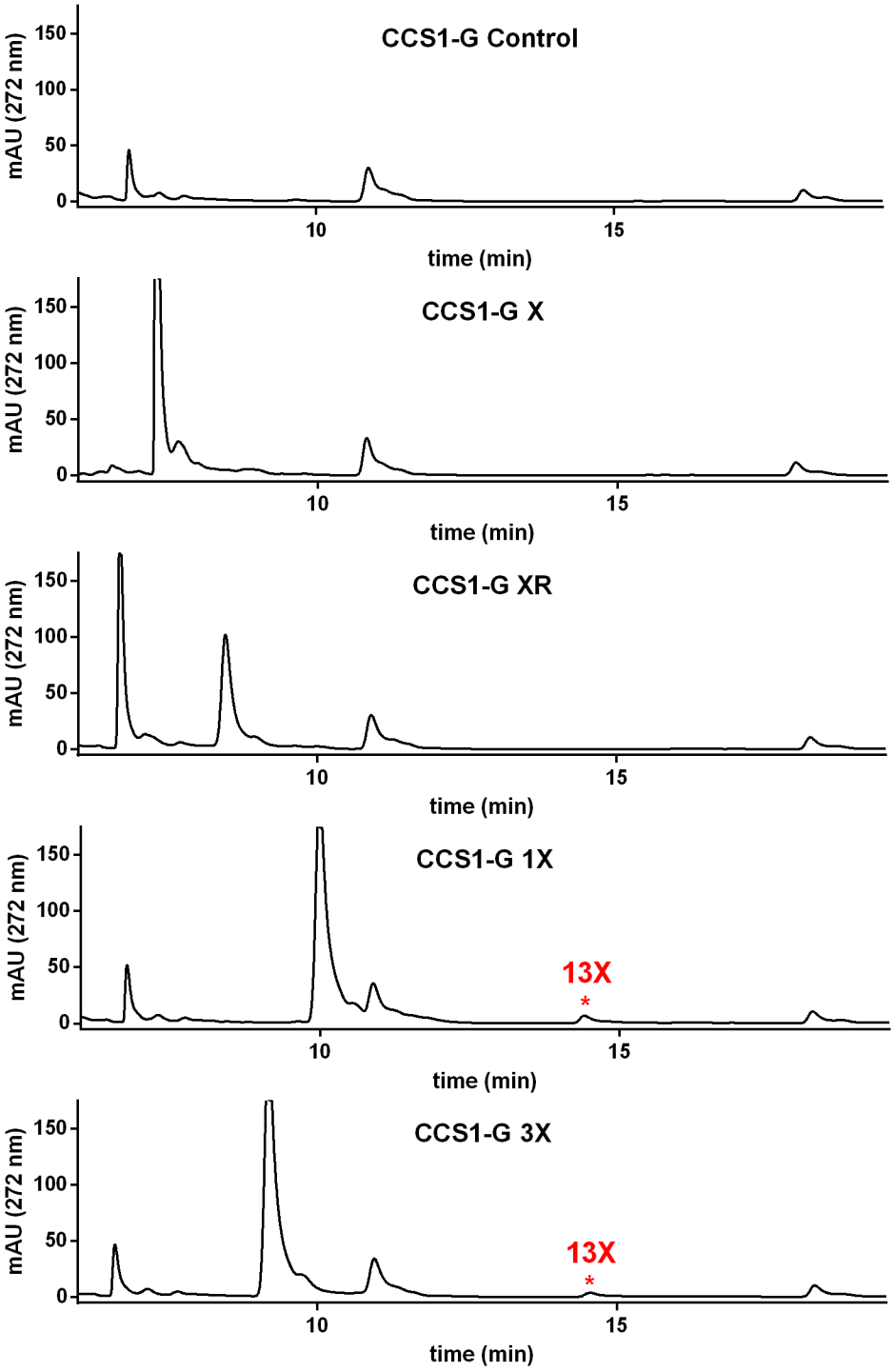

Figure 3.62: Control, X, XR, 1X, and 3X chromatograms from DAD (272 nm) for CCS1-G. Products are marked with an asterisk and are labeled in red.

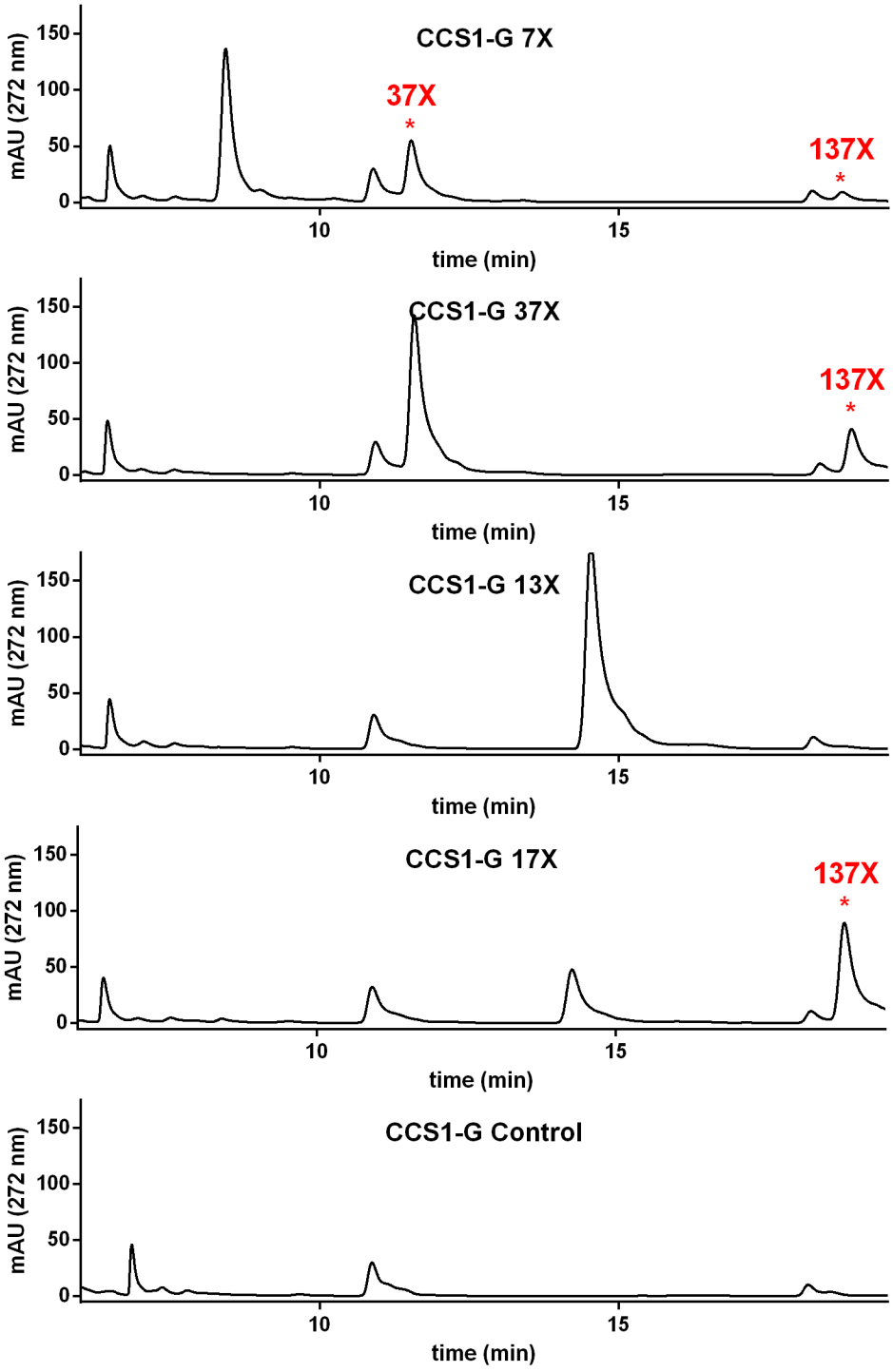

Figure 3.63: 7X, 37X, 13X, 17X, and control chromatograms from DAD (272 nm) for CCS1-G. Products are marked with an asterisk and are labeled in red.

3.15.6.7 CCS1(delC13)

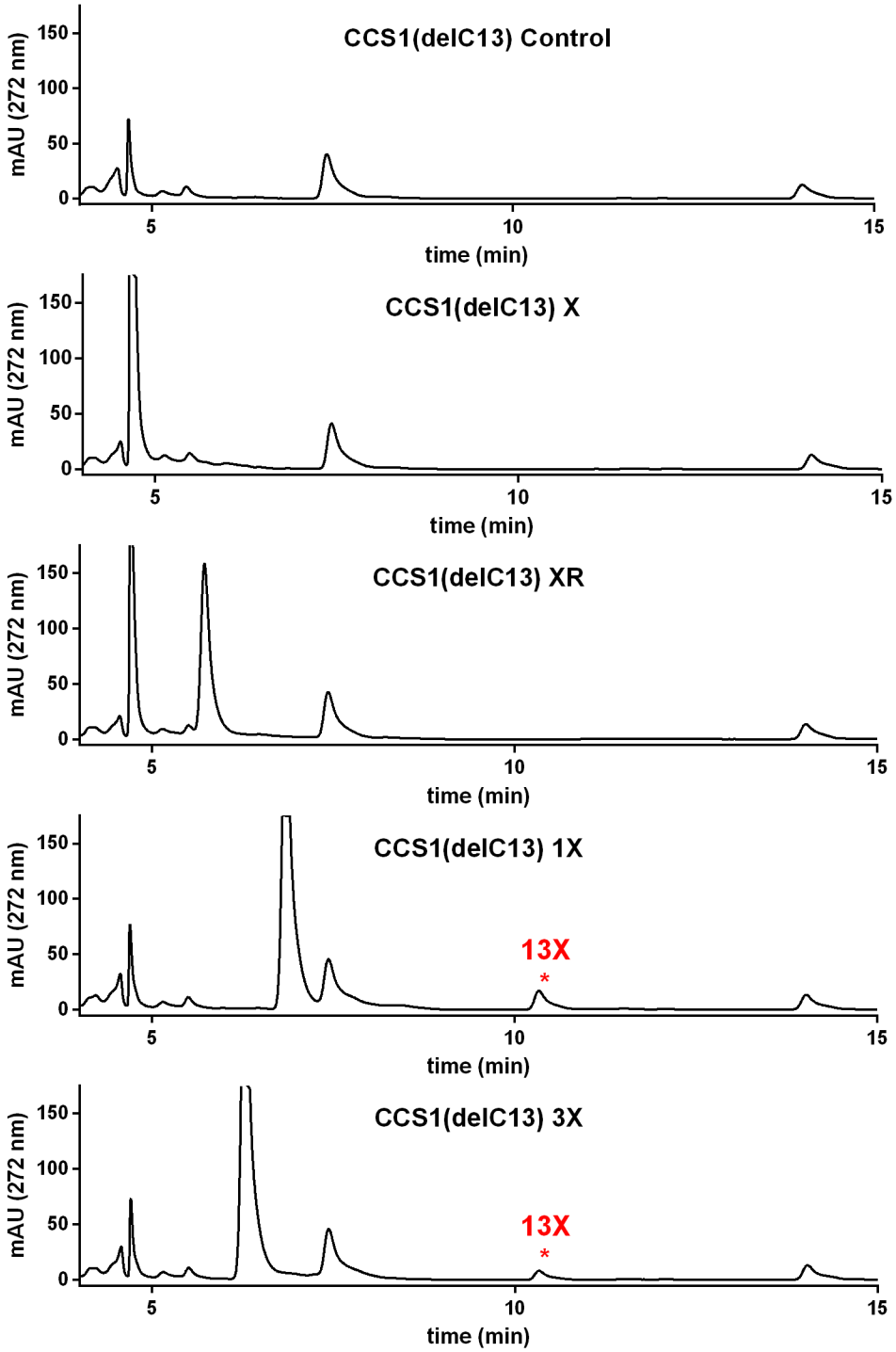

Figure 3.64: Control, X, XR, 1X, and 3X chromatograms from DAD (272 nm) for CCS1(delC13). Products are marked with an asterisk and are labeled in red.

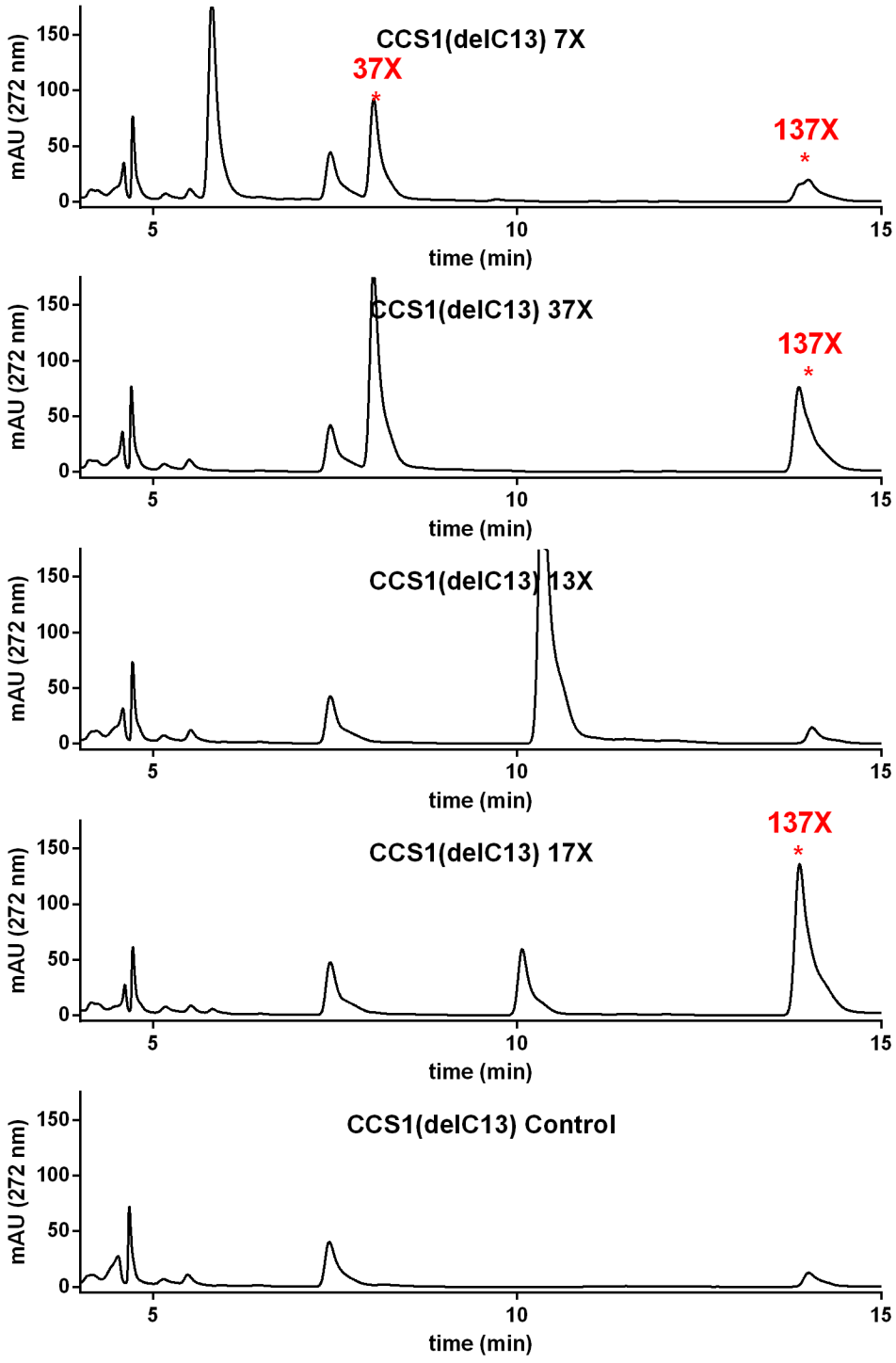

Figure 3.65: 7X, 37X, 13X, 17X, and control chromatograms from DAD (272 nm) for CCS1(delC13). Products are marked with an asterisk and are labeled in red.

3.15.6.8 CsAncCS

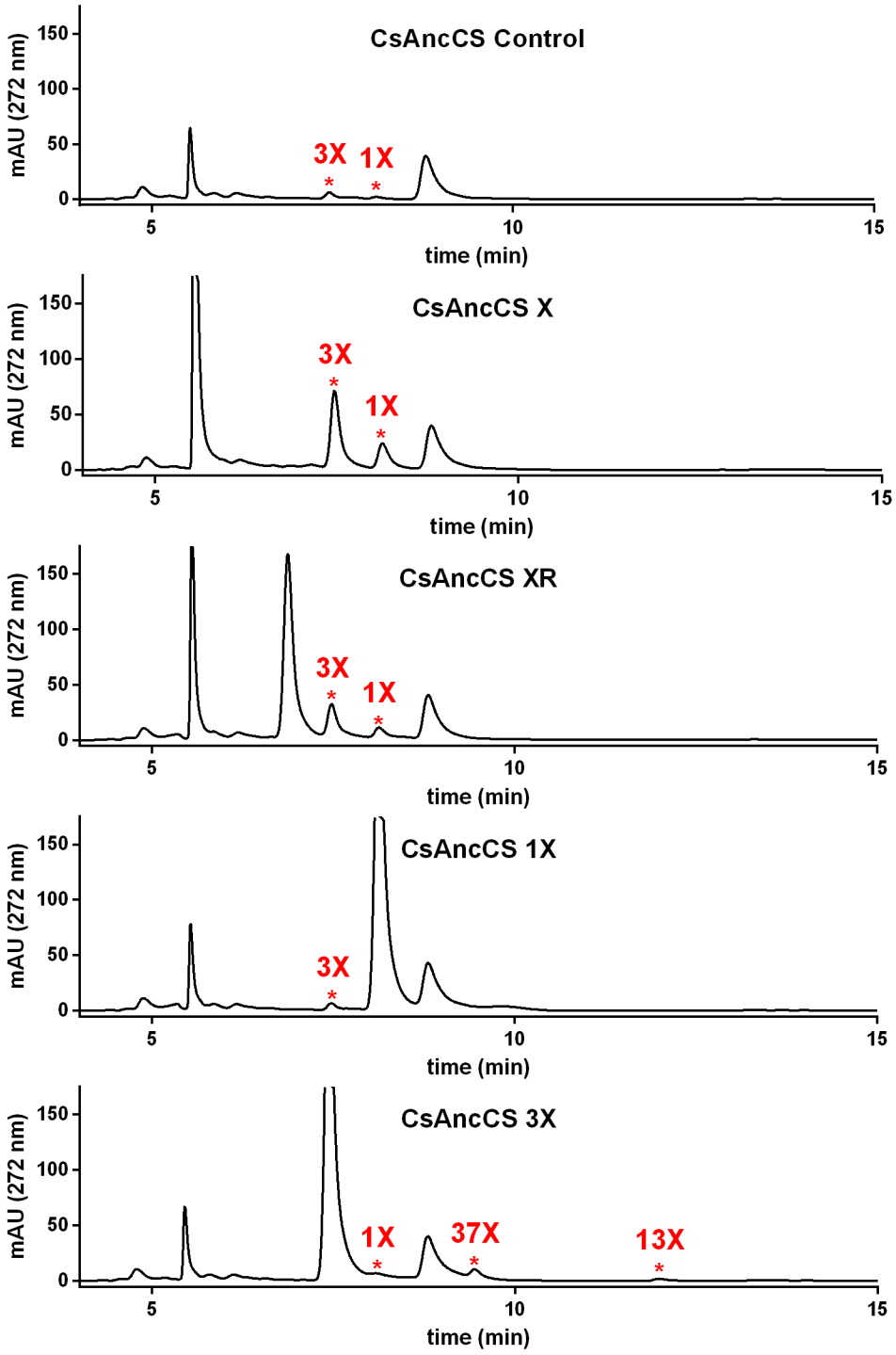

Figure 3.66: Control, X, XR, 1X, and 3X chromatograms from DAD 272 nm for CsAncCS. Note the presence of 3X and 1X in all samples. This likely comes from conversion of endogenous xanthine. Products are marked with an asterisk and are labeled in red.

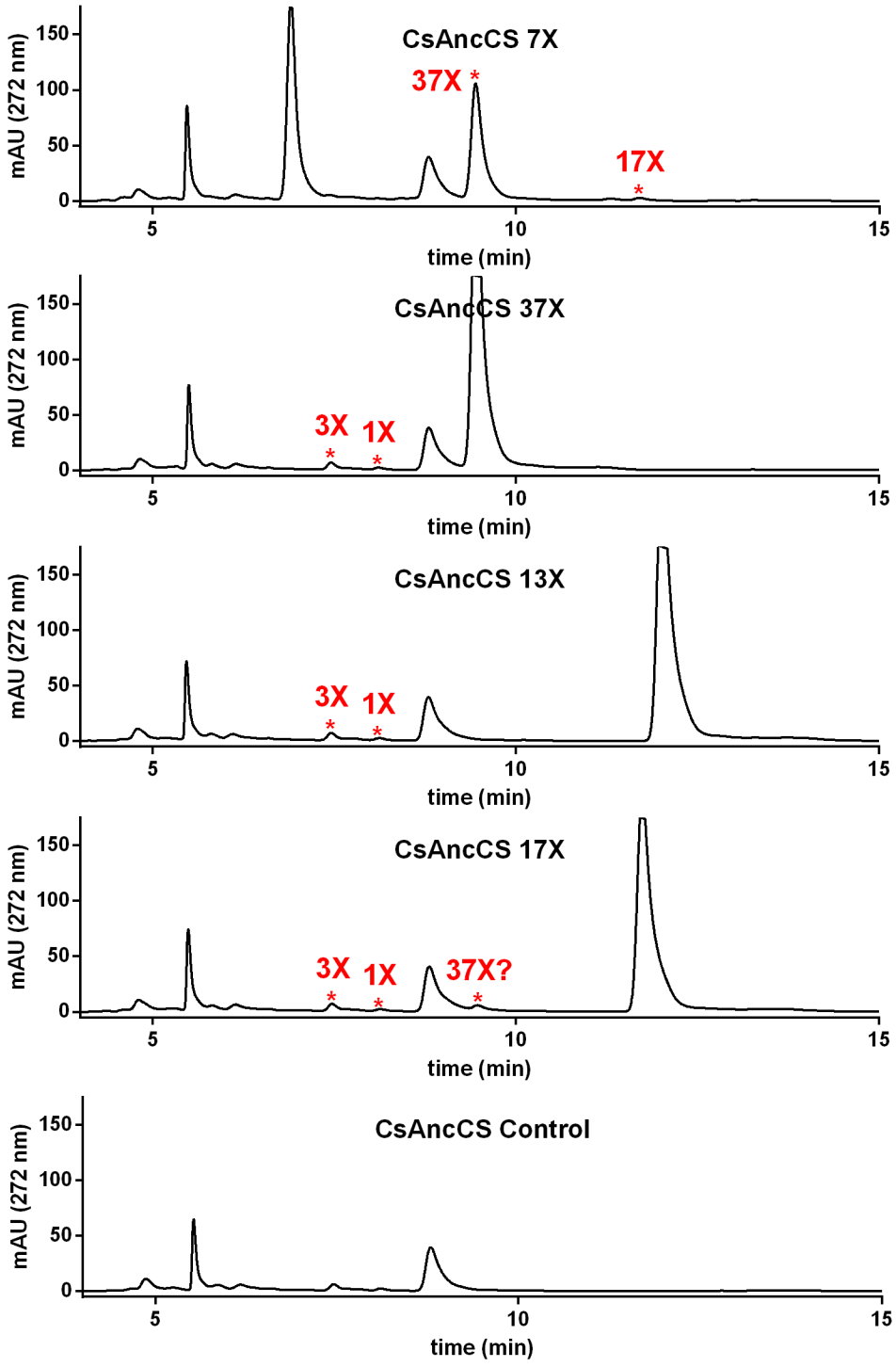

Figure 3.67: 7X, 37X, 13X, 17X, and control chromatograms from DAD (272 nm) for CsAncCS. Note the presence of 3X and 1X in all samples. This likely comes from conversion of endogenous xanthine. Products are marked with an asterisk and are labeled in red.

3.15.6.9 PcAncCS2

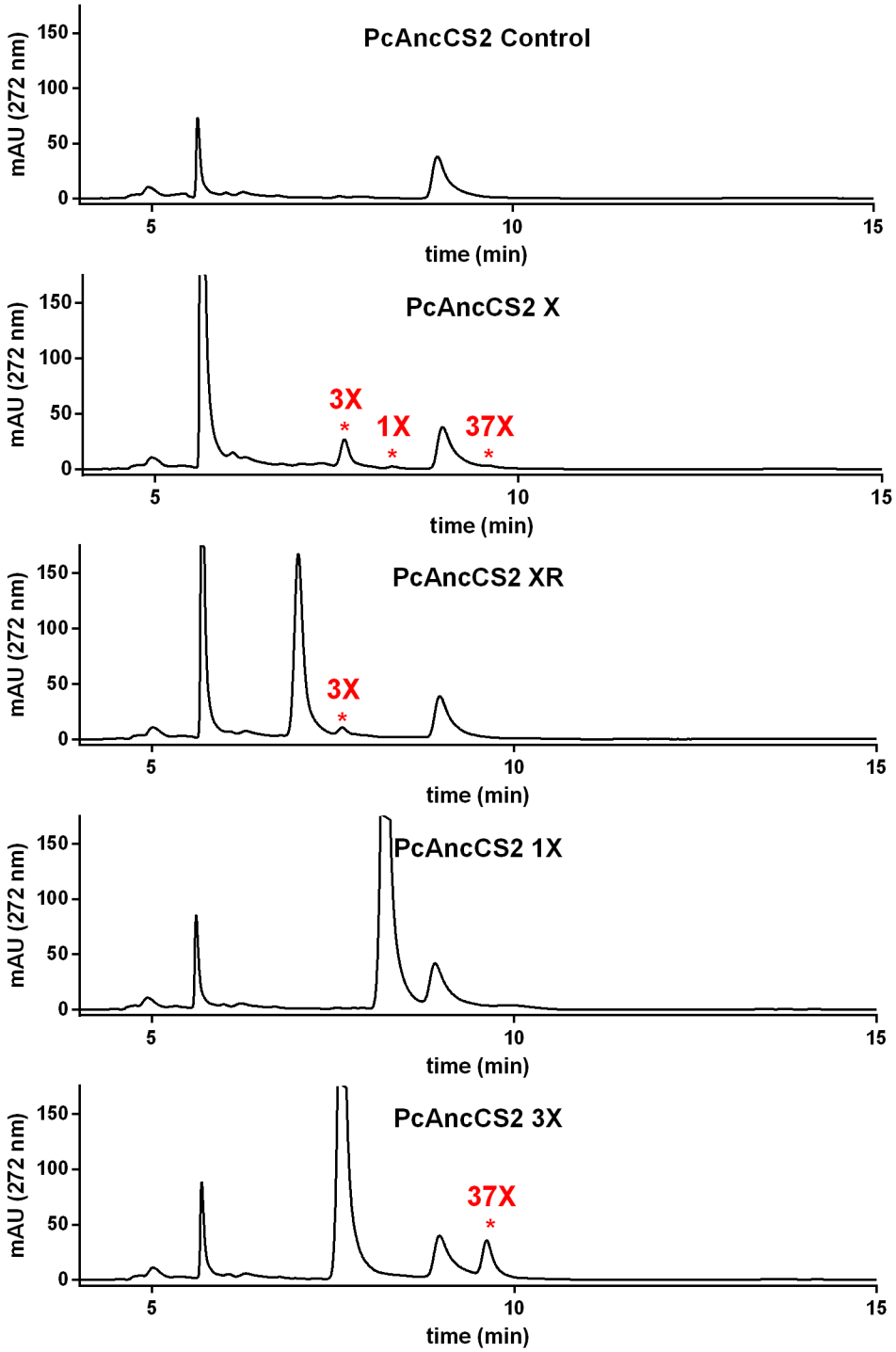

Figure 3.68: Control, X, XR, 1X, and 3X chromatograms from DAD (272 nm) for PcAncCS2. Products are marked with an asterisk and are labeled in red.

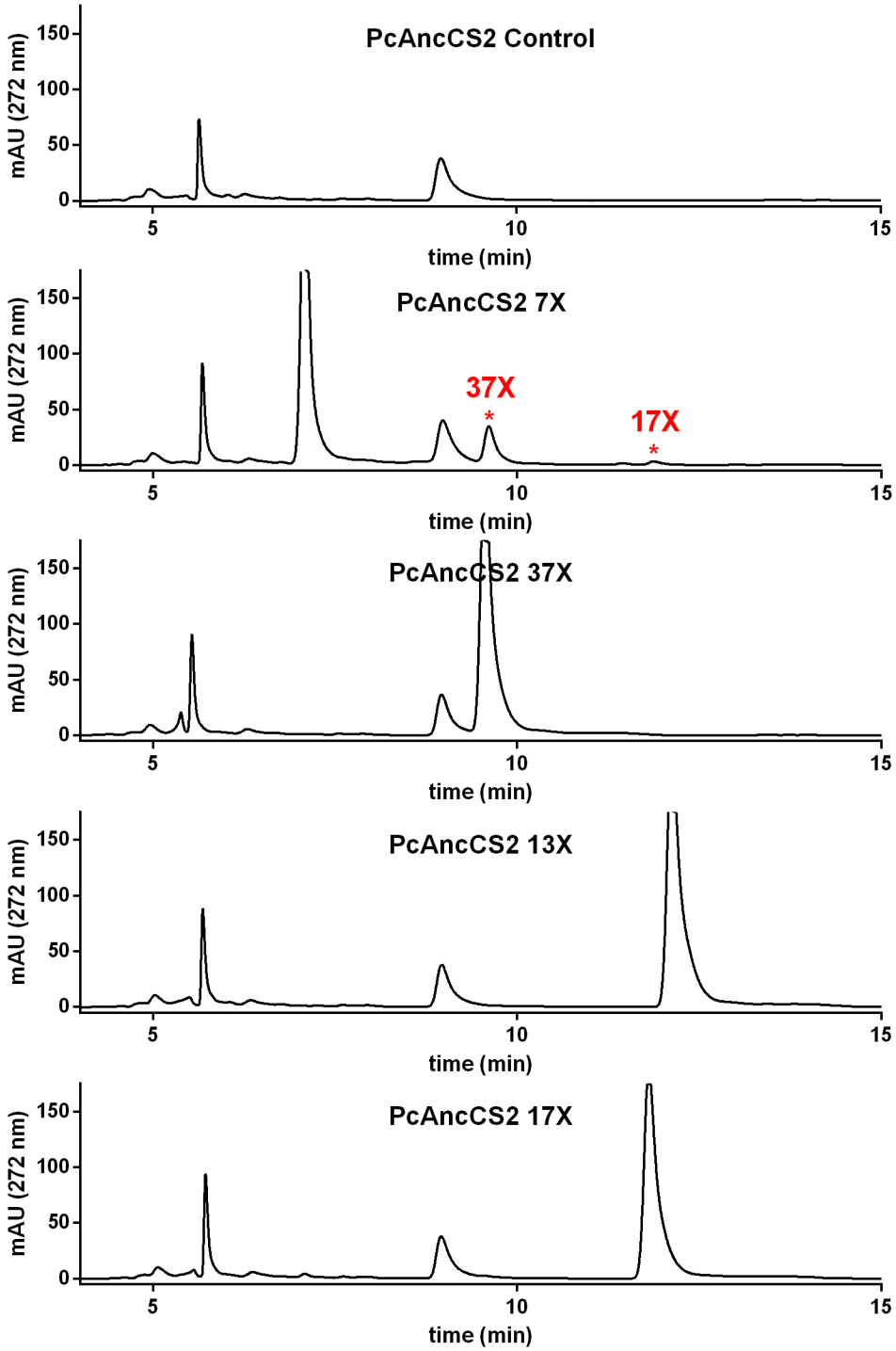

Figure 3.69: 7X, 37X, 13X, 17X, and control chromatograms from DAD (272 nm) for PcAncCS2. Products are marked with an asterisk and are labeled in red.

3.15.6.10 PcCS

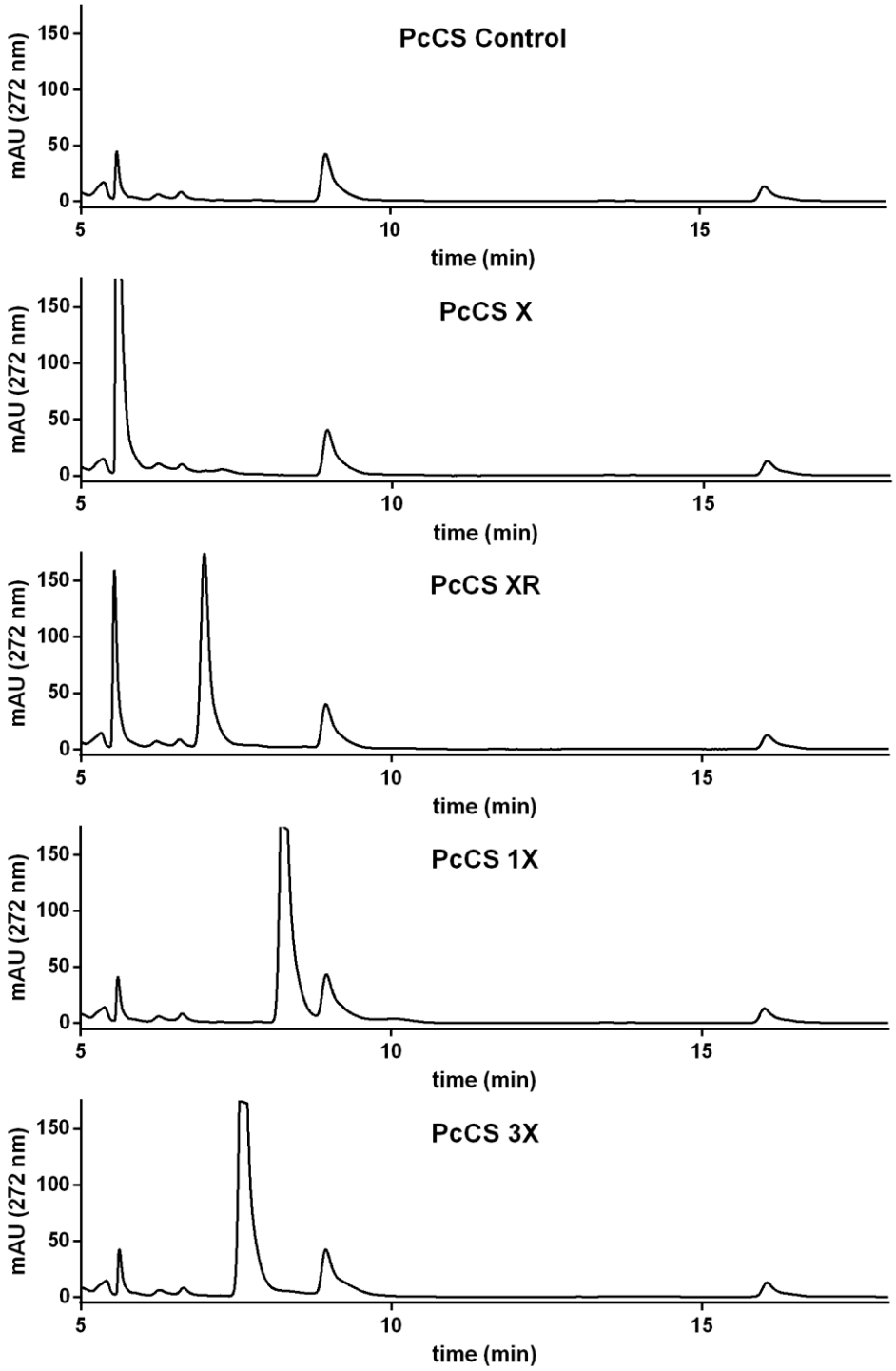

Figure 3.70: Control, X, XR, 1X, and 3X chromatograms from DAD (272 nm) for PcCS. Products are marked with an asterisk and are labeled in red.

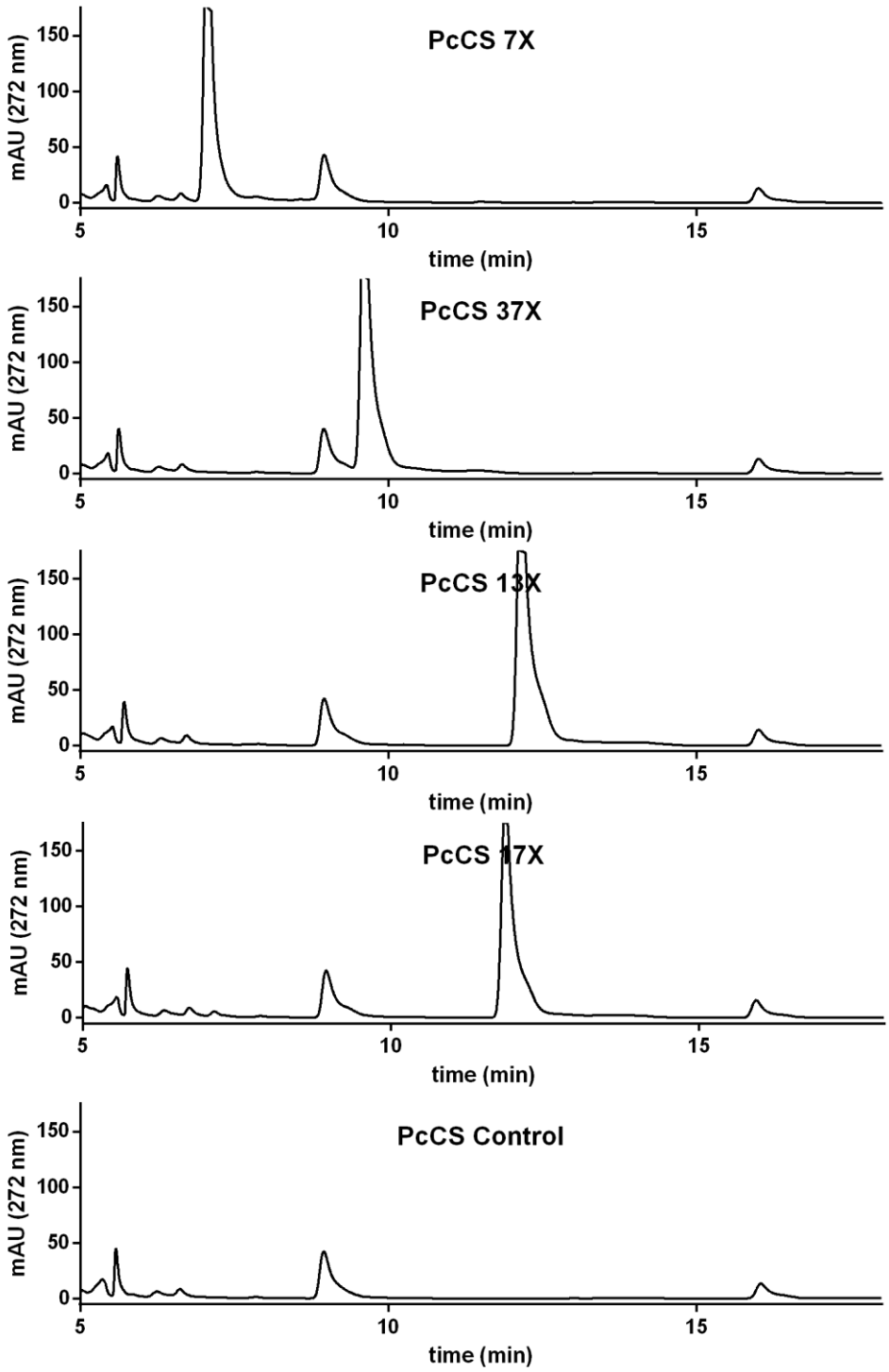

Figure 3.71: 7X, 37X, 13X, 17X, and control chromatograms from DAD (272 nm) for PcCS. Products are marked with an asterisk and are labeled in red.

3.15.6.11 TCS1

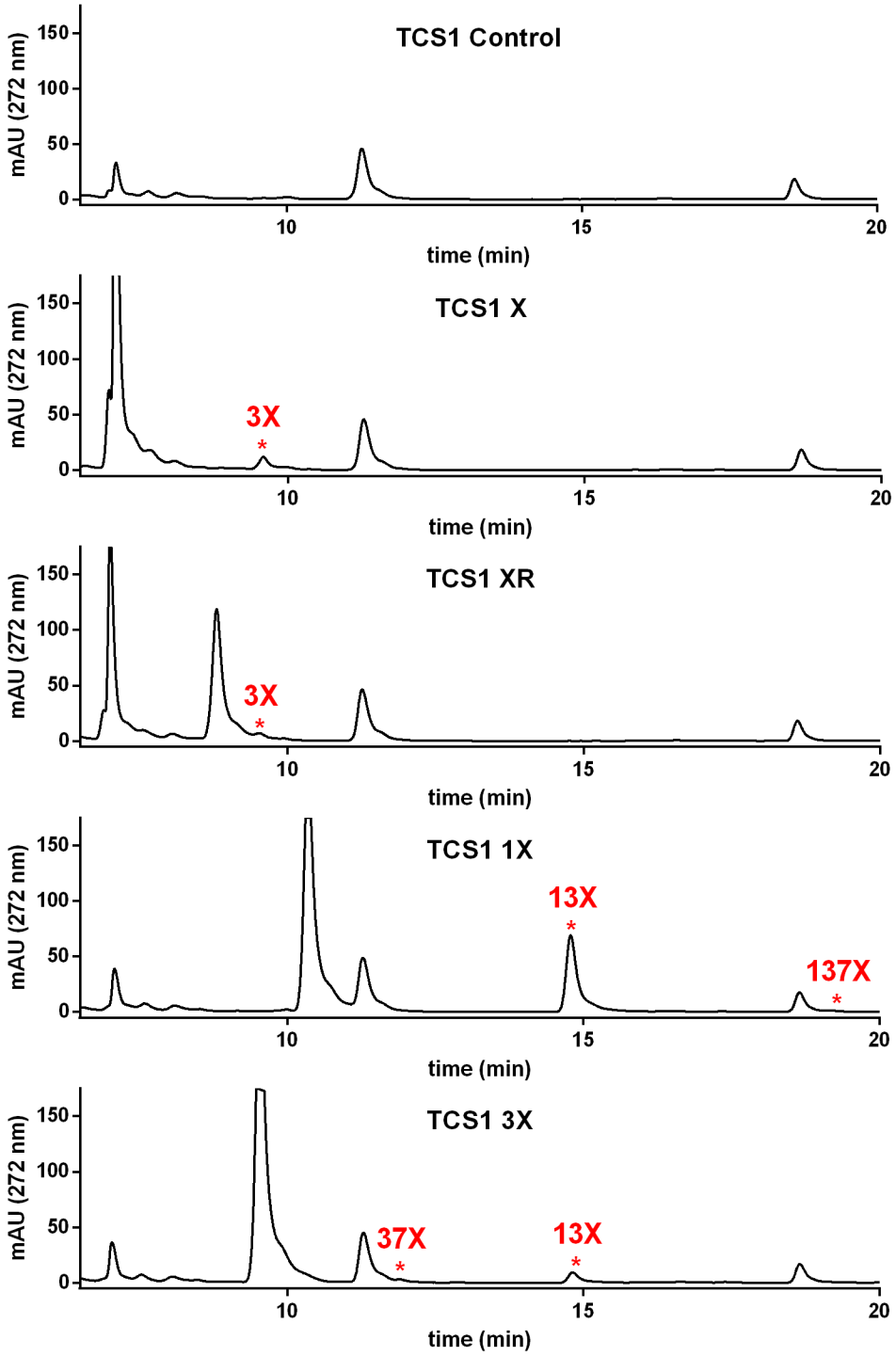

Figure 3.72: Control, X, XR, 1X, and 3X chromatograms from DAD (272 nm) for TCS1. Products are marked with an asterisk and are labeled in red.

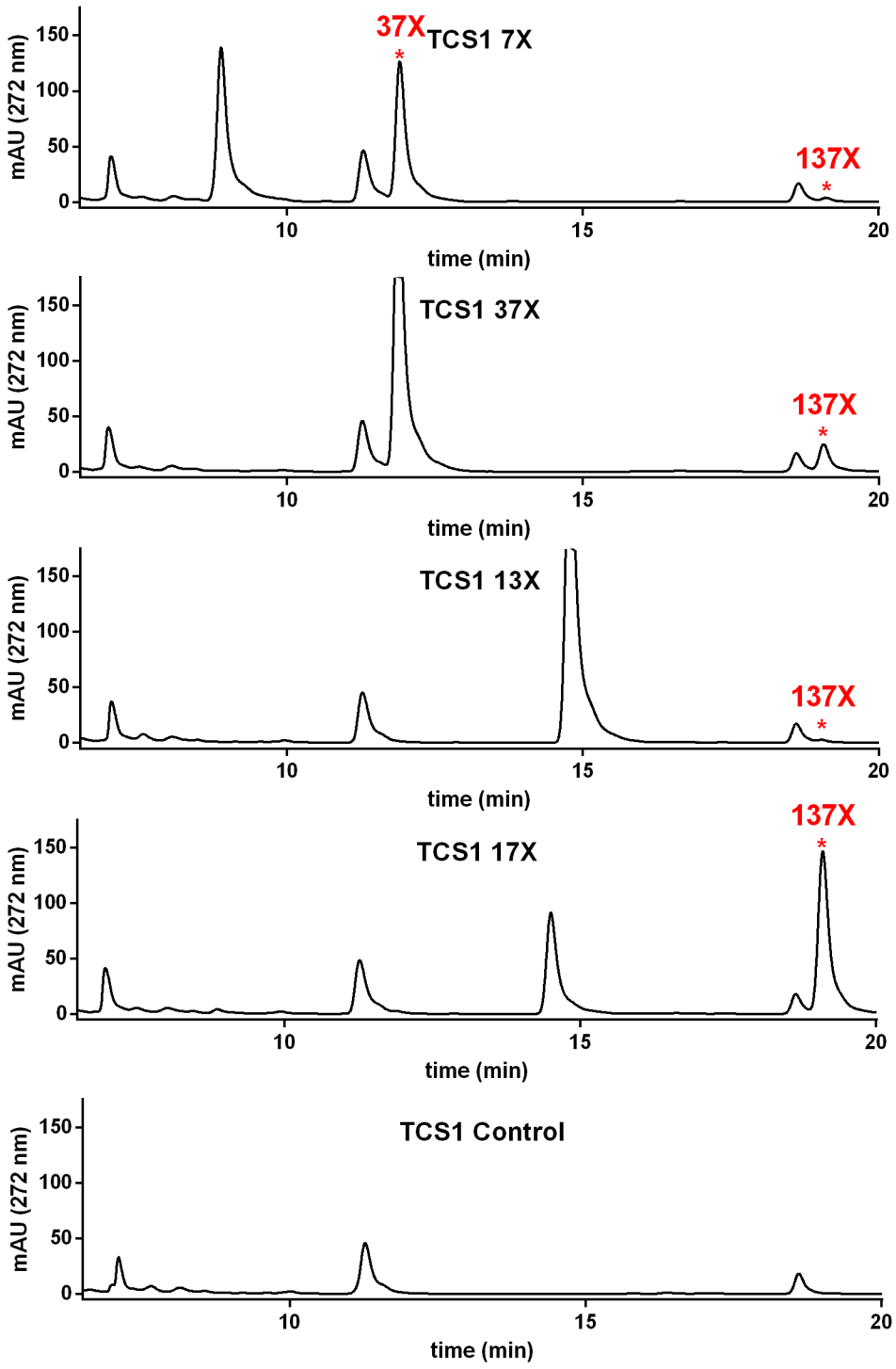

Figure 3.73: 7X, 37X, 13X, 17X, and control chromatograms from DAD (272 nm) for TCS1. Products are marked with an asterisk and are labeled in red.

3.15.6.12 TCS1-G

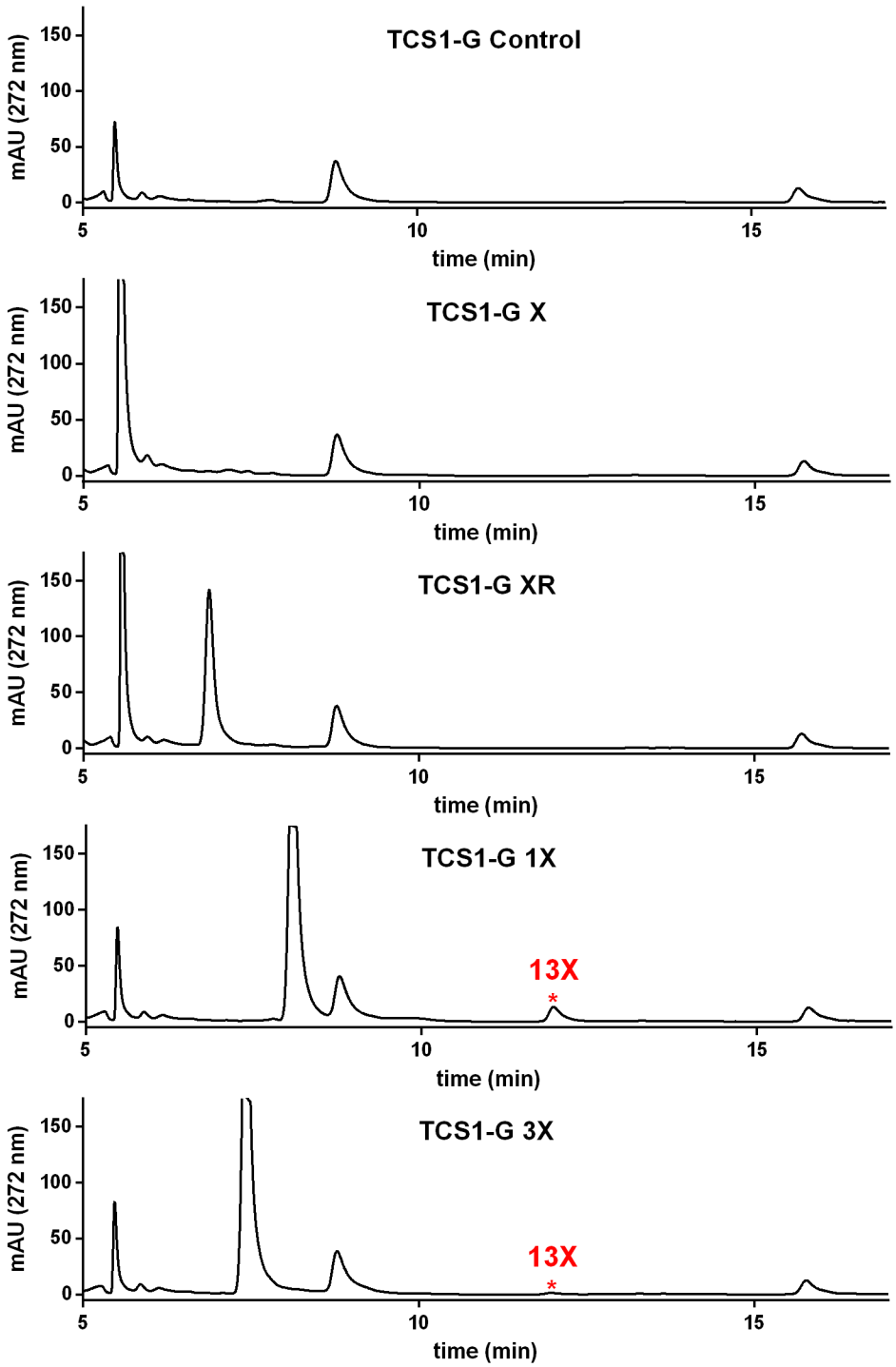

Figure 3.74: Control, X, XR, 1X, and 3X chromatograms from DAD (272 nm) for TCS1-G. Products are marked with an asterisk and are labeled in red.

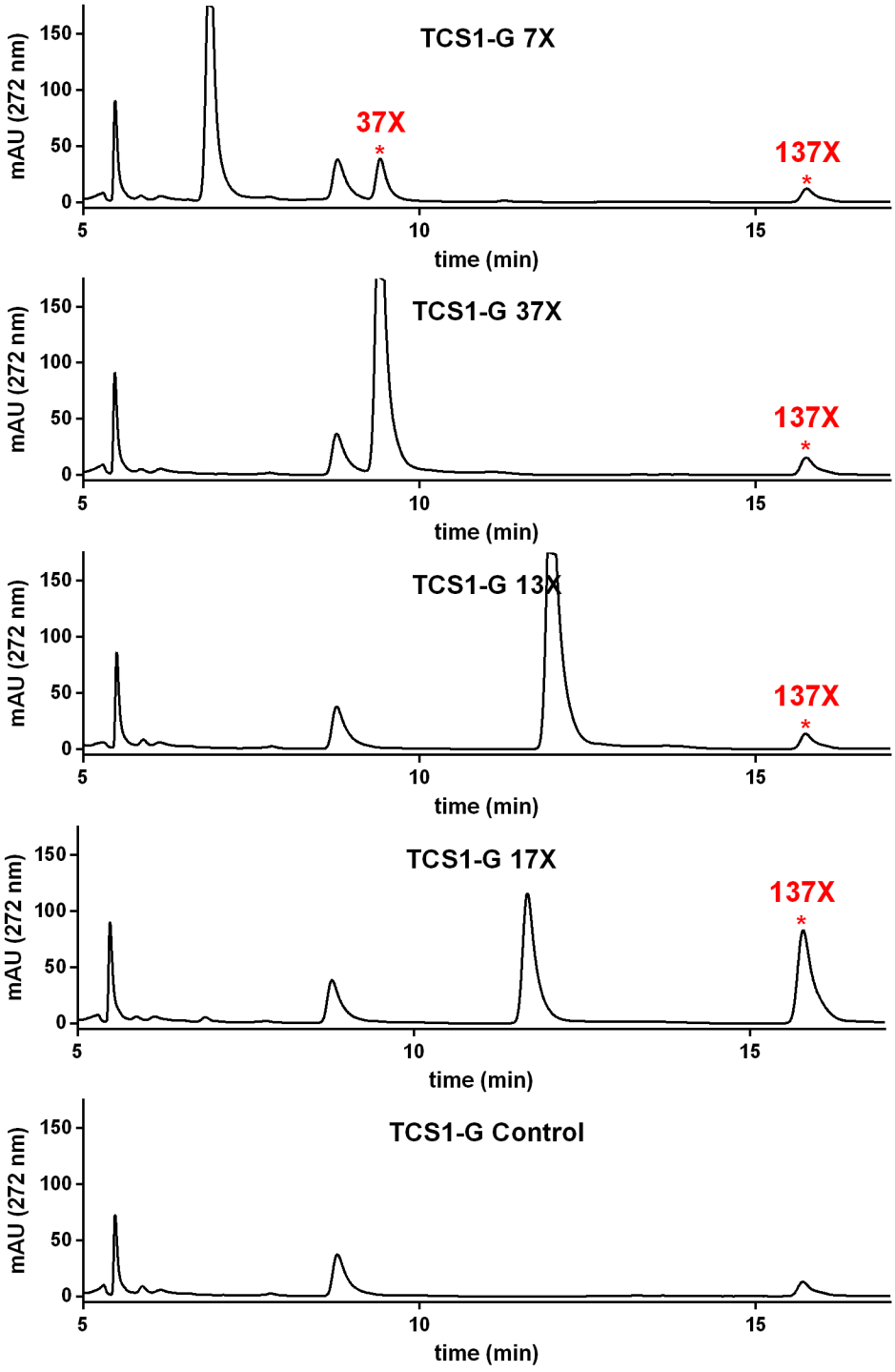

Figure 3.75: 7X, 37X, 13X, 17X, and control chromatograms from DAD (272 nm) for TCS1-G. Products are marked with an asterisk and are labeled in red.

3.15.6.13 TCS2

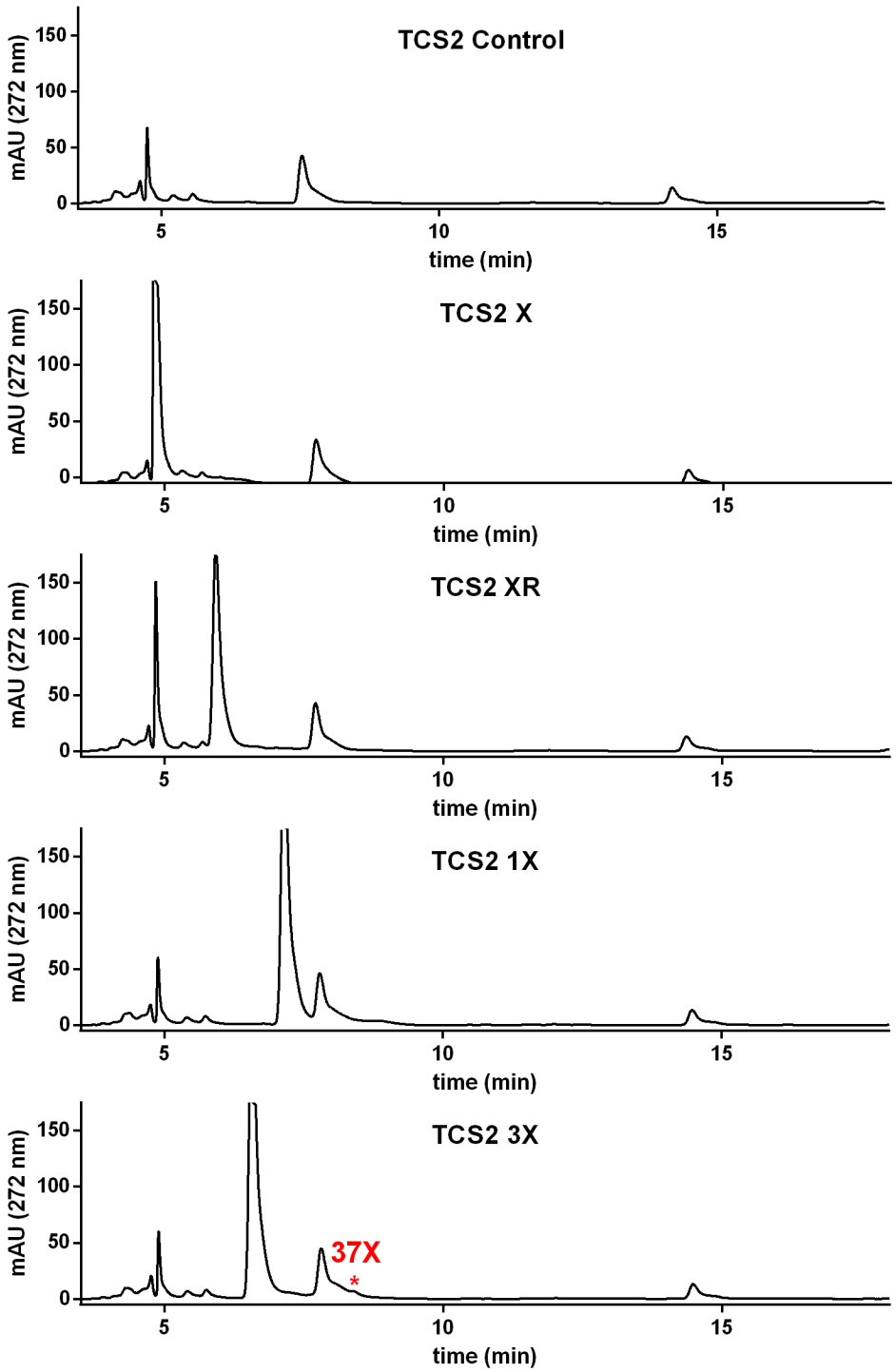

Figure 3.76: Control, X, XR, 1X, and 3X chromatograms from DAD (272 nm) for TCS2. Products are marked with an asterisk and are labeled in red.

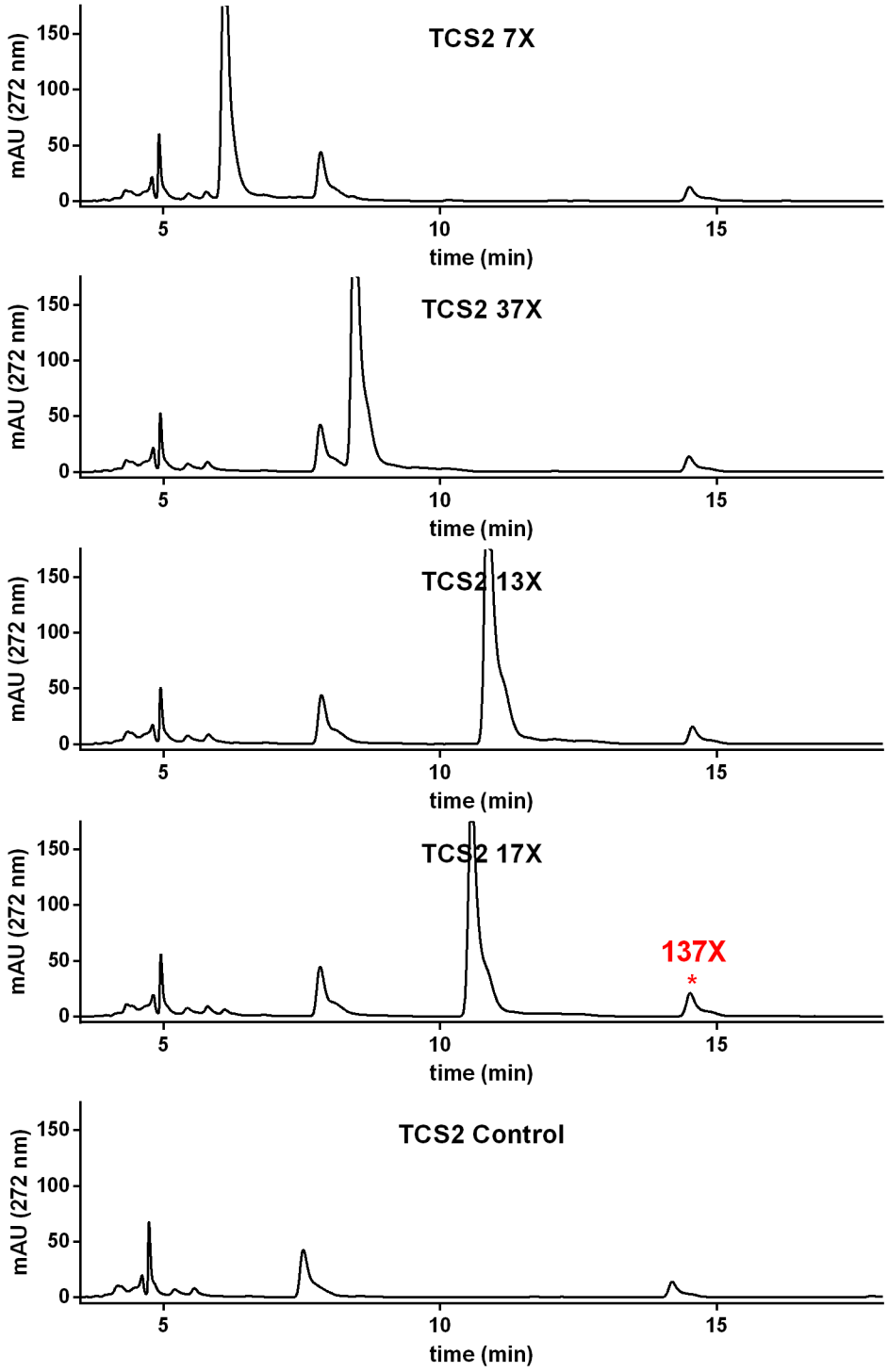

Figure 3.77: 7X, 37X, 13X, 17X, and control chromatograms from DAD (272 nm) for TCS2. Products are marked with an asterisk and are labeled in red.

3.15.6.14 LaG17-synNotch-TetRVP64 + TRE mCherry-P2A-MXMT / Target Cell 0:1 and 1:1 Co-culture

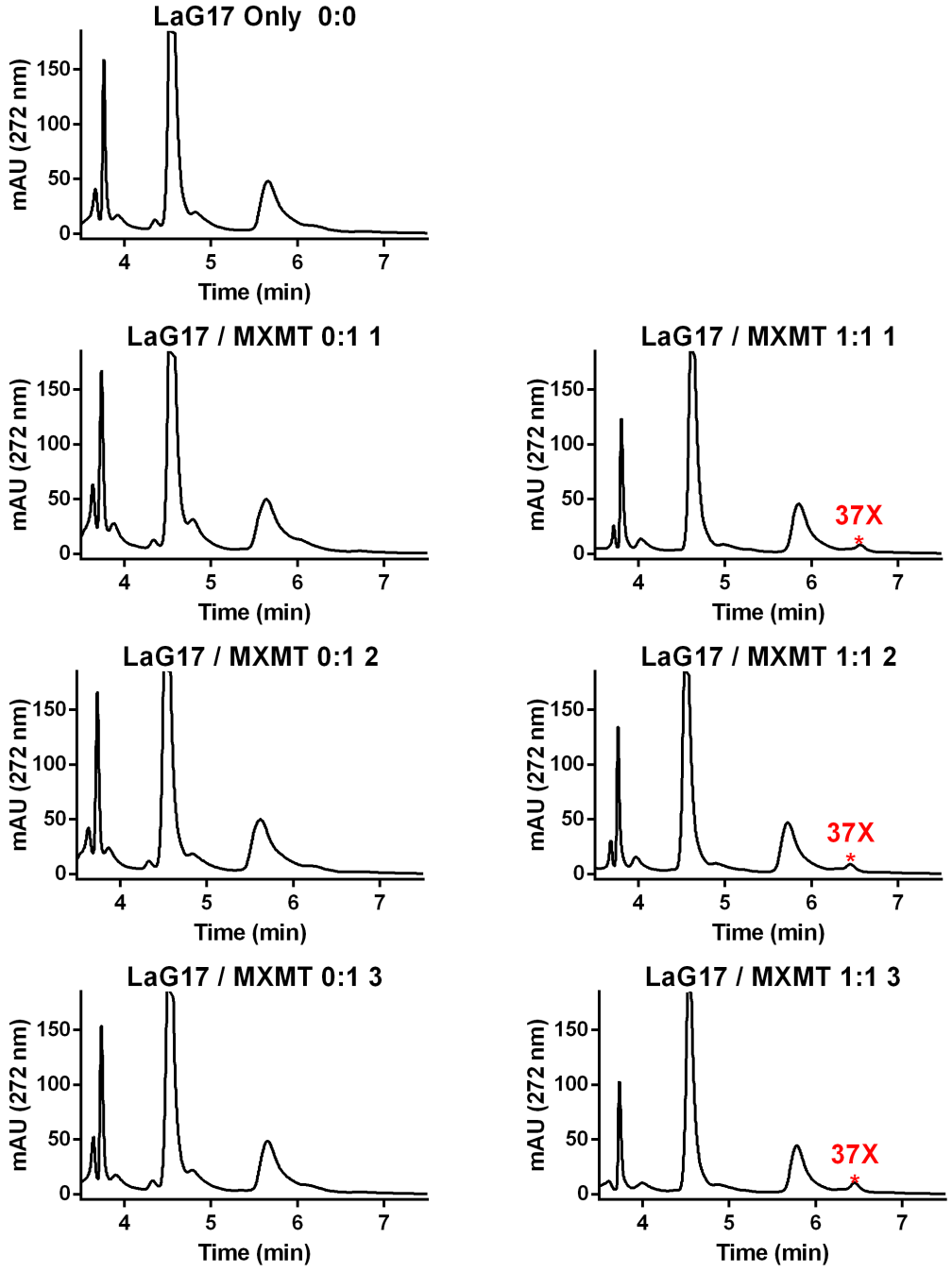

Figure 3.78: Chromatograms from DAD (272 nm) for co-culture experiment of LaG17-synNotch-TetRVP64 + TRE mCherry-P2A-MXMT / Target cells at 0:1 and 1:1 ratios with 200 µM 7X. Integration of control chromatogram was subtracted from each of the experimental conditions to determine concentrations.

3.15.6.14 LaG17-synNotch-TetRVP64 + TRE mCherry-P2A-TCS1 / Target Cell 1:1 Co-culture

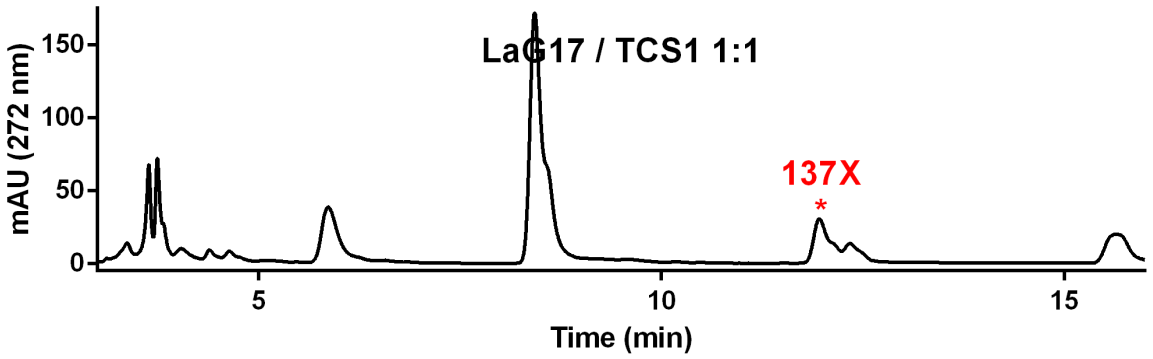

Figure 3.79: Chromatogram from DAD (272 nm) for co-culture experiment of LaG17-synNotch-TetRVP64 + TRE mCherry-P2A-TCS1 / Target cells 1:1 ratios with 200 µM PX. Integration of control chromatogram was subtracted from each of the experimental conditions to determine concentrations. Concentration of caffeine (not corrected for evaporative loss) was determined to be 32.1 µM.

3.15.7 Gene Block Sequences

The following are the Gene Block sequences ordered for the named genes. Start and stop codons are bolded. Names of enzymes are underlined.

PcCS

GCCACC**ATG**GATATGAAAGATGTGCTTTGTATGAACACAGGAGAAGGAGAAAGCAGCTACTTGCTCAATTCTAAATT
CACGAACGTAACAGCAATCAAATCAATCCCAACCCTAAAGAGGGCAATTGAATCACTCTTCAAGGAAGAATCACCAC
CATTTGAACACCTCCTAAATGTGGCAGATTTGGGGTGTGCTTCAGGCTCAACTTCAAATACCATAATGCCAACCGTA
GTCCAAACAGTGGTCAACAAATGCAGAGAATTGAATCACAAAATCCCAGAGTTTCAATTCTACTTGAATGATCTACC
ATCTAATGACTTCAACACACTCTTCAAGGGATTGAATGGTTTTGTGGGTAGTGGTGGTGAAGAATTTGAAAATACTT
CATGTCTTGTGATGGGTGCTCCTGGTTCTTTTCATGGGAGGCTCTTTCCTTTGAATACAATTCATCTTGTTTACTCT
AATTATTCTGTTCATTGGCTCTCCAAGGTACCGGATCTTAGAGATGAAAAAGGTAATCCAATAAACAAAGGAACATT
TTACATATCGAAAACAAGTCCTAGTGGTGTAAGAGAAGCGTACCTTGCTCAATTTCAAAAAGACTTCACATTGTTTC
TAAAGTCACGTGCTGAGGAGATGGTGTCCAATGGTCGAGTTGTGTTGGTTCTCCATGGAAGACTCTCTCAAGATTTC
TCCTGCGAAAAAGAACTTCAATTACCTTGGTTAATTCTCTCCCAAGCCATATCTCGCTTGGTTTCCAAGGGATTGAT
AGATGAAGAGAAATTGGATTCATTTGAGGTACCATACTACACACCATCAGTGCAAGAAGTGAAAGAATTAGTAGAGG
GAGAGGGATCGTATGCGGTGGAGCTCATGGAAACATTTACAATCAGGATCGGAGCCCGAAATGAGGGCATCTGGAGT
GATGCCCGAGGGTTTGGGAACAATCTCAGATCAATCACAGAGACAATGATTTCACACCACTTTGGACCTCAAATTCT
TGATGAATTGTATGATGAGATTCAAGATCTGCCTCTACAAGATTTTGCTACTCAATGTAGCTTTGTTGTTGGTTTGA
AGAGAAATGGAAGTAGCTAA

CaDXMT

CATTGGCCTCTGAGGCCACC**ATG**GAGCTCCAAGAAGTCCTGCATATGAATGGAGGCGAAGGCGATACAAGCTACGCC
AAGAACTCATTCTACAATCTGTTTCTCATCAGGGTGAAACCTATCCTTGAACAATGCATACAAGAATTGTTGCGGGC
CAACTTGCCCAACATCAACAAGTGCATTAAAGTTGCGGATTTGGGATGCGCTTCTGGACCAAACACACTTTTAACAG
TTCGGGACATTGTACAAAGTATTGACAAAGTTGGCCAGGAAAAGAAGAATGAATTAGAACGTCCCACCATTCAGATT
TTTCTGAATGATCTTTTCCAAAATGATTTCAATTCGGTTTTCAAGTCGCTGCCAAGCTTCTACCGCAAACTTGAGAA
AGAAAATGGACGCAAAATAGGATCATGCCTGATAGGCGCAATGCCTGGCTCTTTCTACGGCAGACTCTTCCCCGAGG
AGTCCATGCATTTTTTACACTCTTGTTACTGTTTGCATTGGTTATCTCAGGTTCCCAGCGGTTTGGTGACTGAATTG
GGGATCAGTGCGAACAAAGGGTGCATTTACTCTTCCAAAGCAAGTCGTCCGCCCATCCAGAAGGCATATTTGGATCA
ATTTACGAAAGATTTTACCACATTTCTTAGGATTCATTCGGAAGAGTTGATTTCACGTGGCCGAATGCTCCTTACTT
GGATTTGCAAAGAAGATGAATTCGAGAACCCGAATTCCATAGACTTACTTGAGATGTCAATAAACGACTTGGTTATT
GAGGGACATCTGGAGGAAGAAAAATTGGACAGTTTCAATGTTCCAATCTATGCACCTTCAACAGAAGAAGTAAAGTG
CATAGTTGAGGAGGAAGGTTCTTTTGAAATTTTATACCTGGAGACTTTTAAGGTCCCTTATGATGCTGGCTTCTCTA
TTGATGATGATTACCAAGGAAGATCCCATTCCCCAGTATCCTGCGATGAACATGCTAGAGCAGCGCATGTGGCATCT
GTCGTTAGATCAATTTTCGAACCCATCGTCGCAAGTCATTTTGGAGAAGCTATCATGCCTGACTTATCCCACAGGAT
TGCGAAGAATGCAGCAAAGGTTCTTCGCTCCGGCAAAGGCTTCTATGATAGTCTTATCATTTCTCTCGCCAAAAAGC
CAGAGAAGTCAGACGTG**TAA**GGCCTGTCAGGCCCATT

TCS1
CATTGGCCTCTGAGGCCACC**ATG**GAGCTAGCTACTGCGGGGAAGGTGAACGAAGTGTTGTTCATGAACAGAGGAGAA
GGAGAAAGTAGTTATGCACAAAACTCTTCTTTCACGCAACAAGTGGCCTCAATGGCACAGCCAGCGCTAGAAAATGC
AGTTGAAACTCTCTTCTCCAGAGATTTCCACCTTCAAGCTCTTAACGCAGCGGACTTGGGTTGTGCAGCGGGTCCAA
ACACATTCGCAGTGATTTCTACGATCAAGAGAATGATGGAAAAGAAATGCAGGGAATTGAATTGCCAAACACTGGAA
CTTCAGGTTTACTTGAATGATCTTTTTGGAAATGATTTCAATACCCTCTTCAAAGGCCTGTCGTCTGAGGTTATTGG
TAACAAATGTGAGGAAGTTCCGTGTTATGTGATGGGAGTACCGGGGTCTTTCCATGGCCGGCTTTTTCCTCGTAACA
GCTTACATTTAGTTCATTCCTCTTACAGTGTTCATTGGCTTACTCAGGCACCAAAAGGACTCACAAGCAGAGAAGGC
TTGGCATTAAACAAGGGGAAGATTTACATATCAAAGACAAGCCCTCCTGTTGTAAGAGAAGCCTACTTATCTCAATT
TCATGAAGATTTCACAATGTTTCTCAATGCTAGATCCCAAGAGGTGGTTCCAAATGGTTGTATGGTGTTGATACTTC
GTGGTAGGCAATGTTCTGATCCTTCAGACATGCAGAGCTGCTTTACTTGGGAACTATTAGCTATGGCCATTGCTGAA
TTGGTTTCACAGGGATTGATAGATGAAGATAAATTAGACACCTTCAATATACCCAGCTATTTTGCATCACTTGAGGA
AGTGAAAGATATAGTGGAGAGGGACGGATCATTCACAATTGATCATATAGAGGGGTTTGATCTTGATAGCGTAGAAA
TGCAGGAGAATGATAAATGGGTTAGAGGGGAAAAGTTTACCAAGGTTGTCAGGGCCTTCACAGAGCCTATAATTTCA
AACCAGTTTGGACCTGAAATCATGGACAAACTATATGACAAATTCACTCACATTGTAGTTTCAGATTTGGAAGCAAA
GCTACCGAAGACCACAAGTATCATCCTAGTGCTTTCCAAGATTGATGGA**TAG**GGCCTGTCAGGCCCATT

CaXMT1
GAACTGCAAGAGGTGCTGAGA**ATG**AACGGCGGCGAGGGCGATACAAGCTACGCCAAGAACAGCGCCTACAATCAGCT
GGTGCTGGCCAAAGTGAAGCCCGTGCTGGAACAGTGTGTGCGCGAACTGCTGAGAGCCAACCTGCCTAACATCAACA
AGTGCATCAAGGTGGCCGACCTGGGCTGTGCCTCTGGACCTAATACTCTGCTGACCGTGCGGGACATCGTGCAGAGC
ATCGACAAAGTGGGCCAAGAGAAGAAGAACGAGCTGGAACGGCCAACCATCCAGATCTTTCTGAACGATCTGTTCCC
CAACGACTTCAACAGCGTGTTCAAGCTGCTGCCCAGCTTCTACCGGAAGCTGGAAAAAGAGAACGGCCGGAAGATCG
GCTCCTGCCTGATTGGAGCTATGCCCGGCTCCTTCTACAGCAGACTGTTCCCCGAGGAATCCATGCACTTTCTGCAC
AGCTGCTACTGCCTGCAGTGGCTGTCTCAGGTGCCATCTGGCCTGGTTACAGAGCTGGGCATCTCCACCAACAAGGG
CAGCATCTACAGCTCCAAGGCCTCCAGACTGCCAGTGCAGAAGGCCTACCTGGACCAGTTCACCAAGGACTTCACCA
CCTTTCTGCGGATCCACAGCGAGGAACTGTTCAGCCACGGCAGAATGCTGCTGACCTGCATCTGCAAAGGCGTGGAA
CTGGACGCCAGAAACGCCATCGACCTGCTGGAAATGGCCATCAACGACCTGGTGGTGGAAGGACACCTGGAAGAGGA
AAAGCTGGACAGCTTCAATCTGCCCGTGTACATCCCCAGCGCCGAGGAAGTGAAGTGCATCGTGGAAGAAGAGGGCA
GCTTCGAGATCCTGTACCTGGAAACCTTCAAGGTGCTGTACGACGCCGGCTTCAGCATCGACGACGAGCACATCAAG
GCCGAGTACGTGGCCTCTTCTGTGCGGGCCGTGTATGAGCCTATTCTGGCCAGCCACTTCGGCGAGGCCATCATTCC
CGACATCTTCCACAGATTCGCCAAGCACGCCGCCAAAGTGCTGCCTCTCGGAAAGGGCTTCTACAACAACCTGATCA
TCAGCCTGGCCAAGAAGCCCGAGAAGTCCGACGTG**TAA**GGTAACTA

CCS1
GAACTGCAAGAGGTGCTGCAC**ATG**AATGGCGGCGAGGGCGATACAAGCTACGCCAAGAACAGCAGCTACAACCTGTT
CCTGATCAGAGTGAAGCCCGTGCTGGAACAGTGCATCCAAGAGCTGCTGAGAGCCAACCTGCCTAACATCAACAAGT
GCTTCAAAGTGGGCGACCTGGGCTGTGCCAGCGGACCTAATACCTTTAGCACCGTGCGGGACATCGTGCAGAGCATC
GACAAAGTGGGACAAGAGAAGAAGAACGAGCTGGAACGGCCTACCATCCAGATCTTTCTGAACGACCTGTTCCAGAA
CGACTTCAACAGCGTGTTCAAGCTGCTGCCCAGCTTCTACCGGAACCTGGAAAAAGAGAACGGCCGGAAGATCGGCT

CCTGCCTGATTGGAGCTATGCCCGGCTCCTTCTACAGCAGACTGTTCCCCGAGGAATCCATGCACTTTCTGCACAGC
TGCTACTGCCTGCACTGGCTGTCTCAGGTGCCATCTGGCCTGGTTACAGAGCTGGGCATCTCTGCCAACAAGGGCTG
CATCTACAGCTCCAAGGCCAGCGGGCCTCCTATCAAGAAGGCCTACCTGGACCAGTTCACCAAGGACTTCACCACCT
TTCTGCGGATCCACAGCGAGGAACTGATCAGCAGAGGCCGGATGCTGCTGACCTTCATCTGCAAAGAGGACGAGTTC
GATCACCCCAACAGCATGGACCTGCTGGAAATGAGCATCAACGACCTGGTCATCGAGGGCCACCTGGAAGAGGAAAA
GCTGGACAGCTTCAACGTGCCCATCTACGCCCCTAGCACCGAGGAAGTGAAGCGGATCGTTGAGGAAGAGGGCAGCT
TCGAGATCCTGTACCTGGAAACCTTTTACGCCCCTTACGACGCCGGCTTCAGCATCGACGATGACTACCAGGGCAGA
TCTCACAGCCCTGTGTCCTGTGATGAGCACGCCAGAGCTGCTCACGTGGCATCTGTTGTGCGGAGCATCTACGAGCC
TATCCTGGCCTCTCACTTCGGCGAGGCCATTCTGCCTGATCTGAGCCACCGGATCGCCAAGAATGCCGCCAAGGTGC
TGAGAAGCGGCAAGGGCTTTTACGACAGCGTGATCATCAGCCTGGCCAAGAAGCCCGAGAAGGCCGATATG**TAG**GGT
AACTA

CamelliaAncCS
AGTAGGCCTCTGAGGCCACC**ATG**GAAGAAGTGAAAGAGGCCCTCTTCATGAACAGAGGCGAGGGCGAGTCTAGCTAC
GCCCAGAATAGCAGCTTCACCCAGAAAGTGGCCAGCATGACCATGCCTGTGCTGGAAAACGCCGTGGAAACCCTGTT
CAGCAAGGACTTCCATCTGCTGCAGGCCCTGAATGCCGCCGATCTTGGATGTGCCGCCGGACCTAATACCTTCACCG
TGATCAGCACCATCAAGCGGATGATGGAAAAGAAGTGCCGCGAGCTGAACTGTCAGACCCTGGAACTGCAGGTCTAC
CTGAACGACCTGCCTGGCAACGACTTCAACACCCTGTTTAAGGGCCTGTCCTCCAAGGTGGTCGTGGGCAACAAGTG
CGAAGAGGTGTCCTGCTACGTGATGGGAGTGCCTGGCAGCTTTCACGGCAGACTGTTCCCCAGAAACAGCCTGCACC
TGGTGCACAGCAGCTACTCCGTGCATTGGCTGTCTCAGGCCCCAAAGGGCCTGACCAGTAGAGAAGGACTGGCCCTG
AACAAGGGCAAGATCTACATCAGCAAGACAAGCCCTCCAGTCGTGCGCGAGGCCTACCTGTCTCAGTTCCACGAGGA
CTTCACCATGTTTCTGAACGCTCGGAGCCAAGAGGTGGTGCCCAATGGCTGTATGGTCCTGATCCTGCACGGCAGGC
AGAGCAGCGACCCCAGCAATATGGAAAGCTGCTTCACCTGGGAGCTGCTGGCCATTGCCATTGCCGAACTGGTGTCC
CAGGGCCTGATCGACGAGGACAAGCTGGACACCTTCAACGTGCCCTACTACACCCCTAGCCTCGAGGAAGTGAAGGA
CATCGTCGAGAGAGAGGGCTCCTTCACCATCGACCACATGGAAGGCTTCGAGCTGGACAGCCCTCAGATGCAAGAGA
ACGACAAATGGGTCCGAGGCGAGAAGCTGGCCAAAGCCGTCAGAGCCTTTACCGAGCCTATCATCAGCAATCAGTTC
GGCCACGAGATCATGGATAAGCTGTACGACAAGTTCACCCACATCGTGGTGTCCGACCTGGAAGCCAAGATTCCCAA
GACCACCAGCATCATCCTGGTGCTGAGCAAGATCGTGGGC**TAA**TTCGAAGGCCTGTCAGGCCCTTA

TCS2
AGTAGGCCTCTGAGGCCACC**ATG**AAGGAAGTGAAAGAGGCCCTCTTCATGAACAAAGGCGAGGGCGAGAGCAGCTAC
GCCCAGAATAGCAGCTTTACCCAGACCGTGACCAGCATGACCATGCCTGTGCTGGAAAACGCCGTGGAAACCCTGTT
CAGCAAGGACTTCCATCTGCTGCAGGCCCTGAATGCCGTGGATCTGGGATGTGCTGCCGGACCTACCACCTTCACCG
TGATCAGCACCATCAAGCGGATGATGGAAAAGAAGTGCCGCGAGCTGAACTGTCAGACCCTGGAACTGCAGGTCTAC
CTGAACGACCTGCCTGGCAACGACTTCAACACCCTGTTTAAGGGCCTGCCTAGCAAGGTCGTGGGCAACAAGTGTGA
AGAGGTGTCCTGCTACGTCGTGGGAGTGCCTGGCTCTTTTCACGGCAGACTGTTCCCCAGAAACAGCCTGCACCTGG
TGCACAGCTGTTACTCCGTGCACTGGCTGACACAGGCCCCAAAGGGCCTGACCTCCAAAGAAGGACTGGCCCTGAAC
AAGGGCAAGATCTACATCAGCAAGACAAGCCCTCCAGTCGTGCGCGAGGCCTACCTGTCTCAGTTCCACGAGGACTT
CACCATGTTTCTGAACAGCCGCAGCCAAGAGGTGGTGCCCAATGGCTGTATGGTCCTGATCCTGAGAGGCCGGCTGA
GCAGCGATCCTAGCGATATGGGCAGCTGCTTCACCTGGGAACTGCTGGCCGTGGCCATTGCCGAACTGGTTTCTCAG
GGACTGATCGACGAGGACAAGCTGGACACCTTCAACGTGCCCAGCTACTTCCCCAGCCTGGAAGAAGTGAAGGACAT
CGTCGAGCGGAACGGCAGCTTCACCATCGACCACATGGAAGGCTTCGAGCTGGACAGCCCCGAGATGCAAGAGAACG
ACAAATGGGTCCGAGGCGAGAAGTTCGCCACAGTGGCCAGAGCCTTTACCGAGCCTATCATCAGCAATCAGTTCGGC
CACGAGATCATGGATAAGCTGTACGAGAAGTTTACCCACATCGTGGTGTCCGACTTCGAGGCCAAGATTCCCAAGAT
CACCAGCATCATCCTGGTGCTGTCCAAGATCGTGGGC**TAA**TTCGAAGGCCTGTCAGGCCCTTA

CaMXMT
AGTAGGCCTCTGAGGCCACC**ATG**GAACTGCAAGAGGTGCTGCACATGAACGAAGGCGAGGGCGATACCAGCTACGCC
AAGAACGCCAGCTACAATCTGGCCCTGGCCAAAGTGAAGCCCTTCCTGGAACAGTGCATCAGAGAGCTGCTGCGGGC
CAACCTGCCTAACATCAACAAGTGCATCAAGGTGGCCGACCTGGGCTGTGCCTCTGGACCTAATACTCTGCTGACCG
TGCGGGACATCGTGCAGAGCATCGACAAAGTGGGCCAAGAGGAAAAGAACGAGCTGGAACGGCCTACCATCCAGATC
TTTCTGAACGACCTGTTCCAGAACGACTTCAACAGCGTGTTCAAGCTGCTGCCCAGCTTCTACCGGAAGCTGGAAAA
AGAGAACGGCCGGAAGATCGGCTCCTGCCTGATTTCTGCCATGCCTGGCAGCTTTTACGGCCGGCTGTTCCCCGAGG
AATCCATGCACTTTCTGCACAGCTGCTACAGCGTGCACTGGCTGTCTCAGGTGCCATCTGGCCTGGTTATCGAACTC
GGCATCGGAGCCAACAAGGGCAGCATCTACAGCAGCAAGGGCTGCAGACCTCCAGTGCAGAAGGCCTACCTGGACCA
GTTCACCAAGGACTTCACCACCTTTCTGCGGATCCACAGCAAAGAGCTGTTCAGCCGGGGCAGAATGCTGCTGACCT
GCATCTGCAAGGTGGACGAGTTCGACGAGCCCAATCCACTGGACCTGCTGGACATGGCCATCAACGACCTGATCGTG

GAAGGCCTGCTGGAAGAAGAAAAGCTGGACAGCTTCAACATCCCGTTCTTCACCCCTAGCGCCGAGGAAGTGAAGTG
CATTGTGGAAGAGGAAGGCAGCTGCGAGATCCTGTACCTGGAAACCTTCAAGGCCCACTACGACGCCGCCTTCAGCA
TCGACGATGATTACCCTGTGCGGAGCCACGAGCAGATCAAGGCCGAATATGTGGCCAGCCTGATCAGAAGCGTGTAC
GAGCCTATCCTGGCCAGCCACTTTGGCGAGGCCATCATGCCTGATCTGTTCCACAGACTGGCCAAGCACGCCGCTAA
AGTGCTGCATATGGGCAAGGGATGCTACAACAACCTGATCATCAGCCTGGCCAAGAAGCCCGAGAAGTCCGACGTG**T**
AATTCGAAGGCCTGTCAGGCCCTTA

PaulliniaCupanaAncCS2

AGTAGGCCTCTGAGGCCACC**ATG**GACGTGAAGGACGTGCTGTGCATGAACAAAGGCGAGGGCGAGAGCAGCTACCTG
CTGAACAGCAAGTTCACCAACATCACCGCCGTGAAGTCTATCCCCACACTGAAGAGAGCCATCGAGAGCCTGTTCAA
AGAGGAAAGCCCTCCATTCGAGCATCTGCTGAACGTGGCCGATCTGGGCTGTGCCTCTGGCAGCACAAGCAACACCA
TCATGAGCACCGTGGTGCAGACCGTGGTCAACAAGTGCAGAGAGCTGAACCACAAGATCCCCGAGTTCCAGTTCTAC
CTGAACGACCTGCCTAGCAACGACTTCAACACCCTGTTCAAGGGCCTGAGCGGCTTTGTTGGCTCTGGCGGCGAGGA
ATTCGAGAACACCAGCTGTCTGGTCATGGGAGCCCCTGGCAGCTTTCACGGCAGACTGTTCCCTCTGAACACCATCC
ACCTGGTGTACAGCAACTACAGCGTGCACTGGCTGAGCAAGGTGCCCGACCTGAGAGATGAGAAGGGCAACCCCATC
AACAAGGGCACCTTCTACATCAGCAAGACAAGCCCCTCTGCCGTGCGCGAAGCTTATCTGGCCCAGTTCCAGAAGGA
CTTCACCCTGTTTCTGAAGTCCAGAGCCGAGGAAATGGTGTCCAACGGCAGAGTGGTGCTGGTGCTGCATGGAAGGC
TGAGCCAGGATTTCAGCTGCGAGAAAGAACTGCAGCTGCCTTGGCTGATCCTGTCTCAGGCCATCAGCAGACTGGTG
TCTAAGGGACTGATCGACGAGGAAAAGCTGGACAGCTTCGAGGTGCCCTACTACACCCCTAGCGCTCAAGAAGTGAA
AGAGCTGGTCGAAGGCGAAGGCAGCTACGCCGTGGAACTGATGGAAACCTTCACCATCCGGATCGGCGCCAGAAACG
AAGGCATTTGGAGCGACGCCAGAGGCTTCGGCAACAACCTGAGATCCATCACCGAGACAATGATCAGCCACCACTTC
GGCCCTCAGATCCTGGACGAGCTGTACGACGAGATCCAGGACCTGCCACTGCAGGACTTCGCCACACAGTGCAGCTT
TGTCGTGGGCCTGAAGCGGAAT**TAA**TTCGAAGGCCTGTCAGGCCCTTA

CaXMT1

GAACTGCAAGAGGTGCTGAGA**ATG**AACGGCGGCGAGGGCGATACAAGCTACGCCAAGAACAGCGCCTACAATCAGCT
GGTGCTGGCCAAAGTGAAGCCCGTGCTGGAACAGTGTGTGCGCGAACTGCTGAGAGCCAACCTGCCTAACATCAACA
AGTGCATCAAGGTGGCCGACCTGGGCTGTGCCTCTGGACCTAATACTCTGCTGACCGTGCGGGACATCGTGCAGAGC
ATCGACAAAGTGGGCCAAGAGAAGAAGAACGAGCTGGAACGGCCAACCATCCAGATCTTTCTGAACGATCTGTTCCC
CAACGACTTCAACAGCGTGTTCAAGCTGCTGCCCAGCTTCTACCGGAAGCTGGAAAAAGAGAACGGCCGGAAGATCG
GCTCCTGCCTGATTGGAGCTATGCCCGGCTCCTTCTACAGCAGACTGTTCCCCGAGGAATCCATGCACTTTCTGCAC
AGCTGCTACTGCCTGCAGTGGCTGTCTCAGGTGCCATCTGGCCTGGTTACAGAGCTGGGCATCTCCACCAACAAGGG
CAGCATCTACAGCTCCAAGGCCTCCAGACTGCCAGTGCAGAAGGCCTACCTGGACCAGTTCACCAAGGACTTCACCA
CCTTTCTGCGGATCCACAGCGAGGAACTGTTCAGCCACGGCAGAATGCTGCTGACCTGCATCTGCAAAGGCGTGGAA
CTGGACGCCAGAAACGCCATCGACCTGCTGGAAATGGCCATCAACGACCTGGTGGTGGAAGGACACCTGGAAGAGGA
AAAGCTGGACAGCTTCAATCTGCCCGTGTACATCCCCAGCGCCGAGGAAGTGAAGTGCATCGTGGAAGAAGAGGGCA
GCTTCGAGATCCTGTACCTGGAAACCTTCAAGGTGCTGTACGACGCCGGCTTCAGCATCGACGACGAGCACATCAAG
GCCGAGTACGTGGCCTCTTCTGTGCGGGCCGTGTATGAGCCTATTCTGGCCAGCCACTTCGGCGAGGCCATCATTCC
CGACATCTTCCACAGATTCGCCAAGCACGCCGCCAAAGTGCTGCCTCTCGGAAAGGGCTTCTACAACAACCTGATCA
TCAGCCTGGCCAAGAAGCCCGAGAAGTCCGACGTG**TAA**GGTAACTA

CCS1

GAACTGCAAGAGGTGCTGCAC**ATG**AATGGCGGCGAGGGCGATACAAGCTACGCCAAGAACAGCAGCTACA
ACCTGTTCCTGATCAGAGTGAAGCCCGTGCTGGAACAGTGCATCCAAGAGCTGCTGAGAGCCAACCTGCC
TAACATCAACAAGTGCTTCAAAGTGGGCGACCTGGGCTGTGCCAGCGGACCTAATACCTTTAGCACCGTG
CGGGACATCGTGCAGAGCATCGACAAAGTGGGACAAGAGAAGAAGAACGAGCTGGAACGGCCTACCATCC
AGATCTTTCTGAACGACCTGTTCCAGAACGACTTCAACAGCGTGTTCAAGCTGCTGCCCAGCTTCTACCG
GAACCTGGAAAAAGAGAACGGCCGGAAGATCGGCTCCTGCCTGATTGGAGCTATGCCCGGCTCCTTCTAC
AGCAGACTGTTCCCCGAGGAATCCATGCACTTTCTGCACAGCTGCTACTGCCTGCACTGGCTGTCTCAGG
TGCCATCTGGCCTGGTTACAGAGCTGGGCATCTCTGCCAACAAGGGCTGCATCTACAGCTCCAAGGCCAG
CGGGCCTCCTATCAAGAAGGCCTACCTGGACCAGTTCACCAAGGACTTCACCACCTTTCTGCGGATCCAC
AGCGAGGAACTGATCAGCAGAGGCCGGATGCTGCTGACCTTCATCTGCAAAGAGGACGAGTTCGATCACC
CCAACAGCATGGACCTGCTGGAAATGAGCATCAACGACCTGGTCATCGAGGGCCACCTGGAAGAGGAAAA
GCTGGACAGCTTCAACGTGCCCATCTACGCCCCTAGCACCGAGGAAGTGAAGCGGATCGTTGAGGAAGAG

GGCAGCTTCGAGATCCTGTACCTGGAAACCTTTTACGCCCCTTACGACGCCGGCTTCAGCATCGACGATG
ACTACCAGGGCAGATCTCACAGCCCTGTGTCCTGTGATGAGCACGCCAGAGCTGCTCACGTGGCATCTGT
TGTGCGGAGCATCTACGAGCCTATCCTGGCCTCTCACTTCGGCGAGGCCATTCTGCCTGATCTGAGCCAC
CGGATCGCCAAGAATGCCGCCAAGGTGCTGAGAAGCGGCAAGGGCTTTTACGACAGCGTGATCATCAGCC
TGGCCAAGAAGCCCGAGAAGGCCGATATGTAGGG**TAA**CTA

3.15.8 Mass Spectrum for BG-Biotin

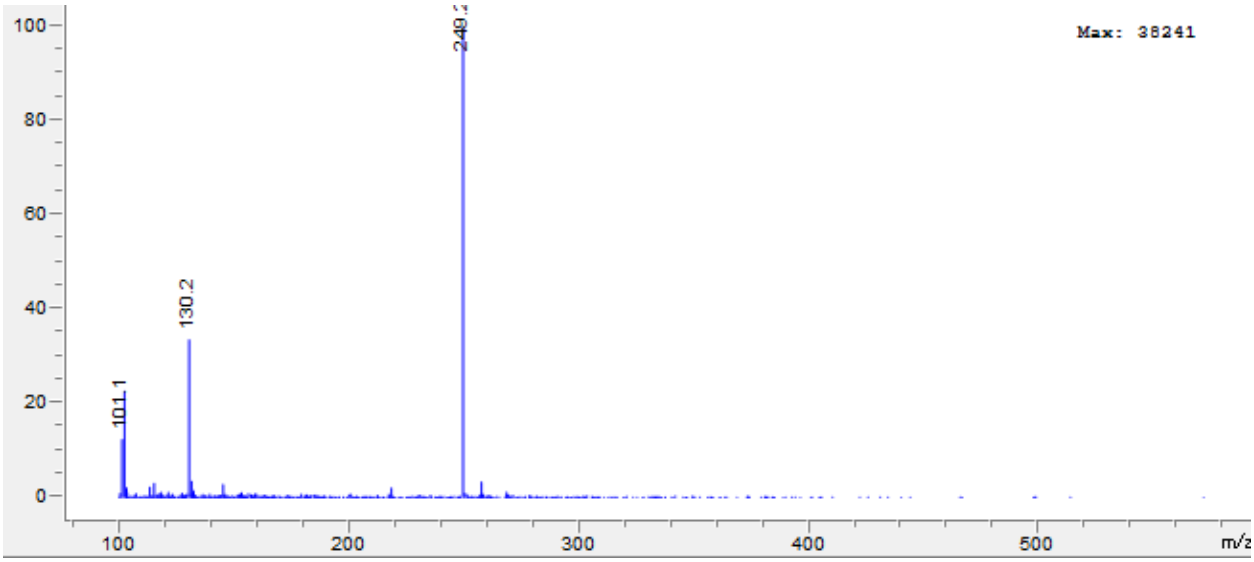

Figure 3.80: Mass spectrum for BG-Biotin. Shows m/2z $[M+2H]^{2+}$ calc 249.11; found 249.2.

3.15.9 Mass Spectrum for BG-PEG4-Biotin

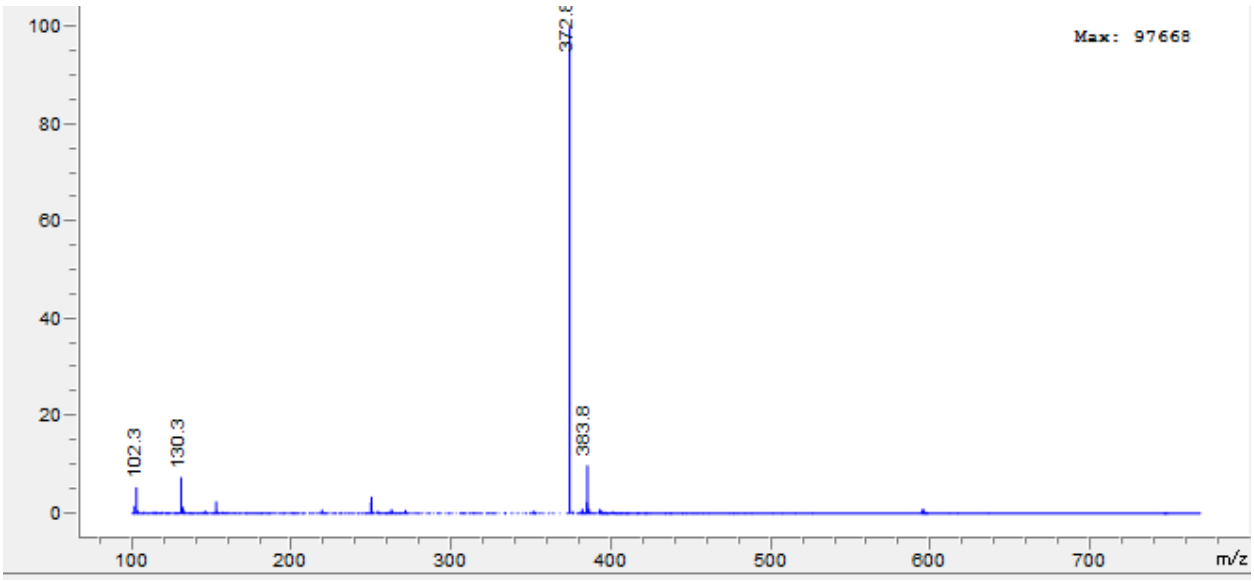

Figure 3.81: Mass spectrum for BG-PEG4-Biotin. Shows m/2z $[M+2H]^{2+}$ calc 372.68; found 372.8. Also shows m/2z $[M+H+Na]^{2+}$ calc 383.67; found 383.15.

3.15.10 LaG17 SDS-PAGE

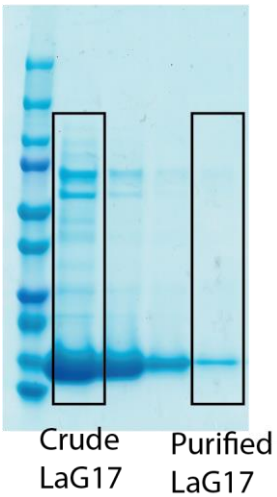

Figure 3.82: SDS-PAGE gel of crude and purified LaG17.

3.15.11 CCS1 and CCS1(delC13) Product Yields

Experimental conditions were the same as in the standard substrate activity assay. Concentrations are stated as final concentration in 1.5 mL after normalizing for evaporative loss in wells.

Table 3.15: Yield of products produced by CCS1 and CCS1(delC13) at 200 µM or 1000 µM substrate

		Concentration (µM)				
Enzyme	**[Substrate]**	*7X*		*37X*	*17X*	*Substrate*
		37X	*137X*	*137X*	*137X*	*Product(s)*
CCS1	200 µM	102.1	7.7	116.6	114	
	1000 µM	66.6	15.1	85.1	148.2	
CCS1(delC13)	200 µM	121.3	8.4	133.6	143.3	
	1000 µM	73	14	100.3	167.1	

3.15.12 Substrate Activity Assay Product Yields

Yields are calculated from concentration determined per well multiplied by volume of each well.

Table 3.16: Yield of each product from substrates assayed for all enzyme cell lines. Yield of 7X not calculated from XR for TCS2 and CaXMT1 due to difficulties in determining yield.

	Product Yield (nmoles)												
Enzyme	X		1X		3X		7X			37X	13X	17X	Substrate
	1X	3X	13X	137X	13X	37X	37X	17X	137X	137X	137X	137X	Product
CaDXMT										32.4		126.6	
CaMXMT	-	-	-	-	-	-	180.6	-	-	-	-	-	
CCS1			18.6		9.8		99.9		22.7	127.7		222.3	
CCS-G			7.35		4.2		96.5		11.6	9.9		161.1	
CCS1(delC13)			23.9		11.6		19.5		21	15.5		25.7	
CsAncCS	27.3	71.6			2.6	11.9	134.0	2.6					
PcAncCS2						43.8	39.6	3.8					
PcCS													
TCS1		11.6	112.8	2.6	14.3	tr.	184.5		6.2	37.4	4.2	241.8	
TCS1-G			18.8	0.9	1.8		47.0			3.9	2.7	134.1	

13.15.13 qPCR Experiment Results and Data

13.15.13.1 qPCR Data Tables

Table 3.17: Raw Ct Values for qPCR of Juxtacrine-Induced CCS1 Reporter Cells

Sample Name	Ct for CCS1	Ct for Notch
CCS1 0-1	15.92387	13.67257
CCS1 0-2	15.92719	13.57328
CCS1 0-3	16.31047	13.49401
CCS1 0.25-1	16.02952	12.78988
CCS1 0.25-2	16.00682	13.21113
CCS1 0.25-3	15.84349	13.71481
CCS1 0.5-1	13.85773	11.30057
CCS1 0.5-2	15.30472	12.01477
CCS1 0.5-3	15.55745	13.07764
CCS1 1.0-1	15.23175	13.43937
CCS1 1.0-2	15.36848	13.32988
CCS1 1.0-3	15.28742	13.37788
CCS1 1.5 -1	12.21545	12.32589
CCS1 1.5 -2	12.34758	11.36882
CCS1 1.5 -3	12.65342	11.52799

Table 3.18: Calculated Average Fold-Changes for qPCR of Juxtacrine-Induced CCS1 Reporter Cells

Sample	Fold-Change	Fold-Change – 1 Std. Dev.	Fold-Change + 1 Std. Dev.
CCS1 0:1	1.00	0.847	1.18
CCS1 0.25:1	0.842	0.606	1.17
CCS1 0.5:1	0.811	0.334	1.97
CCS1 1.0:1	1.47	1.39	1.57
CCS1 1.5:1	3.50	2.38	5.16

13.15.13.2 qPCR Data Figures

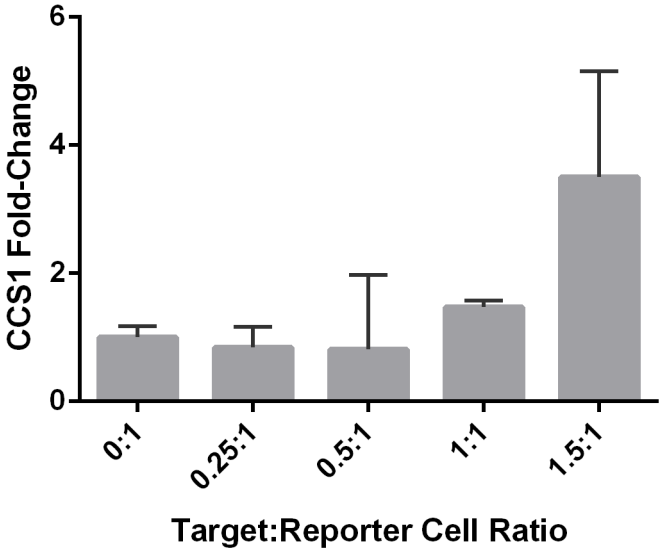

Figure 3.83: Graph of qPCR results showing CCS1 induction (as fold-change) at various target:reporter cell ratios relative to synNotch.

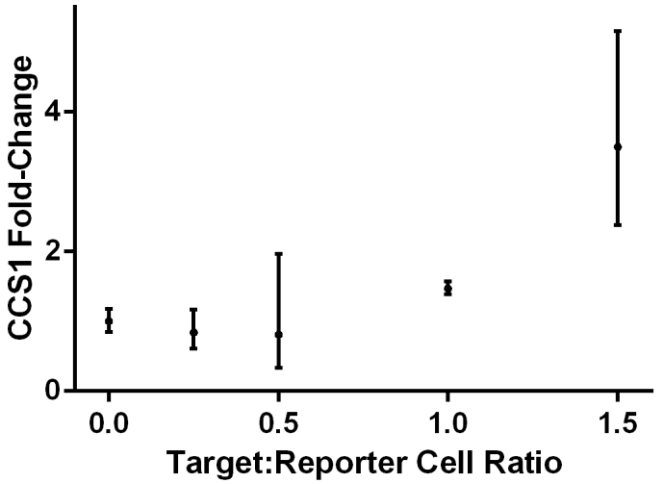

Figure 3.84: Graph of qPCR results showing CCS1 induction (as fold-change) at various target:reporter cell ratios relative to synNotch. The x-axis position indicates target:reporter cell ratio.

13.15.14 Additional Co-cuture Experiment Data and Results

Table 3.19: Data for plot of [Caffeine] vs Target:Reporter Cell Ratio for LaG17-synNotch + TRE mCherry-P2A-CCS1 / Target Cell Co-Culture Experiment. Cells were incubated in 200 µM PX for 72 h.

Target:Reporter Cell Ratio	[Caffeine] (µM)
0.00	1.03
0.25	3.68
0.50	3.15
1.00	5.19
1.50	7.15
2.00	9.06
2.50	9.03
3.00	14.5

Table 3.20: Data for plot of [Caffeine] vs Target:Reporter Cell Ratio for LaG17-synNotch + TRE mCherry-P2A-CCS1 / Target Cell Co-Culture Experiment with High Target:Reporter ratios. Cells were incubated in 200 µM PX for 72 h.

Target:Reporter Cell Ratio	[Caffeine] (µM)
0.1	1.69
0.2	1.86
0.5	3.70
1.0	10.14
1.5	9.55
2.0	13.8
3.0	13.5
4.0	12.0
5.0	15.7

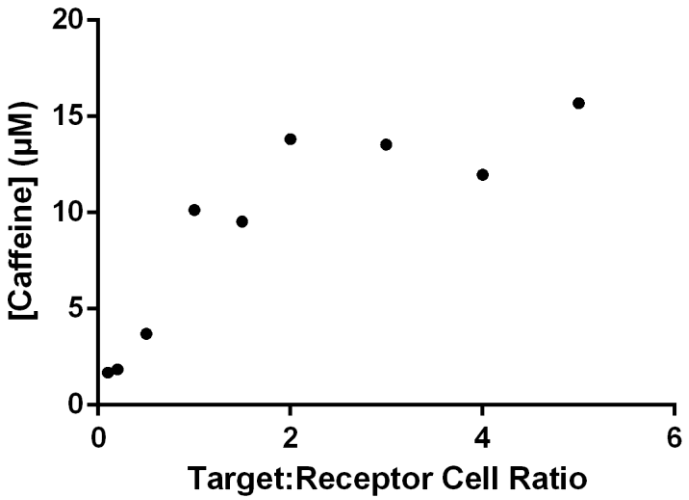

Figure 3.85: Plot of caffeine concentration (not evaporation-loss corrected) vs Target:Receptor cell ratio for higher cell ratios showing appearance of a plateau in response. Maximal response appears to be the same as in previous

Chapter three, in part, is being prepared for submission for publication of the material. Cisneros, B. T., Devaraj, N. K. The dissertation author is the primary investigator and author of this material.

References

(1) Cook, H. C. Origins of ... Tinctorial Methods in Histology. *J. Clin. Pathol.* **1997**, *50* (9), 716–720. https://doi.org/10.1136/jcp.50.9.716.

(2) Rusk, N. The Fluorescence Microscope. *Nat. Cell Biol.* **2009**, *11* (S1), S8–S9. https://doi.org/10.1038/ncb1941.

(3) Heimstadt Oskar. Das Fluoreszenzmikroskop. *Z. Wiss. Mikrosk.* **1911**, *28*, 330–337.

(4) van Ooij, C. *Milestone 7: Recipe for Fluorescent Antibodies*; 2009; Vol. 11. https://doi.org/10.1038/ncb1932.

(5) Coons, A. H.; Creech, H. J.; Norman, J. R.; Berliner, E. The Demonstration of Pneumococcal Antigen in Tissues by the Use of Fluorescent Antibody. *J. Immunol.* **1942**, *45*, 159–170.

(6) Graham, R. C.; Karnovsky, M. J. The Early Stages of Absorption of Injected Horseradish Peroxidase in the Proximal Tubules of Mouse Kidney: Ultrastructural Cytochemistry by a New Technique. *J. Histochem. Cytochem.* **1966**, *14* (4), 291–302. https://doi.org/10.1177/14.4.291.

(7) Nakane, P. K.; Pierce, G. B. Enzyme-Labeled Antibodies for the Light and Electron Microscopic Localization of Tissue Antigens. *J. Cell Biol.* **1967**, *33* (2), 307–318. https://doi.org/10.1083/jcb.33.2.307.

(8) Bobrow, M. N.; Harris, T. D.; Shaughnessy, K. J.; Litt, G. J. Catalyzed Reporter Deposition, a Novel Method of Signal Amplification Application to Immunoassays. *J. Immunol. Methods* **1989**, *125* (1–2), 279–285. https://doi.org/10.1016/0022-1759(89)90104-X.

(9) Kerstens, H. M. J.; Poddighe, P. J.; Hanselaar, A. G. J. M. A Novel in Situ Hybridization Signal Amplification Method Based on the Deposition of Biotinylated Tyramine. *J. Histochem. Cytochem.* **1995**, *43* (4), 347–352. https://doi.org/10.1177/43.4.7897179.

(10) Adams, J. C. Biotin Amplification of Biotin and Horseradish Peroxidase Signals in Histochemical Stains. *J. Histochem. Cytochem.* **1992**, *40* (10), 1457–1463. https://doi.org/10.1177/40.10.1527370.

(11) Chao, J.; DeBiasio, R.; Zhu, Z.; Giuliano, K. A.; Schmidt, B. F. Immunofluorescence Signal Amplification by the Enzyme-Catalyzed Deposition of a Fluorescent Reporter Substrate (CARD). *Cytometry* **1996**, *23* (1), 48–53. https://doi.org/10.1002/(SICI)1097-0320(19960101)23:1<48::AID-CYTO7>3.0.CO;2-I.

(12) Gould, S. J.; Subramani, S. Firefly Luciferase as a Tool in Molecular and Cell Biology. *Analytical Biochemistry*. November 15, 1988, pp 5–13. https://doi.org/10.1016/0003-

2697(88)90353-3.

(13) Stewart, G. S. A. B.; Williams, P. Lux Genes and the Applications of Bacterial Bioluminescence. *Journal of General Microbiology*. 1992, pp 1289–1300. https://doi.org/10.1099/00221287-138-7-1289.

(14) Silhavy, T. J.; Beckwith, J. R. Uses of Lac Fusions for the Study of Biological Problems. *Microbiological Reviews*. 1985, pp 398–418.

(15) Dilella, A. G.; Hope, D. A.; Chen, H.; Trumbauer, M.; Schwartz, R. J.; Smith, R. G. Utility of Firefly Luciferase as a Reporter Gene for Promoter Activity in Transgenic Mice. *Nucleic Acids Res.* **1988**, *16* (9), 4159. https://doi.org/10.1093/nar/16.9.4159.

(16) Chalfie, M.; Tu, Y.; Euskirchen, G.; Ward, W. W.; Prasher, D. C. Green Fluorescent Protein as a Marker for Gene Expression. *Science (80-.).* **1994**, *263* (5148), 802–805. https://doi.org/10.1126/science.8303295.

(17) Shaner, N. C.; Campbell, R. E.; Steinbach, P. A.; Giepmans, B. N. G.; Palmer, A. E.; Tsien, R. Y. Improved Monomeric Red, Orange and Yellow Fluorescent Proteins Derived from Discosoma Sp. Red Fluorescent Protein. *Nat. Biotechnol.* **2004**, *22* (12), 1567–1572. https://doi.org/10.1038/nbt1037.

(18) Matz, M. V.; Fradkov, A. F.; Labas, Y. A.; Savitsky, A. P.; Zaraisky, A. G.; Markelov, M. L.; Lukyanov, S. A. Fluorescent Proteins from Nonbioluminescent Anthozoa Species. *Nat. Biotechnol.* **1999**, *17* (10), 969–973. https://doi.org/10.1038/13657.

(19) Thurston, C. F. The Structure and Function of Fungal Laccases. *Microbiology* **1994**, *140* (1), 19–26. https://doi.org/10.1099/13500872-140-1-19.

(20) Andersen, S. O. Insect Cuticular Sclerotization: A Review. *Insect Biochem. Mol. Biol.* **2010**, *40* (3), 166–178. https://doi.org/10.1016/J.IBMB.2009.10.007.

(21) Alexandre, G.; Zhulin, I. B. Laccases Are Widespread in Bacteria. *Trends Biotechnol.* **2000**, *18* (2), 41–42. https://doi.org/10.1016/S0167-7799(99)01406-7.

(22) Alcalde, M. Laccases: Biological Functions, Molecular Structure and Industrial Applications. In *Industrial Enzymes*; Springer Netherlands: Dordrecht, 2007; pp 461–476. https://doi.org/10.1007/1-4020-5377-0_26.

(23) Abadulla, E.; Tzanov, T.; Costa, S.; Robra, K. H.; Cavaco-Paulo, A.; Gübitz, G. M. Decolorization and Detoxification of Textile Dyes with a Laccase from Trametes Hirsuta. *Appl. Environ. Microbiol.* **2000**, *66* (8), 3357–3362. https://doi.org/10.1128/AEM.66.8.3357-3362.2000.

(24) Kunamneni, A.; Plou, F.; Ballesteros, A.; Alcalde, M. Laccases and Their Applications: A Patent Review. *Recent Pat. Biotechnol.* **2008**, *2* (1), 10–24.

https://doi.org/10.2174/187220808783330965.

(25) Rodríguez Couto, S.; Toca Herrera, J. L. Industrial and Biotechnological Applications of Laccases: A Review. *Biotechnol. Adv.* **2006**, *24* (5), 500–513. https://doi.org/10.1016/J.BIOTECHADV.2006.04.003.

(26) Osma, J. F.; Toca-Herrera, J. L.; Rodríguez-Couto, S. Uses of Laccases in the Food Industry. *Enzyme Res.* **2010**, *2010*, 918761. https://doi.org/10.4061/2010/918761.

(27) Mogharabi, M.; Faramarzi, M. A. Laccase and Laccase-Mediated Systems in the Synthesis of Organic Compounds. *Adv. Synth. Catal.* **2014**, *356* (5), 897–927. https://doi.org/10.1002/adsc.201300960.

(28) Slagman, S.; Zuilhof, H.; Franssen, M. C. R. Laccase-Mediated Grafting on Biopolymers and Synthetic Polymers: A Critical Review. *ChemBioChem* **2018**, *19* (4), 288–311. https://doi.org/10.1002/cbic.201700518.

(29) Ray, S.; Das, N.; Bishayi, B. Development of a Simple Method for a New Immunoconjugate Utilizing Laccase. *Res. J. Immunol.* **2012**, *5* (1), 1–16. https://doi.org/10.3923/rji.2012.1.16.

(30) Zherdev, A. V; Bizova, N. A.; Yaropolov, A. I.; Lyubimova, N. V; Morozava, O. V; Dzantiev, B. B. Laccase from Coriolus Hirsutus as Alternate Label for Enzyme Immunoassay. *Appl. Biochem. Biotechnol.* **1999**, *76* (3), 203.

(31) Skorobogatko, O. V.; Gindilis, A. L.; Troitskaya, E. N.; Shuster, A. M.; Yaropolov, A. I. Laccase as a New Enzymatic Label for Enzyme Immunoassay. *Anal. Lett.* **1994**, *27* (15), 2997–3012. https://doi.org/10.1080/00032719408000307.

(32) Rodríguez-Delgado, M. M.; Alemán-Nava, G. S.; Rodríguez-Delgado, J. M.; Dieck-Assad, G.; Martínez-Chapa, S. O.; Barceló, D.; Parra, R. Laccase-Based Biosensors for Detection of Phenolic Compounds. *TrAC Trends Anal. Chem.* **2015**, *74*, 21–45. https://doi.org/10.1016/J.TRAC.2015.05.008.

(33) Zumárraga, M.; Bulter, T.; Shleev, S.; Polaina, J.; Martínez-Arias, A.; Plou, F. J.; Ballesteros, A.; Alcalde, M. In Vitro Evolution of a Fungal Laccase in High Concentrations of Organic Cosolvents. *Chem. Biol.* **2007**, *14* (9), 1052–1064. https://doi.org/10.1016/J.CHEMBIOL.2007.08.010.

(34) Mate, D. M.; Gonzalez-Perez, D.; Falk, M.; Kittl, R.; Pita, M.; De Lacey, A. L.; Ludwig, R.; Shleev, S.; Alcalde, M. Blood Tolerant Laccase by Directed Evolution. *Chem. Biol.* **2013**, *20* (2), 223–231.

(35) Gijlswijk, R. P. M. van; Zijlmans, H. J. M. A. A.; Wiegant, J.; Bobrow, M. N.; Erickson, T. J.; Adler, K. E.; Tanke, H. J.; Raap, A. K. Fluorochrome-Labeled Tyramides: Use in Immunocytochemistry and Fluorescence In Situ Hybridization. *J. Histochem. Cytochem.*

1997, *45* (3), 375–382. https://doi.org/10.1177/002215549704500305.

(36) Bobrow, M. N.; Litt, G. J.; Shaughnessy, K. J.; Mayer, P. C.; Conlon, J. The Use of Catalyzed Reporter Deposition as a Means of Signal Amplification in a Variety of Formats. *J. Immunol. Methods* **1992**, *150* (1–2), 145–149. https://doi.org/10.1016/0022-1759(92)90073-3.

(37) Martell, J. D.; Deerinck, T. J.; Sancak, Y.; Poulos, T. L.; Mootha, V. K.; Sosinsky, G. E.; Ellisman, M. H.; Ting, A. Y. Engineered Ascorbate Peroxidase as a Genetically Encoded Reporter for Electron Microscopy. *Nat. Biotechnol.* **2012**, *30* (11), 1143–1148. https://doi.org/10.1038/nbt.2375.

(38) Martell, J. D.; Deerinck, T. J.; Lam, S. S.; Ellisman, M. H.; Ting, A. Y. Electron Microscopy Using the Genetically Encoded APEX2 Tag in Cultured Mammalian Cells. *Nat. Protoc.* **2017**, *12* (9), 1792–1816. https://doi.org/10.1038/nprot.2017.065.

(39) Lee, S.-Y.; Kang, M.-G.; Park, J.-S.; Lee, G.; Ting, A. Y. Y.; Rhee, H.-W. APEX Fingerprinting Reveals the Subcellular Localization of Proteins of Interest. **2016**, *15* (8), 1837–1847. https://doi.org/10.1016/j.celrep.2016.04.064.

(40) Chen, C.-L.; Hu, Y.; Udeshi, N. D.; Lau, T. Y.; Wirtz-Peitz, F.; He, L.; Ting, A. Y.; Carr, S. A.; Perrimon, N. Proteomic Mapping in Live Drosophila Tissues Using an Engineered Ascorbate Peroxidase. *Proc. Natl. Acad. Sci. U. S. A.* **2015**, *112* (39), 12093–12098. https://doi.org/10.1073/pnas.1515623112.

(41) Berger, J.; Hauber, J.; Hauber, R.; Geiger, R.; Cullen, B. R. Secreted Placental Alkaline Phosphatase: A Powerful New Quantitative Indicator of Gene Expression in Eukaryotic Cells. *Gene* **1988**, *66* (1), 1–10. https://doi.org/10.1016/0378-1119(88)90219-3.

(42) Schönhuber, W.; Fuchs, B.; Juretschko, S.; Amann, R. Improved Sensitivity of Whole-Cell Hybridization by the Combination of Horseradish Peroxidase-Labeled Oligonucleotides and Tyramide Signal Amplification. *Appl. Environ. Microbiol.* **1997**, *63* (8), 3268–3273.

(43) Wang, G.; Achim, C. L.; Hamilton, R. L.; Wiley, C. A.; Soontornniyomkij, V. Tyramide Signal Amplification Method in Multiple-Label Immunofluorescence Confocal Microscopy. *Methods* **1999**, *18* (4), 459–464. https://doi.org/10.1006/METH.1999.0813.

(44) Foreman, J.; Demidchik, V.; Bothwell, J. H. F.; Mylona, P.; Miedema, H.; Torres, M. A.; Linstead, P.; Costa, S.; Brownlee, C.; Jones, J. D. G.; et al. Reactive Oxygen Species Produced by NADPH Oxidase Regulate Plant Cell Growth. *Nature* **2003**, *422* (6930), 442–446. https://doi.org/10.1038/nature01485.

(45) Nakamura, J.; Purvis, E. R.; Swenberg, J. A. Micromolar Concentrations of Hydrogen Peroxide Induce Oxidative DNA Lesions More Efficiently than Millimolar Concentrations in Mammalian Cells. *Nucleic Acids Res.* **2003**, *31* (6), 1790–1795.

https://doi.org/10.1093/nar/gkg263.

(46) Hampton, M. B.; Orrenius, S. Dual Regulation of Caspase Activity by Hydrogen Peroxide: Implications for Apoptosis. *FEBS Lett.* **1997**, *414* (3), 552–556. https://doi.org/10.1016/S0014-5793(97)01068-5.

(47) Forman, H. J. Use and Abuse of Exogenous H2O2 in Studies of Signal Transduction. *Free Radic. Biol. Med.* **2007**, *42* (7), 926–932. https://doi.org/10.1016/J.FREERADBIOMED.2007.01.011.

(48) Lee, C. R.; Patel, J. C.; Neill, B. O. '; Rice, M. E. Inhibitory and Excitatory Neuromodulation by Hydrogen Peroxide: Translating Energetics to Information. *J Physiol J. Physiol. Neurosci. S* **2015**, *59316*, 3431–3446. https://doi.org/10.1113/jphysiol.2014.273839.

(49) Veal, E. A.; Day, A. M.; Morgan, B. A. Hydrogen Peroxide Sensing and Signaling. *Mol. Cell* **2007**, *26* (1), 1–14. https://doi.org/10.1016/J.MOLCEL.2007.03.016.

(50) Gross, A. J.; Sizer, I. W. The Oxidation of Tyramine, Tyrosine, and Related Compounds by Peroxidase. *J. Biol. Chem.* **1959**, *234* (6), 1611–1614.

(51) Mattinen, M.-L.; Kruus, K.; Buchert, J.; Nielsen, J. H.; Andersen, H. J.; Steffensen, C. L. Laccase-Catalyzed Polymerization of Tyrosine-Containing Peptides. *FEBS J.* **2005**, *272* (14), 3640–3650. https://doi.org/10.1111/j.1742-4658.2005.04786.x.

(52) Hollmann, F.; Arends, I. W. C. E. Enzyme Initiated Radical Polymerizations. *Polymers (Basel).* **2012**, *4* (4), 759–793. https://doi.org/10.3390/polym4010759.

(53) Oudgenoeg, G.; Hilhorst, R.; Piersma, S. R.; Boeriu, C. G.; Gruppen, H.; Hessing, M.; Voragen, A. G. J.; Laane, C. Peroxidase-Mediated Cross-Linking of a Tyrosine-Containing Peptide with Ferulic Acid. *J. Agric. Food Chem.* **2001**, *49* (5), 2503–2510. https://doi.org/10.1021/jf000906o.

(54) Wan, Y.-Y.; Lu, R.; Xiao, L.; Du, Y.-M.; Miyakoshi, T.; Chen, C.-L.; Knill, C. J.; Kennedy, J. F. Effects of Organic Solvents on the Activity of Free and Immobilised Laccase from Rhus Vernicifera. *Int. J. Biol. Macromol.* **2010**, *47* (4), 488–495. https://doi.org/10.1016/J.IJBIOMAC.2010.07.003.

(55) Kurniawati, S.; Nicell, J. A. Characterization of Trametes Versicolor Laccase for the Transformation of Aqueous Phenol. *Bioresour. Technol.* **2008**, *99* (16), 7825–7834. https://doi.org/10.1016/J.BIORTECH.2008.01.084.

(56) Bollag, J. M.; Leonowicz, A. Comparative Studies of Extracellular Fungal Laccases. *Appl. Environ. Microbiol.* **1984**, *48* (4), 849–854.

(57) Harkin, J. M.; Obst, J. R. Syringaldazine, an Effective Reagent for Detecting Laccase and

Peroxidase in Fungi. *Experientia* **1973**, *29* (4), 381–387. https://doi.org/10.1007/BF01926734.

(58) Haigler, H.; Ash, J. F.; Singer, S. J.; Cohen, S. Visualization by Fluorescence of the Binding and Internalization of Epidermal Growth Factor in Human Carcinoma Cells A-431. *Proc. Natl. Acad. Sci. U. S. A.* **1978**, *75* (7), 3317–3321.

(59) Lake, M. C.; Aboagye, E. O. Luciferase Fragment Complementation Imaging in Preclinical Cancer Studies. *Oncoscience* **2014**, *1* (5), 310–325. https://doi.org/10.18632/oncoscience.45.

(60) Yewale, C.; Baradia, D.; Vhora, I.; Patil, S.; Misra, A. Epidermal Growth Factor Receptor Targeting in Cancer: A Review of Trends and Strategies. *Biomaterials* **2013**, *34* (34), 8690–8707. https://doi.org/10.1016/J.BIOMATERIALS.2013.07.100.

(61) Rizzolio, S.; Tamagnone, L. Epidermal Growth Factor (EGF) Receptor Endocytosis Assay in A549 Cells. *Bio-protocol* **2016**, *3* (15). https://doi.org/10.21769/bioprotoc.847.

(62) Kawamoto, T.; Mendelsohn, J.; Anh Le. Relation of Epidermal Growth Factor Receptor Concentration to Growth of Human Epidermoid Carcinoma A431 Cells. *J. Biol. Chem.* **1984**, *259* (12), 7761–7766.

(63) Morsut, L.; Roybal, K. T.; Xiong, X.; Gordley, R. M.; Coyle, S. M.; Thomson, M.; Lim, W. A. Engineering Customized Cell Sensing and Response Behaviors Using Synthetic Notch Receptors. *Cell* **2016**, *164* (4), 780–791. https://doi.org/10.1016/j.cell.2016.01.012.

(64) Yee, J. K.; Miyanohara, A.; LaPorte, P.; Bouic, K.; Burns, J. C.; Friedmann, T. A General Method for the Generation of High-Titer, Pantropic Retroviral Vectors: Highly Efficient Infection of Primary Hepatocytes. *Proc. Natl. Acad. Sci. U. S. A.* **1994**, *91* (20), 9564–9568.

(65) Schneider, C. A.; Rasband, W. S.; Eliceiri, K. W. NIH Image to ImageJ: 25 Years of Image Analysis. *Nat. Methods* **2012**, *9* (7), 671–675.

(66) Schindelin, J.; Rueden, C. T.; Hiner, M. C.; Eliceiri, K. W. The ImageJ Ecosystem: An Open Platform for Biomedical Image Analysis. *Mol. Reprod. Dev.* **2015**, *82* (7–8), 518–529. https://doi.org/10.1002/mrd.22489.

(67) Cisneros, B. T.; Devaraj, N. K. Laccase-Mediated Catalyzed Fluorescent Reporter Deposition for Live-Cell Imaging. *ChemBioChem* **2019**, cbic.201900593. https://doi.org/10.1002/cbic.201900593.

(68) Blomberg, B. A.; Codreanu, I.; Cheng, G.; Werner, T. J.; Alavi, A. Beta-Cell Imaging: Call for Evidence-Based and Scientific Approach. *Mol. Imaging Biol.* **2013**, *15* (2), 123–130. https://doi.org/10.1007/s11307-013-0620-4.

(69) Rice, B. W.; Cable, M. D.; Nelson, M. B. In Vivo Imaging of Light-Emitting Probes. **2001**. https://doi.org/10.1117/1.1413210.

(70) Close, D. M.; Xu, T.; Sayler, G. S.; Ripp, S. In Vivo Bioluminescent Imaging (BLI): Noninvasive Visualization and Interrogation of Biological Processes in Living Animals. *Sensors*. January 2011, pp 180–206. https://doi.org/10.3390/s110100180.

(71) Barnes, P. J. Theophylline. *Am. J. Respir. Crit. Care Med.* **2013**, *188* (8), 901–906. https://doi.org/10.1164/rccm.201302-0388PP.

(72) ZOUMAS, B. L.; KREISER, W. R.; MARTIN, R. THEOBROMINE AND CAFFEINE CONTENT OF CHOCOLATE PRODUCTS. *J. Food Sci.* **1980**, *45* (2), 314–316. https://doi.org/10.1111/j.1365-2621.1980.tb02603.x.

(73) Fulgoni, V. L.; Keast, D. R.; Lieberman, H. R. Trends in Intake and Sources of Caffeine in the Diets of US Adults: 2001–2010. *Am. J. Clin. Nutr.* **2015**, *101* (5), 1081–1087. https://doi.org/10.3945/ajcn.113.080077.

(74) Barone, J. J.; Roberts, H. Human Consumption of Caffeine. In *Caffeine*; Springer Berlin Heidelberg, 1984; pp 59–73. https://doi.org/10.1007/978-3-642-69823-1_4.

(75) Pendelll, D. *Pharmako/Dynamis*; North Atlantic Books: Berkeley, CA, 2009.

(76) Mitchell, D. C.; Knight, C. A.; Hockenberry, J.; Teplansky, R.; Hartman, T. J. Beverage Caffeine Intakes in the U.S. *Food Chem. Toxicol.* **2014**, *63*, 136–142. https://doi.org/10.1016/j.fct.2013.10.042.

(77) Ashihara, H.; Crozier, A. Biosynthesis and Metabolism of Caffeine and Related Purine Alkaloids in Plants. *Adv. Bot. Res.* **1999**, *30* (C), 117–205. https://doi.org/10.1016/S0065-2296(08)60228-1.

(78) Huang, R.; O'Donnell, A. J.; Barboline, J. J.; Barkman, T. J.; O'Donnell, A. J.; Barboline, J. J.; Barkman, T. J. Convergent Evolution of Caffeine in Plants by Co-Option of Exapted Ancestral Enzymes. *Proc. Natl. Acad. Sci.* **2016**, *113* (38), 10613–10618. https://doi.org/10.1073/pnas.1602575113.

(79) Xia, E. H.; Zhang, H. Bin; Sheng, J.; Li, K.; Zhang, Q. J.; Kim, C.; Zhang, Y.; Liu, Y.; Zhu, T.; Li, W.; et al. The Tea Tree Genome Provides Insights into Tea Flavor and Independent Evolution of Caffeine Biosynthesis. *Mol. Plant* **2017**, *10* (6), 866–877. https://doi.org/10.1016/j.molp.2017.04.002.

(80) Denoeud, F.; Carretero-Paulet, L.; Dereeper, A.; Droc, G.; Guyot, R.; Pietrella, M.; Zheng, C.; Alberti, A.; Anthony, F.; Aprea, G.; et al. The Coffee Genome Provides Insight into the Convergent Evolution of Caffeine Biosynthesis. *Science (80-.).* **2014**, *345* (6201), 1181–1184. https://doi.org/10.1126/science.1255274.

(81) Wei, C.; Yang, H.; Wang, S.; Zhao, J.; Liu, C.; Gao, L.; Xia, E.; Lu, Y.; Tai, Y.; She, G.; et al. Draft Genome Sequence of Camellia Sinensis Var. Sinensis Provides Insights into the Evolution of the Tea Genome and Tea Quality. *Proc. Natl. Acad. Sci. U. S. A.* **2018**, *115* (18), E4151–E4158. https://doi.org/10.1073/pnas.1719622115.

(82) Weckerle, C. S.; Stutz, M. A.; Baumann, T. W. Purine Alkaloids in Paullinia. *Phytochemistry* **2003**, *64* (3), 735–742. https://doi.org/10.1016/S0031-9422(03)00372-8.

(83) Ashihara, H.; Kubota, H. Patterns of Adenine Metabolism and Caffeine Biosynthesis in Different Parts of Tea Seedlings. *Physiol. Plant.* **1986**, *68* (2), 275–281. https://doi.org/10.1111/j.1399-3054.1986.tb01926.x.

(84) Kato, M.; Mizuno, K.; Crozier, A.; Fujimura, T.; Ashihara, H. Caffeine Synthase Gene from Tea Leaves. *Nature* **2000**, *406* (6799), 956–957. https://doi.org/10.1038/35023072.

(85) Schimpl, F. C.; Kiyota, E.; Mayer, J. L. S.; Gonçalves, J. F. D. C.; Da Silva, J. F.; Mazzafera, P. Molecular and Biochemical Characterization of Caffeine Synthase and Purine Alkaloid Concentration in Guarana Fruit. *Phytochemistry* **2014**, *105*, 25–36.

(86) Uefuji, H.; Ogita, S.; Yamaguchi, Y.; Koizumi, N.; Sano, H. Molecular Cloning and Functional Characterization of Three Distinct N -Methyltransferases Involved in the Caffeine Biosynthetic Pathway in Coffee Plants. *Plant Physiol.* **2003**, *132* (1), 372–380. https://doi.org/10.1104/pp.102.019679.

(87) Mizuno, K.; Kato, M.; Irino, F.; Yoneyama, N.; Fujimura, T.; Ashihara, H. The First Committed Step Reaction of Caffeine Biosynthesis: 7-Methylxanthosine Synthase Is Closely Homologous to Caffeine Synthases in Coffee (*Coffea Arabica* L.) [1]. *FEBS Lett.* **2003**, *547* (1–3), 56–60. https://doi.org/10.1016/S0014-5793(03)00670-7.

(88) Kato, M.; Mizuno, K.; Fujimura, T.; Iwama, M.; Irie, M.; Crozier, A.; Ashihara, H. Purification and Characterization of Caffeine Synthase from Tea Leaves. *Plant Physiol.* **1999**, *120* (2), 579–586. https://doi.org/10.1104/pp.120.2.579.

(89) Mizuno, K.; Okuda, A.; Kato, M.; Yoneyama, N.; Tanaka, H.; Ashihara, H.; Fujimura, T. Isolation of a New Dual-Functional Caffeine Synthase Gene Encoding an Enzyme for the Conversion of 7-Methylxanthine to Caffeine from Coffee (Coffea Arabica L.). **2003**, *534* (1–3), 75–81. https://doi.org/10.1016/S0014-5793(02)03781-X.

(90) Yoneyama, N.; Morimoto, H.; Ye, C. X.; Ashihara, H.; Mizuno, K.; Kato, M. Substrate Specificity of N-Methyltransferase Involved in Purine Alkaloids Synthesis Is Dependent upon One Amino Acid Residue of the Enzyme. *Mol. Genet. Genomics* **2006**, *275* (2), 125–135. https://doi.org/10.1007/s00438-005-0070-z.

(91) Figueirêdo, L.; Faria-Campos, A.; Astolfi-Filho, S.; Azevedo, J. Identification and Isolation of Full-Length CDNA Sequences by Sequencing and Analysis of Expressed Sequence Tags from Guarana (Paullinia Cupana). *Genet. Mol. Res.* **2011**, *10* (2), 1188–

1199. https://doi.org/10.4238/vol10-2gmr1124.

(92) Medrano, J. F.; Cantu, D.; Hulse-Kemp, A.; Van Deynze, A. The UC Davis Coffea arabica Genome Project http://phytozome.jgi.doe.gov.

(93) Xia, E.; Li, F.; Tong, W.; Yang, H.; Wang, S.; Zhao, J.; Liu, C.; Gao, L.; Tai, Y.; She, G.; et al. The Tea Plant Reference Genome and Improved Gene Annotation Using Long-Read and Paired-End Sequencing Data. *Sci. data* **2019**, *6* (1), 122. https://doi.org/10.1038/s41597-019-0127-1.

(94) Li, M.; Sun, Y.; Pan, S. A.; Deng, W. W.; Yu, O.; Zhang, Z. Engineering a Novel Biosynthetic Pathway in: Escherichia Coli for the Production of Caffeine. *RSC Adv.* **2017**, *7* (89), 56382–56389. https://doi.org/10.1039/c7ra10986e.

(95) Jin, L.; Bhuiya, M. W.; Li, M.; Liu, X. Q.; Han, J.; Deng, W. W.; Wang, M.; Yu, O.; Zhang, Z. Metabolic Engineering of Saccharomyces Cerevisiae for Caffeine and Theobromine Production. *PLoS One* **2014**, *9* (8), e105368. https://doi.org/10.1371/journal.pone.0105368.

(96) McKeague, M.; Wang, Y.-H. H.; Cravens, A.; Win, M. N.; Smolke, C. D. Engineering a Microbial Platform for de Novo Biosynthesis of Diverse Methylxanthines. *Metab. Eng.* **2016**, *38*, 191–203.

(97) Huang, R. Evolution of Caffeine Biosynthetic Enzymes and Pathways in Flowering Plants, 2017.

(98) Kowarz, E.; Löscher, D.; Marschalek, R. Optimized Sleeping Beauty Transposons Rapidly Generate Stable Transgenic Cell Lines. *Biotechnol. J.* **2015**, *10* (4), 647–653. https://doi.org/10.1002/biot.201400821.

(99) Ivics, Z.; Hackett, P. B.; Plasterk, R. H.; Izsvák, Z. Molecular Reconstruction of Sleeping Beauty, a Tc1-like Transposon from Fish, and Its Transposition in Human Cells. *Cell* **1997**, *91* (4), 501–510. https://doi.org/10.1016/S0092-8674(00)80436-5.

(100) Izsvák, Z.; Ivics, Z.; Plasterk, R. H. Sleeping Beauty, a Wide Host-Range Transposon Vector for Genetic Trensformation in Vertebrates. *J. Mol. Biol.* **2000**, *302* (1), 93–102. https://doi.org/10.1006/jmbi.2000.4047.

(101) Jin, Z.; Maiti, S.; Huls, H.; Singh, H.; Olivares, S.; Mátés, L.; Izsvák, Z.; Ivics, Z.; Lee, D. A.; Champlin, R. E.; et al. The Hyperactive Sleeping Beauty Transposase SB100X Improves the Genetic Modification of T Cells to Express a Chimeric Antigen Receptor. *Gene Ther.* **2011**, *18* (9), 849–856. https://doi.org/10.1038/gt.2011.40.

(102) Ogawa, M.; Herai, Y.; Koizumi, N.; Kusano, T.; Sano, H. 7-Methylxanthine Methyltransferase of Coffee Plants. Gene Isolation and Enzymatic Properties. *J. Biol. Chem.* **2001**, *276* (11), 8213–8218. https://doi.org/10.1074/jbc.M009480200.

(103) Alexiou, M.; Leese, H. J. *Purine Utilisation, de Novo Synthesis and Degradation in Mouse Preimplantation Embryos*; 1992; Vol. 114.

(104) Lu, S. C.; Mato, J. M. S-Adenosylmethionine in Liver Health, Injury, and Cancer. *Physiol. Rev.* **2012**, *92* (4), 1515–1542. https://doi.org/10.1152/physrev.00047.2011.

(105) Stead, L. M.; Brosnan, J. T.; Brosnan, M. E.; Vance, D. E.; Jacobs, R. L. Is It Time to Reevaluate Methyl Balance in Humans? *Am. J. Clin. Nutr.* **2006**, *83* (1), 5–10. https://doi.org/10.1093/ajcn/83.1.5.

(106) Martínez-López, N.; Varela-Rey, M.; Ariz, U.; Embade, N.; Vazquez-Chantada, M.; Fernandez-Ramos, D.; Gomez-Santos, L.; Lu, S. C.; Mato, J. M.; Martinez-Chantar, M. L. S-Adenosylmethionine and Proliferation: New Pathways, New Targets. In *Biochemical Society Transactions*; 2008; Vol. 36, pp 848–852. https://doi.org/10.1042/BST0360848.

(107) Rosenzweig, A.; Blenis, J.; Gomes, A. P. Beyond the Warburg Effect: How Do Cancer Cells Regulate One-Carbon Metabolism? *Front. Cell Dev. Biol.* **2018**, *6*. https://doi.org/10.3389/fcell.2018.00090.

(108) Poulton, J. E. Transamination and Demethylation Reactions in the Metabolism of Secondary Plant Products. In *The Biochemistry of Plants, Vol. 7*; Stumpf, P. K., Conn, E. E., Eds.; Academic Press: New York, 1981; pp 667–723.

(109) Waldhauser, S. S. M.; Gillies, F. M.; Crozier, A.; Baumann, T. W. Separation of the N-7 Methyltransferase, the Key Enzyme in Caffeine Biosynthesis. *Phytochemistry* **1997**, *45* (7), 1407–1414. https://doi.org/10.1016/S0031-9422(97)00187-8.

(110) Costa, S.; Almeida, A.; Castro, A.; Domingues, L. Fusion Tags for Protein Solubility, Purification, and Immunogenicity in Escherichia Coli: The Novel Fh8 System. *Frontiers in Microbiology*. Frontiers Research Foundation 2014. https://doi.org/10.3389/fmicb.2014.00063.

(111) Kodama, Y.; Shinya, T.; Sano, H. Dimerization of N-Methyltransferases Involved in Caffeine Biosynthesis. *Biochimie* **2008**, *90* (3), 547–551. https://doi.org/10.1016/j.biochi.2007.10.001.

(112) Marianayagam, N. J.; Sunde, M.; Matthews, J. M. The Power of Two: Protein Dimerization in Biology. *Trends in Biochemical Sciences*. November 2004, pp 618–625. https://doi.org/10.1016/j.tibs.2004.09.006.

(113) Renatus, M.; Stennicke, H. R.; Scott, F. L.; Liddington, R. C.; Salvesen, G. S. Dimer Formation Drives the Activation of the Cell Death Protease Caspase 9. *Proc. Natl. Acad. Sci. U. S. A.* **2001**, *98* (25), 14250–14255. https://doi.org/10.1073/pnas.231465798.

(114) Nakane, M.; Arai, K.; Saheki, S.; Kuno, T.; Buechler, W.; Murad, F. Molecular Cloning and Expression of CDNAs Coding for Soluble Guanylate Cyclase from Rat Lung. *J. Biol.*

Chem. **1990**, *265* (28), 16841–16845.

(115) Mizuno, K.; Kurosawa, S. ichi; Yoshizawa, Y.; Kato, M. Essential Region for 3-N Methylation in N-Methyltransferases Involved in Caffeine Biosynthesis. *Zeitschrift fur Naturforsch. - Sect. C J. Biosci.* **2010**, *65* (3–4), 257–265. https://doi.org/10.1515/znc-2010-3-414.

(116) Roybal, K. T.; Rupp, L. J.; Morsut, L.; Walker, W. J.; Mcnally, K. A.; Park, J. S.; Lim, W. A. Precision Tumor Recognition by T Cells With Combinatorial Antigen-Sensing Circuits. *Cell* **2016**, *164*, 770–779. https://doi.org/10.1016/j.cell.2016.01.011.

(117) Toda, S.; Blauch, L. R.; Tang, S. K. Y.; Morsut, L.; Lim, W. A. Programming Self-Organizing Multicellular Structures with Synthetic Cell-Cell Signaling. *Science (80-.).* **2018**, *361* (6398), 156–162. https://doi.org/10.1126/science.aat0271.

(118) Gordley, R. M.; Bugaj, L. J.; Lim, W. A. Modular Engineering of Cellular Signaling Proteins and Networks Introduction: Why Design and Engineer Signaling Proteins? *Curr. Opin. Struct. Biol.* **2016**, *39*, 106–114. https://doi.org/10.1016/j.sbi.2016.06.012.

(119) Roybal, K. T.; Lim, W. A. Synthetic Immunology: Hacking Immune Cells to Expand Their Therapeutic Capabilities INTRODUCTION: IMMUNE CELLS ARE AN IDEAL PLATFORM FOR INTERFACING WITH DISEASE. *Annu. Rev. Immunol* **2017**, *35*, 229–253. https://doi.org/10.1146/annurev-immunol.

(120) He, L.; Huang, J.; Perrimon, N.; Potter, C. J.; Venken, K. Development of an Optimized Synthetic Notch Receptor as an in Vivo Cell–Cell Contact Sensor. *Proc. Natl. Acad. Sci.* **2017**, 201703205. https://doi.org/10.1073/pnas.1703205114.

(121) Artavanis-Tsakonas, S.; Rand, M. D.; Lake, R. J. Notch Signaling: Cell Fate Control and Signal Integration in Development. *Science*. April 30, 1999, pp 770–776. https://doi.org/10.1126/science.284.5415.770.

(122) Kopan, R.; Ilagan, M. X. G. The Canonical Notch Signaling Pathway: Unfolding the Activation Mechanism. *Cell*. April 17, 2009, pp 216–233. https://doi.org/10.1016/j.cell.2009.03.045.

(123) Kopan, R. *Notch: A Membrane-Bound Transcription Factor*; 2002; Vol. 115, pp 1095–1097.

(124) Gordon, W. R.; Zimmerman, B.; He, L.; Miles, L. J.; Huang, J.; Tiyanont, K.; McArthur, D. G.; Aster, J. C.; Perrimon, N.; Loparo, J. J.; et al. Mechanical Allostery: Evidence for a Force Requirement in the Proteolytic Activation of Notch. *Dev. Cell* **2015**, *33* (6). https://doi.org/10.1016/j.devcel.2015.05.004.

(125) Lecourtois, M.; Schweisguth, F. Indirect Evidence for Delta-Dependent Intracellular Processing of Notch in Drosophila Embryos. *Curr. Biol.* **1998**, *8* (13), 771–775.

https://doi.org/10.1016/s0960-9822(98)70300-8.

(126) Fridy, P. C.; Li, Y.; Keegan, S.; Thompson, M. K.; Nudelman, I.; Scheid, J. F.; Oeffinger, M.; Nussenzweig, M. C.; Fenyö, D.; Chait, B. T.; et al. A Robust Pipeline for Rapid Production of Versatile Nanobody Repertoires. *Nat. Methods* **2014**, *11* (12), 1253–1260. https://doi.org/10.1038/nmeth.3170.

(127) Gossen, M.; Bujard, H. Tight Control of Gene Expression in Mammalian Cells by Tetracycline-Responsive Promoters. *Proc. Natl. Acad. Sci. U. S. A.* **1992**, *89* (12), 5547–5551. https://doi.org/10.1073/pnas.89.12.5547.

(128) Agha-Mohammadi, S.; O'Malley, M.; Etemad, A.; Wang, Z.; Xiao, X.; Lotze, M. T. Second-Generation Tetracycline-Regulatable Promoter: Repositioned Tet Operator Elements Optimize Transactivator Synergy While Shorter Minimal Promoter Offers Tight Basal Leakiness. *J. Gene Med.* **2004**, *6* (7), 817–828. https://doi.org/10.1002/jgm.566.

(129) Szymczak-Workman, A. L.; Vignali, K. M.; Vignali, D. A. A. Design and Construction of 2A Peptide-Linked Multicistronic Vectors. *Cold Spring Harb. Protoc.* **2012**, *7* (2), 199–204. https://doi.org/10.1101/pdb.ip067876.

(130) Eng, J.; Kleinman, W. A.; Singh, L.; Singh, G.; Raufman, J. P. Isolation and Characterization of Exendin-4, an Exendin-3 Analogue, from Heloderma Suspectum Venom. Further Evidence for an Exendin Receptor on Dispersed Acini from Guinea Pig Pancreas. *J. Biol. Chem.* **1992**, *267* (11), 7402–7405.

(131) Kolterman, O. G.; Buse, J. B.; Fineman, M. S.; Gaines, E.; Heintz, S.; Bicsak, T. A.; Taylor, K.; Kim, D.; Aisporna, M.; Wang, Y.; et al. Synthetic Exendin-4 (Exenatide) Significantly Reduces Postprandial and Fasting Plasma Glucose in Subjects with Type 2 Diabetes. *J. Clin. Endocrinol. Metab.* **2003**, *88* (7), 3082–3089. https://doi.org/10.1210/jc.2002-021545.

(132) Wu, Z.; Liu, S.; Hassink, M.; Nair, I.; Park, R.; Li, L.; Todorov, I.; Fox, J. M.; Li, Z.; Shively, J. E.; et al. Development and Evaluation of 18F-TTCO-Cys40-Exendin- 4: A PET Probe for Imaging Transplanted Islets. *J. Nucl. Med.* **2013**, *54* (2), 244–251. https://doi.org/10.2967/jnumed.112.109694.

(133) Wu, Z.; Todorov, I.; Li, L.; Bading, J. R.; Li, Z.; Nair, I.; Ishiyama, K.; Colcher, D.; Conti, P. E.; Fraser, S. E.; et al. In Vivo Imaging of Transplanted Islets with ^{64} Cu-DO3A-VS-Cys ^{40} -Exendin-4 by Targeting GLP-1 Receptor. *Bioconjug. Chem.* **2011**, *22* (8), 1587–1594. https://doi.org/10.1021/bc200132t.

(134) Reiner, T.; Thurber, G.; Gaglia, J.; Vinegoni, C.; Liew, C. W.; Upadhyay, R.; Kohler, R. H.; Li, L.; Kulkarni, R. N.; Benoist, C.; et al. Accurate Measurement of Pancreatic Islet - Cell Mass Using a Second-Generation Fluorescent Exendin-4 Analog. *Proc. Natl. Acad. Sci.* **2011**, *108* (31), 12815–12820. https://doi.org/10.1073/pnas.1109859108.

(135) Zhang, B.; Yang, B.; Zhai, C.; Jiang, B.; Wu, Y. The Role of Exendin-4-Conjugated Superparamagnetic Iron Oxide Nanoparticles in Beta-Cell-Targeted MRI. *Biomaterials* **2013**, *34* (23), 5843–5852. https://doi.org/10.1016/j.biomaterials.2013.04.021.

(136) Waldo, G. S.; Standish, B. M.; Berendzen, J.; Terwilliger, T. C. Rapid Protein-Folding Assay Using Green Fluorescent Protein. *Nat. Biotechnol.* **1999**, *17* (7), 691–695. https://doi.org/10.1038/10904.

(137) Rajan, S.; Dickson, L. M.; Mathew, E.; Orr, C. M. O.; Ellenbroek, J. H.; Philipson, L. H.; Wicksteed, B. Chronic Hyperglycemia Downregulates GLP-1 Receptor Signaling in Pancreatic β-Cells via Protein Kinase A. *Mol. Metab.* **2015**, *4* (4), 265–276. https://doi.org/10.1016/j.molmet.2015.01.010.

(138) Keppler, A.; Pick, H.; Arrivoli, C.; Vogel, H.; Johnsson, K. Labeling of Fusion Proteins with Synthetic Fluorophores in Live Cells. *Proc. Natl. Acad. Sci. U. S. A.* **2004**, *101* (27), 9955–9959. https://doi.org/10.1073/pnas.0401923101.

(139) Keppler, A.; Gendreizig, S.; Gronemeyer, T.; Pick, H.; Vogel, H.; Johnsson, K. A General Method for the Covalent Labeling of Fusion Proteins with Small Molecules in Vivo. *Nat. Biotechnol.* **2003**, *21* (1), 86–89. https://doi.org/10.1038/nbt765.

(140) Michael Green, N. Avidin and Streptavidin. *Methods Enzymol.* **1990**, *184* (C), 51–67. https://doi.org/10.1016/0076-6879(90)84259-J.

(141) Wilchek, M.; Bayer, E. A. Introduction to Avidin-Biotin Technology. *Methods Enzymol.* **1990**, *184* (C), 5–13. https://doi.org/10.1016/0076-6879(90)84256-G.

(142) Roux, K. J.; Kim, D. I.; Burke, B.; May, D. G. BioID: A Screen for Protein-Protein Interactions. *Curr. Protoc. Protein Sci.* **2018**, *91* (1), 19.23.1-19.23.15. https://doi.org/10.1002/cpps.51.

(143) Wu, K. K. Analysis of Protein-DNA Binding by Streptavidin-Agarose Pulldown. *Methods Mol. Biol.* **2006**, *338*, 281–290. https://doi.org/10.1385/1-59745-097-9:281.

(144) Kendall, C.; Ionescu-Matiu, I.; Dreesman, G. R. Utilization of the Biotin/Avidin System to Amplify the Sensitivity of the Enzyme-Linked Immunosorbent Assay (ELISA). *J. Immunol. Methods* **1983**, *56* (3), 329–339. https://doi.org/10.1016/S0022-1759(83)80022-2.

(145) Wu, S.-C.; Wong, S.-L. Engineering Soluble Monomeric Streptavidin with Reversible Biotin Binding Capability* □ S. **2005**. https://doi.org/10.1074/jbc.M501733200.

(146) Lim, K. H.; Huang, H.; Pralle, A.; Park, S. Stable, High-Affinity Streptavidin Monomer for Protein Labeling and Monovalent Biotin Detection. *Biotechnol. Bioeng.* **2013**, *110* (1), 57–67. https://doi.org/10.1002/bit.24605.

(147) Roybal, K. T.; Williams, J. Z.; Morsut, L.; Rupp, L. J.; Kolinko, I.; Choe, J. H.; Walker, W. J.; McNally, K. A.; Lim, W. A. Engineering T Cells with Customized Therapeutic Response Programs Using Synthetic Notch Receptors. *Cell* **2016**, *167* (2), 419-432.e16. https://doi.org/10.1016/j.cell.2016.09.011.

(148) Keeley, M. B.; Busch, J.; Singh, R.; Abel, T. TetR Hybrid Transcription Factors Report Cell Signaling and Are Inhibited by Doxycycline. *Biotechniques* **2005**, *39* (4), 529–536. https://doi.org/10.2144/000112002.

(149) Bojar, D.; Scheller, L.; Hamri, G. C.-E. El; Xie, M.; Fussenegger, M.; Charpin-El Hamri, G.; Xie, M.; Fussenegger, M. Caffeine-Inducible Gene Switches Controlling Experimental Diabetes. *Nat. Commun.* **2018**, *9* (1), 2318. https://doi.org/10.1038/s41467-018-04744-1.

(150) Franco, E. J.; Sonneson, G. J.; DeLegge, T. J.; Hofstetter, H.; Horn, J. R.; Hofstetter, O. Production and Characterization of a Genetically Engineered Anti-Caffeine Camelid Antibody and Its Use in Immunoaffinity Chromatography. *J. Chromatogr. B Anal. Technol. Biomed. Life Sci.* **2010**, *878* (2), 177–186. https://doi.org/10.1016/j.jchromb.2009.06.017.

(151) Sonneson, G. J.; Horn, J. R. Hapten-Induced Dimerization of a Single-Domain VHH Camelid Antibody. *Biochemistry* **2009**, *48* (29), 6693–6695. https://doi.org/10.1021/bi900862r.

(152) Ladenson, R. C.; Crimmins, D. L.; Landt, Y.; Ladenson, J. H. Isolation and Characterization of a Thermally Stable Recombinant Anti-Caffeine Heavy-Chain Antibody Fragment. *Anal. Chem.* **2006**, *78* (13), 4501–4508. https://doi.org/10.1021/ac058044j.

(153) Carvalho, J. J.; Weller, M. G.; Panne, U.; Schneider, R. J. A Highly Sensitive Caffeine Immunoassay Based on a Monoclonal Antibody. In *Analytical and Bioanalytical Chemistry*; 2010; Vol. 396, pp 2617–2628. https://doi.org/10.1007/s00216-010-3506-1.

(154) Cullen, B. R.; Malim, M. H. Secreted Placental Alkaline Phosphatase as a Eukaryotic Reporter Gene. *Methods Enzymol.* **1992**, *216* (C), 362–368. https://doi.org/10.1016/0076-6879(92)16033-G.

(155) Schukur, L.; Geering, B.; Charpin-El Hamri, G.; Fussenegger, M. Implantable Synthetic Cytokine Converter Cells with AND-Gate Logic Treat Experimental Psoriasis. *Sci. Transl. Med.* **2015**, *7* (318). https://doi.org/10.1126/scitranslmed.aac4964.

(156) Yin, Y.; Katahira, R.; Ashihara, H. *Metabolism of Purine Alkaloids and Xanthine in Leaves of Maté (Ilex Paraguariensis)*; 2015; Vol. 10.

(157) O'Donnell, A. J. Evolutionary Convergence of the Caffeine Biosynthetic Pathway in Chocolate Followed Duplication of a Constrained Ancestral Enzyme, Western Michigan University, 2015.

(158) McCarthy, A. A.; McCarthy, J. G. The Structure of Two N-Methyltransferases from the Caffeine Biosynthetic Pathway. *Plant Physiol.* **2007**, *144* (2), 879–889. https://doi.org/10.1104/pp.106.094854.

(159) Jørgensen, K.; Rasmussen, A. V.; Morant, M.; Nielsen, A. H.; Bjarnholt, N.; Zagrobelny, M.; Bak, S.; Møller, B. L. Metabolon Formation and Metabolic Channeling in the Biosynthesis of Plant Natural Products. *Current Opinion in Plant Biology*. Elsevier Ltd 2005, pp 280–291. https://doi.org/10.1016/j.pbi.2005.03.014.

(160) Zubieta, C.; Ross, J. R.; Koscheski, P.; Yang, Y.; Pichersky, E.; Noel, J. P. Structural Basis for Substrate Recognition in the Salicylic Acid Carboxyl Methyltransferase Family. *Plant Cell* **2003**, *15* (8), 1704–1716. https://doi.org/10.1105/tpc.014548.

(161) Jones, S.; Thornton, J. M. Protein-Protein Interactions: A Review of Protein Dimer Structures. *Progress in Biophysics and Molecular Biology*. 1995. https://doi.org/10.1016/0079-6107(94)00008-W.

(162) Mei, G.; Di Venere, A.; Rosato, N.; Finazzi-Agrò, A. The Importance of Being Dimeric. *FEBS Journal*. December 2, 2005, pp 16–27. https://doi.org/10.1111/j.1432-1033.2004.04407.x.

(163) Li, M.; Sun, Y.; Pan, S.; Deng, W.; Yu, O.; Zhang, Z. Engineering a Novel Biosynthetic Pathway in *Escherichia Coli* for the Production of Caffeine. *RSC Adv.* **2017**, *7* (89), 56382–56389. https://doi.org/10.1039/C7RA10986E.

(164) Traut, T. W. Physiological Concentrations of Purines and Pyrimidines. *Molecular and Cellular Biochemistry*. 1994, pp 1–22. https://doi.org/10.1007/BF00928361.

(165) Summers, R. M.; Louie, T. M.; Yu, C. L.; Gakhar, L.; Louie, K. C.; Subramanian, M. Novel, Highly Specific N-Demethylases Enable Bacteria to Live on Caffeine and Related Purine Alkaloids. *J. Bacteriol.* **2012**, *194* (8), 2041–2049. https://doi.org/10.1128/JB.06637-11.

(166) Holzinger, A.; Barden, M.; Abken, H. The Growing World of CAR T Cell Trials: A Systematic Review. *Cancer Immunology, Immunotherapy*. Springer Science and Business Media Deutschland GmbH December 1, 2016, pp 1433–1450. https://doi.org/10.1007/s00262-016-1895-5.

(167) Bruni, A.; Gala-Lopez, B.; Pepper, A. R.; Abualhassan, N. S.; James Shapiro, A. M. Islet Cell Transplantation for the Treatment of Type 1 Diabetes: Recent Advances and Future Challenges. *Diabetes, Metab. Syndr. Obes. Targets Ther.* **2014**, *7*, 211–223. https://doi.org/10.2147/DMSO.S50789.

(168) Rosenberg, S. A.; Restifo, N. P.; Yang, J. C.; Morgan, R. A.; Dudley, M. E. Adoptive Cell Transfer: A Clinical Path to Effective Cancer Immunotherapy. *Nature Reviews Cancer*. April 2008, pp 299–308. https://doi.org/10.1038/nrc2355.

(169) Park, T. S.; Rosenberg, S. A.; Morgan, R. A. Treating Cancer with Genetically Engineered T Cells. *Trends Biotechnol.* **2011**, *29* (11), 550–557. https://doi.org/10.1016/J.TIBTECH.2011.04.009.

(170) Kroeze, W. K.; Sassano, M. F.; Huang, X. P.; Lansu, K.; McCorvy, J. D.; Giguère, P. M.; Sciaky, N.; Roth, B. L. PRESTO-Tango as an Open-Source Resource for Interrogation of the Druggable Human GPCRome. *Nat. Struct. Mol. Biol.* **2015**, *22* (5), 362–369. https://doi.org/10.1038/nsmb.3014.

(171) Gasteiger, E.; Hoogland, C.; Gattiker, A.; Duvaud, S.; Wilkins, M. R.; Appel, R. D.; Bairoch, A. Protein Identification and Analysis Tools on the ExPASy Server. In *The Proteomics Protocols Handbook*; Humana Press, 2005; pp 571–607. https://doi.org/10.1385/1-59259-890-0:571.

(172) Park, Y.; Shin, S.; Jin, H.; Park, J.; Hong, Y.; Choi, J.; Jung, B.; Song, H.; Seo, D. Single-Molecule Rotation for EGFR Conformational Dynamics in Live Cells. *J. Am. Chem. Soc.* **2018**, *140* (45), 15161–15165. https://doi.org/10.1021/jacs.8b09037.

(173) Ye, J.; Coulouris, G.; Zaretskaya, I.; Cutcutache, I.; Rozen, S.; Madden, T. L. Primer-BLAST: A Tool to Design Target-Specific Primers for Polymerase Chain Reaction. *BMC Bioinformatics* **2012**, *13*, 134. https://doi.org/10.1186/1471-2105-13-134.

(174) Livak, K. J.; Schmittgen, T. D. Analysis of Relative Gene Expression Data Using Real-Time Quantitative PCR and the 2-ΔΔCT Method. *Methods* **2001**, *25* (4), 402–408. https://doi.org/10.1006/meth.2001.1262.